FLANGE BRACING REQUIREMENTS FOR METAL BUILDING SYSTEMS

A Dissertation
Presented to
The Academic Faculty

By

Cliff Douglas Bishop

In Partial Fulfillment
Of the Requirements for the Degree
Doctor of Philosophy in Civil Engineering

Georgia Institute of Technology

May 2013

FLANGE BRACING REQUIREMENTS
FOR METAL BUILDING SYSTEMS

Approved By:

Dr. Donald W. White, Advisor
School of Civil and Environmental Engineering
Georgia Institute of Technology

Dr. Bruce R. Ellingwood
School of Civil and Environmental Engineering
Georgia Institute of Technology

Dr. Lawrence F. Kahn
School of Civil and Environmental Engineering
Georgia Institute of Technology

Dr. Reginald DesRoches
School of Civil and Environmental Engineering
Georgia Institute of Technology

Dr. James Craig
School of Aerospace Engineering
Georgia Institute of Technology

Date Approved: April 3, 2013

To Jen, for all her love and support

ACKNOWLEDGEMENTS

I would like to first and foremost, express my deepest gratitude for the guidance provided by my advisor, Professor Don White. His patience, willingness to help, breadth of knowledge, and love of structural engineering is truly unparalleled. Furthermore, Professor White is an outstanding mentor whom I look up to and hold the utmost respect for.

I would also like to extend my thanks to the other members of my doctoral committee, including Professors Bruce Ellingwood, Lawrence Kahn, Reginald DesRoches, and James Craig, and to Mr. Ralf Leistikow. Their comments and suggestions throughout the research and at my defense proved most helpful.

The Metal Building Manufactures Association (MBMA) is greatly acknowledged for funding this research. Additionally, continued interaction with the group's research steering committee provided a valuable link between the theoretical and practical aspects of this research into bracing requirements for metal building structures.

Lastly, I would like to thank Dr. Yoon Duk Kim and Mr. Akhil Sharma for their prior research on metal building systems related to this project and other aspects of metal building structures. Dr. Kim proved not only to be a good friend but also a valuable resource for concerns regarding finite element modeling in Abaqus.

TABLE OF CONTENTS

LIST OF TABLES

LIST OF FIGURES

SUMMARY

The analysis and design of bracing systems for complex frame geometries typically found in metal buildings can prove to be an arduous task given current methods. The American Institute of Steel Construction's Appendix 6 from the 2010 Specification for Structural Steel Buildings affords engineers a means for determining brace strength and stiffness requirements, but only for the most basic cases. Specifically, there are a number of aspects of metal building systems that place their designs outside the scope of AISC's Appendix 6 (Stability Bracing for Columns and Beams). Some of the aspects not considered by Appendix 6 include: the use of web-tapered members, the potential for unequally spaced or unequal stiffness bracing, combination of bracing types including panel and flange diagonal bracing, and the effects of continuity across brace points. In this research, an inelastic eigenvalue buckling procedure is developed for calculation of the ideal bracing stiffness demands in general framing systems. Additionally, the software provides a method of calculating the elastic lateral-torsional buckling load of members with generally stepped and tapered cross-sections, which satisfies an important need for rigorous design assessment. Extensive benchmarking to load-deflection simulations of geometrically imperfect systems is performed and recommendations are developed for determining the required design stiffness and strength of the bracing components based on the use of this type of computational tool.

1. INTRODUCTION

1.1 Problem Statement

Metal buildings are structures that utilize extreme weight efficiency to provide large, open floor space at a relatively inexpensive price. Metal buildings are designed to the limits of applicable codes and standards in order to optimize their economy while still meeting safety standards and client objectives. Thus, provisions in design standards that are overly conservative can unduly influence the steel system costs. Figure 1.1 shows a rendering of a one-bay, two-frame segment of a typical metal building.

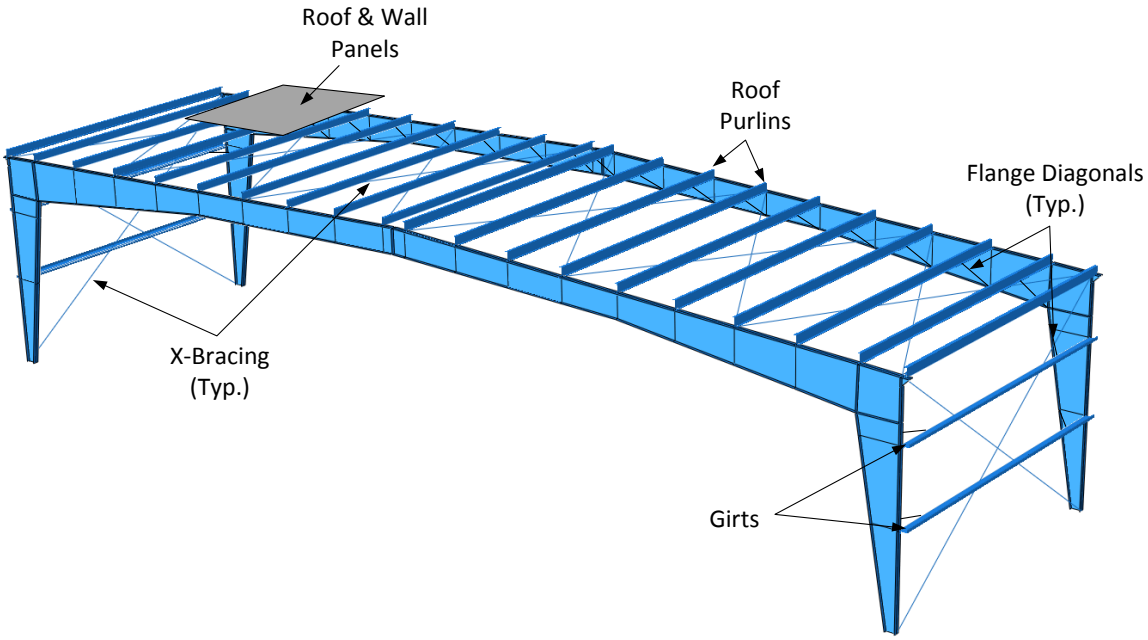

Figure 1.1: Two representative clear-span metal building frames

The American Institute of Steel Construction's *Specification for Structural Steel Buildings* (2010b) Appendix 6 – "Stability Bracing for Columns and Beams" provides simplified methods for designing lateral and torsional braces required for stability and is the

governing specification used by designers of metal buildings when considering bracing systems. However, there are a number of specific attributes of metal building systems that are outside of the scope of Appendix 6. These attributes include:

- Metal building frames make extensive use of web-tapered members where AISC's Appendix 6 only considers prismatic members.
- The bracing stiffnesses provided are assumed to be equal at each brace per Appendix 6. This is often not achieved in practice due to variations in girt or purlin size and in bracing diagonal lengths and angles of inclination.
- Appendix 6 assumes uniform spacing of braces; however, metal building frames generally have unequal spacing of the girts, purlins and/or flange diagonal braces.
- Knee joints and other joints may not provide rigid restraint against twisting and lateral movement at the rafter and column ends, yet the AISC equations are based on the assumption of rigid bracing at the member ends.
- Warping and lateral bending restraint from joints and continuity with more lightly-loaded adjacent member segments is not considered.
- The combined action of diaphragms and discrete flange diagonal braces may contribute significantly to the stability of critical segments. AISC does not offer any guidance for assessing the stiffness provided to the system by multiple bracing types.
- AISC's Appendix 6 targets the design of the braces for a single upper-bound estimate of the stiffness and strength requirements of equal stiffness, uniformly-spaced braces. However, some economy potentially may be gained by

recognizing that the bracing stiffness and strength demands often reduce very sharply as one moves away from a critical bracing location.

Although it is believed that many of the above attributes result in conservative designs, engineers are left to interpret and adapt the current AISC codified equations well beyond the intent of the Specification to design bracing for their buildings. This could lead to inadequate designs and, in extreme situations, to adverse effects on life-safety.

There are also questions concerning brace connection details. Metal building frames have flange diagonals bracing the compression flange of the rafters to the purlins. Since the connections of these components are often made with slotted or oversized holes, it is important to assess the impact of this practice on the bracing strength. Furthermore, many metal building frames are braced by light, threaded rods or cables, which can easily become slack. It may be possible to tolerate a small amount of movement (where “small” generally refers to movements on the order of or less than typical construction tolerances) required to engage the bracing in some cases without severely impacting the effectiveness of the bracing. If the brace stiffness is engaged substantially after a small amount of movement, the response may be similar to the behavior associated with a larger nominal geometric imperfection.

Lastly, the AISC Specification Appendix 6 provisions estimate the maximum brace strength and stiffness demands throughout a given member generally assuming constant brace spacing and constant brace stiffness. However, this method is not practical for members with a large number of brace points along their length. When considering the sample frames shown in Figure 1.1, several questions come to mind:

1. Are the bracing requirements at the knee influenced significantly by the loading, cross-section geometry or arrangement of bracing at the ridge?
2. What constitutes a support point? That is, at what locations is the movement of the frame out-of-plane effectively prevented? Do locations of attachment of the panel or rod bracing provide this restraint?
3. How do the rafters interact with the columns and vice versa with respect to the bracing demands?

Figure 1.2 shows a simplified depiction of the type of problem in question. In this example, the member is subjected to an axial load and full reverse-curvature bending. The member ends are laterally supported by conceptual springs at the top and bottom flange levels, which represent general, non-rigid end bracing. The outset purlins passing over the top flange and the flange diagonal kickers connected to the bottom flange (as shown in Figure 1.1) are modeled as torsional springs that are "activated" by the relative lateral movement between flanges. Figure 1.2 shows these torsional springs as a relative shear stiffness provided between the flanges. Therefore, the torsional bracing flexibility, which is represented by a single torsional brace, can be significantly affected by:

- Bending deformations of the purlins,
- Axial deformations of the flange diagonal brace(s),
- Local deformations and potential slip in the connection of the purlins to the top flange, and in the connection of the flange diagonals to the member and the purlins, and
- Cross-section distortion within the member that is being braced.

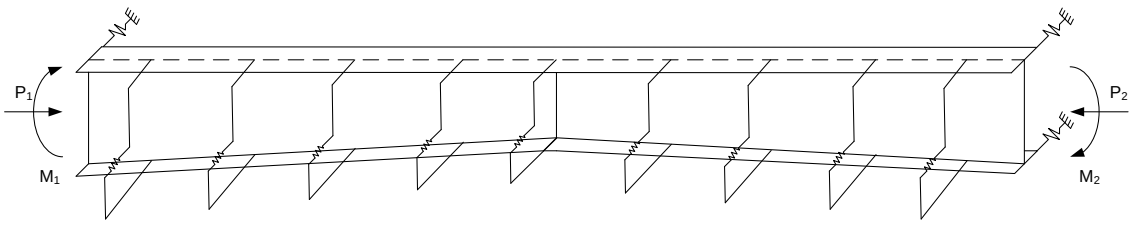

Figure 1.2: Simplified beam model

For the beam model in Figure 1.2 with reference to the four items listed above:

1. Does it make sense to design the braces at the middle of the span (located at cross-sections of low moment) for the same demands as the critical end braces? Strictly speaking, the AISC Appendix 6 provisions give only a single estimate of the maximum brace stiffness and strength demands throughout the member length, based on the assumption of constant brace stiffness and constant brace spacing.
2. At what stiffness do the end springs become effective as lateral supports?
3. How does this member tie to adjacent members, and how does potential warping and lateral bending restraint from continuity with the adjacent members influence the bracing demands in this member?

In general, all the members and their bracing components work together as a system in structural frames such as that shown in Figure 1.1. Therefore, a central question in this research is: What overall physical bracing strength and stiffness demands are needed to develop the required strength the structure?

1.2 Objectives and Scope

The objectives of this research are to:

1. Assess the physical strength and stiffness demands on the stability bracing systems in metal building frames.
2. Investigate and recommend new practical methods of stability bracing design that are more general and more easily applied than current methods.
3. Improve the overall safety of metal building structural systems.

2. BACKGROUND

2.1 Stability Bracing Defined

Stability bracing is defined as bracing in which the primary forces are zero. That is, the bracing system does not directly resist the loads generally carried by the framing system; it exists solely to permit the main framing members to reach higher strengths by limiting the unbraced member lengths. The only forces in the bracing system are due to movements caused by initial geometric imperfections of the members that are being braced. In general, stability bracing must satisfy two main design requirements:

1. It must have sufficient *strength* to resist the loads imparted to it by the members being braced, and
2. It must have sufficient *stiffness* to limit brace-point movement, which subsequently limits the brace forces and the amplified second-order displacements in the members.

In current structural design practice, bracing systems are commonly classified into the following categories (Galambos & Surovek 2008; Ziemian 2010):

1. *Discrete* bracing resists brace-point movement only at the locations of the brace. This form of bracing is also commonly referred to as *nodal* bracing. An example of such bracing is a column that is braced against some other massive non-movable structure by struts that frame in perpendicular to the member at various points along its length. Sharma (2010) refers to this type of bracing as *discrete grounded* bracing to emphasize the fact that nodal bracing is modeled as single

discrete springs normal to the axis of the member and tied to a rigid support on their opposite ends.

2. *Relative* bracing (possibly better described as *shear panel* bracing) resists the relative displacements between two points. Common applications of relative bracing include chevron or X-bracing for braced bays in low to mid-rise steel structures. For metal building systems, wall or roof panels between purlins and cable or rod bracing between adjacent frames provide relative, shear panel bracing for lateral support of the main frame members at the location of these systems through the member depth.
3. *Continuous* bracing provides uninterrupted lateral support for structural members. A composite slab is an example of continuous bracing.
4. *Lean-on* bracing describes bracing in which the lateral support of one member is provided by the flexural stiffness of another adjacent member. This may occur when one frame, loaded to capacity, “leans” on another frame that is more lightly loaded.

Within actual bracing systems, the precise behavior of the different bracing components often does not fit well with these simple definitions. For example, scenarios are often encountered where combinations of bracing types are used. Figure 2.1 provides a simple example. Engineers may question which type of bracing system is employed for each bay. Some may indicate that the bracing in Bay 1 is nodal, since it ties a discrete brace-point at the location of the brace back to another system. However, the bracing in Bay 2 is relative since it resists movement of the mid-point of the column relative to the the top and bottom of the column. In actuality, the bracing in this example is a combination of nodal and relative braces in series.

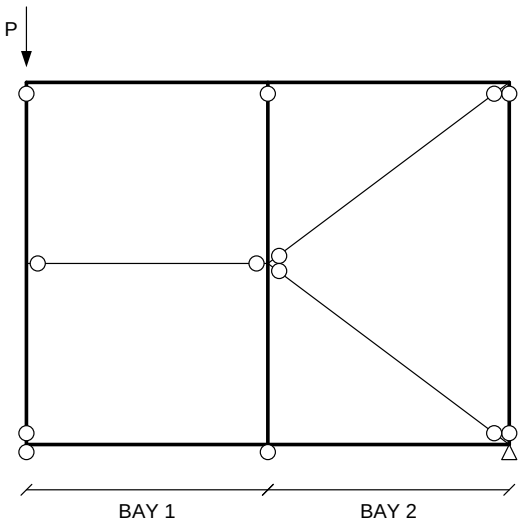

Figure 2.1: Nodal and relative bracing in series

The AISC Specification's Appendix 6 (2010b) focuses on basic bracing situations and offers design equations for relative and nodal lateral bracing of columns and beams and for nodal and continuous torsional bracing of beams.

2.2 Historical Perspective

Historically, braces have been designed using simplified models and rule-of-thumb estimates. The most common traditional rule for strength design of the brace suggests a brace force equal to 2% of the axial load for columns or 2% of the equivalent flange force for beams. This rule can be traced back to the mid-1940's to the structural design firm Seelye, Stevenson & Value in New York City. Seelye (1945) notes one should "brace all columns in two directions… Min. = 2% of load" and for beams, "[the] strength of [the] brace is to be not less than 2% of the flange stress."

Several years later, Throop (1947) wrote an article in Engineering News-Record on "Suggestions for Safe Lateral Bracing Design." Being an Associate Engineer at Seelye,

Stevenson & Value, he subscribed to Seelye's design recommendation. However, he also added that braces must "be within the limits of stiffness requirements by code or good design". Throop went on to suggest specific details that seemed to work well in practice.

Zuk (1956) noted that engineers tend to pick values for brace forces as some small percentage of the axial load and base those values solely on engineering judgment. He performed calculations for several varied brace configurations and column lengths. The results showed that the brace force was indeed usually less than 2% of the axial load (or equivalent beam compression flange force). The only exception was when the brace was located at the centroid of the beam cross-section as opposed to being attached directly to the compression flange. These cases saw maximum values of only 2.35% (Zuk 1956). Research per Sharma (2010), described subsequently in Section 5.3, provides results similar to that of Zuk and shows that the maximum brace forces at the limit load of the structure are usually on the order of 2 to 3 percent of the equivalent flange force for nodal cases involving *full bracing*, which is the situation where further increases in the bracing stiffness or strength have negligible influence on the capacity of the structure.

Winter is often thought of as the father of modern-day bracing requirements. His work in the late-1950's and early-1960's created the foundation on which our current Specification equations are based. Winter (1960) noted in his experiments that an improperly braced beam tended to "twist and deflect sideways with consequent loss of strength." In addition, he went on to demonstrate that the resistance to secondary loads required bracing components to have a certain strength *and* rigidity.

Further research by Yura and Phillips (1992), Yura et al. (1992) and Yura (1993, 1995, 1996) expanded the basic Winter model into equations for strength and stiffness that were codified by AISC. Various forms of Yura's proposed equations can be found in the current AISC Specification Appendix 6.

2.3 AISC Specification Provisions for Stability Bracing of Beams

The AISC equations from the Specification's Appendix 6 and Commentary are based predominantly on the definition of full bracing as the bracing stiffness and strength necessary to develop column or beam strengths based on column flexural buckling or beam lateral-torsional buckling with effective length factors of K = 1.0. In addition, practical estimates of the stiffness and strength requirements are provided for partial torsional and nodal lateral bracing. These approaches, while computationally simple, lack the ability to account for the issues discussed in Section 1.1. The following sections review specific forms of the basic equations detailed in the AISC Specification, including many of the refinements (largely developed by Yura) presented in the corresponding Commentary. Thus, the equations presented below are AISC's most comprehensive approach to designing stability bracing systems. This dissertation presents only the AISC beam lateral and torsional bracing equations. The AISC column bracing equations are closely related to, and in fact, are the conceptual bases for the AISC beam lateral bracing equations.

In the 2010 AISC Specification a new Section 6.4 has been added to Appendix 6. This section addresses beam-columns. The requirements presented in Section 6.4 are an *ad hoc* extension to the strength and stiffness requirements for columns and beams. While these considerations appear to be conservative, very little research has been performed to assess their accuracy or implications (Sharma 2010). Metal building frames are

typically dominated by bending effects. However, further consideration for and a brief discussion of the effects of axial force on the design of stability bracing for beams, i.e., for members that are loaded predominantly in flexure, is presented in this research.

2.3.1 Nodal (Discrete Grounded) Bracing, Stiffness Requirement

A refined estimate of the nodal lateral bracing stiffness requirement defined in the AISC Commentary (2010b) is:

$$\beta_{br} = \psi\left[2\left(4-\frac{2}{n}\right)\frac{\left(\frac{M_r}{h_o}\right)}{L_q}\right]C_{tN}C_d \qquad \text{(2.1, AISC C-A-6-5, AISC 2010b)}$$

where ψ = 1/φ = 1/0.75 = 1.33 for LRFD and ψ = Ω = 2.0 for ASD; n is the number of intermediate brace points within the beam length between the end rigid bracing locations; M_r is the required flexural strength in the beam from LRFD or ASD load combinations; M_r/h_o is the required equivalent flange force from the LRFD or ASD load combinations, taken as the largest value within the member length; L_q is the unbraced length KL obtained by setting the resistance equal to the required moment; C_{tN} is the flange load height factor, taken equal to 1.0 for loading at the centroid of the cross-section or if tipping restraint is provided at the load application point, or taken as 1+1.2/n when the load is applied at and normal to the flange and in a direction toward the cross-section's shear center; and C_d is the double curvature factor, taken equal to 1.0 unless a beam is subjected to double curvature bending and then, taken as $1+(M_S/M_L)^2$ for the brace where an inflection point occurs in the unbraced length on either side of the brace point, and M_S and M_L are the smallest and the largest moments causing compression in either flange within the two unbraced lengths, respectively.

2.3.2 Nodal (Discrete Grounded) Bracing, Strength Requirement

The AISC nodal lateral bracing strength requirement is:

$$P_{br} = 0.01(M_r/h_o)C_{tN}C_d \qquad \text{(2.2, AISC C-A-6-6b, AISC 2010b)}$$

where all the variables have been defined previously.

2.3.3 Relative (Shear Panel) Bracing, Stiffness Requirement

A refined estimate of the relative bracing stiffness from the AISC Commentary (2010b) is:

$$\beta_{\mathrm{br}} = \psi\left[2\frac{(M_r/h_o)}{L_b}\right]C_{tR}C_d \qquad \text{(2.3, C-A-6-3, AISC 2010b)}$$

where C_{tR} is the flange load height factor for relative bracing, which is taken equal to 1.0 for loading at the centroid of the cross-section or if tipping restraint is provided at the load application point, or taken as 1+1.2/*n* when the load is applied at and normal to the flange and in a direction toward the cross-section's shear center; L_b is the unbraced length between the braced points on the member, and all other variables have been defined previously.

2.3.4 Relative (Shear Panel) Bracing, Strength Requirement

The AISC relative bracing strength requirement is:

$$V_{rb} = 0.004(M_r/h_o)C_{tR}C_d \qquad \text{(2.4, C-A-6-6a, AISC 2010b)}$$

where V_{rb} is the required shear strength of the brace and all other variables have been defined previously.

2.3.5 Nodal Torsional Bracing, Stiffness Requirement

The refined torsional bracing stiffness given by the AISC Commentary (2010b) may be written as:

$$\beta_T = \psi\pi^2 h_o^2 \left[\frac{M_r/C_b h_o}{P_{ef,eff}}\right]\left[\frac{M_r/C_b h_o}{L_b}\right]\frac{(n_T+1)}{n_T}C_{tT} \qquad \text{(2.5, A-6-11, AISC 2010b)}$$

where $\psi = 1/\varphi = 1/0.75 = 1.33$ for LRFD and $\psi = \Omega = 3.0$ for ASD (Ω is usually taken equal to $1.5/\varphi$, but it is taken as $1.5^2/0.75$ in this case since the moment term appears twice in the equation); L_b is the spacing between the torsional brace points, assumed constant in the development of the equation; M_r/C_b is the equivalent uniform moment for a given unbraced length within the member span; C_{tT} is the torsional bracing factor accounting for effects of the height of the transverse load, taken equal to 1.2 when the load is applied at and normal to the flange and in a direction toward the cross-section's shear center or otherwise, equal to 1.0; and n_T is the number of intermediate nodal torsional brace points within the member length between the rigid end brace locations, where both twisting and lateral movement of the beam are prevented. Yura et al. (1992) recommend that for $n_T = 1$, the term $(n_T + 1)/n_T$ may be multiplied by 0.75; $P_{ef.eff}$ is the effective flange buckling load, equal to $\pi^2 E I_{eff} / L_b^2$; E is the modulus of elasticity of steel = 29,000 ksi; $I_{eff} = I_{yc}$ for doubly symmetric sections and $(I_{yc} + \frac{t}{c} I_{yt})/2$ for singly symmetric sections; c is the distance between the cross section centroid and the centroid of the compression flange; t is the distance between the cross-section centroid and the centroid of tension flange; I_{yc} is the lateral moment of inertia of the compression flange; and I_{yt} is lateral moment of inertia of the tension flange.

Yura, et al. (1992) and Yura (2001) noted that ignoring cross-section distortion when determining the required bracing stiffness led to poor correlations with experimental and finite element results. Yura demonstrated that treating the different components of bracing (e.g., applied torsional bracing, the member's cross-section web stiffness, or the addition of stiffeners through the web depth) as springs in series provided an acceptable approximation of the observed experimental and simulation results. As such, to take into account the member's loss of effective brace stiffness due to distortion of the cross-section, the AISC Specification uses the following equation:

$$\beta_{Tb} = \frac{\beta_T}{\left(1-\frac{\beta_T}{\beta_{sec}}\right)} \qquad \text{(2.6, A-6-10, AISC 2010b)}$$

where β_T is the overall bracing system required stiffness; β_{sec} is the web distortional stiffness, including the effect of web transverse stiffeners, if any; and β_{Tb} is the required stiffness of the brace itself.

2.3.6 Nodal Torsional Bracing, Strength Requirement

Given the stiffness from Equation 2.5, assuming an initial layover of the web of $\theta_o = 0.002L_b/h_o$, and assuming a corresponding second-order amplification factor of 2.0 for this initial layover (such that the torsional rotation experienced by the brace is $\theta = \theta_o$), the strength requirement may be estimated as:

$$M_{br} = \frac{\beta_T}{\psi}\theta_o = \frac{\beta_T}{\psi}\frac{L_b}{500h_o} = \frac{\beta_T}{\psi}0.002\frac{L_b}{h_o} \qquad \text{(2.7, C-A-6-8, AISC 2010b)}$$

where all the variables have been defined previously.

2.3.7 Bracing Types Used in Metal Building Frames

While nodal bracing is the most simplistic and possibly the most documented bracing type, it is rarely found in practice other than in members with only one or two intermediate brace points. A discrete nodal brace requires that the member being braced is tied back to something that is effectively rigid. As suggested before, this may be the case if a multi-story column is tied by a floor member to a very stiff concrete shear wall. However, for metal building systems, there are often more than two intermediate brace points within the members and there are rarely any opportunities to brace off of something so stiff. Therefore, the two types of bracing implemented and discussed in this research are relative and discrete torsional bracing, as these idealizations are the most consistent with typical metal building design. Both bracing types act by controlling relative movement between two points; however, there are a number of distinct differences between the two types as they are employed in metal building systems.

2.3.7.1 Relative Bracing

Relative bracing, as utilized in metal buildings, is commonly implemented using roof or wall panels as well as truss panels parallel to the plane of the roof or wall with their diagonals composed of cables or rods. This type of bracing is usually applied to one flange and controls relative movement between the bracing points on that same flange through the shear stiffness of these panels. A common model to assess the stiffness provided by cable or rod bracing is shown below in Figure 2.2. Often, engineers consider that the cable or rod in compression is ineffective when determining the stiffness (denoted by the dashed diagonal line in Figure 2.2), since relatively small axial load will cause buckling of the rod. In addition, the chord elements of the truss panels are typically assumed to be rigid relative to the diagonal stiffness. The load application at the

top of the frame (denoted as *P,* in Figure 2.2) divided by the shear deflection of the bracing panel (denoted as Δ in Figure 2.2) gives the relative stiffness provided by the rod or cable system. If one were modeling a system where initial slack in the bracing cables or rods is expected, the relative stiffness of the system would not change; however, the brace would not engage until a certain deflection of the system had been reached. For the design of the main framing system, the Commentary to Appendix 6 (AISC 2010b) implies that an additional imperfection can be added to the initial out-of-plumbness of Δ_o = L/500 in the analysis model to estimate this effect.

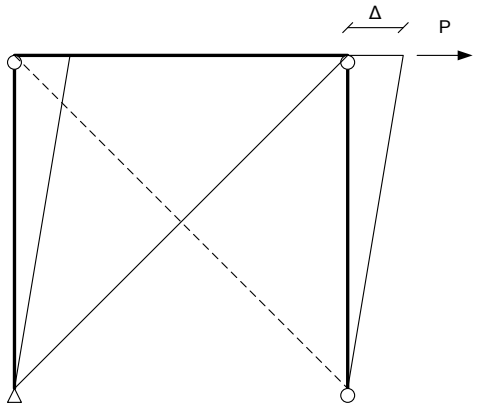

Figure 2.2: Model to determine stiffness provided by relative bracing

2.3.7.2 Torsional Bracing

Torsional bracing, as it pertains to metal buildings, resists relative out-of-plane movement between flanges. Figure 2.3 shows what constitutes typical “torsional bracing” in metal building frames. The continuous purlin framing over the top of the member provides the base from which flange diagonals (indicated here as angle bracing) kick down to provide lateral support to the inside flange. Under this configuration, the top flange movement is tied through the rotational stiffness of the purlin-angle brace system

to the movement of the bottom flange. Commonly, a truss analogy is used to determine the rotational stiffness in the sense that the flange diagonals are considered as truss elements that are tied to the continuous purlin's bending stiffness (indicated by the dashed line in Figure 2.3).

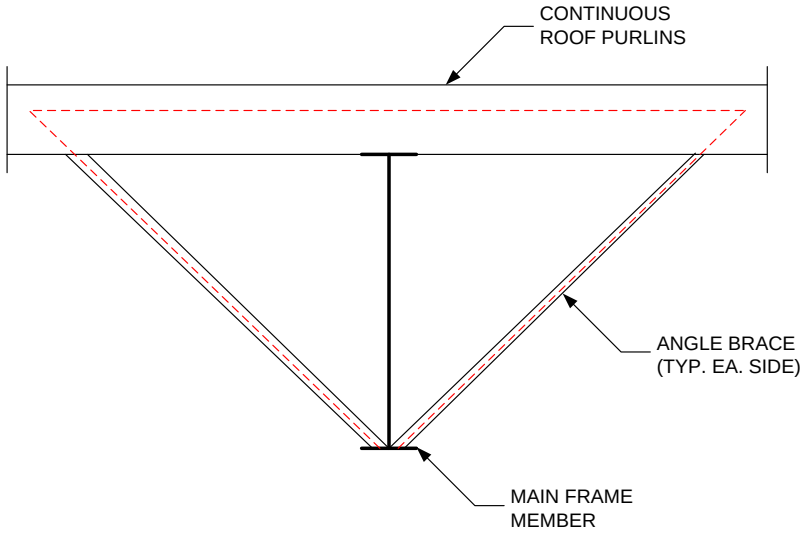

Figure 2.3: Torsional bracing truss analogy provided by flange-diagonal bracing

The estimation of the torsional stiffness for a given bracing system varies widely in current practice. It is beyond the scope of this project to assess what stiffness is provided by a given bracing arrangement, but a few key points are highlighted to demonstrate the variability of stiffness values one may obtain. Figure 2.4 provides a typical continuous purlin model from Mastan2, a matrix analysis based software code developed by McGuire et al. (2000), which will be used in the following discussion.

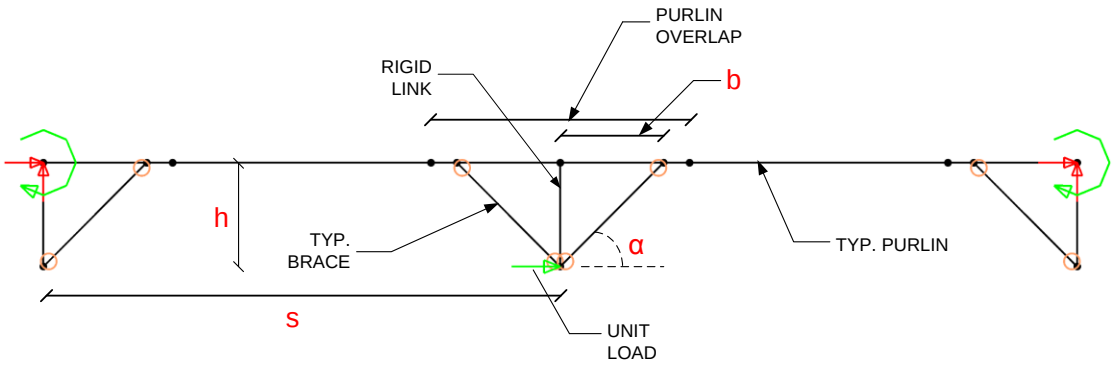

Figure 2.4: Mastan2 model of a continuous purlin over a main frame

The bracing stiffness provided by the continuous purlin over the middle rafter is dependent on a number of factors, including:

- The restraint provided at the ends of the purlin segment (at each end of Figure 2.4),
- The inclination of the bracing diagonals, α,
- The depth of the member, *h*, and
- The purlin overlap.

From a parametric study, the range of stiffness values associated with the torsional restraint at the interior main frame member are from 4 to 10 times *EI*/*s* (where a majority of the results lie near the lower bound), where *E* is Young's Modulus for steel, equal to 29000ksi; *I* is the major axis moment of inertia of the purlin; and *s* is the spacing between the center-line of the adjacent frames. The range of torsional restraint presented above is largely affected by the restraint provided at the adjacent frame in either direction. Whether or not the adjacent frames are buckling at the same time as the frame in question or even the direction of buckling can significantly alter the stiffness.

For example, a rough upper-bound estimate of the torsional restraint provided at the center frame in Figure 2.4 would consider that the adjacent rafters are not buckling and thus, allow for a provided torsional stiffness at the interior rafter equal to 2*(4*EI/s) = 8EI/s, where EI is the flexural stiffness of the purlin and s is the frame spacing.

As indicated previously, it is beyond the scope of this research to assess the actual provided stiffness for a given torsional bracing layout. Therefore, in this research, when an ideal bracing stiffness is determined and a design bracing stiffness is calculated, the onus then lies on the design engineer to ensure that the means by which the bracing is provided is able to achieve the stiffness and strength design requirements.

2.4 Motivational Example: 90 Foot Clear-Span Frame

Sharma (2010) studied the application of the above equations to metal building frame members and compared the requirements to fully-nonlinear finite element simulations using Abaqus (Simulia 2010) for several large-scale metal building frames, an example of which is a ninety foot clear-span frame. Numerous insights can be gained from this example as reported in Kim (2010), Sharma (2010), and White and Kim (2006). The design check calculations for this frame can be found in Kim (2010). An elevation view of one-half of the frame is shown in Figure 2.5.

The ASD gravity load combination with uniform snow load is considered to act on the frame since this produces the largest strength demands for this structure. The ASD loads are increased by a multiplicative factor of 1.6 to correspond to the ultimate design strength load level on the structure. A load-deflection simulation is performed by increasing the applied loads proportionally until the system's maximum strength is achieved. The following observations are noted (Sharma 2010):

1. The AISC equations, configured based on an ad hoc interpretation of their appropriate application to the tapered members, the knee joint of the frame, etc. give significantly conservative estimates of the torsional bracing stiffness demands; however, the AISC brace strength equations tend to underestimate the maximum bracing strength demands in the most critical brace at the limit load of the structure.
2. If the frame is redesigned with wider flanges, the brace strength and stiffness demands are decreased substantially.
3. The torsional brace stiffness provided by representative minimum purlin sizes lies approximately on the “knuckle” of a plot of the system strength versus brace stiffness for this frame. That is, a small decrease in the brace stiffness produces a relatively large decrease in the system strength, while a significant increase in the brace stiffness has a relatively small effect on the frame’s response.

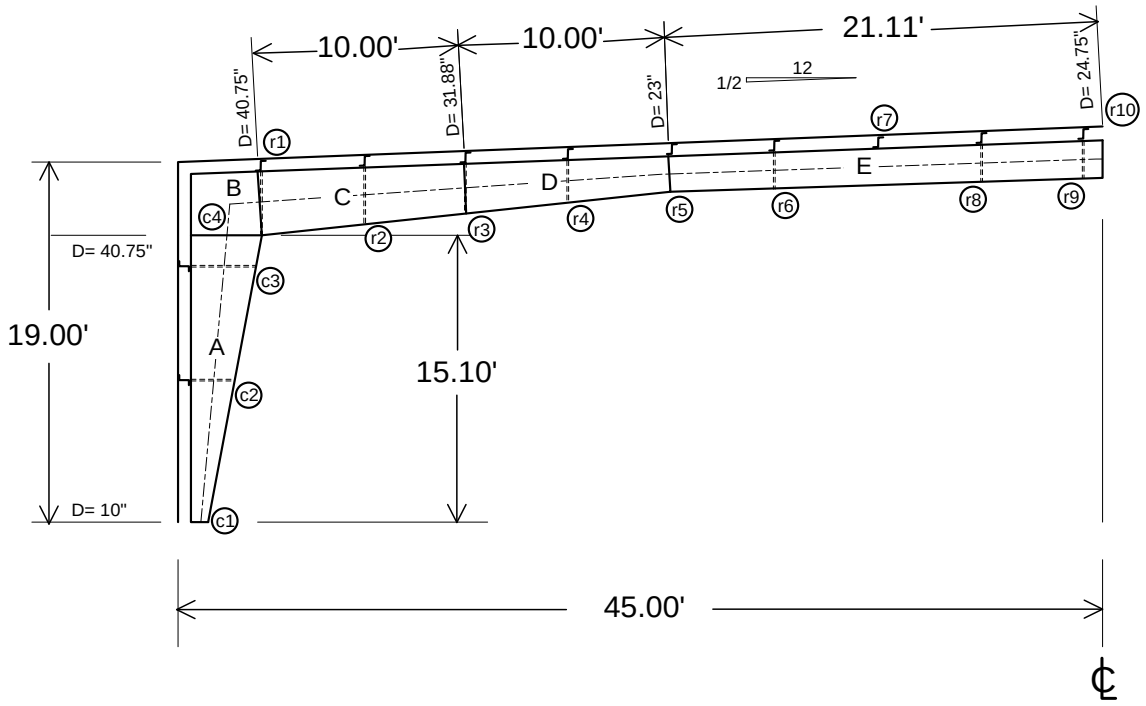

Figure 2.5: Elevation view of a ninety foot clear-span frame (from Kim 2010)

2.5 Toward a Comprehensive Bracing Tool

Due to the complex and interrelated nature of the attributes discussed in Section 1.1, this research focuses first on the development of a comprehensive computational bracing analysis tool for the direct assessment of stability bracing requirements. Any such tool would need to be robust enough to include consideration of all of the items in Section 1.1, yet remain simple enough for use in practical applications. The following is a summary of why such an analysis tool is required for bracing design in metal building structures.

The current AISC Specification equations for stability bracing are derived from solutions of the elastic eigenvalue buckling of members and their bracing systems. However, the nominal flexural strength of columns and rafters of metal building frames is usually

controlled by *inelastic* lateral-torsional buckling, once the frames are in their final constructed configuration. The Appendix 6 equations address this (for LRFD of beam bracing) by a two-staged approximation:

- First, replacing the member elastic critical moment M_{cr} by the design strength ϕM_n, where ϕM_n is generally less than M_{cr} since it is based on the elastic *or inelastic* strength limit, then
- Replacing ϕM_n by the actual required strength M_u, which is generally smaller than ϕM_n for a properly designed beam.

For cases involving partial nodal bracing, the last bulleted item is revised considering that the AISC equations assume that the bracing strength requirement is estimated sufficiently, simply by using L_q in place of L_b (along with the use of M_u), where L_q is taken as the unbraced length that reduces ϕM_n to M_u. This is an acceptable and practical approximation for practical partial bracing cases approaching full bracing, but it tends to be conservative for weak partial bracing, where the amplification of the initial imperfection displacements may become substantial.

A portion of the conservatism observed by Sharma (2010) may be due to the approximations detailed above; however, a larger portion could be due to the fact that a number of metal building system attributes detailed in Section 1.1 are not addressed explicitly by the AISC equations.

Very little prior research has focused on bracing strength and stiffness requirements for inelastic *beams*. Lutz and Fisher (1985) considered the effects of inelasticity in *columns* by starting with the exact solution to the differential equation for buckling of a

continuously supported member from Timoshenko and Gere (1961) and then substituting the tangent modulus, E_t in for E; where E_t is determined based on the level of axial load to be developed in the column. Ultimately, Lutz and Fisher arrived at an equation for the full, continuous bracing stiffness of:

$$k_c = {}^{2.5\,P_{cr}}\Big/_{L_e^2} \tag{2.8}$$

where P_{cr} is the critical buckling load, taken as $P_{cr} = \pi^2 * E_t * I / L_b^2$; I is the cross-section's minor-axis moment of inertia; L_b is the unbraced length and $L_e = \pi\sqrt{(E_t * I / P*)}$, where $P*$ may be taken equal to P_u/ϕ_c (with ϕ_c = 0.9 for LRFD). They go on to suggest similar equations that allow one to determine the required stiffness for columns with a finite number of brace points.

Gil and Yura (1999) and Gil (1996) studied the bracing requirements for inelastic steel columns and inelastic steel columns and beams, respectively. Through experiments and finite element analysis models from Abaqus, they were able to verify new software that they developed for the assessment of the bracing requirements for elastic or inelastic members (a program similar to the one used by Gil (1996) is used by Yura (2001) to determine bracing stiffness demands for *elastic* members and is formally introduced in Chapter 4 of this thesis). Gil showed, using a single internal braced model based on the incremental theory of plasticity, that the brace demands as a function of applied load increased linearly past the yield load until a state of full bracing was reached. Therefore, Gil concluded that Winter's model was able to adequately predict the required stiffness of the bracing independent of the level of yielding in the member. However, they only assessed the capacity versus stiffness requirements for cases where one discrete brace,

either lateral or torsional, was placed at the compact-section member's mid-span. Ultimately, they concluded that an elastic model of the member being braced was sufficient to determine the brace stiffness demands, since there is clear evidence in the cases they analyzed that the state of yielding in the member does not directly affect the brace stiffness demands.

Ales and Yura (1999) performed two experiments to determine if Winter's model could be used for bracing of inelastic members. They point out that failures during prior experiments investigating bracing demands have led to the misconception that bracing for inelastic members requires larger braces. Ales and Yura suggest that Winter's model can be used to accurately predict the required ideal stiffness for members with full bracing (which must be factored to limit large amplification of brace point displacement). Additionally, they cite the equations from Timoshenko & Gere (1961) for bracing requirements for continuous lateral bracing, where the tangent modulus replaces the elastic modulus for members loaded into their inelastic range. Two experiments were conducted where a compact S-shape member was loaded in 4-point bending with three, equally spaced interior lateral braces. The lateral brace stiffness provided was equal to 1.2x the ideal requirement from Winter's model. They observed that the buckled shape of the member was one where buckling occurred between brace points, thus validating Winter's model for use in bracing of inelastic members.

Li and Yura (2002) investigated, through both lab experiments and finite element simulations in Abaqus, the effects of varied brace stiffness on the ability to develop the plastic rotation capacity of beam sections. They performed experiments on six beams; three with moment gradient and three with uniform bending. They found that for bracing stiffness in the range 30 to 100% of the AISC requirement (based on an elastic

eigenvalue buckling solution), the brace stiffness was sufficient to force buckling between the brace points (i.e., the brace stiffness was large enough to be considered full bracing). For the moment gradient case in particular, Li and Yura observed brace forces ranging from 2 to 8% of the equivalent flange load (taken as the moment at the brace divided by the web depth) for stiffnesses in the range of less than 50% of the AISC requirement, but saw a substantial drop in the brace forces (below 2%) for stiffnesses larger than approximately 200% of the AISC requirement (i.e., $2/\phi$ times the ideal bracing requirement). Their main conclusions were that the AISC bracing stiffness requirements were sufficient to characterize the needs for inelastic members and that brace forces could become quite large for inelastic members where an appropriate multiple of the ideal bracing stiffness requirements was not used.

In many situations in practice, bracing for beams and/or frames is much more complicated than that for columns. Generally, columns, beams and frames can have multiple brace points along their length with any combination of the many attributes that are not accounted for in the AISC (2010b) provisions of Appendix 6 (listed in Section 1.1). This gap in the current state-of-the-art is where this research is targeted; specifically, this research addresses the determination of the strength and stiffness requirements for any general stability bracing system.

Tran (2009) showed a useful "exact" calculation of column inelastic buckling strengths using the inelastic column stiffness reduction factor, τ_a. He performed "exact" inelastic eigenvalue buckling analyses for the column shown in Figure 2.6 (exact in the sense that the solution is based on τ_a in a fashion such that the eigenvalue for a given bracing stiffness directly gives the column inelastic, or elastic, design strength ϕP_n) and having the following attributes:

- Prismatic, nodal-laterally braced W14x90 column
- F_y = 50 ksi
- Five equal unbraced lengths, $L_b = L_{by}$ = 15 ft
- Equal brace stiffness, β = 20 kips/in.
- Constant axial load, *P*

A comparison of the inelastic eigenvalue buckling analysis results with the AISC Direct Analysis Method solution for the column maximum strength as well as distributed plasticity simulation results is shown in Figure 2.7, where *DM*, *InE*, and *DP* represent the Direct Analysis Method results, the inelastic eigenvalue buckling solution, and the distributed plasticity solution, respectively.

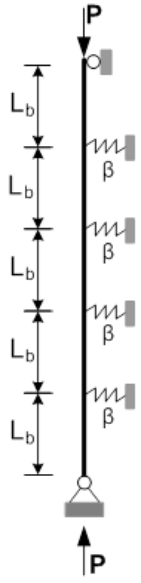

Figure 2.6: Sample column, W14x90 with four interior lateral braces

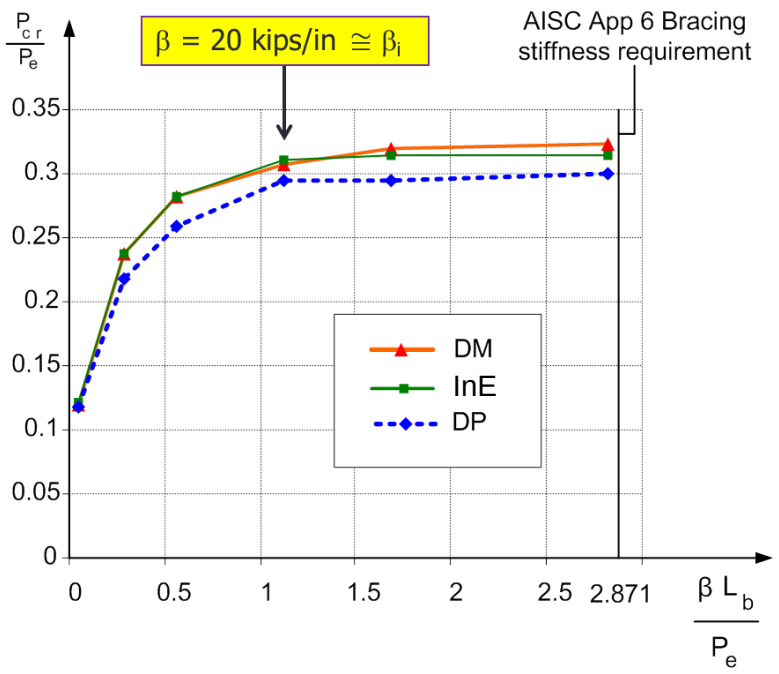

Figure 2.7: Comparison of analysis results

One can observe from Figure 2.7 that all of these solutions produce similar results, and all suggest that a bracing stiffness significantly less than the AISC Appendix 6 requirement is sufficient to develop the full-bracing resistance for this example. Tran (2009) showed that for this problem, the use of nodal bracing stiffness equal to the ideal bracing stiffness, labeled as β_i = 20 kips/inch in Figure 2.7, resulted in brace strength demands only slightly larger than 2% as determined from distributed plasticity simulation studies.

Although the solution by the DM is reasonably accurate, the Direct Analysis Method (often thought of as a reasonable approximation of the results from a rigorous distributed plasticity simulation analysis, or a physical test, and thus providing the best design assessment for stability requirements) may not be a feasible option for assessing

stability bracing demands in problems like this due to the following fact: With the DM, as well as with the simulation analysis, an appropriate magnitude and pattern of the initial geometric imperfections must be imposed on the member to estimate the maximum strength demand on a given brace. This means that one must consider geometric imperfections in a manner similar to the way that load combinations are considered in general strength design. For each specific brace, an imperfection needs to be identified that produces the maximum demand on that brace. Although procedures have been identified by Sharma (2010) and others to determine the "critical" imperfection for a given brace, these procedures are relatively complex and in general, may require a number of trials to truly identify the critical imperfection. Of equal importance is that these procedures would generally need to be executed for each brace within the structural system. This level of effort can be tolerated for research studies; however, it is not practical for ordinary design.

In contrast, the "exact" inelastic eigenvalue buckling analysis gives similar results for the member capacity compared to the DM or DP solutions with much less computational effort. However, one should note that an eigenvalue analysis only provides the designer with an estimate of the required bracing *stiffness* and the overall system strength.

As has been discussed extensively (see Yura (2001), for example), to be effective, a brace must provide sufficient stiffness *and* strength to resist the loads imparted to it by the braced member. Yura shows, using a simple pinned-end column with a single lateral brace at the top, that for a given initial imperfection, two times the ideal bracing stiffness must be provided if the amplification from the initial state is to be equal to the original deflection (that is, two times the ideal stiffness must be provided for the total deflection to be two times the initial imperfection). The bracing stiffness is tied directly to the brace

force, where a larger bracing stiffness leads to less force. Therefore, some multiple of the ideal bracing stiffness should be provided in an effort to keep brace forces manageable. (It should be noted that in this example, the flexural stiffness of the member is never engaged in resisting the brace point movement.) Additionally, Yura (1995) shows that the brace forces are most reasonable when bracing stiffness requirements are set such that the member buckles between brace points with K = 1.0. Yura notes that five times the ideal bracing stiffness is needed to reach 95% of the K = 0.7 limit as compared to that needed to reach the elastic buckling load assuming K = 1.0. Therefore, given a specified bracing stiffness, the force demands on the brace required to develop a member capacity based on K = 0.7 would increase dramatically once the force level increases beyond the capacity corresponding to the K = 1.0 case; up to this level, the brace forces in the column are actually reduced due to the additional rotational restraint at one end.

Despite the potential for large brace forces when continuity across a brace point is considered, Sharma (2010) and Tran (2009) have shown through numerous finite element simulations that the brace force is usually in the range of 2 to 3% of the effective flange force for nodal bracing cases approaching full bracing. In fact, 2% was often enough to allow the frame to reach 95% of its rigidly-braced capacity. Therefore, one can combine the brace stiffness requirement from an inelastic eigenvalue analysis with say, a 2 to 4% brace strength rule (for frames not specifically required to sustain large cyclical loadings) for a complete determination of the bracing requirements.

Creation of a new computational bracing analysis tool is needed in this research because no current structural analysis software provides the specific necessary elements or combination of analysis methods to produce the type of solutions illustrated

in Figure 2.7 for general member and/or frame geometries and general bracing arrangements. The targeted bracing analysis tool must be able to address such aspects as warping and bending restraint, roof and wall panel stiffness, combined relative and nodal torsional bracing, combined effects of axial and flexural loading, unequal brace spacing, web taper, and steps in the cross-section geometry. The computational tool needs to be able to solve for the in-plane elastic and/or inelastic state of a member or frame at a given design load level, or at an envelope of all the maximum internal forces based on a range of design loadings, and then determine the ideal bracing stiffness demands (i.e., the required ideal bracing stiffness) to sufficiently stabilize the structure in this elastic/inelastic state.

For speed and efficiency, the bracing tool also must be able to obtain the above solutions with a minimal computational effort (i.e., a minimum number of degrees of freedom). As depicted in Figure 2.8, the webs of the members in the targeted computational tool are modeled using plane stress elements for the initial planar load-deflection analysis and shell elements for the subsequent 3D inelastic eigenvalue buckling analysis. However, the flanges are modeled using beam elements.

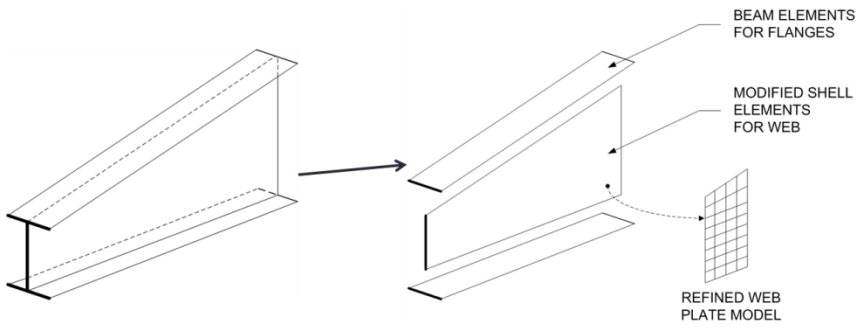

Figure 2.8: Discretization scheme for the member

One additional significant problem that occurs for the above type of model is that, for I-section members having non-compact or slender webs, the eigenvalue buckling solutions are commonly dominated by web local buckling modes. However, it is well known that these types of I-section member webs generally exhibit a stable post-buckling response. That is, the web local buckling behavior in essence has a secondary effect on the overall member flexural and lateral-torsional buckling response, and hence on the member bracing demands. Therefore, for an eigenvalue buckling analysis to provide an efficient solution, something must be done to parse the inconsequential web buckling modes from the general solution. In this research, this is accomplished by using multiple elements through the web depth to determine the web stiffness but using only *one* element through the depth to determine the web's geometric stiffness properties. Thus, with four-node shell elements, the membrane and bending stiffness of the web is captured accurately, but the member is unable to buckle through the web depth due to the lack of internal web nodes in the geometric stiffness (essentially restricting buckling to the web/flange juncture). Prior simulations in Abaqus (Simulia 2012) have shown that modifying the web in a similar manner, that is, by coarsely modeling the webs as a single element through the depth of the web, yields elastic eigenvalue buckling results that are similar to those from load-deflection solutions.

The application of the above computational tool can provide a direction for engineers to better assess their needs for bracing requirements and therefore, provide safe building designs.

3. RESEARCH METHODOLOGY

3.1 Qualification of Simulations

Due to the complexity of the stability bracing systems in metal building frames combined with the wide range of factors discussed in Section 1.1 that can influence the bracing response, a large number of member and frame tests are needed to develop meaningful (and generalizable) bracing data. Simulation provides one such economical approach to generate this data. Furthermore, stability bracing force demands generally are sensitive to the pattern of the geometric imperfections. Therefore, evaluating maximum required bracing forces for design generally necessitates the determination of the critical geometric imperfection. Forcing initial geometric imperfections on physical members that cause the largest demands on the bracing system in an experimental test can prove difficult. However, critical geometric imperfections can be generated with relative ease for simulation studies. Validation of simulation methods against experimental test data on members from which detailed physical geometric imperfections and residual stress measurements have also been taken provides an important validation of the simulation models. These simulation models can then be applied to provide detailed assessments of the true maximum design bracing strength and stiffness demands.

3.2 Simulations Using Abaqus

3.2.1 FEA Modeling

Abaqus 6.12 (Simulia 2012) is used to create the benchmark simulations used to answer the fundamental questions of this research. A four-node linear-order displacement-based quadrilateral shell element with selective reduced integration, known as the “S4R” element in Abaqus, is used to model the member web and flanges in this work. Eight

elements are used through the web depth and across the flange width. This finite element discretization is sufficient to attain overall convergence of the general elastic and inelastic frame load-displacement results, which of course drive the bracing force demands. In addition, the use of eight elements through the web depth facilitates the application of the residual stress patterns discussed subsequently. For uniform depth members, the shell finite element discretization along the member length is set such that the element aspect ratio in the web is approximately equal to 1.0. For tapered members, a uniform shell element discretization is employed along the length such that the maximum aspect ratio in the web is approximately 2.0.

In this research, all non-rigid bracing in the out-of-plane direction is modeled in Abaqus using shear springs. This is accomplished using the “Spring2” element which directly ties two specified points on the member together through a user-defined shear stiffness. For example, to model a diaphragm brace, one would place a Spring2 element between the two adjacent purlin locations in the model and then provide stiffness between those points based on the panel’s shear stiffness (in units of force per length). Similarly, torsional bracing is modeled in this research by dividing the torsional bracing stiffness (in force-length per radian) by the depth of the section at the brace point squared. This approach creates an equivalent shear stiffness that then can be modeled using the readily available Spring2 element.

Finally, all the analyses are performed in Abaqus using a specific form of the Riks arc length solution algorithm (Simulia 2012). This is a load-displacement analysis algorithm capable of continuing the solution through limit points by introducing an additional constraint equation that varies the applied load during the full Newton-Raphson nonlinear iterative steps. By loading a given structure through its maximum load limit,

the fact that the limit load has been obtained can be ensured, and the characteristics of the failure mode and post-peak response can be better understood. The Riks method assumes that all the loading is proportional, i.e., that all the load magnitudes vary in proportion to a single scalar load parameter. Abaqus implements its Riks solution scheme including an automatic increment size control containing various heuristics to apply a fraction of the applied load and to seek convergence (and equilibrium) most efficiently. The reader is referred to Abaqus's documentation for further details on the Riks solution algorithm.

3.2.2 Modeling of Residual Stresses and Initial Geometric Imperfections

The Abaqus-generated simulations conducted in this research are intended to mimic experimental tests. Thus, one must include the variances of the member from its ideal plumb and straight geometry as well as the residual stresses that are induced during the fabrication process in the simulations. The following sub-sections discuss these aspects in detail.

3.2.2.1 Residual Stresses

Figure 3.1 shows the residual stress pattern employed in the Abaqus simulations conducted in this research. This is selected as a nominal residual stress distribution that provides a close representation of the column inelastic flexural and beam inelastic lateral-torsional buckling strength curves in the AISC (2010b) Specification. The flange residual stress distribution is the same as that recommended by ECCS (1983) for rolled I-section beam members with $h/b_f > 1.2$, and the web residual compression is representative of that observed in welded I-section members with non-compact and slender webs (Avent and Wells, 1979; Nethercot, 1974). White (2008) discusses a large set of experimental data upon which the AISC lateral-torsional and flange local buckling

strength curves are based and shows that the influence of the type of I-section (rolled or welded) on the strengths is of minor significance based on this data. This justifies the use of the single nominal residual stress pattern for the flanges shown in Figure 3.1. For I-section members with non-compact or slender webs, an interesting result is that the web typically cannot sustain substantial stresses in uniform axial compression over most of its depth without exhibiting local buckling. Therefore, the maximum uniform web compressive residual stress is taken as $0.1F_y$ or the elastic buckling stress of the web under uniform axial compression, F_{crw}, assuming simply-supported conditions at the juncture of the web with the flanges. The web residual tension is taken over a depth of $h/8$ at its top and bottom such that the total residual stress in the web is self-equilibrating. Of course, the flange residual stresses shown in Figure 3.1 are also self-equilibrating. For web-tapered members, the above web residual stresses are calculated at the middle of each tapered length, where a new “tapered length” is defined with each change in the taper angle. This is a simplification of the potential web residual stresses in a physical tapered member with a non-compact or slender web, which may in fact vary along the member length as a function of the web buckling resistance to the longitudinal residual compression.

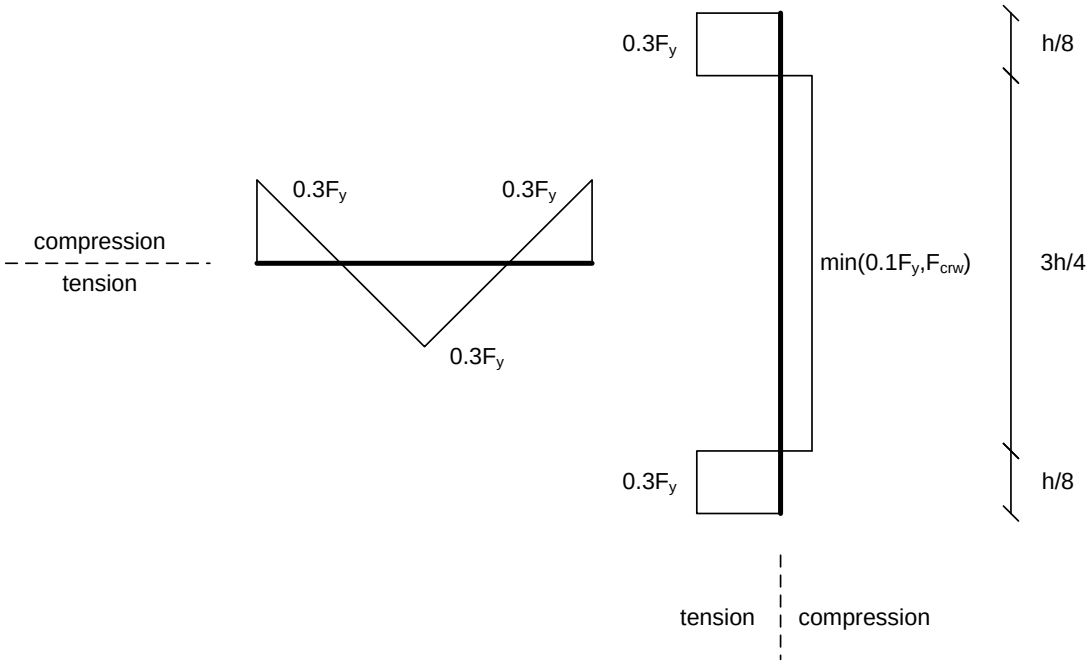

Figure 3.1: Residual stress pattern for flanges (left) and web (right)

It should be noted that the shell elements in Abaqus are generally single-point integrated and thus, a single residual stress is specified within each element. Representative contours for the flange and web residual stresses of a sample prismatic beam (with h_o = 34.66 in., t_w = 0.19 and F_y = 50 ksi) are shown below in Figures 3.2 and 3.3. Here, the flange stresses vary per Figure 3.1 from -10.12 ksi in the elements adjacent to the flange tips to 10.12 ksi in the elements adjacent to the juncture with the web. The web stresses per Figure 3.1 are -2.91 ksi in uniform axial compression and 8.74 ksi in the elements adjacent to the juncture with the flanges.

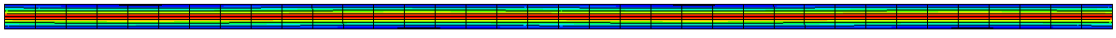

Figure 3.2: Initial residual stress gradient in the flanges (plan view, from Abaqus)

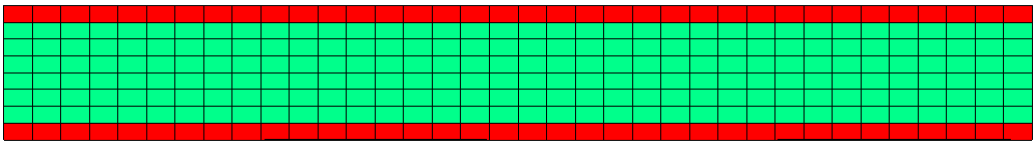

Figure 3.3: Initial residual stress gradient in the web (elevation view, from Abaqus)

3.2.2.2 Nominal Geometric Imperfections

There are four types of geometric imperfections that can have a significant impact on I-section member capacities and the corresponding strength demands placed on their bracing systems:

1. Out-of-alignment of the brace points,
2. Out-of-straightness, or sweep, of the flanges *between* the brace points,
3. Out-of-flatness of the web, and
4. Tilt of the flanges.

In practice, these imperfections are generally limited by fabrication and erection tolerances that are stipulated in various specifications and codes, each applicable to a specific area of construction. The MBMA (2006) Metal Building Systems Manual specifies limits on fabrication tolerances for items (2) through (4) as shown in Figures 3.4 through 3.7. It should be noted that in these figures, the length *L* is the overall fabricated length of a given structural member. Regarding erection tolerances, the MBMA Manual refers the engineer to the AISC (2010a) Code of Standard Practice. Section 7.12 of the Code of Standard Practice states that: “The accumulation of mill tolerances and fabrication tolerances shall not cause the erection tolerances to be exceeded.” Furthermore, the AISC erection tolerances are defined relative to member working points and working lines, where generally, these terms are defined by AISC (2010a) as:

- For horizontal members, the working points are taken as the centerline of the top flange or top surface at each end.
- For members other than horizontal member, the working points are taken as the center of the member at each end.
- The working line is a straight line that connects the member's working points.

The Code of Standard Practice's base erection tolerances for out-of-straightness and out-of-alignment that are permissible for columns are shown in Figure 3.8. Furthermore, the base out-of-alignment of other members containing splices is as shown in Figure 3.9. The out-of-alignment of cantilever segments with respect to the ideal reference line is also 1/500. For the assessment of bracing system demands, the above limits are commonly simplified to a base limit on the out-of-straightness between brace points of L_b/1000, where L_b is the distance between brace points, and a base limit on the out-of-alignment (or in the case of vertical columns, out-of-plumbness) of 1/500 between the brace points.

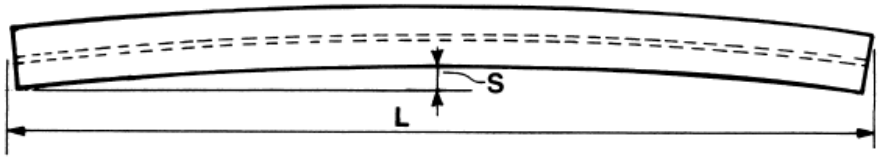

Figure 3.4: Member out-of-straightness, *S*, limited to 1/4 in. x L (ft) / 10 in units of ft. (MBMA 2006)

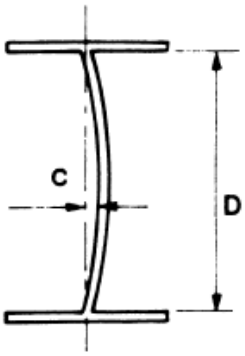

Figure 3.5: Web out-of-flatness, *C*, limited to *D*/72 (MBMA 2006)

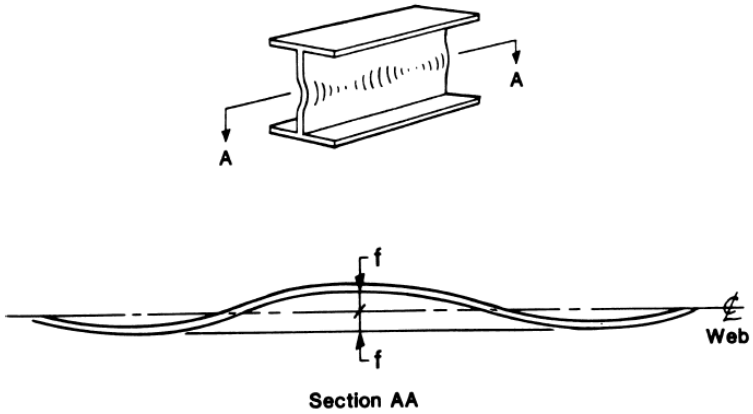

Figure 3.6: Web out-of-flatness, *f*, limited to *D*/72 (MBMA 2006)

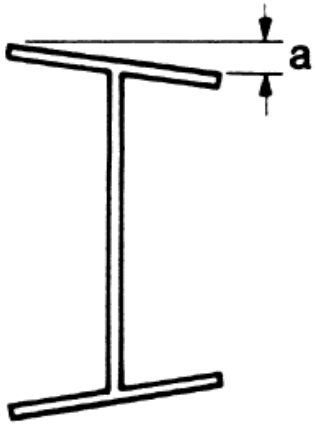

Figure 3.7: Flange tilt, *a*, limited to 3° or 1/4 in. maximum (MBMA 2006)

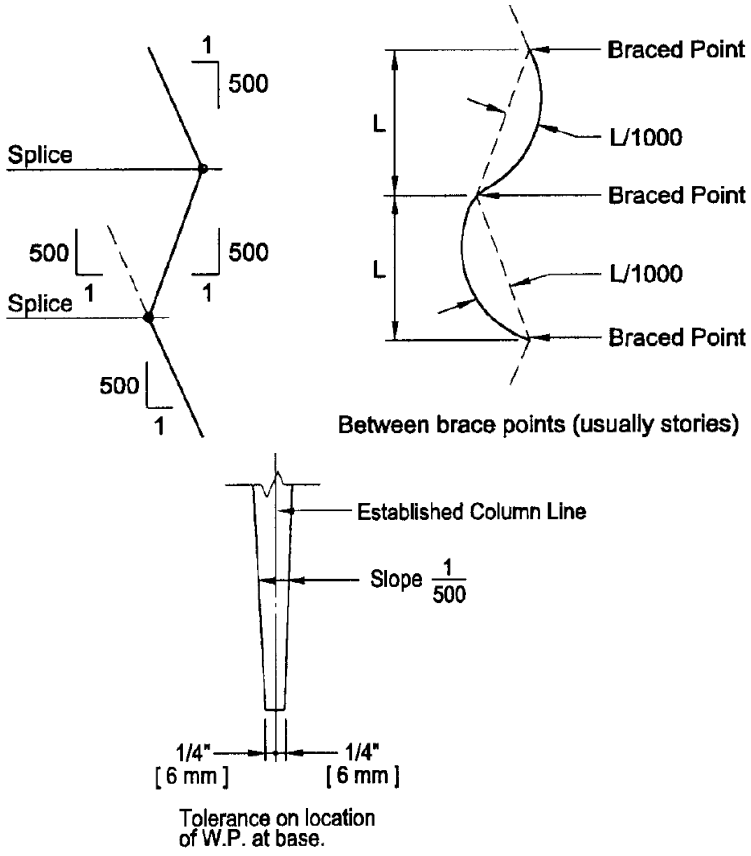

Figure 3.8: COSP (2010a) column out-of-straightness and out-of-alignment tolerances

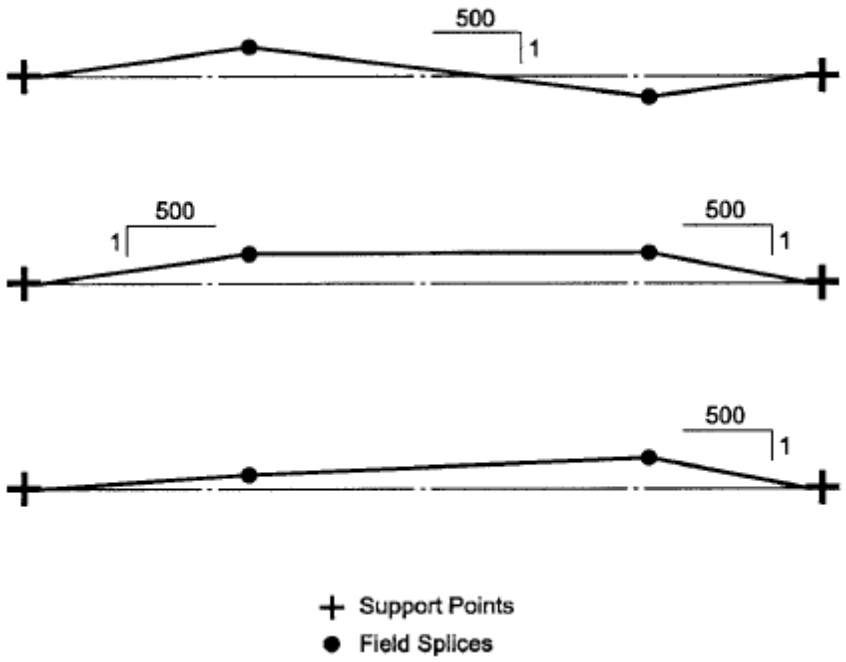

Figure 3.9: COSP (2010a) out-of-alignment tolerance for spliced members

Definition of "Critical" Imperfection

Appropriate patterns and combinations of the above geometric imperfections must be considered for the rigorous computational assessment of design brace force demands. Generally, these patterns and combinations are different for each brace or for each component of the bracing system. There is no firmly established single method for determining these patterns and combinations, but the commonly accepted criterion is that the "critical" imperfection that should be used for the assessment of a given brace or bracing component involves the patterns and combinations that maximize the brace force. Furthermore, it has been observed generally that the out-of-alignment between the brace locations is the dominant imperfection that drives the brace force demands, but that the member out-of-straightness between the brace points and the member

cross-section “local” imperfections also can have a measurable influence on these forces.

One should note that if the goal of the structural analysis is to assess the overall structural capacity, then the “critical” patterns of the flange out-of-alignment and flange sweep are taken typically as those that give the maximum affinity of the imperfection pattern with the fundamental buckling mode of the structure, neglecting any local buckling modes.

In the context of rigorously determining the design bracing forces, the critical imperfections are not necessarily the same as those that minimize the structure capacity. For stability bracing, the corresponding out-of-plane displacements under loading are zero. Furthermore, the brace point displacements in the fundamental buckling mode may in some cases be equal to zero.

Wang and Helwig (2005) have studied the influence of various out-of-alignment geometric imperfections in columns and beams for structural members that are fully braced. They observed that the critical out-of-alignment is one in which the orientation on each side of a selected brace is 1/500 but in opposite directions. Also, for beams, they find that the critical imperfection for the bracing system in fully-braced members is one in which the tension flange is assumed to remain straight and the compression flange is given an out-of-alignment of 1/500 on each side of the brace point or brace points under consideration. In other words, the out-of-alignment of the braces is alternated at 1/500 in opposite directions within each unbraced length as one moves along the member length. By extension, the out-of-straightness that contributes additively to this out-of-alignment effect is either the one that bows the compression

flange outward in the same direction on each side of the selected brace, or in some cases, the maximum brace force demands are produced by setting the out-of-straightness to zero and simply “kinking” the members at each of the brace points. It should be noted that generally, if the out-of-alignment and out-of-straightness of each of a member’s flanges are placed in opposite directions out of the plane of a frame, the overall twist induced at a given member cross-section can be quite large. Therefore, this research adopts a practice similar to that described by Sharma (2010) in that the out-of-alignment and out-of-straightness are generally applied only to the compression flange (for beam problems) or only to the flange having the larger compression, for beam-column problems. Coupling the above discussion of the imperfection shapes with the tolerable imperfection magnitudes for out-of-straightness between brace points and out-of-plumbness of the braced points as specified in AISC’s Code of Standard Practice (2010a), one has a complete description of the imperfections required for a general load-deflection analysis model.

For more general cases involving partial bracing, the determination of the geometric imperfection that produces the maximum brace force demands is significantly more complex. In these cases, an influence line approach detailed by Sharma (2010) is adopted in this research. In this procedure, the design loads are first applied to the structure in a second-order elastic analysis. Then, unit loads are applied at each brace point and at the middle of each unbraced length, and the corresponding force induced at the bracing component under consideration is plotted versus the location of the unit loads. This gives the influence line for a given bracing component. Next, equivalent lateral loads corresponding to the out-of-alignment and out-of-straightness are considered with the influence line to determine the critical imperfection.

Inclusion of Local Buckling Modes

Local buckling modes in the webs of I-shaped sections typically have a minor effect on the bracing force demands for loading less than or equal to the maximum strength of the structure. However, if web local buckling modes are not included in the load-displacement simulation, the solution performance in software such as Abaqus (Simulia 2012) can often be hampered due to numerical problems believed to be associated with continuing the nonlinear solutions in the vicinity of branch points within the solution space. In this research, the local buckling modes from an elastic eigenvalue buckling analysis of the structure are selected such that the corresponding local buckling displacements are additive with the other geometric imperfections in the vicinity of the brace under consideration. Figure 3.10 shows a number of modes included in the simulation of a representative prismatic, slender-web beam. Generally, the selected local buckling modes are scaled such that the fabrication tolerances shown previously in Figures 3.4-3.9 are not exceeded.

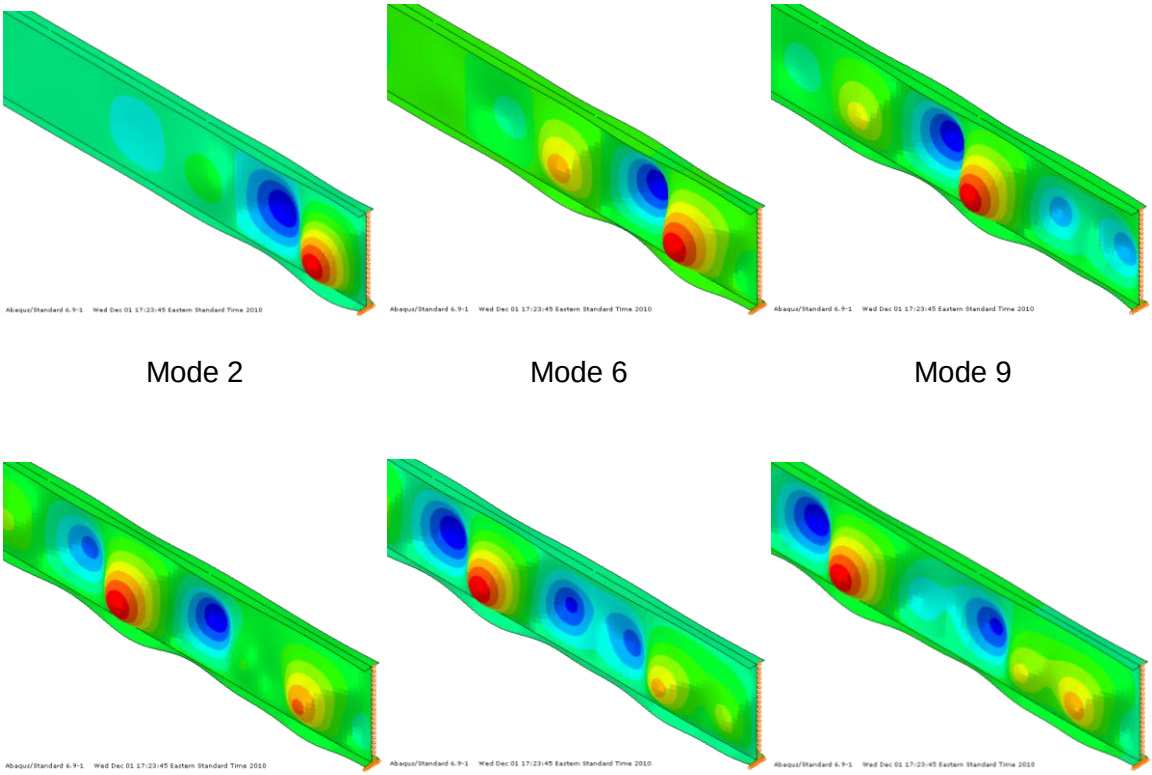

Figure 3.10: Representative local buckling modes for a prismatic, slender-web member (from Abaqus)

Canting of the Frame:

Lastly, an imperfection is included that considers an overall lateral out-of-plumbness within the plane of the frame equal to the specified tolerances of AISC's Code of Standard Practice (2010a). Section 7.13.1.1 of the Code of Standard Practice (2010a) dictates that for an individual column, "the distance of the working line from a vertical plumb line shall not be more than 1/500 between working points." Therefore, for all frames modeled in this research using Abaqus, the structure is leaned 1/500 relative to its base. Figure 3.11 shows a typical displaced shape for this geometric imperfection.

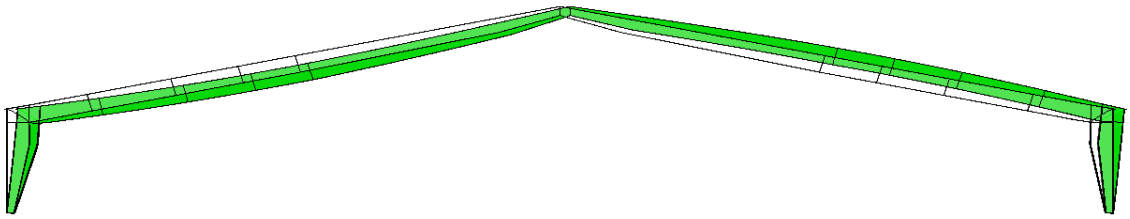

Figure 3.11: Displaced shape induced by canting of the frame L_{column}/500 from its base (from Abaqus)

3.3 Inelastic Buckling Solutions using SINBAD

A new software package referred to as the System for INelastic Bracing Analysis and Design (SINBAD) is developed in this research to address the need for a comprehensive bracing tool as described in Section 2.5. This section describes SINBAD's implementation and how this software may be used to provide a more efficient and accurate assessment of stiffness demands for flange bracing than is possible using the AISC Specification's Appendix 6 equations.

3.3.1 Software Overview

SINBAD is in essence a stand-alone, special purpose finite element program that performs 3D eigenvalue buckling analyses based on the elastic or inelastic state of a planar structure caused by the application of in-plane loads. The solutions from SINBAD may be used to either determine member or framing system out-of-plane buckling capacities or to determine ideal stiffnesses of the corresponding out-of-plane bracing system. The in-plane inelastic analysis capabilities of SINBAD involve a complete spread of plasticity (or plastic zone) analysis of the structure including any appropriate in-plane geometric imperfections as well as specified nominal residual stresses.

SINBAD is written in Matlab (MathWorks 2011) and includes both an analysis engine and a graphical user interface (GUI).

SINBAD has two distinct modules: members and frames. The members module is used exclusively to assess the bracing requirements for individual members. For example, one could analyze a given physical beam or one may import a subset of a frame (e.g., one of the columns) for analysis as an isolated member. That is, the member module is only useful to model *one* member. In the frame module, SINBAD provides the ability to assess the bracing requirements for an entire framing system. The frame can have any generalized geometry but must have no more than two exterior columns and two rafters (one on each side of a ridge location). The input to SINBAD may be accomplished either by a set of Microsoft Excel worksheet forms or via a general application programmer interface. Appendix A describes the member or frame geometry and loading input from the Excel worksheets.

To analyze a member or frame using the stand-alone program, the user starts SINBAD, which then opens the GUI and allows the user to select either the member or frame modules for analysis. SINBAD then imports the geometry and load data from the Microsoft Excel file. Next, SINBAD carries out the elastic or inelastic in-plane analysis and then the out-of-plane buckling analysis. After the analysis is completed, results including in-plane planar displacements, in-plane stress states, and buckled mode shapes can be viewed directly from the GUI. Appendix B provides several screen shots and further descriptions of the basic program layout as well as the typical results one may view following an analysis.

3.3.2 FEA Modeling

The following sub-sections describe some of the individual components that comprise SINBAD. The inelastic buckling analysis solutions in SINBAD are conducted generally in two steps:

1. The 2D (planar) elastic/inelastic state of the structure is calculated given a prescribed loading condition, and
2. A 3D eigenvalue buckling analysis is performed based on the stress state determined in Step 1.

By limiting the stress determination to a planar solution, significant time savings are realized relative to the requirements for a general 3D simulation such as that conducted in Abaqus. After the state of stress is determined, the program must "upgrade" the model to its 3D counterpart in order to assess the out-of-plane stability of the system in question. Details about how this solution is achieved efficiently are provided in the following sections.

3.3.2.1 Beam Elements

All flanges and stiffeners are modeled in SINBAD using 2-node cubic Hermitian beam elements with one additional internal axial degree of freedom providing for a linear variation in the interpolated strains along the member length for both axial and bending deformations (White 1985). For the planar solution, there are a total of 7 degrees of freedom: two translations and one out-of-plane rotation at each end plus an additional axial degree of freedom at the middle of the element. The interior axial degree of freedom is removed via static condensation (McGuire, et al. 2000) to leave a total of 6 global degrees of freedom. For the 3D model, a total of 13 degrees of freedom are used

for the beam element: three translations and three rotations at the member ends plus one additional axial degree of freedom at the middle of the element. Again, static condensation is performed to render the element with 12 global degrees of freedom for the global solution. Figures 3.12 and 3.13 show the layout of the beam element's degrees of freedom for the planar case and the 3D case, respectively.

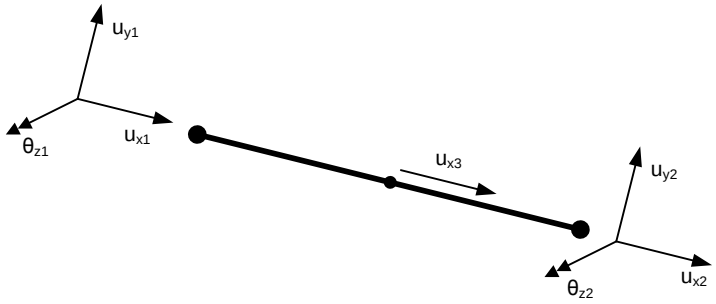

Figure 3.12: Degrees of freedom for uncondensed planar beam element

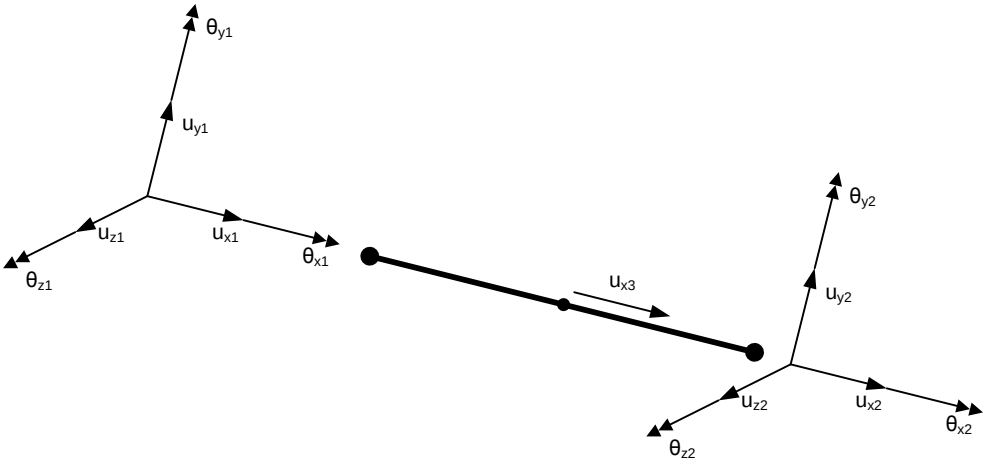

Figure 3.13: Degrees of freedom for uncondensed 3D beam element

To track the spread of plasticity through the beam element, White (1985) proposed a fiber model that subdivides each element into a predefined grid. Figure 3.14 shows a typical grid with 12 fibers through half the width of the flange ($b_f/2$) and 2 fibers through the thickness of the flange (t_f). It is only necessary to model the grid over one-half of the flange width since the planar solution is symmetric about the plane of the structure. In addition, tracking the spread of yielding throughout the element is performed on an "as needed" basis. That is, the fiber grid is only created when the global element has detected yielding. This reduces the memory requirements and substantially increases the computation speed. The process for the fiber grid creation and its use is as follows:

1. During the beam element's material state determination, the element looks for yielding at four points: the top and bottom of the flange at the flange tip and at the mid-width of the flange. These points are selected due to the nature of the residual stress pattern (discussed in Section 3.2.2.1) and the fact that these extreme points are the first to yield under load.
2. If the element detects that yielding is imminent, it creates a fiber grid to be able to track yielding as it spreads through the flange thickness and/or width.
3. Next, the material state determination is called for each fiber to assess whether or not yielding is occurring under the current load application. If the fiber is not yielded, the modulus remains elastic. If the fiber is yielding, the modulus changes based on the material model curve (discussed in Section 3.3.2.4).
4. After each fiber has passed through its state determination, the fibers are integrated over the flange area to determine the current stress-resultants and forces as well as the effective elastic cross-section properties (*A*, area; *Q*, first

moment of the area; and *I*, moment of inertia) considering the inelastic tangent stiffness at all of the fiber locations.

5. Finally, the element uses the above cross-sectional properties to determine its tangent stiffness matrix used in the global incremental-iterative solution.

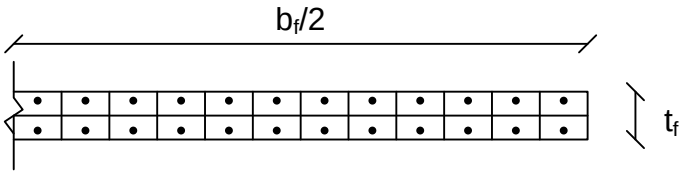

Figure 3.14: Beam fiber model for tracking the spread of plasticity

The above steps are performed for the cross-section at each end of the beam element. From the above cross-section calculations, only the axial force and moment are determined at each end of the element. The element end shears are determined based on element equilibrium per Equation 3.1 (White 1985).

$$F_{y1} = -F_{y2} = \frac{(M_1+M_2)}{L} \tag{3.1}$$

where F_{y1} is the shear in the vertical direction at end 1, F_{y2} is the shear in the vertical direction at end 2, M_1 is the moment at end 1, M_2 is the moment at end 2 (where all signs are in keeping with the element sign conventions from Figure 3.12), and *L* is the element length.

Also, to enforce element force equilibrium in the axial direction of the element, the end cross-section axial forces are taken as:

$$F_{x2} = -F_{x1} = \frac{(P_1+P_2)}{2} \tag{3.2}$$

where F_{x1} is the axial force at end 1, F_{x2} is the axial force at end 2, and P_1 and P_2 are the axial forces at end 1 and end 2, respectively, from the element cross-section stress resultants (White 1985).

The beam element's geometric stiffness matrix (also commonly known as the stress-stiffness matrix) is modified from the standard cubic Hermitian formulation from McGuire, Gallagher, and Ziemian (2000). Only the external geometric stiffness matrix is used in this research. This is consistent with the common subdivision of the flanges into a large number of beam elements along the member length to track the spread of plasticity and avoids potential mesh discretization problems in which, in some cases, the beam elements may "buckle" between the nodes if the complete beam element geometric stiffness of the cubic Hermitian element is employed. The external geometric stiffness matrix is shown in its entirety in Appendix C.

3.3.2.2 Shell Elements

The basis for the shell element used in SINBAD comes from a formulation named the SBMITC element. It is the combination of two distinct types of elements: a Q6CDRL element for plane stress and a PBMITC element for plate bending and is discussed in Will and Zarco (2011). In this research, a modification is made to this element to remove the drilling degree of freedom. Therefore, the element used is a combination of the QM6 and PBMITC elements.

Plane Stress (QM6)

The QM6 element is created from a general four-node isoparametric quadrilateral element (Q4) with the following two modifications:

1. To prevent shear locking, bending deformation modes are included by adding incompatible modes to the element's displacement field. This reduces the element's tendency to be overly stiff when subjected to bending-type deformations and creates the commonly known Q6 element (Cook, et al. 2002).
2. The determinant of the Jacobian is evaluated only at the middle of the element. This modification allows the Q6 element to represent constant stress (or shear) states for shapes other than rectangles and thus, the element is able to pass all patch tests and is renamed the QM6 element (Cook, et al. 2002).

Plate Bending (PBMITC)

The plate bending aspect of the shell element used in SINBAD is based on a four-node mixed interpolation of tensorial components element originally derived by Bathe and Dvorkin (1985). The inclusion of the mixed interpolation removes shear locking of the element while avoiding spurious zero-energy modes. Essentially, the bending formulation is the same as the regular Mindlin element, but the shear components invoke a reduction operator that allows the element to avoid shear locking (Will and Zarco 2011). After determination of the bending and shear stiffness, the terms are combined to formulate the total stiffness for the PBMITC element.

For use in SINBAD, this combined plate element and plane stress element is renamed the QM6MITC element. The element retains five degrees of freedom per node (two stretching and three bending) for the full-3D solution as shown in Figure 3.15. However, to make the element compatible with the displacement field associated with the beam element discussed previously, an additional "null" drilling degree of freedom is included at nodes common to both the web shell and flange beam elements.

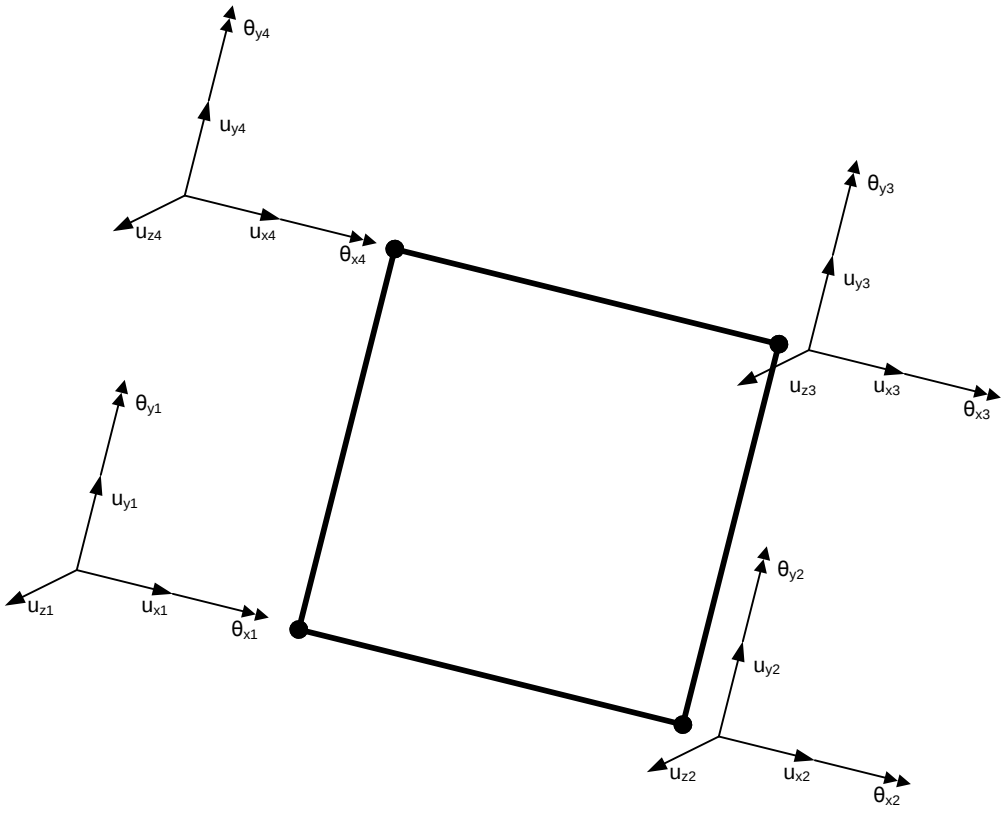

Figure 3.15: Degrees of freedom for the 3D shell element

For the planar case, only the two membrane displacements and the “null” drilling degrees of freedom, at the attachment to the beam elements, are retained for solution efficiency. The degrees of freedom necessary to represent the case of a membrane are shown in Figure 3.16.

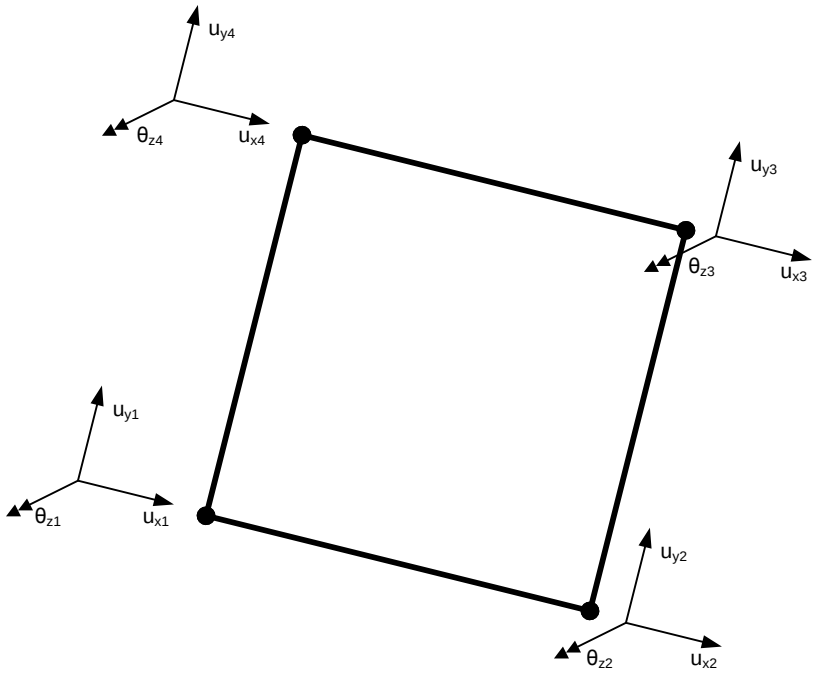

Figure 3.16: Degrees of freedom for the planar membrane element

An important aspect of this research focuses on a formulation of the geometric stiffness for the web shell finite elements such that web local buckling modes do not appear in the SINBAD 3D eigenvalue buckling solutions. As discussed previously, due to the nature of the web being stable in its post-buckled state plus the fact that the brace demands are usually driven by lateral bending of the flanges, removing the local web modes provides a substantial improvement in the efficiency of the solution algorithm while focusing on solving for the member or frame out-of-plane buckling.

From Cook, et. al. (2002), the general formulation for the formation of the geometric stiffness matrix for a planar element can be described by Equation 3.3.

$$\left[k_g\right] = \int [G]^T \begin{bmatrix} \sigma_x & \tau_{xy} \\ \tau_{xy} & \sigma_y \end{bmatrix} [G]\, dV \tag{3.3}$$

where G is derived from the element shape functions, σ_x is the stress in direction x, σ_y is the stress in direction y, τ_{xy} is the element shear stress, and V is the element volume. For integration using Gauss quadrature, one can transform this volume integral to a series of summations over the element's area and thickness.

The element used in SINBAD takes this formulation one step further. As discussed previously, if one used the conventional shell geometric stiffness directly, web local buckling modes would dominate the results. Figure 3.17 shows an elevation view of an I-section member web that is one element wide and four elements tall. Referencing Figure 3.17, the following solution scheme is proposed to eliminate the handling of local web buckling modes:

1. Determine the stress at each Gauss point within each "sub-element" from the in-plane analysis (in Figure 3.17, 16 gauss points, each with three stress measures).
2. Use Gauss quadrature to integrate the stress at each Gauss point over the volume of the "super-element" (where the super-element is composed of all the sub-elements through the depth of the web) to obtain a single geometric stiffness for each web super-element.

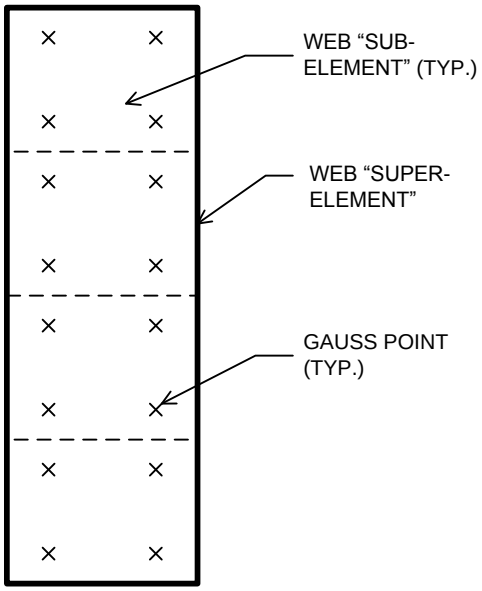

Figure 3.17: Web sub-elements for calculation of the geometric stiffness matrix

Before discussing the last element type used in SINBAD, it is informative to step back and look at an essential function in the Matlab (Mathwoks 2011) library for sparse matrices. Since a large portion of a typical global stiffness matrix is made up of zeros, efficiency can be gained by a method that opts for only allocating memory associated with non-zero values. Matlab has a built-in function known as “Sparse” that does exactly this. Sparse works by keeping only the non-zero values and their position indices within the matrix, which cuts down extensively on the memory required to store a full matrix. The reader is referred to the Matlab documentation for further information on this powerful function.

3.3.2.3 Spring Elements

There are three distinct types of bracing (as termed by AISC 2010b) employed in SINBAD and shown in Figures 3.18 through 3.20:

1. Nodal (discrete grounded)bracing,
2. Relative (shear panel) bracing, and
3. Nodal torsional bracing.

When implementing nodal bracing, SINBAD simply adds the grounded spring's stiffness directly into the global stiffness matrix for the out-of-plane translational degree of freedom associated with the brace location. For relative bracing, SINBAD treats the bracing as a "shear" spring incorporating a basic 2x2 element stiffness matrix that resists the relative out-of-plane movement of two connected points. Lastly, nodal torsional bracing is modeled in a manner similar to the relative bracing with the added step that the program must first divide the user input torsional bracing stiffness (in units of force x length/radian) by the web-depth squared to determine an equivalent shear stiffness. It is also important to note here that the spring elements are only required for the out-of-plane buckling solution. Since the 2D, nonlinear solution only deals with deflections in-plane, the degree of freedom associated with the out-of-plane movement of the springs is not activated and thus not required in the planar global stiffness matrix.

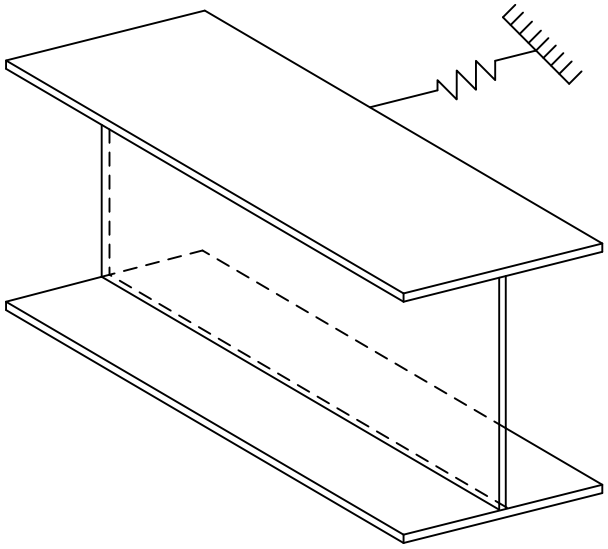

Figure 3.18: Schematic showing the application of nodal lateral bracing

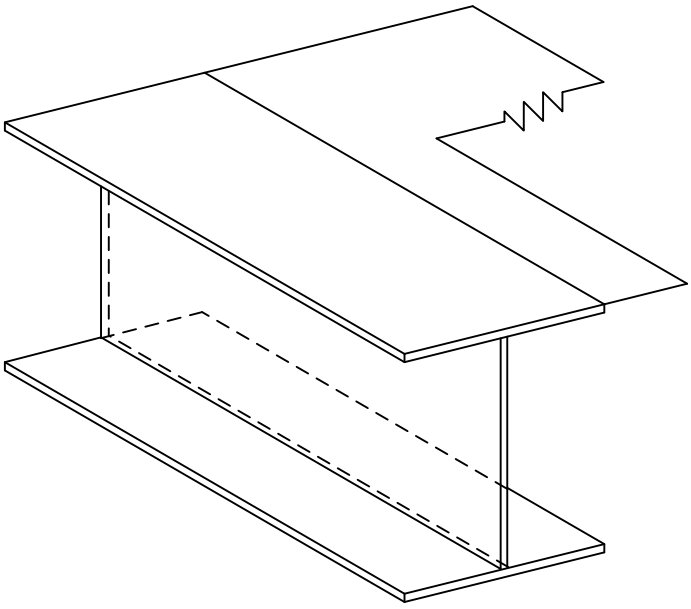

Figure 3.19: Schematic showing the application of relative bracing

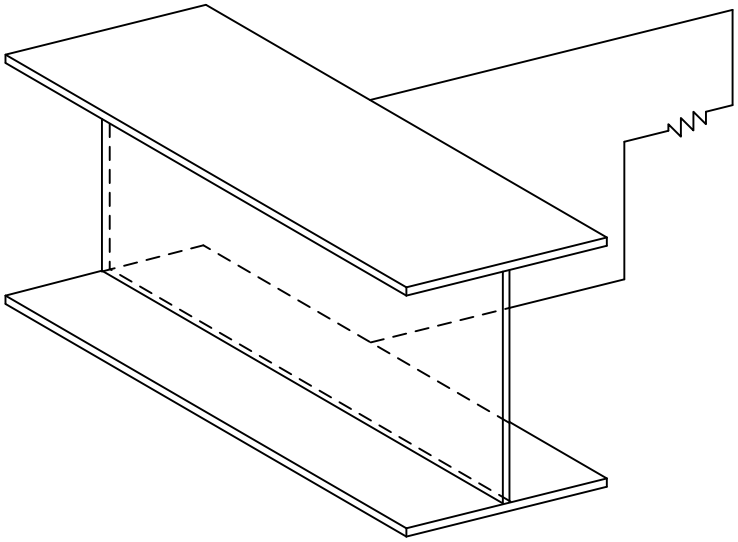

Figure 3.20: Schematic showing the application of nodal torsional bracing

3.3.2.4 Material Description

Figure 3.21 shows the uniaxial stress-strain relationship implemented in SINBAD. The material model considers that the steel remains elastic at modulus E up to F_y (and ε_y), experiences minimal hardening at modulus E_t from ε_y up to $\varepsilon_{st} = 10\varepsilon_y$, and then experiences strain hardening at E_{st} above ε_{st}.

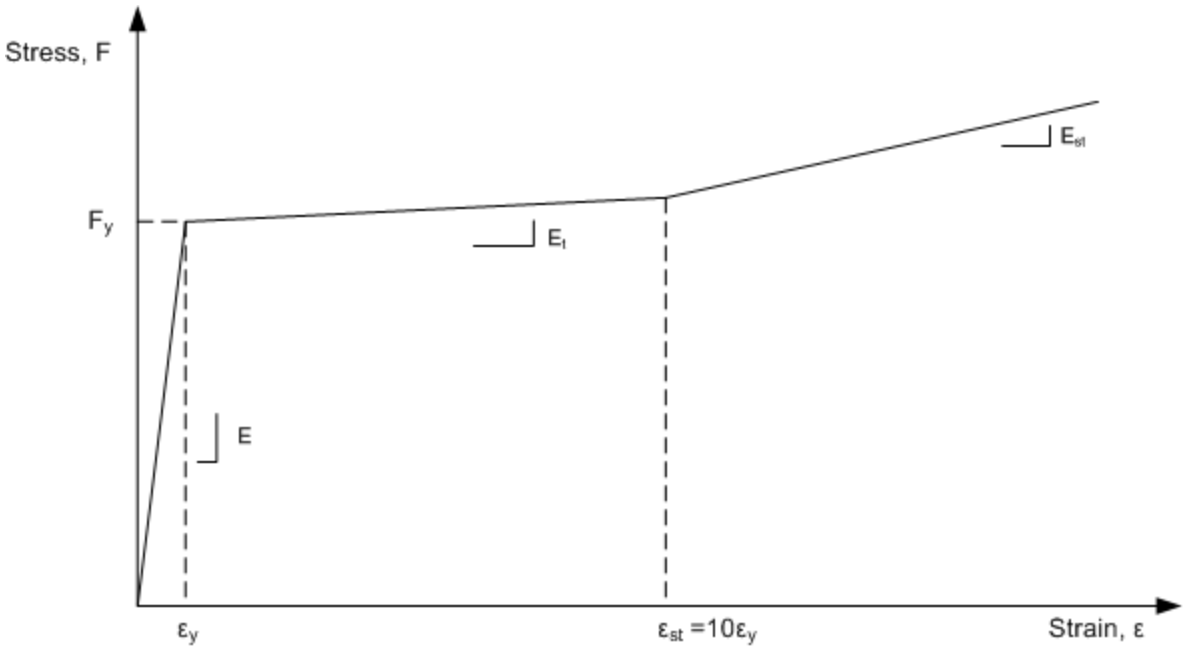

Figure 3.21: Material stress-strain curve

For purposes of numerical stability, that tangent modulus is taken *E*/100 within the yield plateau of the material stress strain curve. It should be noted that this stiffness value is approximately equal to the bounding stiffness exhibited by typical structural steels upon cyclic loading of the material (see White 1988, for example). SINBAD uses E = 29,000 ksi for the steel elastic modulus and E_{st} = 900 ksi for the steel strain-hardening modulus.

3.3.2.5 Residual Stresses

The residual stress pattern used in SINBAD is similar to the pattern discussed in Section 3.2.2.1. The only slight variation comes from the way in which the residual stresses are applied. As discussed previously, Abaqus tracks only one stress value per element. Therefore, specifying the web residual stresses, a single residual stress is applied within each shell element. What ensues is effectively a step function to approximate the linear stress pattern dictated per Figure 3.1. SINBAD is similar except for the fact that it tracks

stresses at two Gauss points within its plane stress / shell elements. The residual stress at the location of a given Gauss point is taken from the pattern shown in Figure 3.1.

3.3.2.6 Boundary Conditions

SINBAD is capable of handling any general boundary conditions in the member module. The boundary conditions for the member module may include simple or fixed supports as well as torsional restraints including restraint of warping (or flange lateral bending).

For the frame module, it is assumed that the base of the columns is “pinned” to the foundation. This assumption comes from typical design considerations where the base plate is often thin enough that the restraint provided in the plane of the frame is small. However, it is assumed that warping is restrained at the column base.

3.3.3 In-Plane Solution Algorithm

As initially discussed in the program overview and description of the element formulations, SINBAD’s solution algorithm includes a nonlinear, in-plane solution and an out-of-plane, eigenvalue buckling solution. The separation of analysis techniques in this manner allows for an economical and efficient solution by not requiring the program to maintain all six degrees of freedom for the symmetric, in-plane solution. When required for the buckling analysis, the program “converts” to a full 3D solution. This section gives the basic groundwork for the nonlinear, in-plane solution employed by SINBAD.

3.3.3.1 Planar Degrees of Freedom

As mentioned previously, the in-plane solution only operates on three degrees of freedom: translations in the horizontal and vertical directions as well as the rotation about the out-of-plane axis. This allows for a significant reduction in processing time and

memory requirements, especially if one considers the exponential gains realized by the use of sparse matrices.

3.3.3.2 Solution Procedure

SINBAD uses the full Newton-Raphson (N-R) iteration algorithm for the planar analysis. For brevity and since these details are assumed to be common knowledge, a description of the N-R algorithm is not presented here. Instead, the reader is referred to, e.g., Crisfield (1991), Cook, et. al. (2002), or any other fundamental text on finite element analysis. Additionally, SINBAD utilizes an adaptive arc length constraint algorithm based on a minimum residual displacement constraint that aims to reduce the number of iterations necessary for satisfactory convergence (Clarke and Hancock 1990).

The adaptive arc length method begins by setting the initial increment size equal to the user-specified value. Based on the number of iterations required for convergence in the previous load increment, SINBAD dynamically updates the current increment size. Furthermore, during each iteration, SINBAD invokes a minimum residual displacement constraint to aid in analysis convergence. When SINBAD has reached the desired load level, the in-plane solution procedure terminates.

At this point, the complete state of stress is known for each element from its planar solution and SINBAD is ready to conduct the 3D inelastic eigenvalue buckling analysis. Before this is discussed in Section 3.3.4, a few intermediate details will be presented on the process for the nonlinear material state determination for the beam and shell elements.

3.3.3.3 State Determination for Beam Elements

Within each N-R iteration, SINBAD performs the necessary beam state determination in order to determine the current state of stress within the element. The material formulation for the beam element is a one-dimensional plasticity model. For each increment in load, the state of the element and the increment in strain from the previous equilibrium step are used to update the state of the element.

3.3.3.4 State Determination for Shell Elements

Similar to the beam element state determination, SINBAD performs the shell element state determination for each N-R iteration and within each load step. A backward-Euler integration of the rate constitutive equations is employed that is similar to the elastic-predictor return-mapping algorithm proposed by Simo and Taylor (1986) to account for plane-stress conditions. Crisfield (1991) more succinctly details the specific implementation of this elastic predictor return-mapping algorithm.

3.3.4 Inelastic Eigenvalue Buckling Solution Algorithm

At the completion of the state determination, the planar state of stress is known for all of the elements. Now, the program performs a four-step process in order to upgrade and perform the necessary calculations to determine the system eigenvalues and eigenvectors. The steps are:

1. Add the three additional out-of-plane degrees of freedom into the planar load and displacement vectors and reorder the total degrees of freedom.
2. Update the total stiffness matrix for the following elements:
    a. Beam elements – a 3D form of the element discussed in White (1985) is implemented.

b. Shell elements – the 3D element stiffness is constructed from the final stresses of the planar solution; however, it is assumed that the shear stiffness of the shell elements remains elastic.
c. Spring elements – these elements, where not required for the planar solution, are now incorporated into the global stiffness matrix.

3. Calculate the local element and global system geometric stiffness matrices based on the principles discussed previously.
4. Perform the inelastic eigenvalue buckling solution using the built-in Matlab function considering sparse matrices.

Out of this analysis comes the ten smallest (closest to zero) eigenvalues and the associated normalized eigenvectors. Ten eigenvalues were selected as the number to report as this is generally enough higher-order buckling modes to be useful without inundating the user with results. Based on the way in which the Matlab *eigs* function calculates the eigenvalues given the global stiffness and stress stiffness matrices, a negative sign on the eigenvalue indicates that the structure buckles with the load applied in the direction specified. Conversely, a positive sign indicates the buckling load ratio if the load is reversed. In SINBAD, only the negative eigenvalues are retained.

The eigenvalues are presented to the engineer through the GUI. The engineer may select the eigenvalue of interest and apply any arbitrary scaling factor in order for the program to present the buckled mode shape (i.e., the associated eigenvector) graphically for review.

This chapter has summarized the development of SINBAD, including all element formulations and a summary of the solution algorithm.

Now that the background of the solution scheme for SINBAD has been discussed, it is important to note a key issue before any analysis results are presented.

As discussed in this chapter, SINBAD performs an eigenvalue buckling solution based on the elastic or inelastic state of the in-plane structure. Specifically, given the distribution of stresses and yielding in the member as well as the magnitude and location of out-of-plane bracing, SINBAD creates the 3D stiffness and stress stiffness matrices and performs an eigenvalue buckling analysis in order to seek the lowest fraction of applied load that will cause out-of-plane buckling of the system. This procedure provides an assessment of the ideal bracing stiffness only, i.e., initial imperfections are not considered in the buckling solution and thus, an undetermined out-of-plane movement occurs only at the onset of buckling.

In contrast to SINBAD, the Riks procedure utilized in Abaqus (Simulia 2012) is of the load-deflection class of analysis solutions. That is, out-of-plane movement occurs from the onset of the loading when initial imperfections are provided at the beginning of the analysis. This type of solution most closely mimics reality, where initial imperfections are unavoidable. Therefore, given properly seeded imperfection patterns, any requirement for bracing stiffness arrived at through a load-deflection solution is the actual, *not ideal*, brace stiffness requirement.

Due to the inherent differences between these analyses, one might expect that the solutions from the eigenvalue buckling analysis performed by SINBAD and the load-deflection simulation performed in Abaqus will differ in general. A large portion of the remainder of this thesis investigates the relationship between the ideal bracing stiffness results from SINBAD and the structure's load capacity and the bracing force demands

from Abaqus. One goal is to investigate how the ideal bracing stiffness determined by SINBAD from an eigenvalue buckling analysis can be used as an index to estimate the bracing strength and stiffness demands that one might expect in the physical structure.

Specifically,

- Chapter 4 utilizes the eigenvalue buckling solution from SINBAD to determine the ideal bracing stiffness for members and compares these results to simulations from Abaqus. Again, it is to be expected that the solution results will differ and thus, the key to this research will be to explain how the eigenvalue buckling results for the ideal bracing stiffness can be used to estimate the physical response.
- Chapter 5 correlates SINBAD to Abaqus using a series of frame examples.
- Chapter 6 discusses some conditions which must be met in order to use SINBAD properly and suggests one method by which the results from SINBAD can be utilized as part of a comprehensive procedure for designing stability bracing systems.

4. APPLICATION OF SINBAD TO MEMBERS

4.1 Introduction

As introduced previously, SINBAD is divided into two distinct modules: one for the design of individual members (member module) and one explicitly for the design of a *group* of members (frame module). This chapter looks specifically at assessing the performance of SINBAD for members only. It is then suggested, through a comparison to the solutions from Abaqus (Simulia 2012), the proper scaling of the ideal stiffness results from SINBAD to accurately predict the bracing demands in physical structures. Subsequently, Chapter 5 will detail the results for the frame module.

In this chapter, it is instructive to first discuss what is meant by an "ideal" stiffness. Next, *elastic* eigenvalue buckling results from SINBAD are validated against analysis solutions that have been employed in determining the AISC Specification provisions of Appendix 6 (2010b). Third, it is shown how SINBAD can be used to aide in the design of web-tapered members by providing the elastic buckling load ratio, γ_e. Fourth, comparisons are made between the SINBAD elastic and inelastic eigenvalue buckling results and the AISC lateral-torsional buckling resistance equations for beams. Finally, results from Abaqus, as well as the AISC Appendix 6 bracing strength requirement equations (where appropriate), are correlated with the elastic and inelastic eigenvalue buckling results for a wide range of inelastic members.

4.2 Ideal Bracing Stiffness

Generally, the ideal bracing stiffness is defined as the stiffness required to brace a perfectly straight member such that a particular out-of-plane eigenvalue buckling resistance is achieved. Figure 4.1 shows an initially straight member and two buckling

modes that are dependent on the bracing stiffness. In this case, if the ideal stiffness is zero (effectively, there is no brace), the member would buckle at $P_e = \pi^2*E*I / (2*L_b)^2$. If the brace ideal bracing stiffness is equal to the stiffness required to force buckling between brace points (known as ideal "full" bracing), then the buckling load would increase to $P_e = \pi^2*E*I / (L_b)^2$, as shown in Figure 4.1(c). Lastly, if the brace stiffness is somewhere between these two extremes (which is commonly termed "partial" bracing), then the buckling load would also lie somewhere in-between. Part Figure 4.1(b) shows the buckled shape for a hypothetical ideal partial bracing stiffness corresponding to a perfectly straight column.

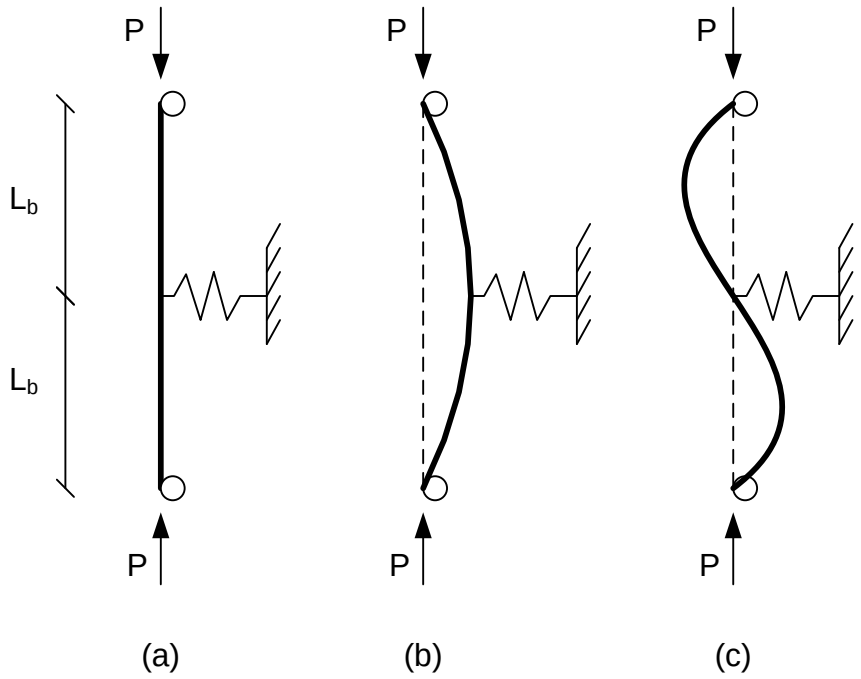

Figure 4.1: (a) Initially perfect column, (b) buckling with partial bracing, (c) buckling with full bracing

In the context described here and employed throughout this research, "full bracing" (either ideal or actual) is defined as the bracing stiffness level required to force the

braced member to buckle between brace points. One example of such full bracing for the ideal bracing case in the context of a column is shown in Figure 4.1(c). Furthermore, for physical members where initial imperfections are unavoidable, full bracing is still defined as the level of applied stiffness where the member buckles between brace points. The consideration of the effects on brace force demands caused by the amplification of the initial imperfections is discussed below.

Due to the fact that physical columns and beams have inherent geometric imperfections, the members displace laterally and the initial imperfections are thus amplified immediately upon application of load (Timoshenko and Gere 1961). This amplification of the initial imperfections drives the brace force demands, since brace point displacement times the bracing stiffness (assumed to remain elastic) generates the brace forces. Therefore, one finds that while theoretically it is possible to provide the ideal stiffness for a given member assuming the member is perfectly straight, practically, one must often provide some multiple of that value to keep the brace forces (and brace strength design requirements) manageable. It is common in the design by AISC LRFD to use a multiple of $2/\phi$ where the resistance factor $\phi = 0.75$ on the ideal bracing stiffness as a general rule to limit the amplification of brace point movement and the resulting brace forces (Yura 2001). In the corresponding design of bridge structures by AASHTO LRFD, Yura (2001) recommends simply a multiple of two. In other cases, for example Helwig and Yura (2008a & b), investigators have determined that a multiple of the ideal bracing stiffness larger than $2/\phi$ is necessary to adequately control the brace point movements. Other investigators, e.g., Tran (2009) and Sharma (2010), have shown that in numerous column, beam, and frame bracing problems, the second-order load-deflection response

of the structure is such that the second-order amplification of the brace forces is limited even at brace stiffnesses approaching the ideal bracing values.

Since the out-of-plane eigenvalue buckling analysis solutions in SINBAD do not account for initial imperfections (in general, out-of-plane imperfections are not considered in an eigenvalue buckling solution), any resulting bracing requirement obtained from SINBAD is simply an ideal bracing requirement. Therefore, it must be scaled appropriately to ensure that brace forces (and their corresponding force demands) do not become excessive within the load-deflection stability bracing behavior of the physical structure. All plots and figures presented henceforth from SINBAD show the ideal stiffness results.

4.3 Comparison to Benchmark Elastic Buckling Cases

4.3.1 Introduction

The foundation of the AISC Appendix 6 (2010b) equations lies in the elastic buckling response of members obtained from an eigenvalue analysis. Yura (1993, 1995, 1996) is credited with largely deriving these fundamental equations and presenting them in a form conducive to design. This section compares results from SINBAD for a number of elastic buckling cases for beams versus elastic eigenvalue buckling results from Yura (2001), which also have been independently confirmed by Tran (2009). In his paper, Yura (2001) describes BASP, a program used to produce his plots; therefore, all future references in this thesis will be to BASP. All of the cases presented in this section are different bracing applications and loadings applied to a rolled W16x26 wide-flange section. The total member length is 20 feet with one brace applied at mid-span (providing an unbraced length, L_b = 10 feet). The boundary conditions are such that at each end of the member, rigid body motion and twist of the cross-section are prevented yet warping and flange lateral bending remain uninhibited. Additionally, Tran (2009)

studied the beam cases presented in Yura (2001) and provides fairly good agreement from his independent analyses and the results from BASP.

In order to show agreement with the results from BASP, the SINBAD analyses for the ideal bracing *stiffness* versus applied load are performed using nominal E, theoretically infinite F_y, and zero residual stresses.

Also included in this section is an assessment of the brace *forces* versus the bracing stiffness. These plots are created by applying initial geometric imperfections to models in Abaqus and then recording the maximum brace force (or moment) when the member is at its capacity. It should be noted that for the assessment of brace forces, analyses in SINBAD and Abaqus are both performed with the inclusion of residual stresses and the application of the nominal E and F_y values.

Five examples from Yura (2001) and Tran (2009) are presented below:

1. A beam subjected to uniform bending with one interior lateral brace at mid-span. This model is known as LB1 in Tran (2009) and corresponds to Figure 6 from Yura (2001).
2. A beam subjected to a moment gradient by the application of a point load at mid-span either at the top flange or at the centroid of the cross section and having one interior lateral brace at the application of the load. Additionally, these two models have a 1/4" thick x 4” wide stiffener at the location of the applied load. This model is known as LB3 in Tran (2009) and corresponds to Figure 8 from Yura (2001).
3. A beam subjected to full reverse curvature bending by the application of equal and opposite moments at each end. Two bracing scenarios are considered: one

with a lateral brace at mid-span connected to the top flange only and one with a lateral brace at mid-span applied to both the top flange and the bottom flange. This model is known as LB4 in Tran (2009) and corresponds to Figure 10 from Yura (2001).

4. A beam subjected to uniform bending with one interior torsional brace at mid-span applied to the top flange. This model also has a 1/4" thick x 4” wide stiffener at the mid-span of the beam. This model is known as TB1 in Tran (2009) and corresponds to Figure 14 from Yura (2001).
5. A beam subjected to a moment gradient by the application of a point load at mid-span either at the top flange or at the centroid of the cross-section and having one interior torsional brace applied to the top flange. This model has a 1/4" thick x 4” wide stiffener applied at the application of the load. This model is known as TB2 in Tran (2009) and corresponds to Figure 17 from Yura (2001).

Individual figures detailing the specific analysis specimens are shown in each member’s subsection.

4.3.2 Uniform Bending with Lateral Bracing

The case, as shown in Figure 4.2, is a twenty foot W16x26 segment with one discrete nodal lateral brace applied to the top flange at mid-span.

Figure 4.2: W16x26 under uniform bending with one interior lateral brace at mid-span

Figure 4.3 shows the comparison between BASP and SINBAD for the case of uniform moment applied to the section (causing compression on the top flange). From the first two data sets shown on the plot, one will notice that the two solutions for elastic buckling are in good agreement.

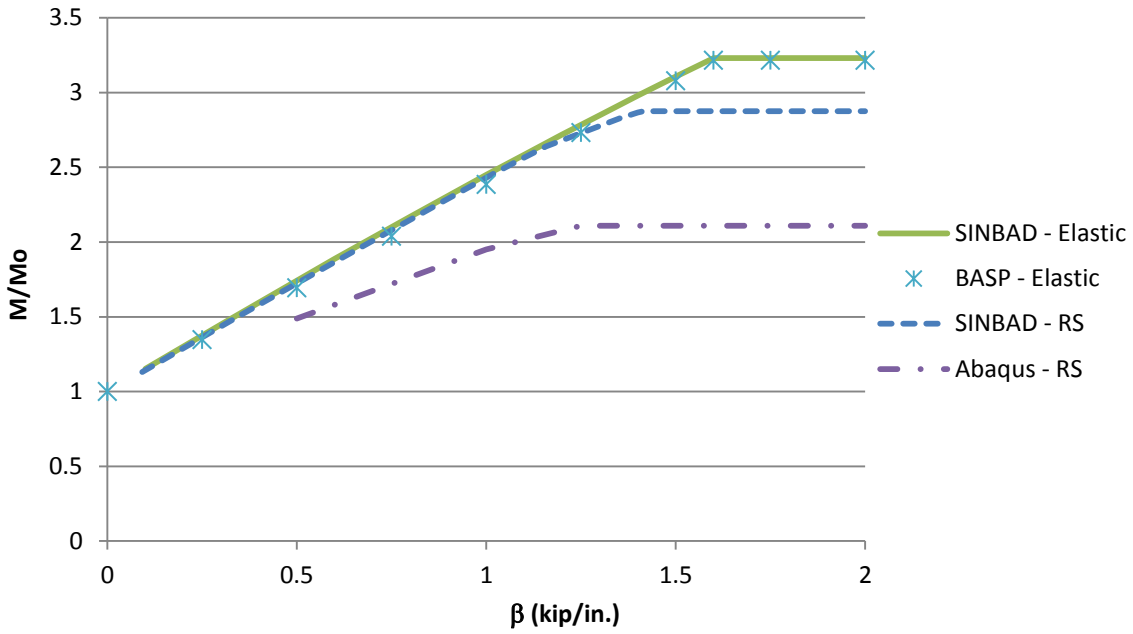

Figure 4.3: Comparison of SINBAD, BASP, and Abaqus for uniform moment (1 lateral brace)

Also shown in Figure 4.3 is a comparison of results from Abaqus versus those from SINBAD for the case of inelastic buckling using nominal E and F_y and including residual stresses. The difference in the capacities reached by SINBAD versus Abaqus will be described later. The intent of including these inelastic results now is purely to provide the reader with an opportunity to directly observe the effect that yielding of the cross-section plays on the capacity of the section and the bracing stiffness requirements. For this specific example, one will notice that the capacity of the section based on an elastic

analysis is reduced approximately 35% when the section is allowed to yield. Similarly, the stiffness demands at which full bracing is reached reduce from around 1.6 kip/in. for the elastic buckling case to 1.25 kip/in. for the inelastic buckling case (a drop of just over 20%).

Figure 4.4 is a plot of the percentage of equivalent flange force (deteremined by dividing the applied moment by the distance between flange centroids) versus bracing stiffness as determined from Abaqus. The maximum brace force is almost 3% of the equivalent flange force if very weak partial bracing is used, yet drops to under 2% as the full bracing limit is reached.

For this example, one may also notice that the brace foces do not become unbounded as the stiffness is reduced below the level required to reach full bracing (see Figure 4.4 for say, less than around 1.2 kip/in.). This could be due to the fact that the capacity of the member reduces as the brace stiffness decreases. Therefore, the brace force does *increase* since the stiffness of the brace provides less restraint to out-of-plane movement, but the load supported by the member *decreases*. Overall, the effect is shown in Figure 4.4 as a brace force demand higher than at the full bracing condition, but not necessarily unmanageable.

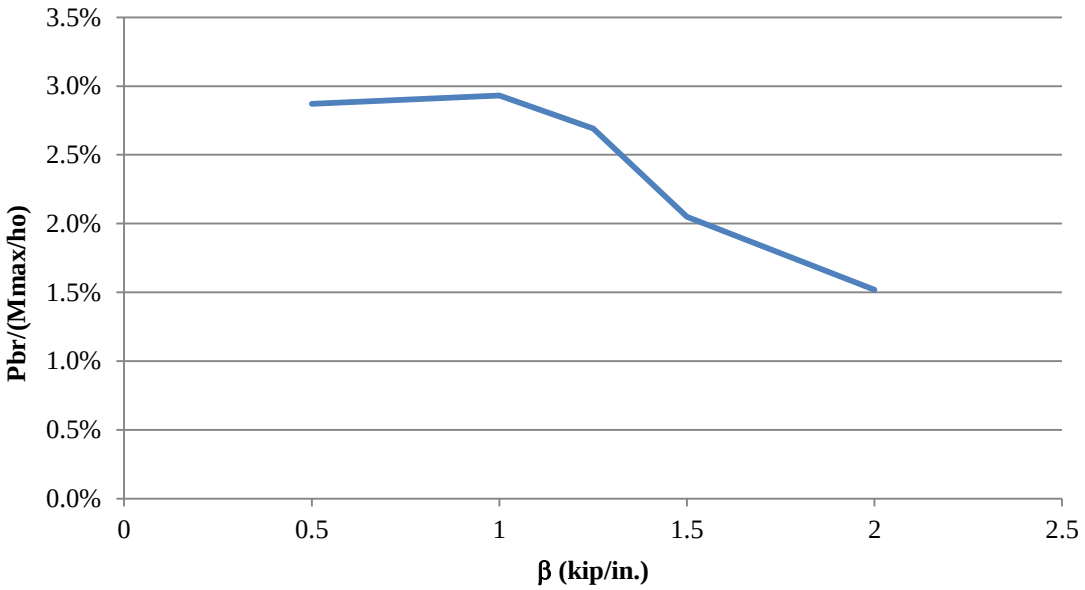

Figure 4.4: Percent of equivalent flange force versus brace stiffness for a W16x26 with uniform moment (lateral brace)

4.3.3. Moment Gradient (M1/M2 = 0.5) with Lateral Bracing

Figure 4.5 shows elevation and cross-section views of a W16x26 beam subjected to a point load at the center of the span and one interior nodal lateral brace applied to the top flange. Two variations of the point load application are discussed: one with the load applied at the top flange (Case 1) and one with the load applied at the centroid of the cross-section (Case 2).

Figure 4.5: W16x26 with a moment gradient and one interior lateral brace at mid-span

Figure 4.6 compares BASP's and SINBAD's solutions. Again, the results coincide fairly well for elastic buckling for either Case 1 or Case 2. The results for inelastic buckling are also shown in Figure 4.6 but only for Case 1 (point load at the top flange). Similar to before, the results suggest that the member is able to support less capacity in its yielded state and consequently, requires less bracing stiffness to reach a fully braced condition.

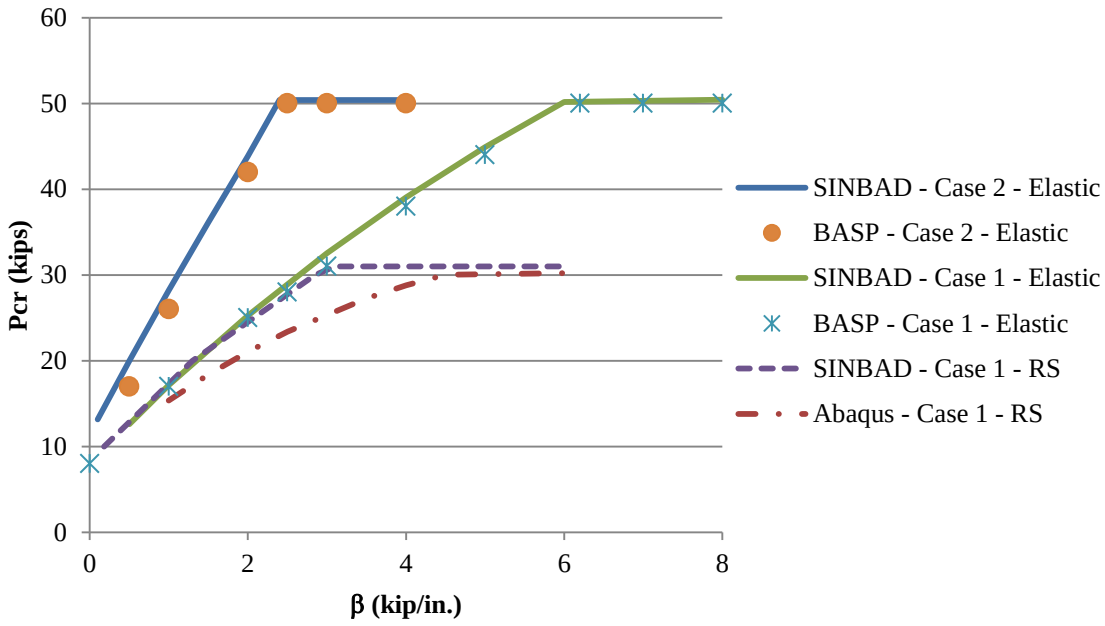

Figure 4.6: Comparison of SINBAD, BASP, and Abaqus for moment gradient (lateral brace)

The brace force percentage versus stiffness of the lateral brace is shown in Figure 4.7. In this example, the brace forces are larger than the previous example under uniform bending; on the order of 4-5% of the equivalent flange force. This may be attributed to the fact that the top flange point load is applied at the location of the only brace along the member. Therefore, this one brace must directly restrain the out-of-plane movement at a location where the externally applied force enters the beam versus the previous example

where moments applied at the ends of the beam means that the mid-span brace is restraining forces that are already internal to the beam.

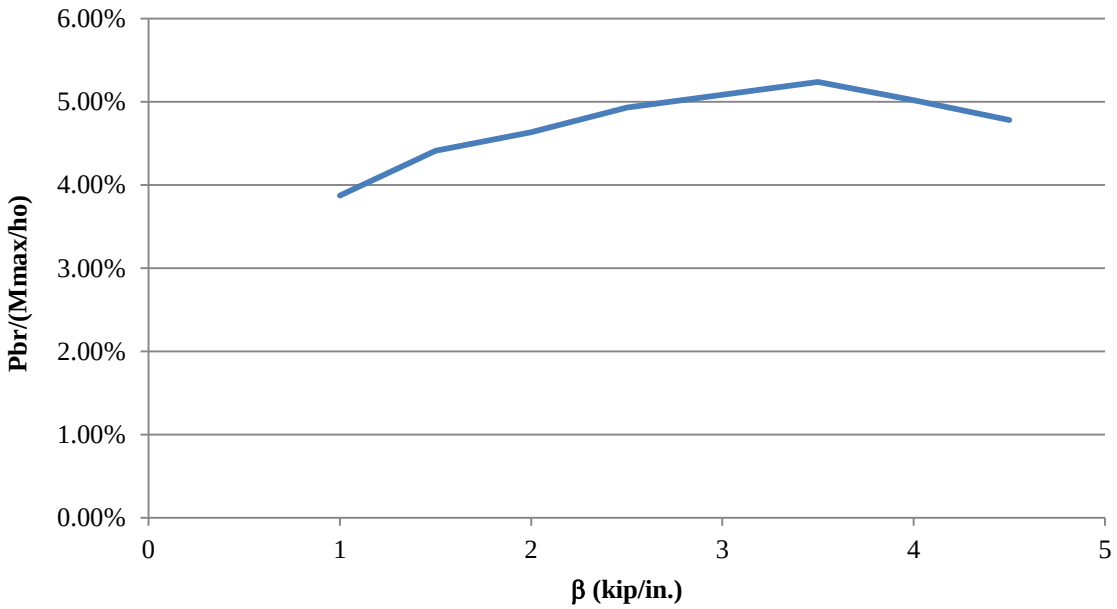

Figure 4.7: Percent of equivalent flange force versus brace stiffness for a W16x26 with a moment gradient (lateral brace)

4.3.4 Moment Gradient (M1/M2 = -1) with Lateral Bracing

Figure 4.8 shows elevation and cross-section views of a W16x26 beam subjected to full reverse curvature bending and interior nodal lateral brace(s) applied at mid-span. Two variations of the lateral bracing are discussed: one with the nodal lateral brace at the top flange only (Case 1), and one with a nodal lateral brace affixed to both the top flange and the bottom flange (Case 2). These two cases were selected to illustrate the effect that load-height plays on the bracing demands. Essentially, a tipping effect occurs due to the load being applied above the cross-section centroid which acts to further destabilize the member and thus, leads to increase brace stiffness demands. The reader is further

referred to Yura (2001) for a more in-depth discussion of this tipping effect and how it works in experimental applications and practice.

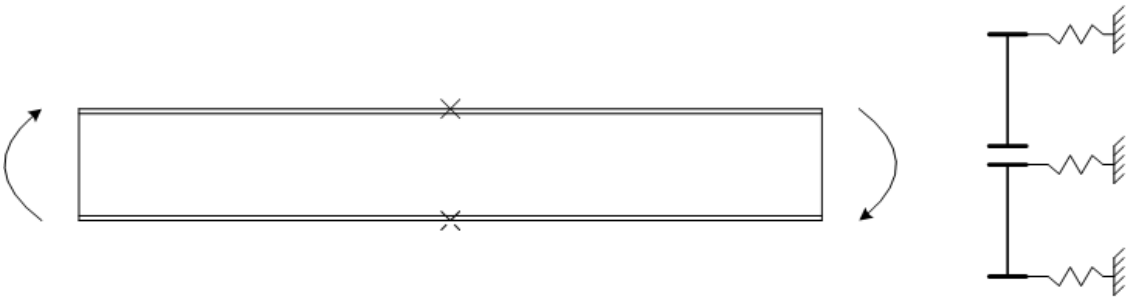

Figure 4.8: W16x26 with a full reverse curvature bending and interior lateral brace(s) at mid-span

Figure 4.9 shows the results for the comparison of SINBAD to BASP for the elastic buckling case and of SINBAD to Abaqus for the case of inelastic buckling. Once again, the elastic buckling results are in fairly good agreement. Also shown in Figure 4.9 are the inelastic buckling results for the case with lateral bracing on both the top and bottom flanges. There is a significant drop in the capacity of the section realized in either SINBAD or Abaqus, but more importantly, the bracing stiffness required to reach full bracing is significantly decreased (from around 25 kip/in. based on the elastic model to around 10-15 kip/in. from the inelastic model).

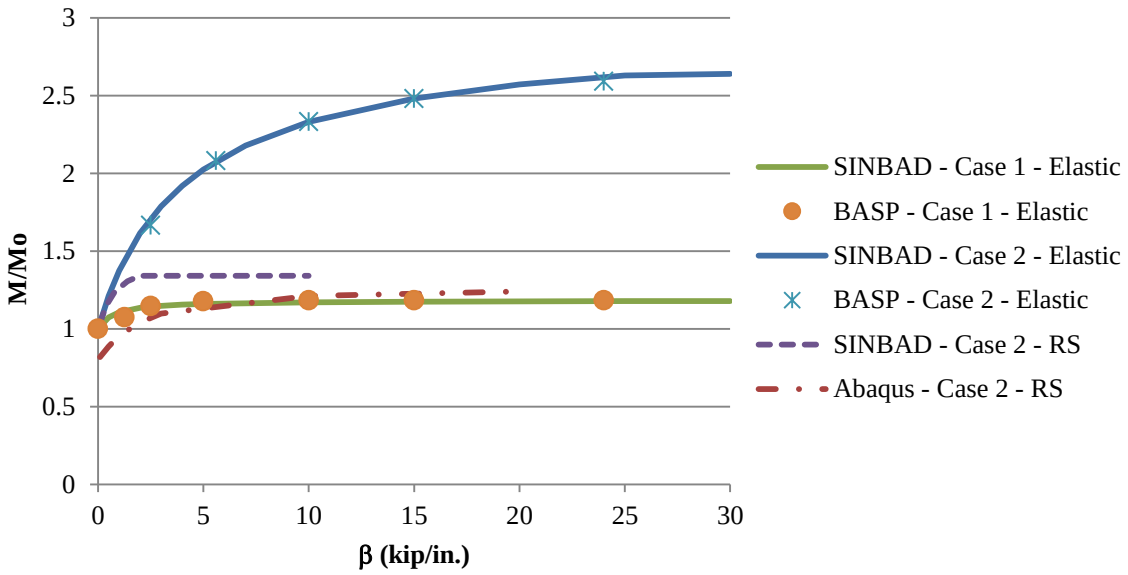

Figure 4.9: Comparison of SINBAD, BASP, and Abaqus for reverse curvature bending (lateral brace)

Figure 4.10 plots the brace force as a percentage of the equivalent flange force versus the bracing stiffness. In this figure, force percentages for both the top and bottom flanges are shown and have strength demands under 0.8%.

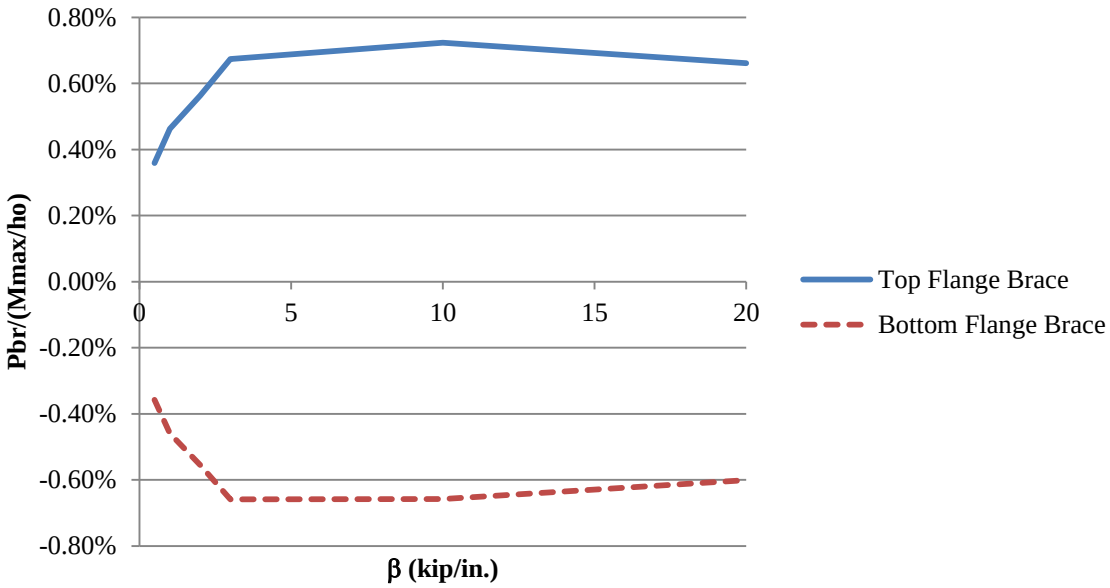

Figure 4.10: Percent of equivalent flange force versus brace stiffness for a W16x26 with a reverse curvature bending (lateral brace)

4.3.5 Uniform Bending with Torsional Bracing

This example is a W16x26 subjected to uniform bending with one torsional brace attached at mid-span. There is a 1/4" thick x 4” stiffener attached to the cross-section at mid-span. An elevation and cross-section view of this example is shown in Figure 4.11.

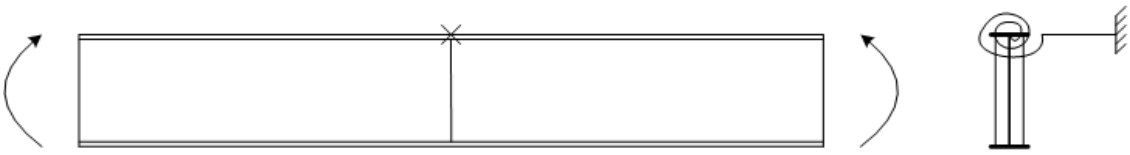

Figure 4.11: W16x26 under uniform bending and one torsional brace at mid-span

The results for this example are shown in Figure 4.12. The elastic buckling capacity as a function of brace stiffness from SINBAD is in close agreement with BASP. Again the

reduced capacity of the section due to the inclusion of inelasticity in the analysis varies between SINBAD and Abaqus, yet the stiffness requirement to reach full bracing stays relatively unchanged despite the analysis program or the effects of yielding.

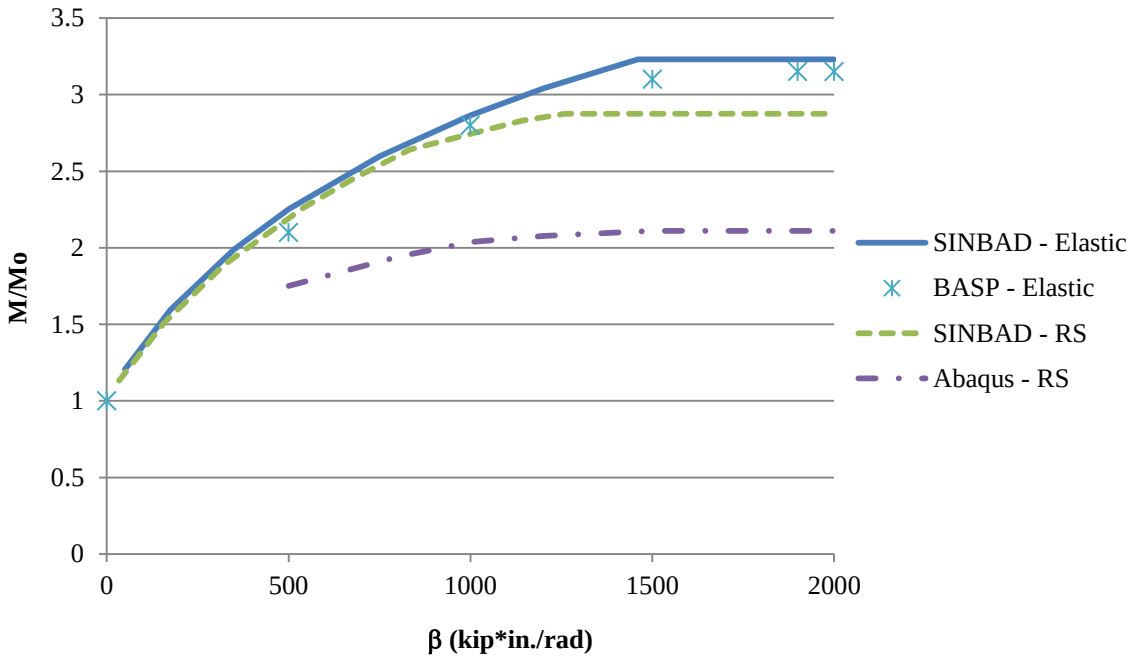

Figure 4.12: Comparison of SINBAD, BASP, and Abaqus for uniform bending (torsional brace)

The brace moment as a percentage of the maximum applied moment versus bracing stiffness is shown in Figure 4.13. As in the previous plots, there is a general decrease in the brace force as the condition of full bracing is approached.

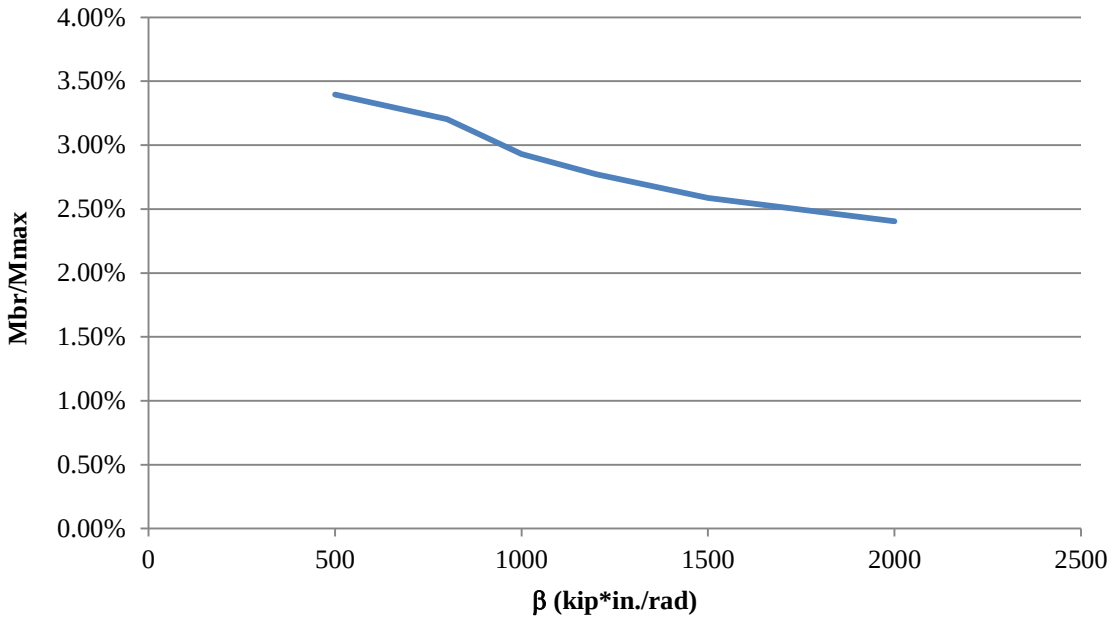

Figure 4.13: Brace force as a percentage of applied moment versus brace stiffness for a W16x26 under uniform bending (torsional brace)

4.3.6 Moment Gradient (M1/M2 = 0.5) with Torsional Bracing

This last example is a W16x26 with a point load and one torsional brace applied at mid-span. There are two cases investigated here: one with the load application at the top flange (Case 1) and one with the load applied at the centroid of the cross-section (Case 2). Figure 4.14 provides an elevation view and cross-section views for this example.

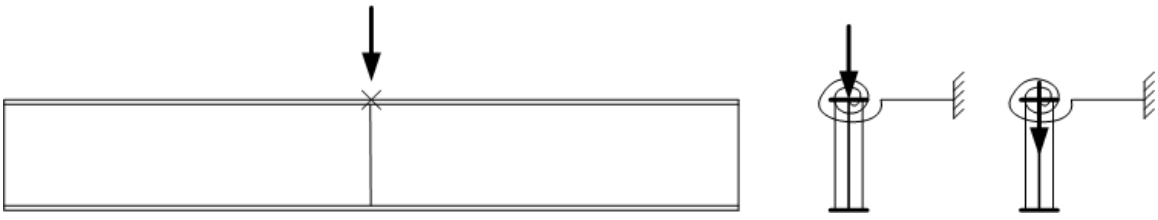

Figure 4.14: W16x26 under moment gradient and one torsional brace at mid-span

The comparisons of SINBAD, BASP, and Abaqus are shown in Figure 4.15. Note that the elastic solutions from SINBAD are slightly more conservative than those from BASP as evidenced by the horizontal shift of the required bracing stiffness to the left. The demands on the bracing for the member including the effects of yielding are slightly less than those predicted by BASP for the elastic solution and roughly comparable to those predicted by SINBAD for the elastic solution.

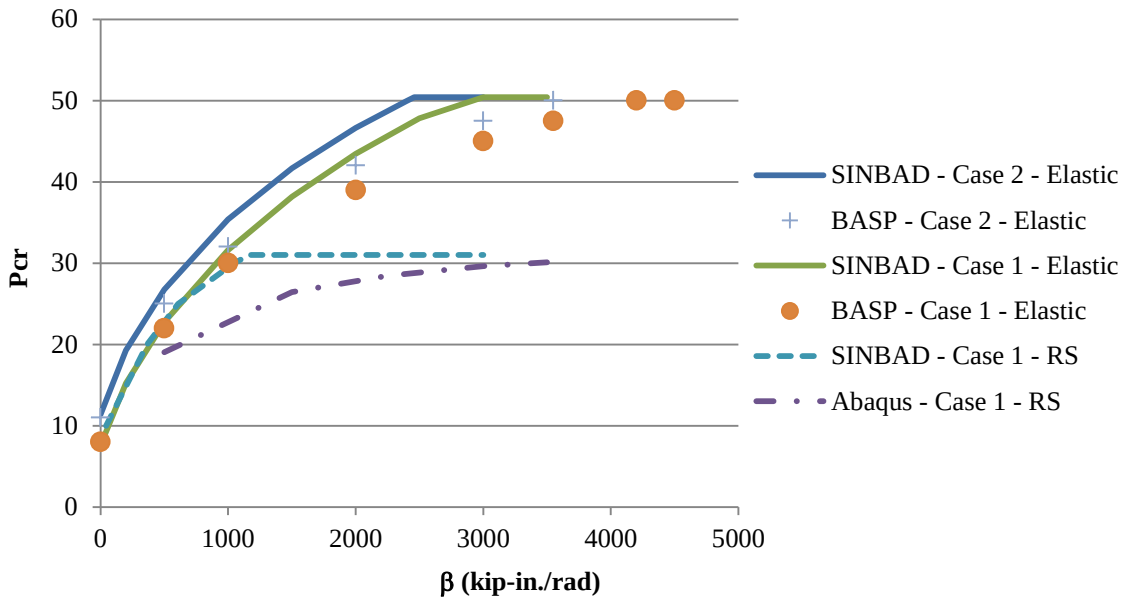

Figure 4.15: Comparison of SINBAD, BASP, and Abaqus for moment gradient (torsional brace)

For the application of top flange loading, Figure 4.16 shows the brace force requirements as a percentage of the maximum moment on the cross-section at the brace location. As discussed previously for the case with lateral bracing a point load applied to the top flange, the brace forces are somewhat higher than cases under uniform bending.

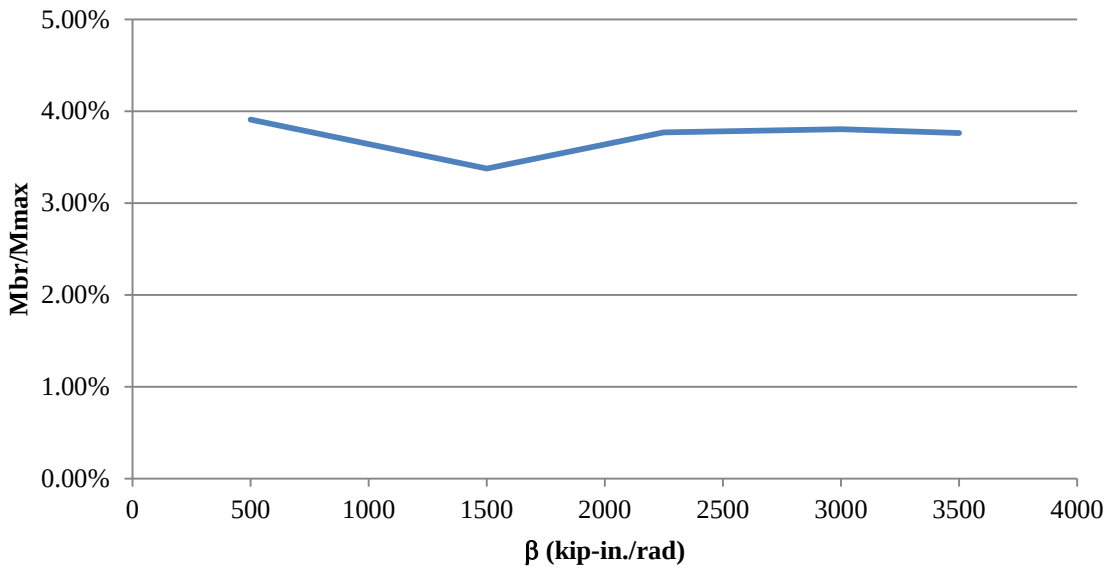

Figure 4.16: Brace force as a percentage of applied moment versus brace stiffness for a W16x26 under moment gradient (torsional brace)

4.4 Elastic Buckling Load Ratio

While the previous section has shown that SINBAD provides sufficient accuracy for predicting the bracing requirements for members buckling elastically, this section advances the notion of the elastic buckling load to help the engineer determine the resistances provided by web-tapered members. Engineers designing web-tapered members often consult AISC's Steel Design Guide 25 (hereafter referred to as DG 25) for guidance on such designs (Kaehler, White, and Kim 2011). The crux of DG 25 lies in the determination of the controlling elastic buckling load ratio, which is defined as,

$$\gamma_e = \frac{F_e}{f_r} \qquad \text{(4.1, 2.2-1, Kaehler, White and Kim 2011)}$$

where F_e is the axial stress at the most highly stressed cross-section, $f_r = P_r/A_g$ at the most highly stressed cross-section, where P_r is the required member axial load

resistance, and A_g is the gross member area (Kaehler, White, and Kim 2011). DG 25 later notes that this calculation works well only for single linear tapers with no section transitions. Furthermore, DG 25 permits the designer to calculate the value directly using an elastic buckling analysis with relatively few restrictions (see Appendix B, Kaehler, White, and Kim 2011).

The main point of this research was not to develop a method for determining the elastic buckling load ratio used in the design of members, yet can be determined directly from the rigorous computational tool. Two examples are presented that show the power of SINBAD to capture the elastic buckling load ratio directly while accounting for two specific items DG 25 does not consider; namely, the warping and flange lateral bending restraint provided by segments adjacent to the one in question and bracing stiffness provided that may be less than the full bracing requirement. No designs are performed in this section nor are any considerations given to determining any member's specific capacity. In all of these comparisons, the γ_e reported from SINBAD is simply the eigenvalue determined from an elastic analysis, since the eigenvalue is a multiplier of the applied load at which incipient buckling would occur if the member remains elastic. Specifically in SINBAD, the residual stresses are turned off and the yield stress is set to a "high" value to ensure that yielding does not preclude elastic buckling.

4.4.1 Design Guide 25 – Example 5.3

Example 5.3 from DG 25 is a doubly-symmetric, single linear-tapered beam that is subjected to a moment gradient. Figure 4.17 is a recreation of Figure 5.6 from DG 25, showing the nominal section geometry and applied moment diagram (calculated using factored loads). Table 4.1 shows the comparison between the design calculations in DG 25 and the results from SINBAD.

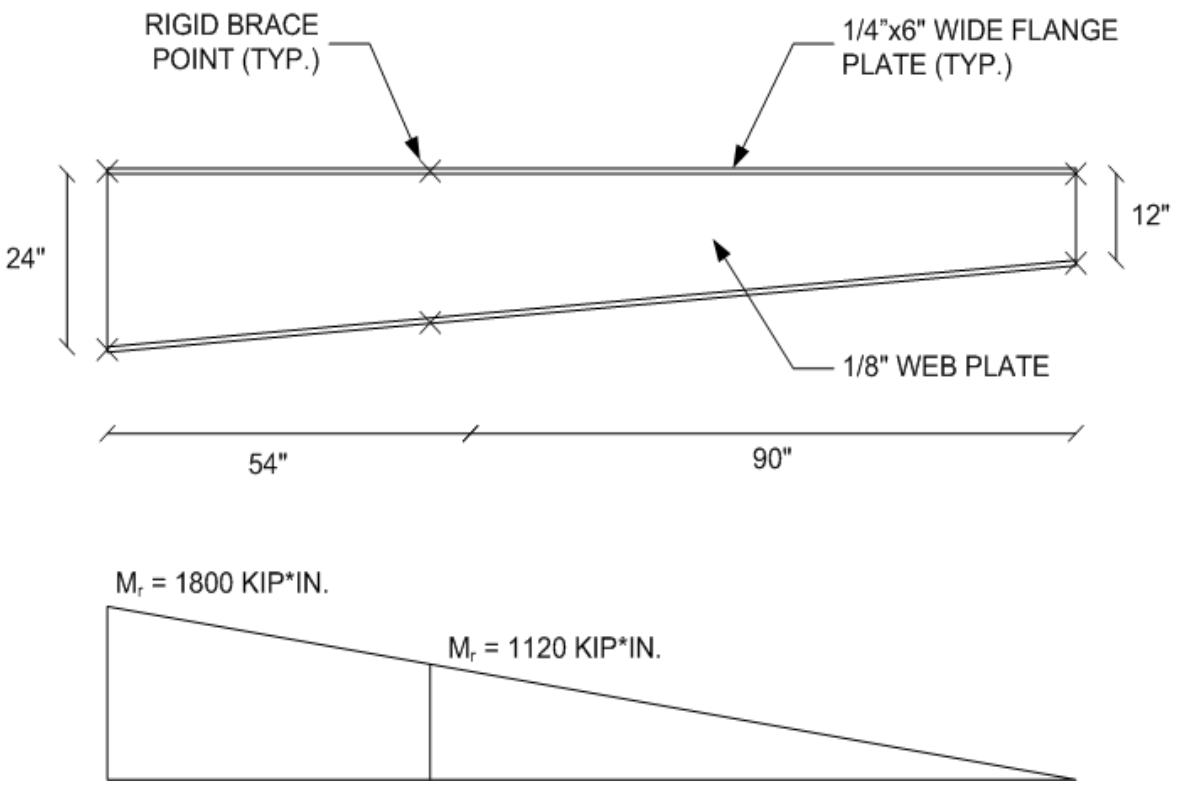

Figure 4.17: Tapered beam example showing section properties and the applied moment diagram

Table 4.1: DG 25 versus SINBAD for calculation of γ_e for example 5.3

Section	**$(\gamma_{eLTB})_{Cb=1}$**	**C_b**	**$(\gamma_{eLTB})*C_b$**	**γ_e SINBAD**	**DG25 v. SINBAD**
Left	6.1	1.08	6.59	6.733	-2.1%
Right	2.91	1.47	4.28	3.978	7.6%
Whole Beam	-	-	-	5.659	-

$(\gamma_{eLTB})_{Cb=1}$ is the elastic buckling load ratio determined with C_b set equal to 1.

Referencing Table 4.1 for the first (left) unbraced length, SINBAD predicts γ_e = 6.733 versus a prediction of 6.59 from DG 25. In this case, DG 25 is suggesting that the member would be able to support 2% less load than the rigorous eigenvalue buckling solution would suggest. Conversely, for the second (right) unbraced length, DG 25 is

7.6% higher than the solution from SINBAD. It should be noted that the results shown from SINBAD in Table 4.1 are for analysis models where each unbraced segment is assumed to have torsionally simply-supported (fork) boundary conditions in order to mimic the end conditions assumed in DG 25.

The last row shows that the elastic buckling load ratio for the entire beam model is 5.7. DG 25 does not explicitly perform this calculation, since the design of web-tapered members (or general, prismatic members for that matter) is commonly based on evaluating each unbraced length in isolation, assuming simply-supported end conditions (corresponding to a lateral-torsional buckling effective length factor of $K = 1$). However, to be considered as an unbraced length for section capacity checks, the bracing provided must be at the full or rigid bracing stiffness (i.e., no brace point movement is allowed). In real structures with bracing other than "rigid", the brace point will displace out-of-plane immediately upon application of the load.

Therefore, using SINBAD to calculate an elastic buckling load ratio based on the entire member provides a more realistic prediction of γ_e based on three main considerations:

1. The bracing stiffness and strengths provided in the physical member may be less than those required to reach full bracing. However, SINBAD provides a rigorous means by which the engineer can capture the ideal stiffness demands for these cases.
2. There may be significant restraint provided by adjacent members due to continuity across the brace points. Regions of the member that are more lightly loaded or with reserve capacity may be able to "assist" more heavily stressed segments by providing warping and lateral bending restraint. SINBAD captures

these effects inherently through the modeling of the entire system and not just individual unbraced lengths.

3. DG 25 is based on equations derived for members with a single linear taper. By modeling the member in SINBAD, a designer is afforded a method to assess γ_e for a wider range of member geometries.

4.4.2 Specimen 4 from Cyclic Testing of Web-Tapered Members

This experimental case comes from cyclic testing of web-tapered rafters performed by Smith (2012a, 2012b). Figure 4.18 shows a diagram of the test setup for his typical experiments and Figure 4.19 shows the overall web-tapered member dimensions for Specimen 4 specifically.

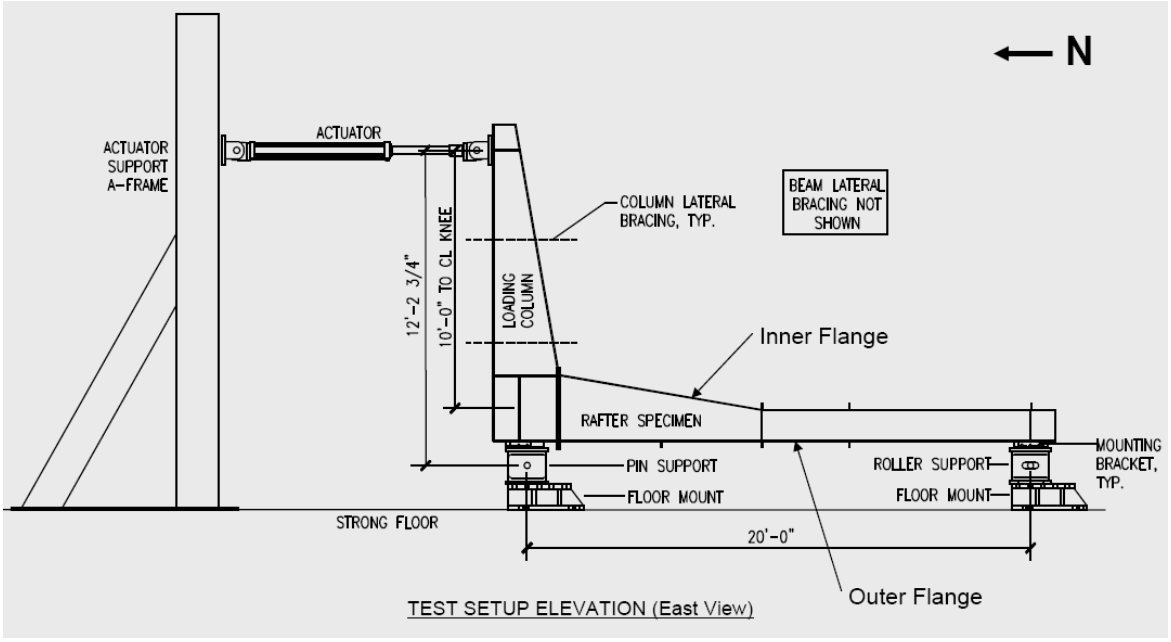

Figure 4.18: Typical cyclic loading test setup (schematic courtesy Smith, 2012a)

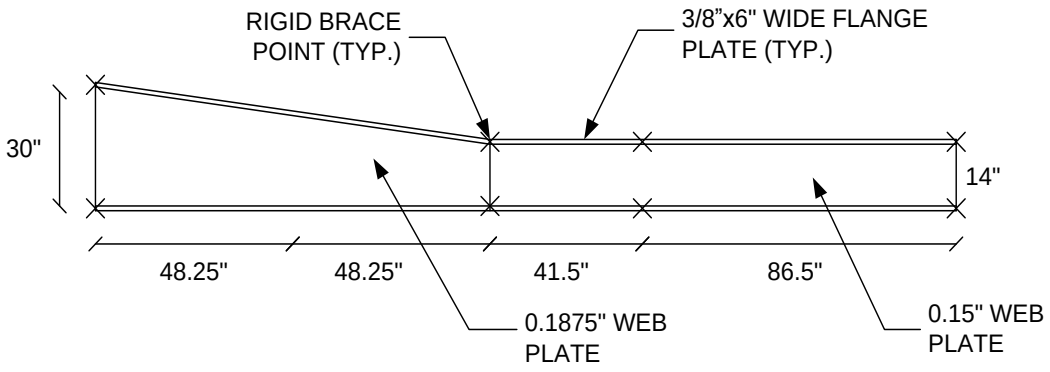

Figure 4.19: Specimen 4 of the cyclic load tests

As denoted in Figure 4.19, the two interior bracing locations were considered to be rigid, i.e., twist and lateral translation of the section is prevented at these four points. The right end is modeled as simply-support with fork boundary conditions for torsion. Finally, the left end of the specimen is considered to be fixed to the rafter (loading apparatus, in this case); providing full warping and restraint to flange lateral bending.

A moment of 4200 kip*in. is applied at the left end and is oriented such that the top flange is in compression. The analysis in SINBAD is performed and the elastic buckling load ratio, γ_e = 3.44. From the hand calculation performed via DG 25 on just the left side (before the pinch point), γ_e = 2.34 (Smith 2012b). Therefore, SINBAD would suggest that considering the effects of continuity across the pinch point would allow the designer to design the section to carry a higher capacity than that predicted by DG 25.

4.5 LTB Curves

Now that the initial benchmarking has been presented for the comparison of SINBAD to elastic buckling solutions, the next logical step is to assess SINBAD’s ability to determine the effects of the spread of plasticity throughout the member on the

eigenvalue buckling capacity. This section presents several lateral-torsional buckling curves for a variety of loadings and cross-section slenderness. As one point of reference to validate SINBAD, one may select the lateral-torsional buckling strength curves produced from AISC (2012b).

When comparing the results from SINBAD to AISC, it is important to keep in mind that SINBAD is an approximation of the inelastic state of the structure given certain idealizations discussed in Chapter 3 in the program's development. Furthermore, it uses these approximations to characterize the member capacity based on an eigenvalue buckling solution. Therefore, invariably, differences will arise for the strength reached by an analysis model prediction based on the eigenvalue buckling capacity (SINBAD, in this case) when compared to experimental results (the AISC strength curves as shown below) or even to another analysis model built on different assumptions or idealizations. In this section it is evident that the capacities predicted by SINBAD as compared to AISC differ, especially for unbraced lengths and cross-section profiles that place the respective sections in the inelastic or plastic buckling regions. Explanations are provided at locations of discrepancies to ensure that the reader understands the differences between the strength predictions.

In all of these cases, SINBAD is executed with nominal yield and stiffness capacities. In order to facilitate a direct comparison, the AISC curve is also computed using nominal values. Additionally, residual stresses are imposed in SINBAD pursuant to 3.2.2.1. The planar boundary conditions are pinned-ended where the fork boundary conditions are assumed for the out-of-plane solution.

4.5.1 LTB Curve for a Compact Section

The first case looks at comparing the LTB curves generated via the AISC Specification (2010b) versus SINBAD for a beam section with compact elements. The W16x26 is selected for this first assessment. The flanges of a W16x26 are 5.5 in. wide by 0.345 in. thick. This gives a $b_f/2*t_f$ ratio of 7.97 whereas the limiting ratio for compact flange elements, λ_p, as determined from AISC Chapter B (2010b) is $0.38*\sqrt{(E/F_y)}$ = 9.15 (for F_y = 50 ksi). Similarly, a 15.01 in. deep web by 0.25 in. thick would yield at h/t_w ratio = 60.04 which is less than $3.76*\sqrt{(E/F_y)}$ = 90.55 (for F_y = 50 ksi). Figure 4.20 shows the results when the solution from SINBAD is plotted against the Specification values for the case of uniform moment. Also, the values of L_p and L_r as well as M_y and $0.7*M_y$ are also plotted for reference during further discussion. It should be noted that for these plots, L_p is calculated using a more conservative approximation as $1.1*r_{ts}*\sqrt{(E/F_y)}$ instead of the codified equation of $1.76*r_y*\sqrt{(E/F_y)}$, where r_{ts} is the effective radius of gyration (in.) and r_y is the radius of gyration about the y-axis (in.).

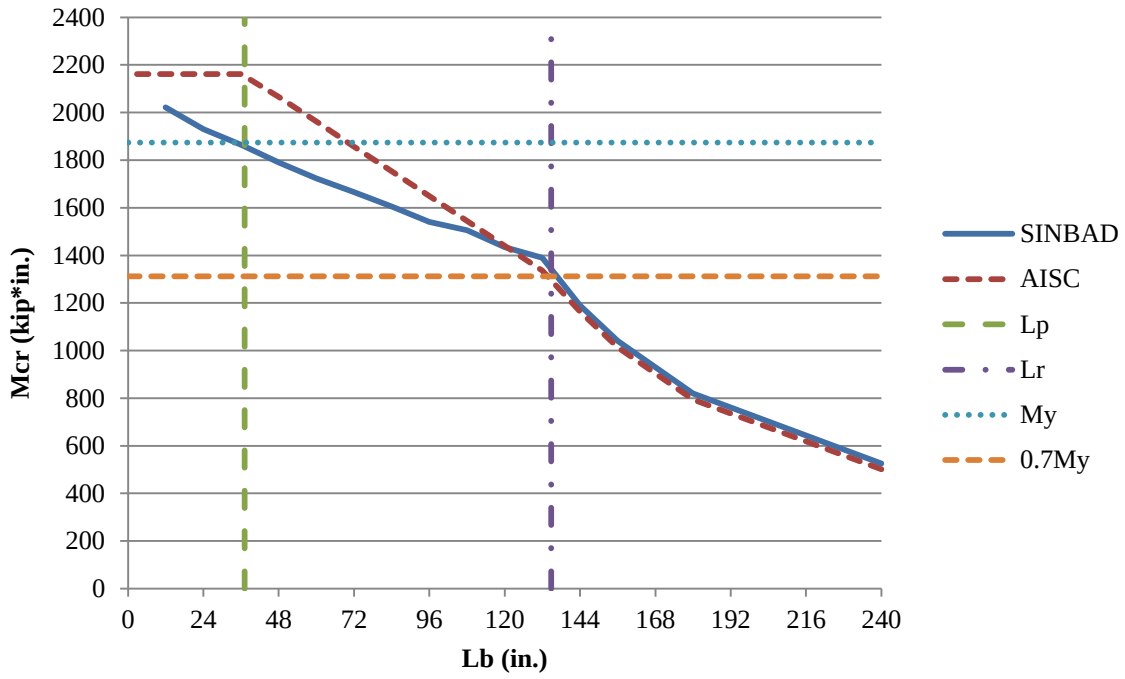

Figure 4.20: LTB strength curves for a W16x26 section under uniform moment

From Figure 4.20, one notices that the elastic buckling region is predicted very well by SINBAD. However, as more and more inelasticity develops in the member (moving from L_r toward L_p), the strength predicted by SINBAD tends to under-predict the AISC values. Once L_p is reached, SINBAD begins to pick up strength at a faster pace until the analyses are discontinued at an unbraced length equal to one foot.

The main difference between the results from a general eigenvalue buckling analysis (SINBAD in this case) and the AISC Specification in the inelastic and plastic buckling regions is due to the lateral movement of the compression flange. The inelastic eigenvalue buckling analysis is based on the state of the structure associated with in-plane deformations. That is, the member is assumed to displace solely in-plane until the critical buckling load is reached. At this point, the member then displaces laterally out-of-

plane an undetermined amount. Conversely, the AISC design curves are a fit to experimental data. Therefore, due to the imperfect nature of the initial geometry in real test specimens, lateral movement of the compression flange initiates immediately with the onset of load. This lateral movement increases as the load increases, exacerbating the compression on one side of the compression flange and relieving compression on the other. Therefore, a potentially higher load may be reached in certain cases in experimental tests when compared to an eigenvalue buckling analysis. The ASCE-WRC Plastic Design Guide (ASCE 1971) discusses this phenomenon in detail and documents these observations for compact-web sections with relatively close brace spacing subjected to uniform moment.

It is also important to note that the residual stresses selected for use in SINBAD may differ from the fit to experimental results that was performed to develop the AISC curves. If one were to sample the residual stresses from a large set of beams, one would find the variability quite high. Furthermore, many experiments on which the design curves are based did not have their residual stresses recorded. Therefore, it is not beyond reason to suspect that a potential difference in the results from AISC and SINBAD from Figure 4.20 may come from the magnitude and distribution of assumed residual stresses.

Figures 4.21 and 4.22 present results from the same beam section discussed above yet with a moment gradient in lieu of uniform bending. Figure 4.21 shows the effect of a moment gradient where $M1/M2 = 0.5$ and Figure 4.22 shows the effect of a moment gradient where $M1/M2 = 0$. Again, one notices from both of these plots that the elastic buckling region is predicted fairly well whereas the inelastic buckling strength predictions from SINBAD comes up less than the AISC values.

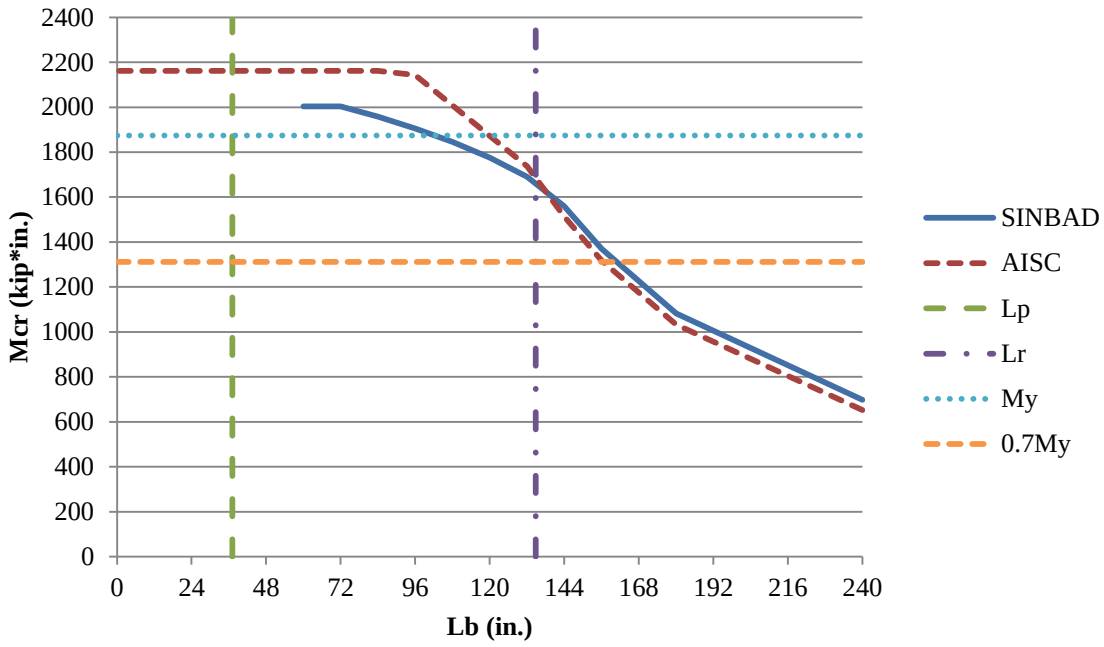

Figure 4.21: LTB strength curves for a W16x26 section with M1/M2 = 0.5

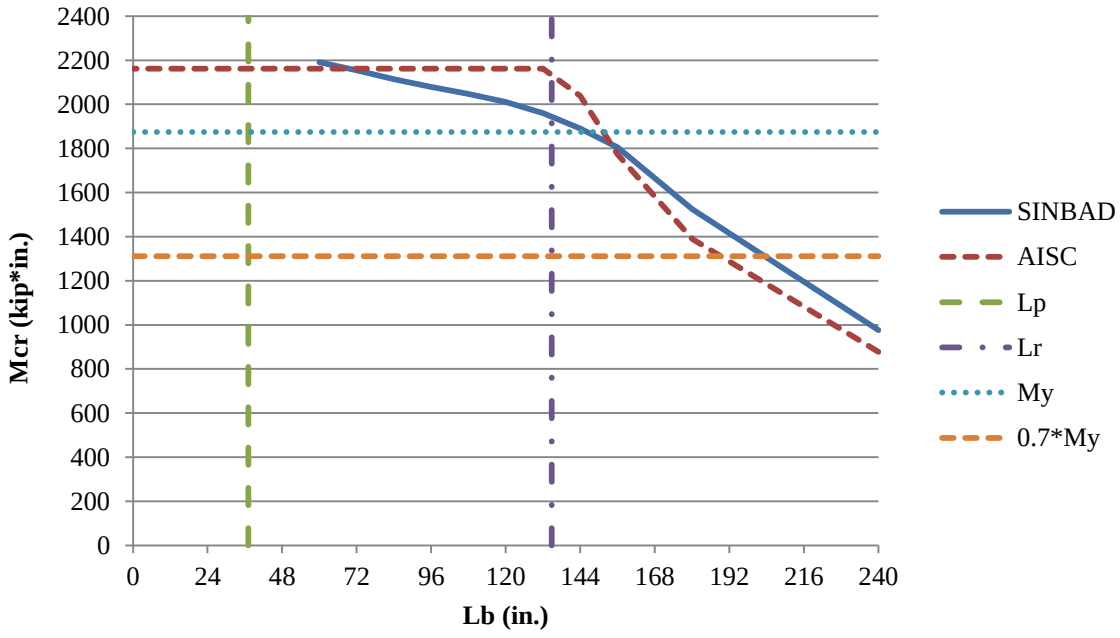

Figure 4.22: LTB strength curves for a W16x26 section with M1/M2 = 0

4.4.2 LTB Curve for a Non-Compact Web Section

In this example, the flanges of the W16x26 are assumed to stay the same but the distance between flange centroids, h_o, is assumed to be double that of the W16x26. Therefore, the flange remains compact and the web slenderness becomes h/t_w = 30.02/0.25 = 120.08. The web compact limit is 90.55 (calculated previously) and the non-compact limit, $\lambda_r = 5.7*\sqrt{(E/F_y)}$ = 137.3 (with F_y = 50 ksi), placing this section in the non-compact range for web slenderness. Henceforth, this section will be referred to as "W16x26-2ho".

Figure 4.23 provides the comparative results for the AISC Specification versus SINBAD for the case of uniform bending. Again, the elastic buckling region is in fairly good agreement, yet the inelastic buckling region still shows that SINBAD tends to under-predict the Specification for the same reasons discussed in the previous sub-section.

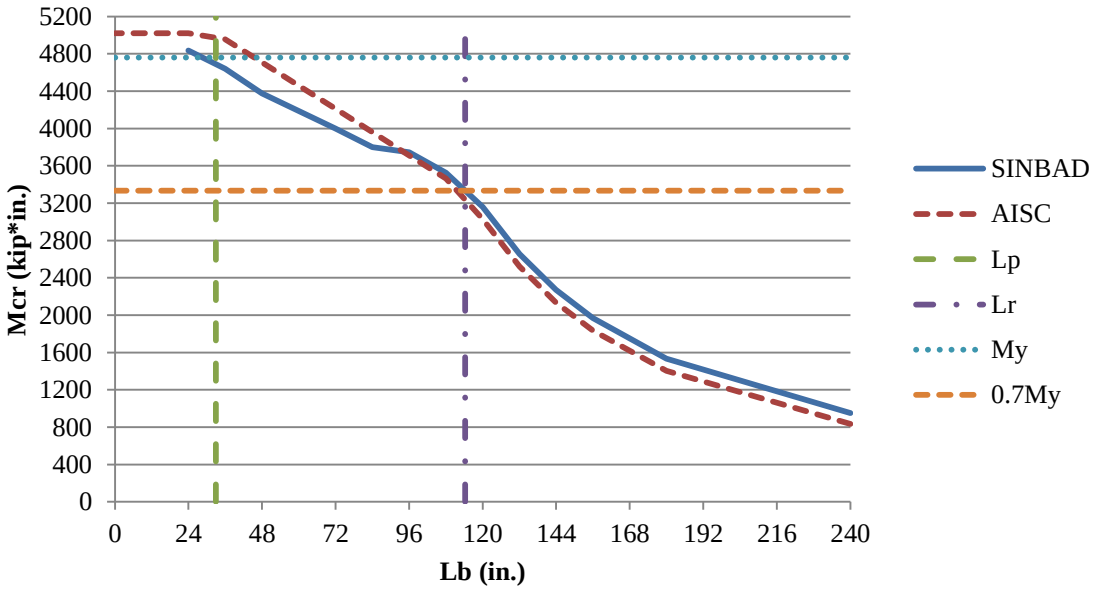

Figure 4.23: LTB strength curves for a W16x26-2ho section with uniform moment

4.4.3 LTB Curve for a Slender Web Section

In this example, the flanges again remain the same dimensions while h_o is set at three times that of the W16x26. The web slenderness becomes h/t_w = 45.03/0.25 = 180.1 which is greater than λ_r calculated prior. This section is known as "W16x26-3ho" in all further references.

Figures 4.24 and 4.25 compare the AISC values with those from SINBAD for the W16x26-3ho under uniform moment and a moment gradient, *M1*/*M2* = 0.5, respectively.

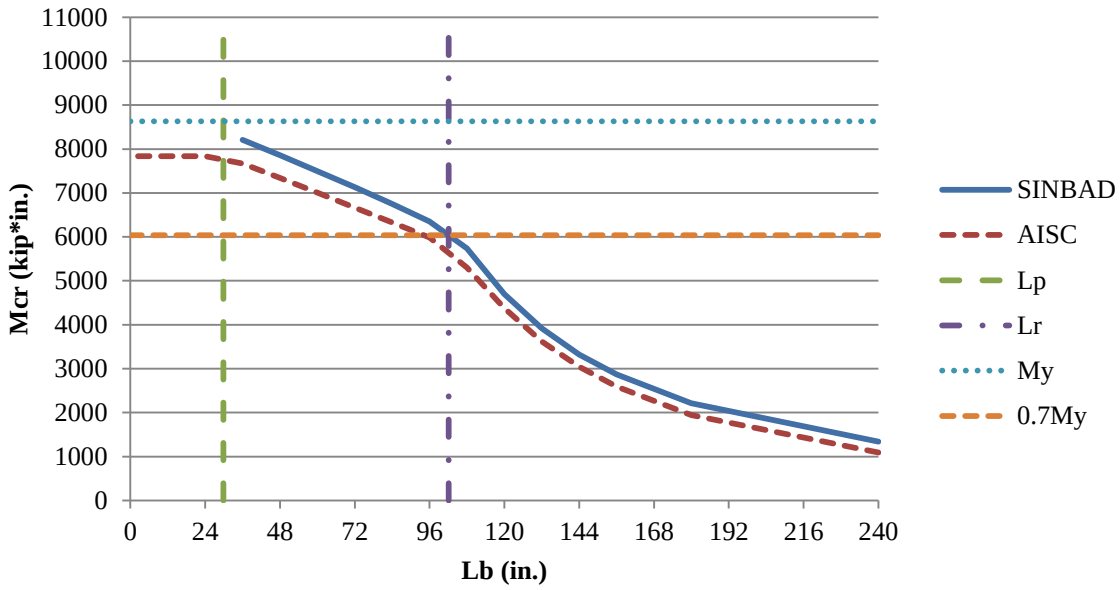

Figure 4.24: LTB strength curves for a W16x26-3ho section with uniform moment

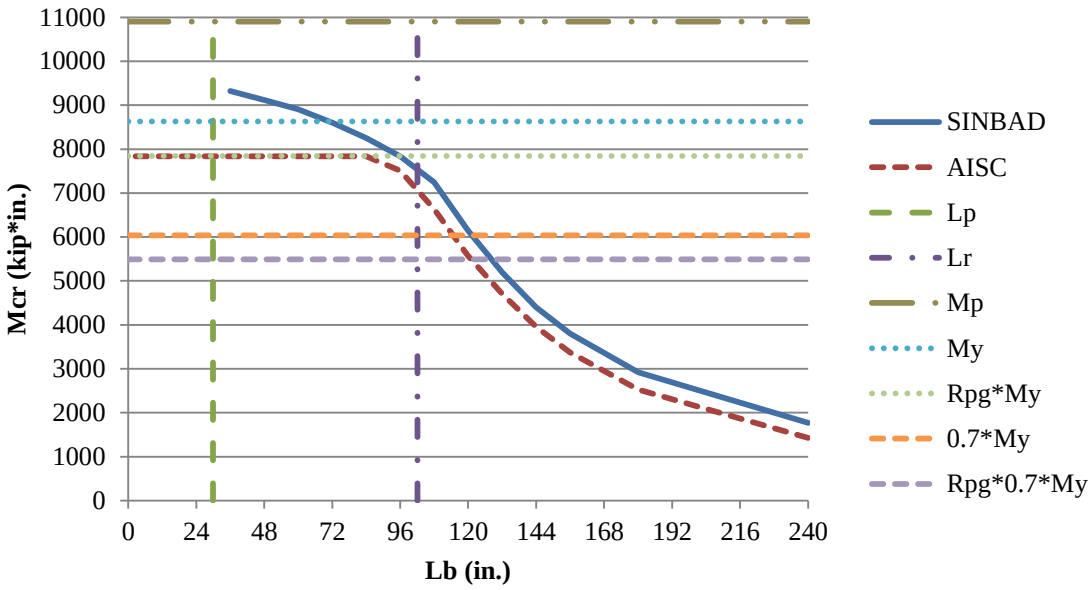

Figure 4.25: LTB strength curves for a W16x26-3ho section with *M1*/*M2* = 0.5

These two figures show a marked contrast from the previous plots for compact and non-compact web sections. The main difference is in the elastic buckling region where SINBAD is now predicting higher strengths versus AISC. This may be attributed to the fact that the Specification ignores the contribution to the strength from the St. Venant torsion constant, *J* (a short discussion on this can be found in the Commentary to F5, AISC 2010b).

For the inelastic buckling region in the case under uniform moment, SINBAD again tracks a bit higher than AISC due to the omission of *J* from the Specification. However, SINBAD begins to predict a large increase in strength for very short unbraced lengths in the case of uniform bending and for relatively moderate unbraced lengths in the case with moment gradient. This variation can be attributed to the fact that SINBAD effectively "condenses out" the ability to develop local buckling in the web (as discussed in Chapter

3). While AISC limits the plateau strength to $R_{pg}*M_y$, where R_{pg} is the bending strength reduction factor that is meant to reduce the strength of the section due to inelastic buckling in the web, SINBAD does not see this effect.

4.6 Bracing of Inelastic Members

4.6.1 Introduction

Now that it has been documented how SINBAD compares to the Specification, it is imperative to discuss the similarities and differences between SINBAD and simulation results from Abaqus. A number of comparisons and observations were made such that the results can loosely be categorized into four main groups based on the web depth of the member in question. Table 4.2 below provides a complete listing of the specimens tested. All boundary conditions for these cases are considered to be pinned-ended with fork boundary conditions for the out-of-plane buckling analysis, unless noted otherwise. Additionally, Figures 4.26 – 4.43 provide a graphical depiction of the test studies detailed in Table 4.2. The members are grouped in Table 4.2 based on their web-depths and web slenderness, with more slender sections listed further down the table.

The examples labeled with a “Case 1” prefix represent the standard W16x26 section discussed in the presentation of the LTB curves. All section properties and test parameters are provided in the first banded set of rows (highlighted) in Table 4.2.

The examples labeled with a “Case 2” prefix are associated with a member where the web is classified via Chapter B (AISC 2010b) as at the non-compact/slender limit. This section was chosen as it provides a slenderness that is as large as possible without having to characterize the web as slender. All section properties and test parameters are provided in the second banded set of rows (un-highlighted) in Table 4.2.

The examples labeled with a “Case 3” prefix are classified via Chapter B (AISC 2010b) as slender. All section properties and test parameters are provided in the third banded set of rows (highlighted) in Table 2. Case 3 has the most number of examples since a majority of the built-up sections used in the metal building industry contain slender web elements.

To determine the initial section properties for the slender web section, ASIC’s DG 25 was consulted for recommendations on appropriate proportioning of the flange and web elements. The first step was to select the flange width. Since all other sections were using the flange plate of a W16x26 rolled section, a 0.345 in. by 5.5 in. plate was similarly selected for the flange. Next, Section 1.2 of DG 25 suggests that $h/b_f \leq 7$ unless closely spaced bracing is provided (Kaehler, White, and Kim 2011), thus a conservative value of $h/b_f = 6$ was selected for these tests, allowing $h = 33$ in. Finally, $h/t_w = 180$ was selected as it is in an appropriate range of slenderness ratios used in the metal building industry, giving $t_w = 0.1833$ in.

Lastly, the examples labeled in Table 4.2 with a “Case 4” prefix present members with webs that are classified via Chapter B (AISC 2010b) as slender. The section selected retains the same flange plate as that of a W16x26 and increases the distance between flange centroids, h_o, to $3*h_o$. All section properties and test parameters are provided in the final banded set of rows (un-highlighted) in Table 4.2. The cross-section properties of Case 4 place it truly outside of the recommended geometry suggested in DG 25. For example, h/b_f for this case is equal to 8.3, where the suggested limit is 7 (Kaehler, White, and Kim 2011).

The plots presented in this section show a representative strength versus stiffness, which is commonly referred to as a “knuckle curve”, to compare the solutions from Abaqus and SINBAD. For these types of graphs, one generally plots the bracing stiffness in kips/inch for relative bracing and kips*inch/radian for torsional bracing on the abscissa and some measurement of strength on the ordinate axis.

Also, plots of the brace force as a percentage of the moment or equivalent moment at the brace will be shown, similar to the results presented previously. The author will wait to make any recommendations on the bracing strength requirements until all the member and frame cases have been presented in their entirety.

Table 4.2: Member bracing test matrix

Case	Figure	L	L_b	No. of Seg.	Brace Type	n_T or n_R	C_b	h_o	t_w	h/t_w	Web Class.	b_f	t_f	Notes:
1a	4.26	192	48	4	T	3	1	15.355	0.25	60.04	C	5.5	0.345	
1b	4.27	192	48	4	R	4	1	15.355	0.25	60.04	C	5.5	0.345	
1c	4.28	432	144	3	T	2	1	15.355	0.25	60.04	C	5.5	0.345	
1d	4.29	192	96	2	T	1	1.3	15.355	0.25	60.04	C	5.5	0.345	
1e	4.30	192	96	2	R	2	1.3	15.355	0.25	60.04	C	5.5	0.345	
2a	4.31	192	48	4	T	3	1	34.664	0.25	137.27	NC	5.5	0.345	
2b	4.32	192	48	4	R	4	1	34.664	0.25	137.27	NC	5.5	0.345	
3a	4.33	192	48	4	T	3	1	33.345	0.1833	180.03	S	5.5	0.345	
3b	4.34	192	48/96/48	3	T	2	1	33.345	0.1833	180.03	S	5.5	0.345	
3c	4.35	192	48/96/48	3	T	3	1	33.345	0.1833	180.53	S	6.6	0.2919	Wide Flanges
3d	4.36	432	144	3	T	2	1	33.345	0.1833	180.03	S	5.5	0.345	
3e	4.37	90	30	3	T	2	1	33.345	0.1833	180.03	S	5.5	0.345	
3f	4.38	192	96	2	T	1	1.3	33.345	0.1833	180.03	S	5.5	0.345	
3g	4.39	192	48	4	T	3	1	33.345	0.1833	180.03	S	5.5	0.345	
3h	4.40	192	48	4	T & R	3/4	1	33.345	0.1833	180.03	S	5.5	0.345	R = 1 kip/in. Comp. FL
3j	4.41	192	48	4	T & R	3/4	1	33.345	0.1833	180.03	S	5.5	0.345	R = 1 kip/in. Ten. FL
4a	4.42	192	48	4	T	3	1	46.065	0.25	182.88	S	5.5	0.345	
4b	4.43	192	48	4	R	4	1	46.065	0.25	182.88	S	5.5	0.345	

Figure 4.26: Case 1a

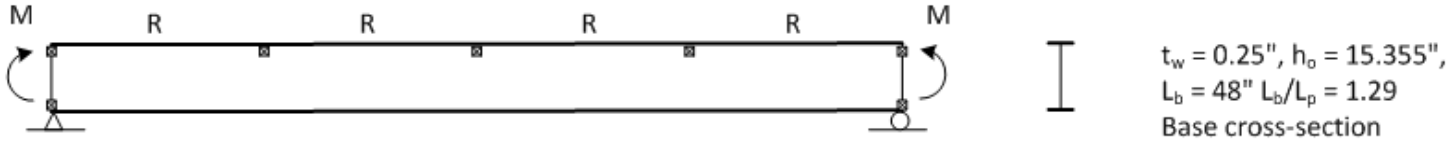

Figure 4.27: Case 1b

Figure 4.28: Case 1c

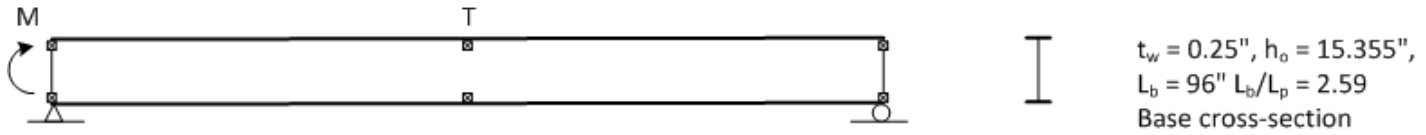

Figure 4.29: Case 1d

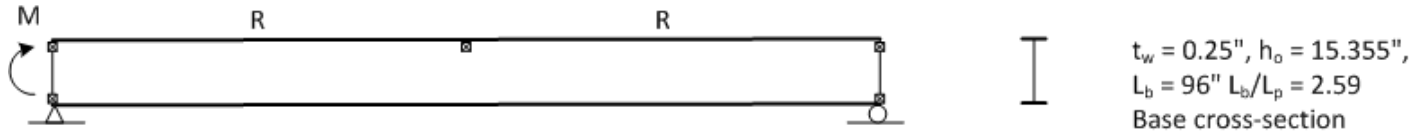

Figure 4.30: Case 1e

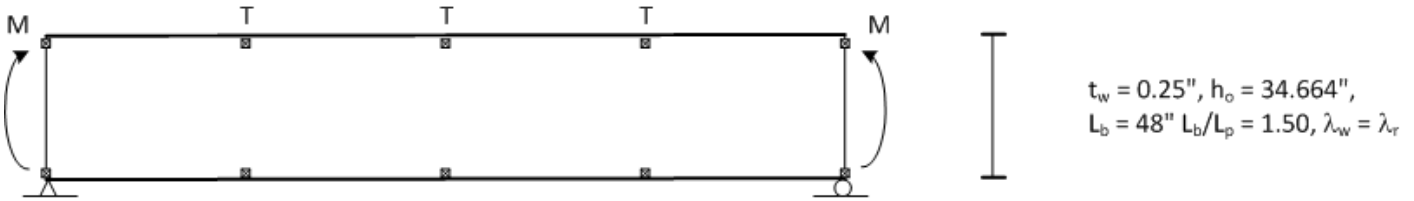

Figure 4.31: Case 2a

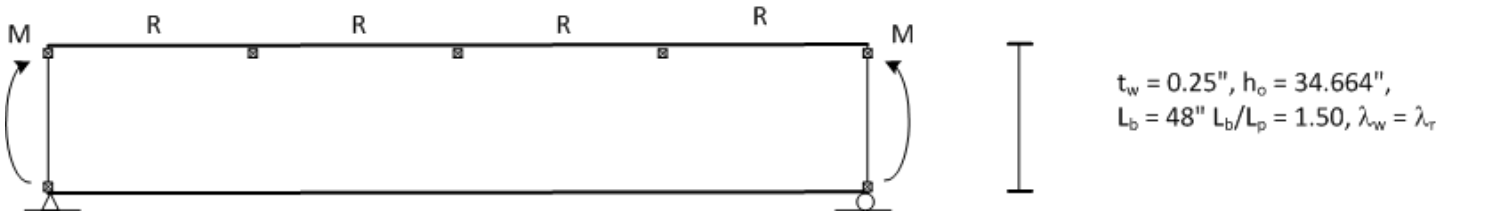

Figure 4.32: Case 2b

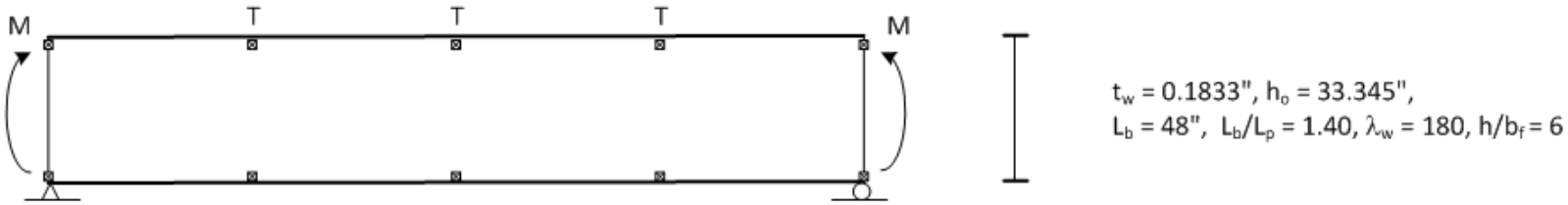

Figure 4.33: Case 3a

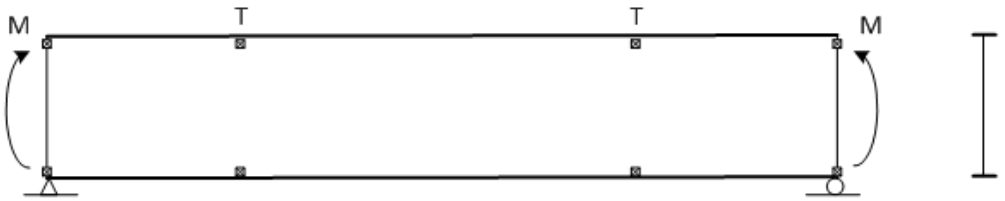

$t_w = 0.1833"$, $h_o = 33.345"$,
$L_b = 48"$, $96"$ & $48"$, $L_{b2}/L_p = 2.8$, $\lambda_w = 180$, $h/b_f = 6$

Figure 4.34: Case 3b

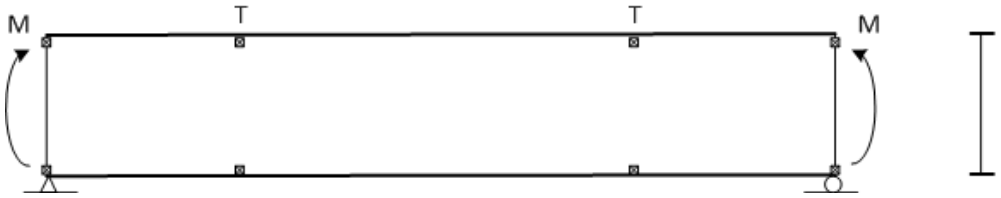

$t_w = 0.1833"$, $h_o = 33.345"$, $b_f = 6.6"$, $t_f = 0.2919"$
$L_b = 48"$, $96"$ & $48"$, $L_{b2}/L_p = 2.8$, $\lambda_w = 180$, $h/b_f = 5$

Figure 4.35: Case 3c

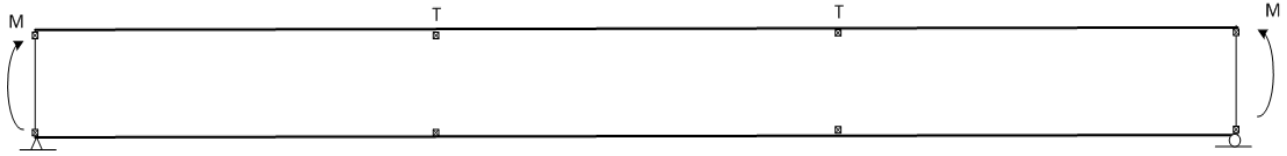

$t_w = 0.1833"$, $h_o = 33.345"$,
$L_b = 144"$, $L_b/L_r = 1.23$, $\lambda_w = 180$, $h/b_f = 6$

Figure 4.36: Case 3d

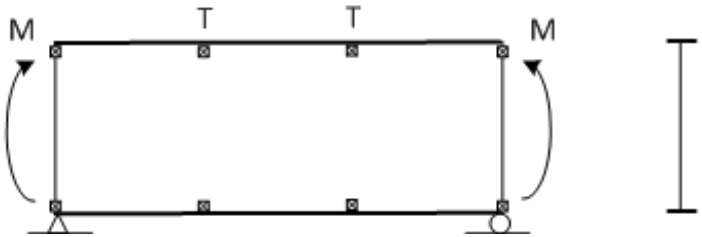

$t_w = 0.1833"$, $h_o = 33.345"$,
$L_b = 30"$, $L_b/L_p = 0.87$, $\lambda_w = 180$, $h/b_f = 6$

Figure 4.37: Case 3e

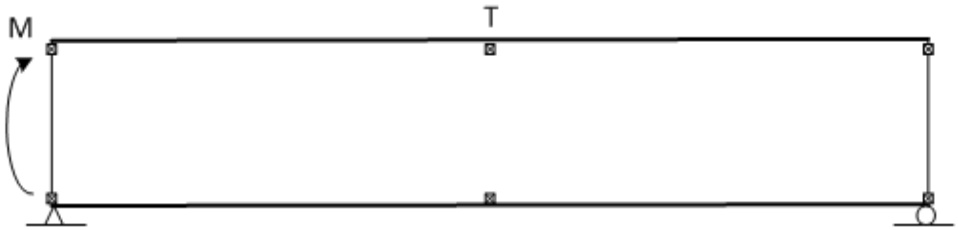

$t_w = 0.1833"$, $h_o = 33.345"$,
$L_b = 96"$, $L_b/L_p = 2.80$, $\lambda_w = 180$, $h/b_f = 6$

Figure 4.38: Case 3f

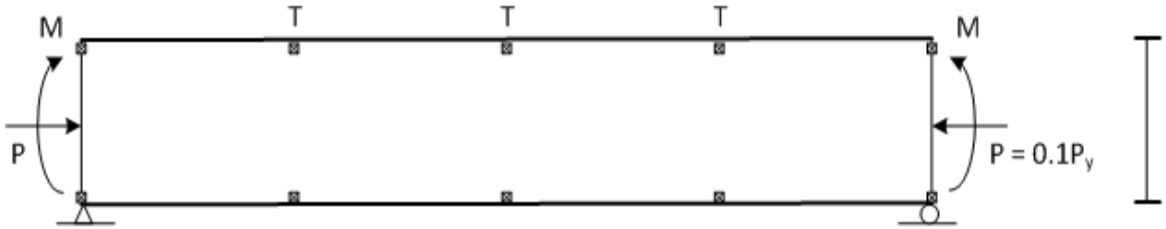

Figure 4.39: Case 3g

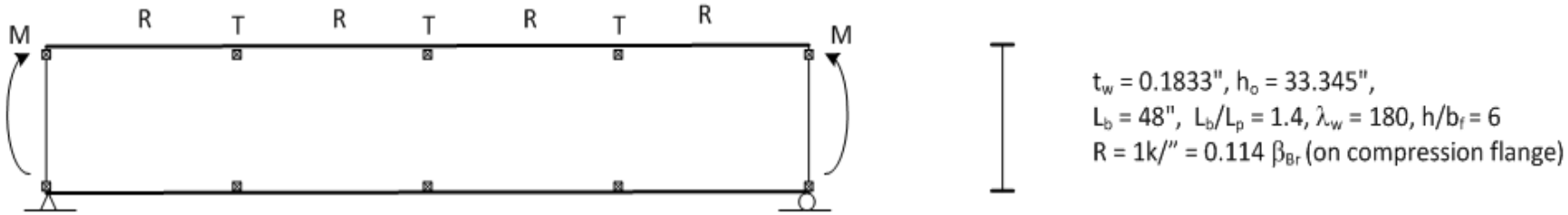

Figure 4.40: Case 3h

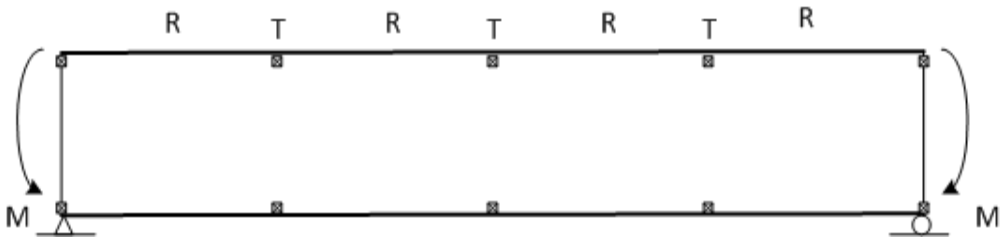

$t_w = 0.1833"$, $h_o = 33.345"$,
$L_b = 48"$, $L_b/L_p = 1.4$, $\lambda_w = 180$, $h/b_f = 6$
$R = 1k/" = 0.114\ \beta_{Br}$ (on tension flange)

Figure 4.41: Case 3j

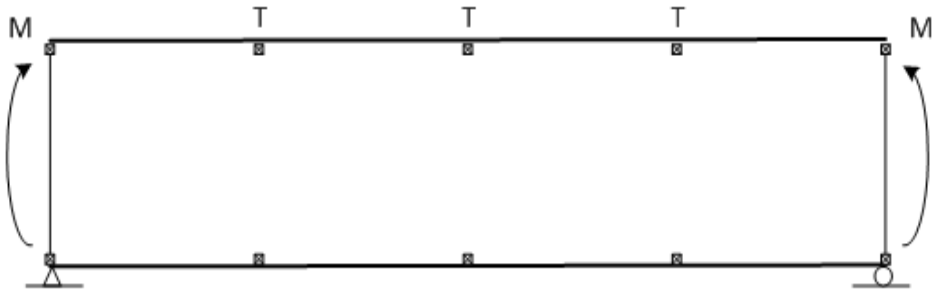

$t_w = 0.25"$, $h_o = 46.065"$,
$L_b = 48"$, $L_b/L_p = 1.61$, $\lambda_w = 183$, $h/b_f = 8.31$

Figure 4.42: Case 4a

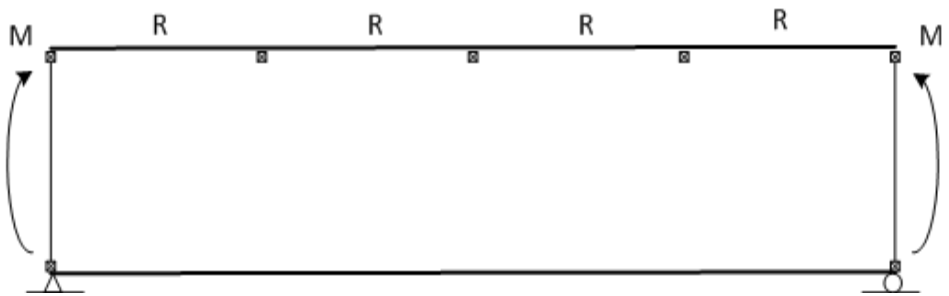

$t_w = 0.25"$, $h_o = 46.065"$,
$L_b = 48"$, $L_b/L_p = 1.61$, $\lambda_w = 183$, $h/b_f = 8.31$

Figure 4.43: Case 4b

4.6.2 Initial Imperfections

As was discussed extensively in Section 3.2.2.2, there are a number of initial imperfections that need to be considered to assess the true capacity of a member using a load-deflection solution. In theory, there are infinite possibilities for combinations of these imperfections that may have the most deleterious effect on any given member or brace. In this research and the results presented herein, it was decided to use imperfection patterns that were in accordance with those in the tolerances of the Code of Standard Practice (2010a) and the Metal Building Systems Manual (MBMA 2006). However, practically, the scope must be limited to a manageable number of imperfections with which to assess the capacity of member via simulations in Abaqus. Therefore, two general classes of imperfections were chosen:

1. An imperfection pattern that would cause the most deleterious effect on the member, and
2. An imperfection pattern that would drive the brace force demands.

More specifically, the “Type 1” imperfection introduced above is obtained by sweeping the compression flange between brace points where the maximum out-of-plane movement is limited by the COSP (2010a) and MBMA (2006). This imperfection pattern will generally create the critical demands on the member if the bracing stiffness is approaching that required for full bracing.

For “Type 2” imperfections, Wang and Helwig (2005) suggest that the largest brace demands are often realized for an initial imperfection pattern where the brace at the maximum moment location is displaced laterally (within construction tolerances) and all other bracing remains in a plumb configuration. This imperfection will tend to produce

the largest brace demands for bracing stiffness somewhat less than full bracing, since full bracing will result in buckling between brace points and thus, very little lateral movement directly at the brace.

Pursuant to the discussion above, all analyses are performed in Abaqus using these two general imperfection types and the capacity values reported in the subsequent plots will be the minimum capacity reached from either of these two imperfection patterns. For the plots showing brace force versus bracing stiffness, the imperfection Type 2 will be used to determine the maximum force demands likely to be experienced by the brace or bracing system.

The specific imperfection patterns employed in Abaqus are shown in the following figures. The x's in the figures represent locations of either internal bracing or the end supports.

- For Cases 1a, 1b, 2a, 2b, 3a, 3g, 3h, 3j, 4a, and 4b (Group 1), the critical beam imperfection (Type 1) is shown in Figure 4.44. The magnitude of the sweep is 1/1000 between brace points. The critical brace pattern (Type 2) is shown in Figure 4.45 where the center brace point is initially displaced 1/500 from the plumb geometry. Both figures are plan views where the movement is purely associated with the compression flange and the tension flange is assumed to remain straight.

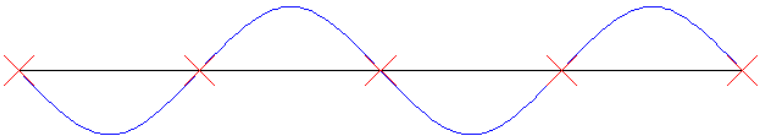

Figure 4.44: Critical member imperfection pattern (Group 1)

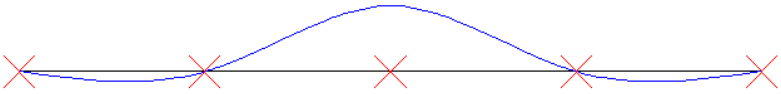

Figure 4.45: Critical brace imperfection pattern (Group 1)

- For Cases 1c, 3d, and 3e (Group 2), the critical beam imperfection (Type 1) is shown in Figure 4.46. The magnitude of the sweep is 1/1000 between brace points. The critical brace pattern (Type 2) is shown in Figure 4.47 where the left brace point is initially displaced 1/500 from the plumb geometry. Both figures are plan views where the movement is purely associated with the compression flange and the tension flange is assumed to remain straight.

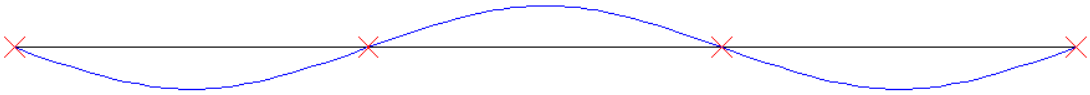

Figure 4.46: Critical member imperfection pattern (Group 2)

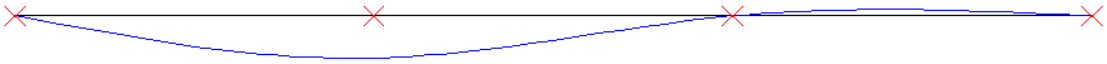

Figure 4.47: Critical brace imperfection pattern (Group 2)

- For Cases 1d, 1e, and 3f (Group 3), the critical beam imperfection (Type 1) is shown in Figure 4.48. Since these members are subjected to a maximum moment on one end and zero moment on the other, the sweep of 1/1000 between brace points is only applied over the compression side of the top flange. The critical brace pattern (Type 2) is shown in Figure 4.49 where the middle brace point is initially displaced 1/500 from the plumb geometry on the compression flange.

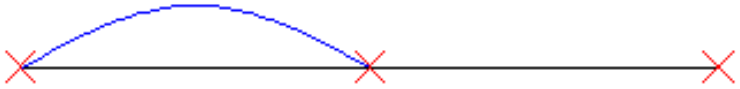

Figure 4.48: Critical member imperfection pattern (Group 3)

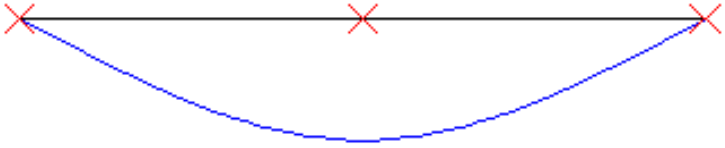

Figure 4.49: Critical brace imperfection pattern (Group 3)

- For Cases 3b and 3c (Group 4), the critical beam imperfection (Type 1) is shown in Figure 4.50. The magnitude of the sweep is 1/1000 between brace points. The critical brace pattern (Type 2) is shown in Figure 4.51 where the brace points are initially displaced 1/500 from the plumb geometry. Both figures are plan views where the movement is purely associated with the compression flange and the tension flange is assumed to remain straight.

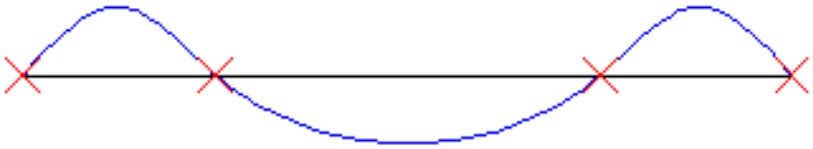

Figure 4.50: Critical member imperfection pattern (Group 4)

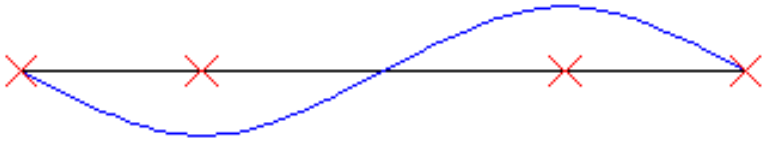

Figure 4.51: Critical brace imperfection pattern (Group 4)

4.6.3 Full Bracing Requirement

As is supported in the following sections, the recommendation from this research will be that the stiffness required to reach full bracing should be provided. This recommendation comes from the fact that the brace forces tend to reduce dramatically as full bracing is approached, since the member or section begins to become more critical between brace points. Additionally, the imperfection patterns discussed above tend to maximize

demands on the stiffness and strength requirements as the full bracing limit is approached.

In this thesis, it will be suggested that the required bracing stiffness shall be the summation of the bracing stiffness required to reach 95% and 90% of the member's rigid braced strength as determined from SINBAD. These specific values were chosen given the following reasoning:

- In general, locating the specific bracing stiffness at the rigidly braced capacity of the member may prove difficult since the plateau of the knuckle curve is flat, where large variations in stiffness may not significantly vary the member's capacity. Therefore, using the stiffness associated with 95% of the rigidly braced strength provides a much easier stiffness value to target using SINBAD.
- 90% was selected as the next metric, since having a stiffness value slightly less than the 95% capacity provides a basic assessment of the shape of the knuckle curve, and more importantly, lets the designer know if he is specifically on the "knuckle".

In the limit that the bracing capacity to brace stiffness relation is a very steep slope, than this procedure essentially provides 2 times the stiffness required to reach 95% of the member's capacity. On the contrary, if one is on or near the plateau of the knuckle curve, than the reduction in stiffness required to reach 90% from 95% may be quite significant, essentially providing only a slight addition to the 95% rigidly braced capacity and thus, only slightly increasing the required bracing stiffness.

It may seem slightly out-of-place to present the recommendation before any results have been provided, but in this case, it will be useful to see where the results are heading

through the presentation of data. At the end of this thesis, the recommendations will be summarized such that the reader is left with a clear understanding of how to use SINBAD to accurately determine the requirements for bracing strength and stiffness.

4.6.4 Members Subjected to Uniform Bending

This section explores how SINBAD compares to simulation results for members subjected to uniform bending. Three different subsections will be presented, categorizing the results into members buckling in the elastic, inelastic, and plastic region. The reader is referred to Table 4.2 and the figures immediately following the table for a tabular and graphical description of the specific member being analyzed.

4.6.4.1 Elastic Buckling Region

Case 1c:

Figure 4.52 shows the results for a compact web member loaded under uniform moment with two equally-spaced interior torsional braces; Case 1c as defined in Table 4.2. The unbraced length, L_b = 144”, places this section in the inelastic buckling region for the given cross-section profile.

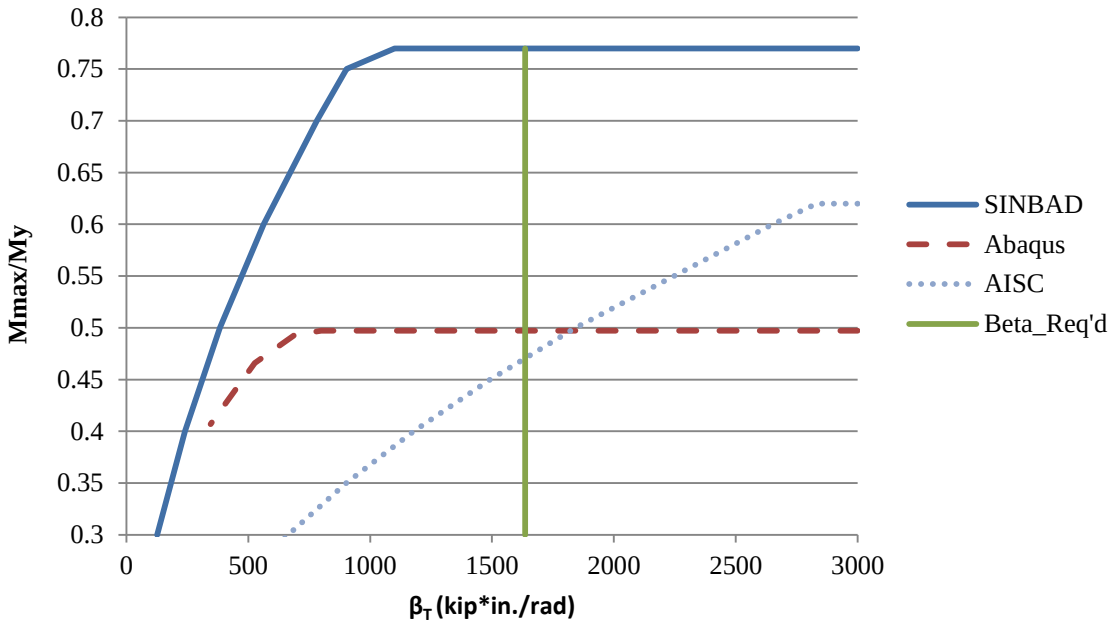

Figure 4.52: Case 1c; compact web section, uniform moment, 2 torsional braces

In the legend for Figure 4.52 (and all subsequent legends in this section), the following nomenclature is used:

- "SINBAD" refers to the results for the strength versus ideal bracing stiffness from an inelastic eigenvalue buckling analysis performed in SINBAD.
- "Abaqus" refers to the results for the strength versus bracing stiffness from a load-deflection simulation including the application of initial imperfections from Abaqus.
- "AISC" is the stiffness requirement from AISC for torsional bracing or relative bracing based on the most refined requirements presented as detailed in the Commentary to Appendix 6 (AISC 2010b) and discussed in Chapter 2.

- "Beta_Req'd" (or $\beta_{Req'd}$ as shown in the text of this thesis) denotes the proposed requirement for bracing stiffness. This metric was highlighted in the previous section and is discussed throughout this section.

The first item of note from Figure 4.52 is the difference in the strengths reached using rigid bracing from SINBAD and the simulation models. In this case, SINBAD over-predicts the capacity reached via the simulation by 50%. This occurs because the member begins to develop significant out-of-plane displacements as the limit load is reached in the Abaqus model. If one couples this knowledge with the given residual stress of 0.3*F_y in compression at the flange tips, the member actually begins to yield, despite the failure being predicted as elastic lateral-torsional buckling. This may suggest that the residual stresses in the experiments used to determine the AISC LTB curves may not be as high as those selected and modeled in the simulation. Despite the difference in capacity, the amount of stiffness required for SINBAD to reach the fully braced capacity of the section lies in the same region as that predicted from Abaqus. Again, SINBAD is an approximation and therefore, will develop inherent difference between solutions as compared to experimental or simulation results.

When looking at the bracing requirement for a particular load level, say at M/M_y = 0.6, Abaqus would suggest that the member could not support this load level. The prediction for the ideal bracing requirement from SINBAD is closer to 600 kip*in./rad. However, to keep brace point displacements manageable enough to control the brace force requirements, it was discussed earlier that some multiple of the ideal stiffness would be required. The curve labeled $\beta_{Req'd}$ (which is based on the bracing stiffness required to reach 95% of the rigidly-braced capacity from SINBAD plus the stiffness required to reach 90% of the rigidly-braced capacity from SINBAD), suggests that a stiffness closer

to 1600 kip*in./rad would be required for each brace. The requirements from AISC is around 2600 kip*in./rad per brace.

A plot of the brace force as a percentage of the applied moment is shown in Figure 4.53. Note that for a $\beta_{Req'd}$ = 1600 kip*in./rad, the brace force demands are on the order of 1.5-2%.

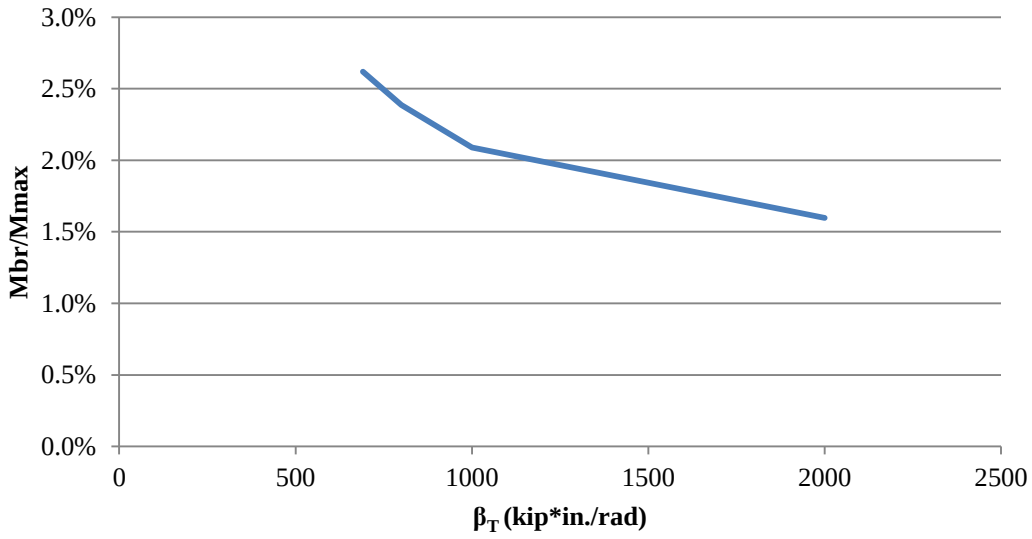

Figure 4.53: Case 1c; brace forces

One of the reasons that the AISC prediction is high relative to the simulation is that even though the Specification equations are based on Ojalvo's derivation for the theoretically exact bracing requirements, the AISC equations ignore the contribution of the member to resist brace point movement (Yura 2001). That is, all out-of-plane displacements must be resisted by the provided bracing, with no consideration of the member's own inherent ability to resist brace point movement. The two plots from SINBAD (including both the

ideal stiffness and the scaled ideal stiffness) consider the member's ability to resist twist of its own section.

Case 3d:

Case 3d is similar to Case 1c in the sense that the type of bracing and loading have stayed the same, yet this case features a deeper, slender web. Figure 4.54 shows the results for the stiffness requirements for Case 3d. As in Case 1c, the capacity reached by SINBAD is higher than that achieved in the simulation yet the level of stiffness required to reach the rigidly-braced capacity in either analysis is roughly the same.

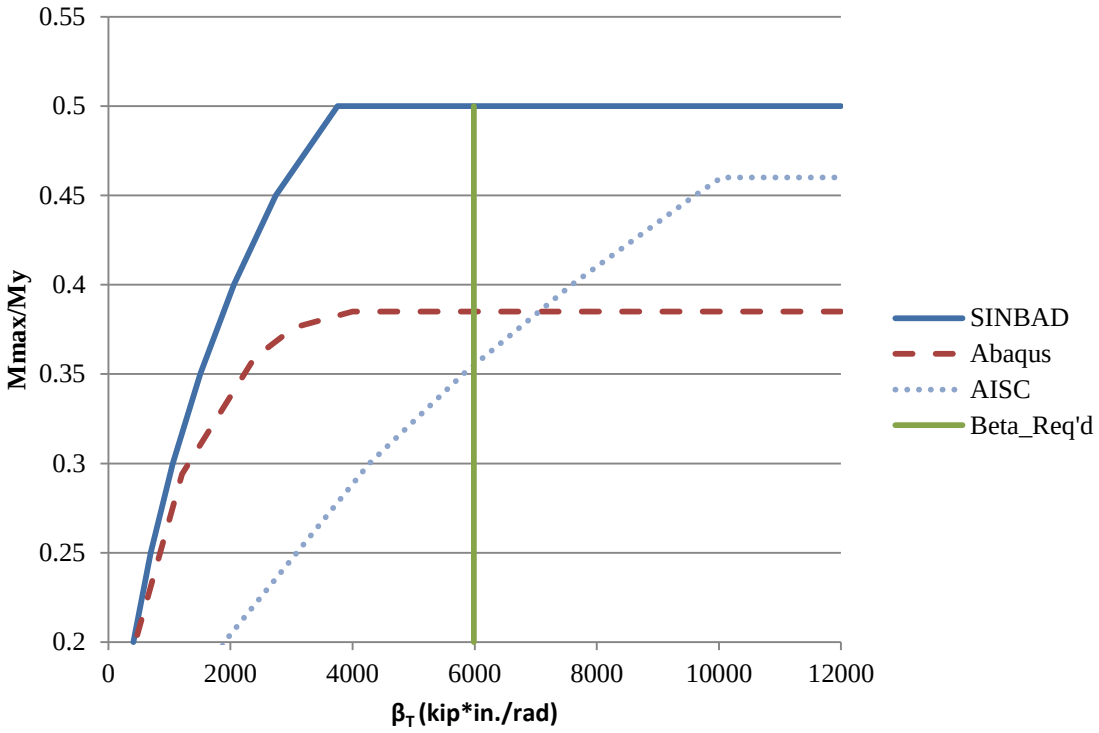

Figure 4.54: Case 3d; slender web section, uniform moment, 2 torsional braces

Figure 4.54 shows that AISC's prediction for the stiffness requirements when the member buckles elastically is generally conservative. However, for lower levels of

applied load, the AISC requirements generally allow for less bracing stiffness as compared to $\beta_{Req'd}$. A plot of the normalized brace force is shown in Figure 4.55 where the normalized brace force is around 2.5% for $\beta_{Req'd}$.

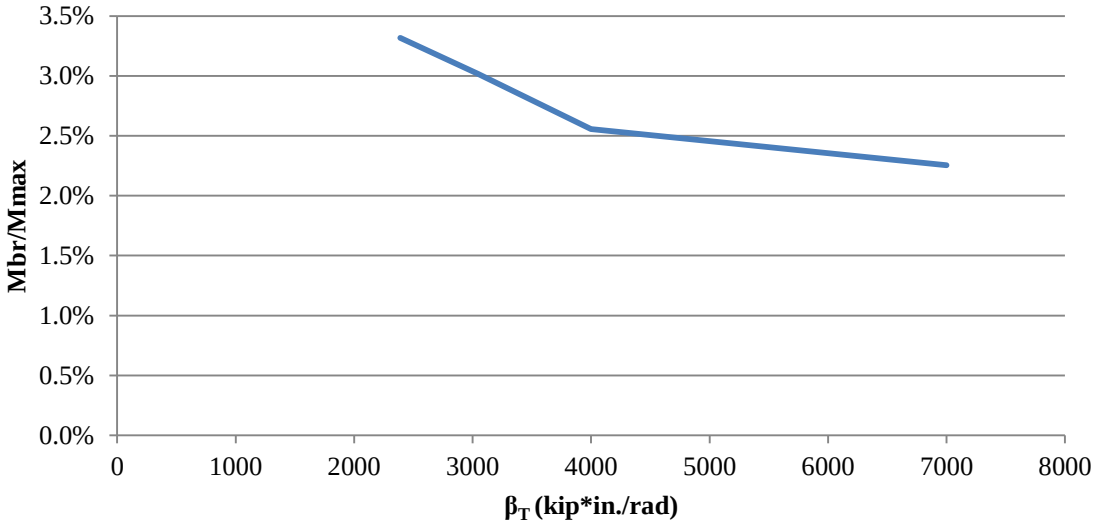

Figure 4.55: Case 3d; brace forces

4.6.4.2 Inelastic Buckling Region

This subsection presents the largest set of results and features requirements torsional bracing and lateral bracing for the full range of web depths tested.

Case 1a:

Case 1a is a compact web section subjected to uniform moment and having a brace spacing that places the member in the inelastic buckling region. The plot of capacity versus stiffness for this example is shown in Figure 4.56.The strengths reached via SINBAD versus Abaqus are close aligned except for the gradual rise in capacity with bracing stiffness from Abaqus as the bracing stiffness is increased. Despite this slow increase in capacity, the recommendation, $\beta_{Req'd}$ = 1600 kip*in./rad still allows the

Abaqus model to reach roughly 90-95% of its capacity. Considering the magnitude of worst-case initial imperfections and the application of residual stresses that may also be conservative, it is the author's suggestion that providing bracing such that the member can reach 90-95% of its rigidly-braced capacity is sufficient.

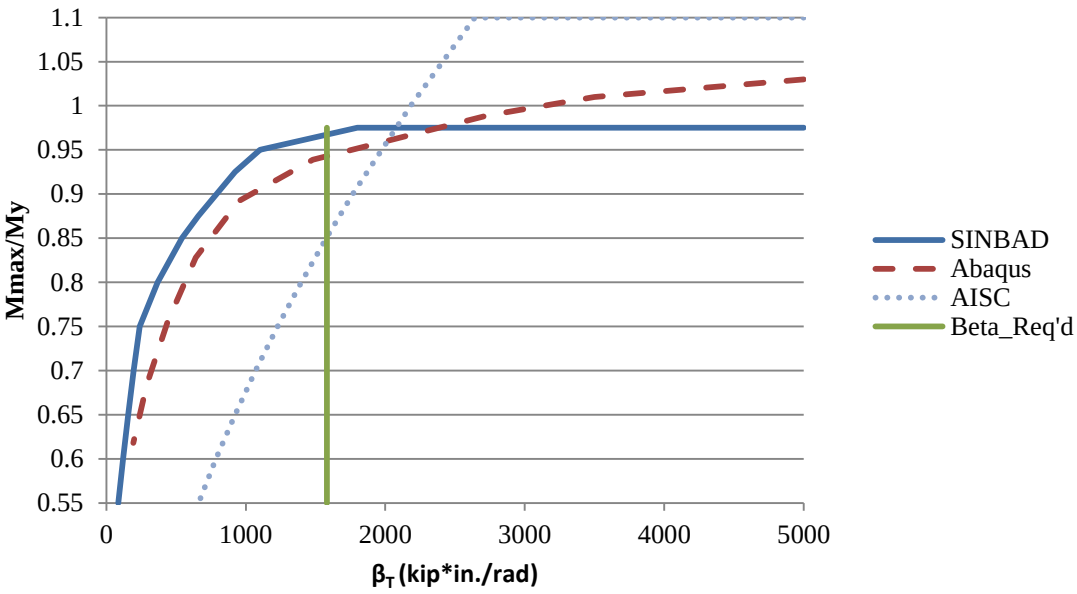

Figure 4.56: Case 1a; compact web section, uniform moment, 3 torsional braces

A plot of the normalized brace forces are shown in Figure 4.57. One will note that the percentage of brace force as compared to the maximum moment applied on the span is around 2% for the bracing stiffness recommended from Figure 4.56. Contrary to what is shown in other plots, there is an increase in brace force as the bracing stiffness approaches full bracing. This can be attributed to the fact that with small level of bracing stiffness, the member moves laterally where the compression flange essentially moves in a half-sine wave shape between end points. As the bracing stiffness becomes larger, the member moves laterally, but the braces begin to restrain the movement more and

more. Ultimately, one may expect the forces to plateau or even decrease as very large levels of stiffness are achieved, since the failure mode or buckling mode will be buckling between braces with very little brace point movement.

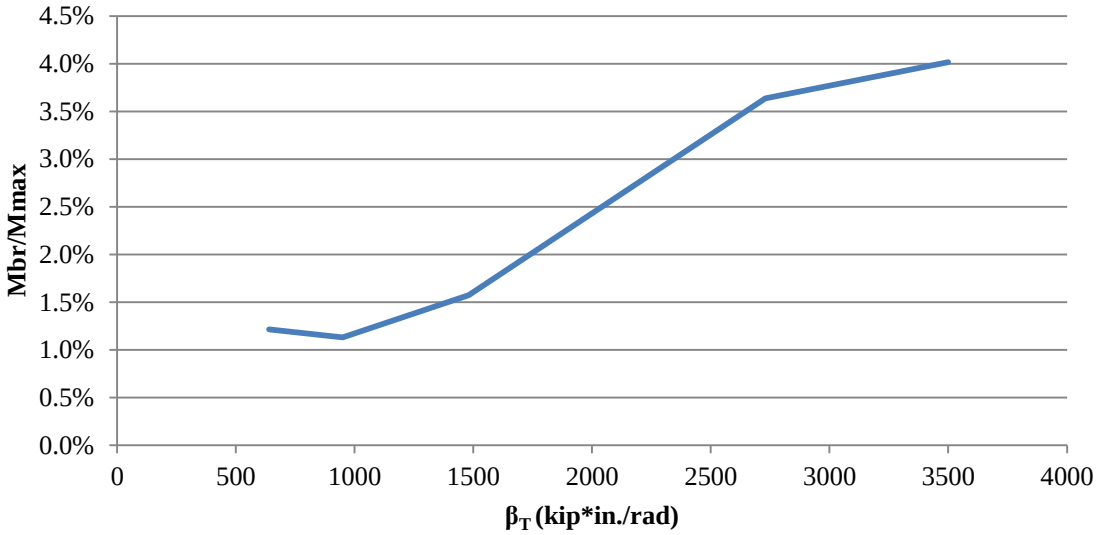

Figure 4.57: Case 1a; brace forces

Case 1b:

Figure 4.58, based on Case 1b from Table 4.2, shows an example similar to Case 1a except that the torsional bracing has been replaced with relative bracing. That is, relative springs are provided between each brace point on the compression flange.

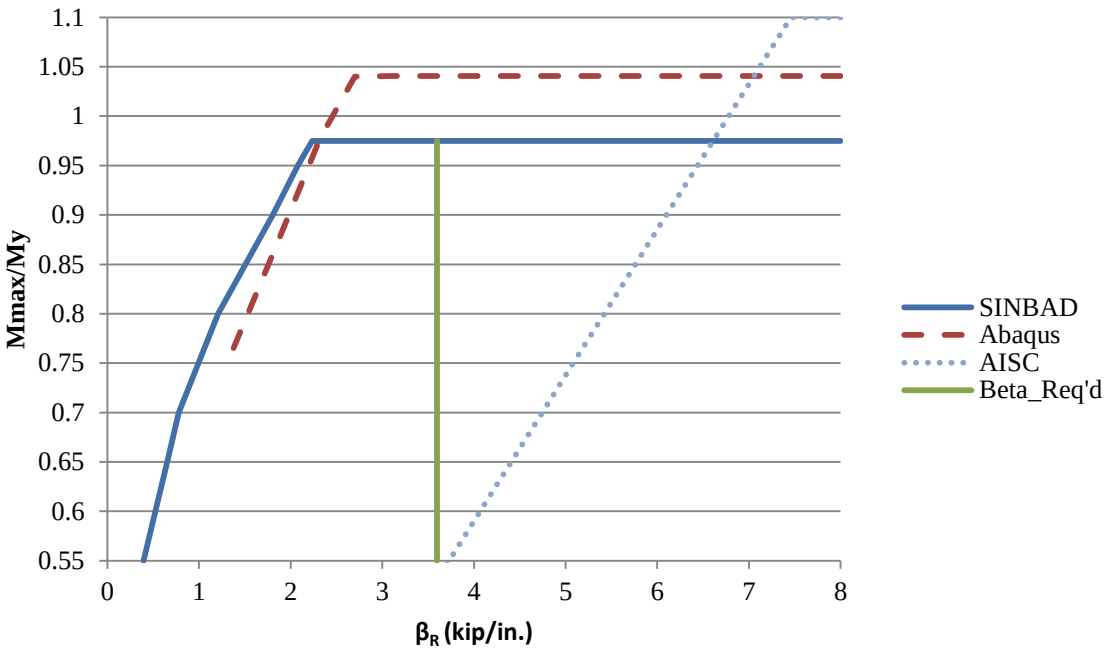

Figure 4.58: Case 1b; compact web section, uniform moment, 4 relative braces

Once again, the simulation results suggest a higher load when the braces are rigid as compared to SINBAD. Also, again one will notice that the AISC Specification requirements are predicting higher stiffness requirements when compared to SINBAD or the simulations. Finally, $\beta_{Req'd}$ provides a level of stiffness that would correspond to full bracing for both the Abaqus and SINBAD models.

Figure 4.59 is a plot of the shear force in the relative brace as a percentage of the equivalent flange force at the location of the center brace (taken as M/ho). For full bracing as shown in Figure 4.58, the brace shear force would be on the order of 2-2.5% yet drops below 1.5% if the required stiffness is used.

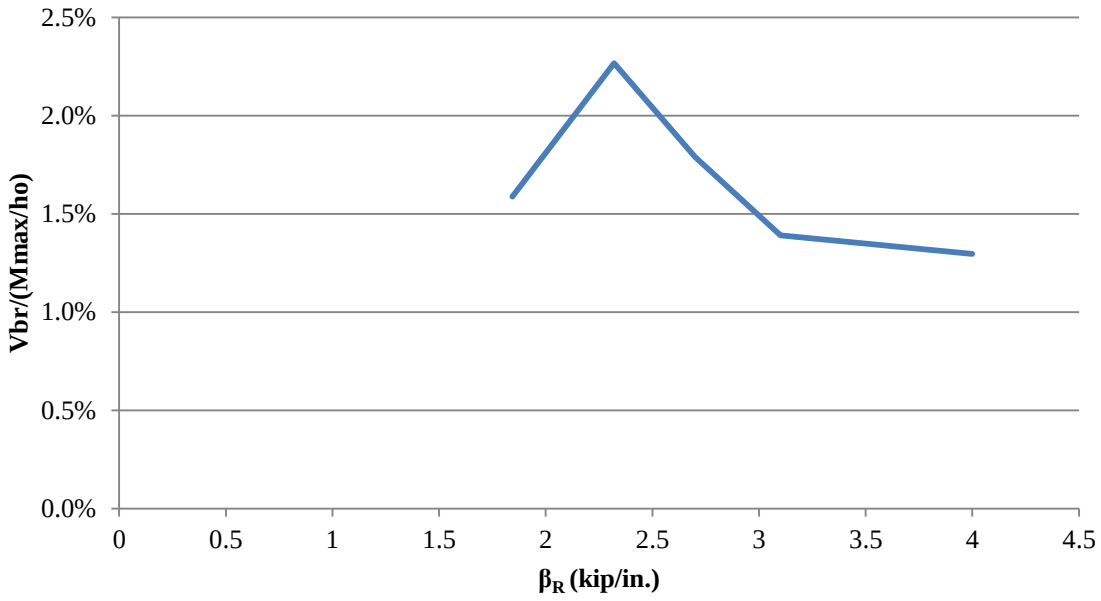

Figure 4.59: Case 1b; brace forces

Case 2a:

Figure 4.60 shows the results of Case 2a. The member has four unbraced lengths, each 48” long (in the inelastic buckling region for this cross-section). There are three, equally spaced interior torsional braces provided and the member is loaded under uniform moment.

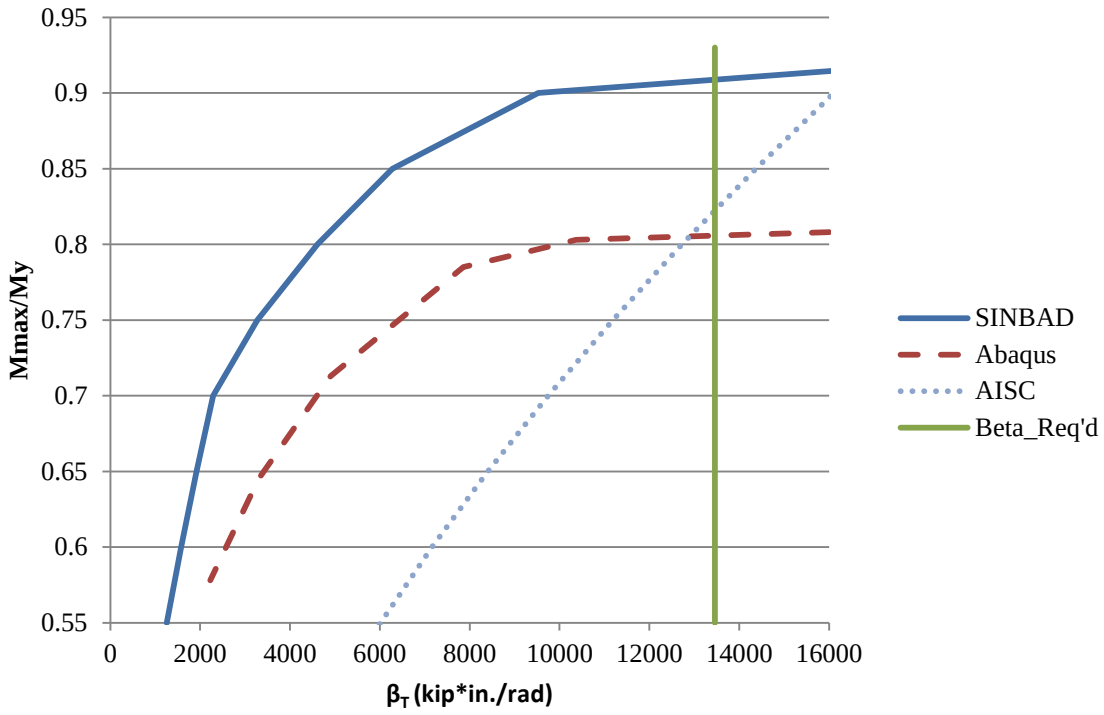

Figure 4.60: Case 2a; non-compact web section, uniform moment, 3 torsional braces

Case 2a is the first plot of many where the strength reached by rigid bracing differs greatly between the results from the simulation and those from SINBAD. As the web becomes more slender, a two-fold effect is felt on the member:

- Stresses in the web can cause the web to buckle which then sheds load to the adjacent flanges, and
- The magnitude of the initial imperfections begin to exert a greater influence on the distribution of the flange stress, potentially causing earlier yielding than may be predicted using an eigenvalue buckling solution.

Figure 4.61 gives one an idea of the extent to which a member may be affected by these items, as determined from Abaqus. In this case, the equivalent plastic strain is contoured

at the maximum load on the member with rigid bracing. Any part of the figure that is not dark blue has yielded; suggesting that almost half of the compression flange has yielded within each unbraced length.

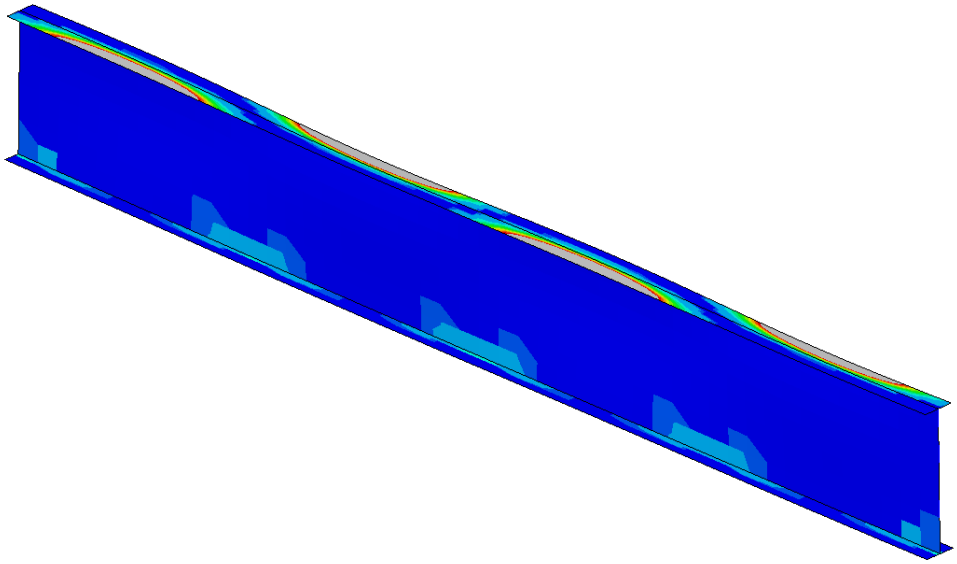

Figure 4.61: Contoured equivalent plastic strain, non-compact web section, uniform moment, rigid bracing

Another aspect to consider when comparing the lower simulation result to the result from SINBAD is that the imperfections assumed may not be realistic for physical members. If one compares simulation results versus an AISC LTB curve, the simulation results often come up lower than the AISC values. This happens as a result of the AISC equations being a fit to experimental data that inherently, do not have the largest magnitude imperfections at the most critical location. On a similar note, the residual stresses also may not be the same as those tested in the laboratory. These items along with testing setup and other uncontrolled experimental variables cause the simulation results to differ from experimental results.

Despite the limitations discussed above, Figure 4.60 shows that $\beta_{Req'd}$ provides an appropriate level of stiffness to develop the fully-braced capacity of the section.

Case 2b:

The counterpart to Figure 4.60 using relative bracing is shown in Figure 4.62. Again it is worth noting the large difference in the strength predicted by Abaqus and SINBAD (SINBAD is almost 18% higher than the simulation). However, one may notice that despite the large relative difference in rigid brace strengths, SINBAD does an appropriate job of predicting the required bracing stiffness through $\beta_{Req'd}$ and provides substantial economy as compared to the AISC equations as the capacity of the structure is reached.

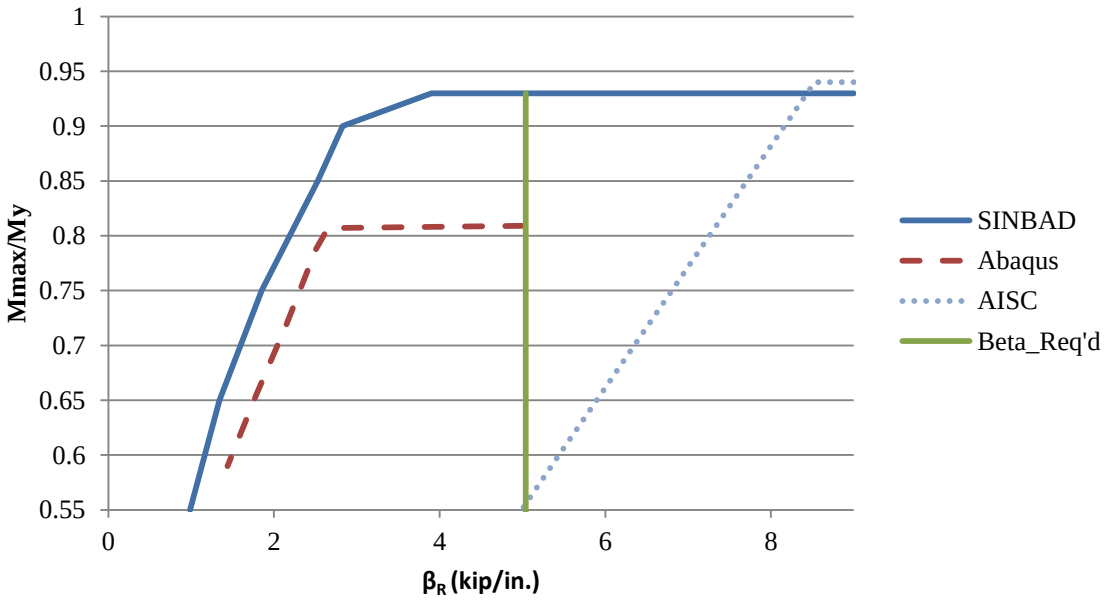

Figure 4.62: Case 2b; non-compact web section, uniform moment, 4 relative braces

Figure 4.63 shows the brace shear force as a percentage of the equivalent flange force for the center brace. At a $\beta_{Req'd}$ around 5 kip/in., the brace shear force is on the order of 1% of M/h_o.

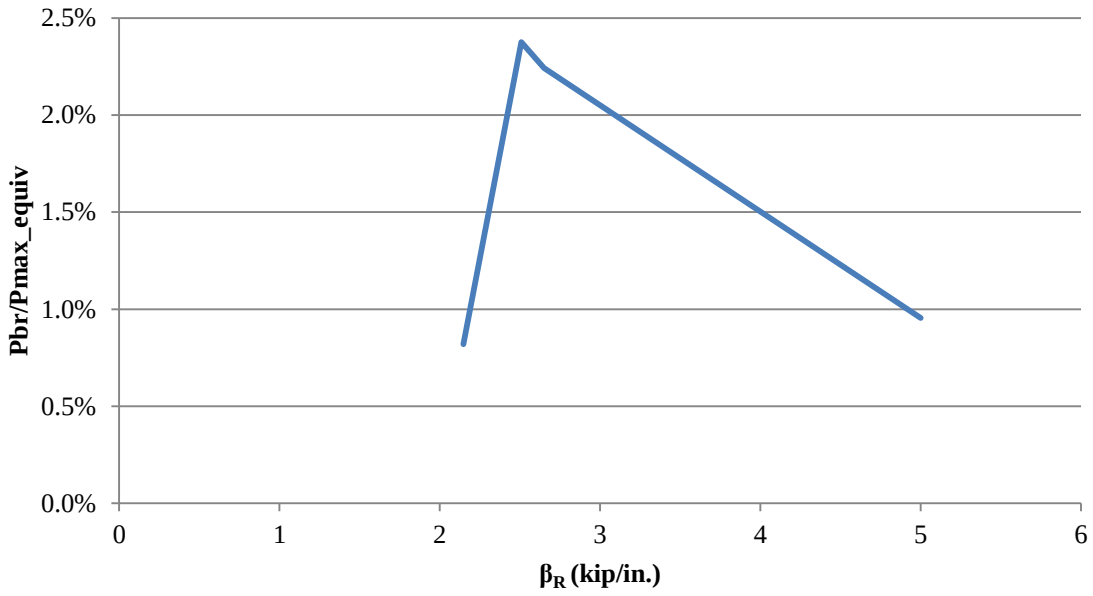

Figure 4.63: Case 2b; brace forces

Case 3a:

Case 3a is the first slender-web case, with results shown in Figure 4.64, and is for a four unbraced length member with three equally spaced torsional braces.

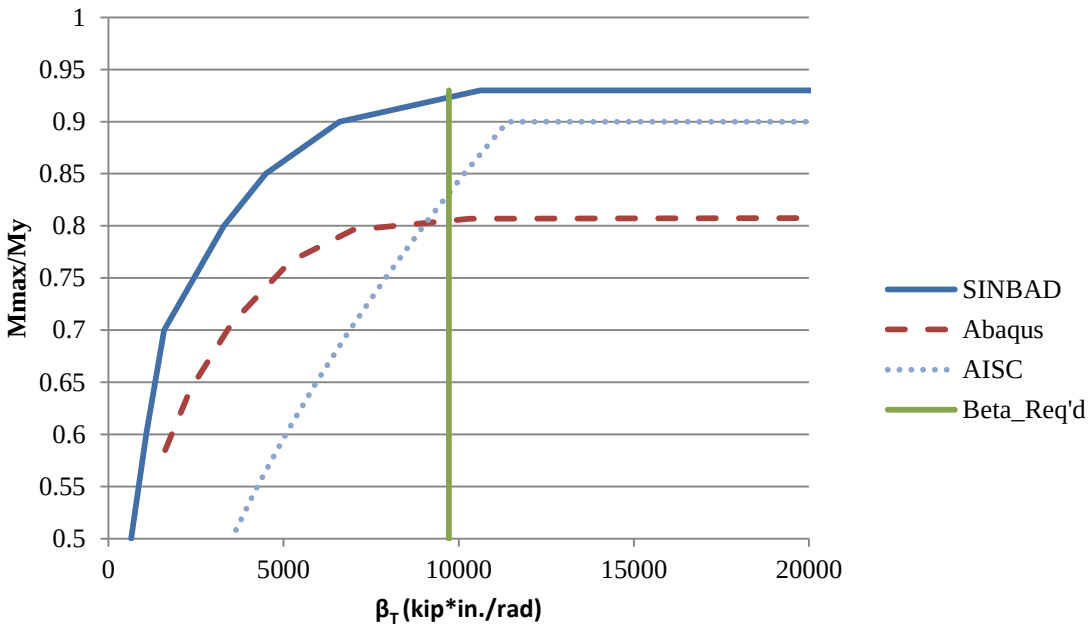

Figure 4.64: Case 3a; slender web section, uniform moment, 3 torsional braces

As discussed previously and shown again here in Figure 4.64, the rigid braced strength reached by Abaqus and SINBAD differ. For slender web cases, an additional complication enters the picture; namely, the influence of residual stresses. Unlike with compact or non-compact web sections, the typical residual stresses applied to slender web sections must be adjusted to account for plate buckling. This concept was discussed in the section on residual stresses in the context that the residual stresses must be limited to the compressive buckling stress of a simply-supported plate. In the field, if stresses were to develop beyond the web plate's buckling capacity, then the web would buckle, relieving the stress in the web and redistributing it to other portions of the member. For general slender members, one is left to sort out the effects due to:

- Residual stresses and applied stresses in the web causing the web plate to buckle and then redistribute the stresses from the web to the flanges and

- Initial imperfections amplifying the stresses in the flanges.

These two items must be accounted for if one expects an eigenvalue buckling solution to pick up these phenomena which are inherently captured via a load-deflection analysis (be it from simulations or a physical structure). The AISC Specification (2010b) attempts to account for the local web buckling and subsequent stress redistribution through the application of R_{pg}.

It is also worth pointing out that AISC's Appendix 6 equations provides adequate stiffness for Case 3a as the limit load of the structure is reached. Also, if one were to consider that the initial imperfections and residual stresses are not as deleterious as modeled in the simulation, one may expect the simulation curve to rise vertically to be closer to SINBAD's prediction. Additionally, $\beta_{Req'd}$ also provides an adequate level of stiffness to develop the fully braced capacity of the member.

A plot of the brace force as a percentage of applied moment is shown in Figure 4.65. For a $\beta_{Req'd}$ just under 10000 kip*in./rad, around 1.5% can be expected for the normalized brace force.

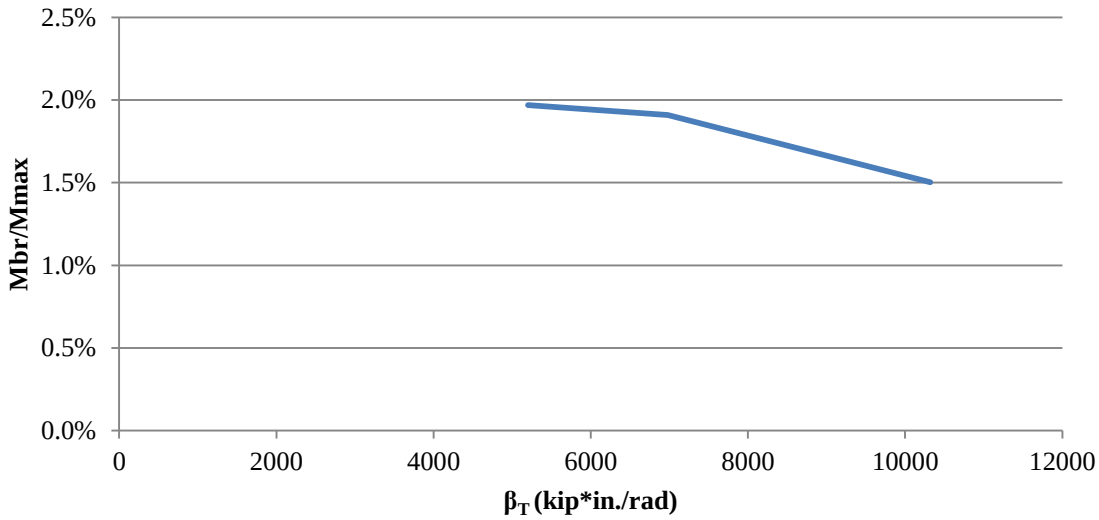

Figure 4.65: Case 3a; brace forces

Case 4a:

This section and the one immediately following also explore how SINBAD compares to simulation results for members with webs that are classified via Chapter B (AISC 2010b) as slender. However, the cross-section properties of Case 4 place it truly outside of the recommended geometry suggested in DG 25. For example, h/b_f for this case is equal to 8.3, where the suggested limit is 7 (Kaehler, White, and Kim 2011). Therefore, only two examples are presented for this particular web depth with emphasis solely on the effect that the web depth has on the comparison of SINBAD to Abaqus.

Figures 4.66 and 4.67 show the capacity versus bracing stiffness and normalized brace force versus bracing stiffness for Case 4a, respectively. Again, the capacity reached by Abaqus is less than that from SINBAD (and more pronounced) due to the same reasons mentioned above. For a $\beta_{Req'd}$ around 27000 kip*in./rad, the fully-braced capacity of the

member can be reached either using SINBAD or Abaqus and the normalized brace force is just under 2%.

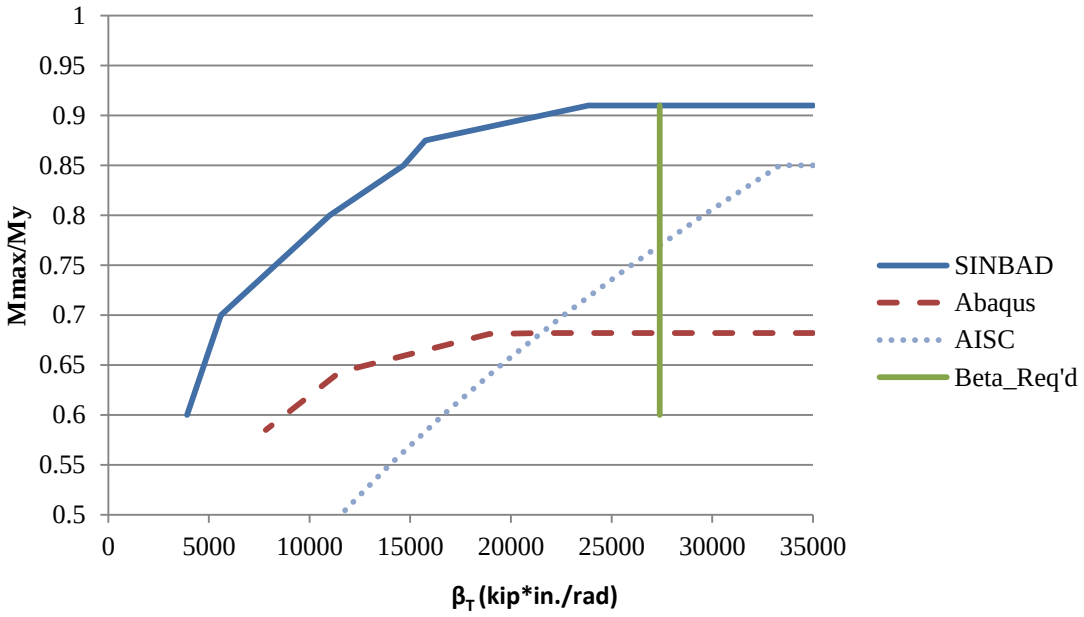

Figure 4.66: Case 4a; slender web section, uniform moment, 3 torsional braces

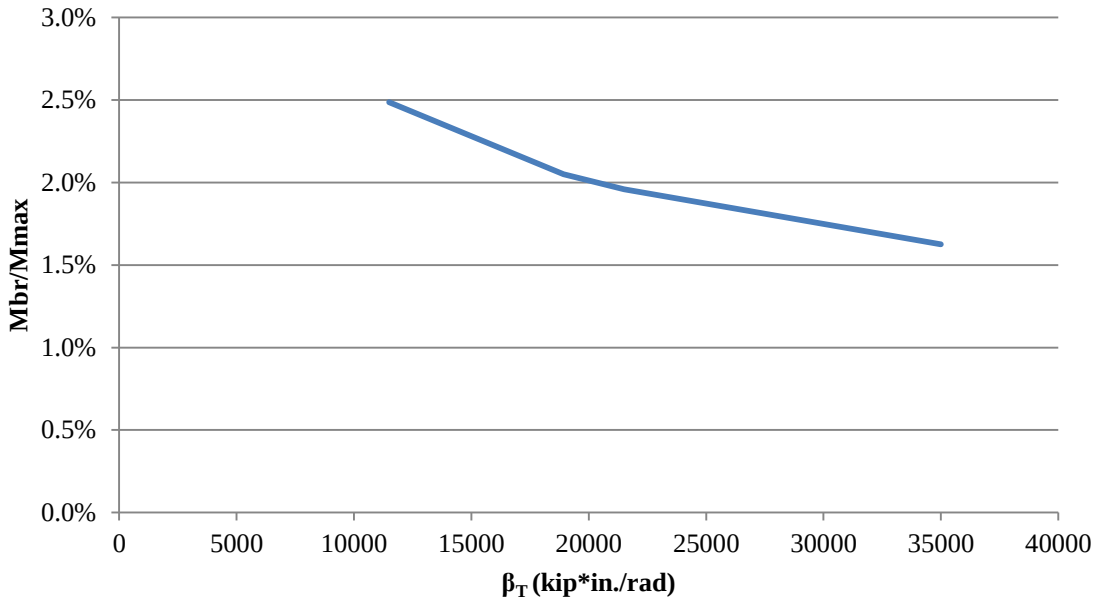

Figure 4.67: Case 4a; brace forces

Case 4b:

Case 4b is similar to Case 4a except that the three torsional braces have been replaced with four relative torsional braces along the compression flange. The stiffness and force plots are shown below in Figures 4.68 and 4.69. SINBAD again predicts a higher capacity, yet the SINBAD and Abaqus models both suggest similar levels of stiffness in order to reach full bracing. While $\beta_{Req'd}$ appears to provide overly-conservative results, the bracing stiffness required is less than that suggested from the AISC equations. The normalized brace forces associated with $\beta_{Req'd}$ are on the order of 0.5%.

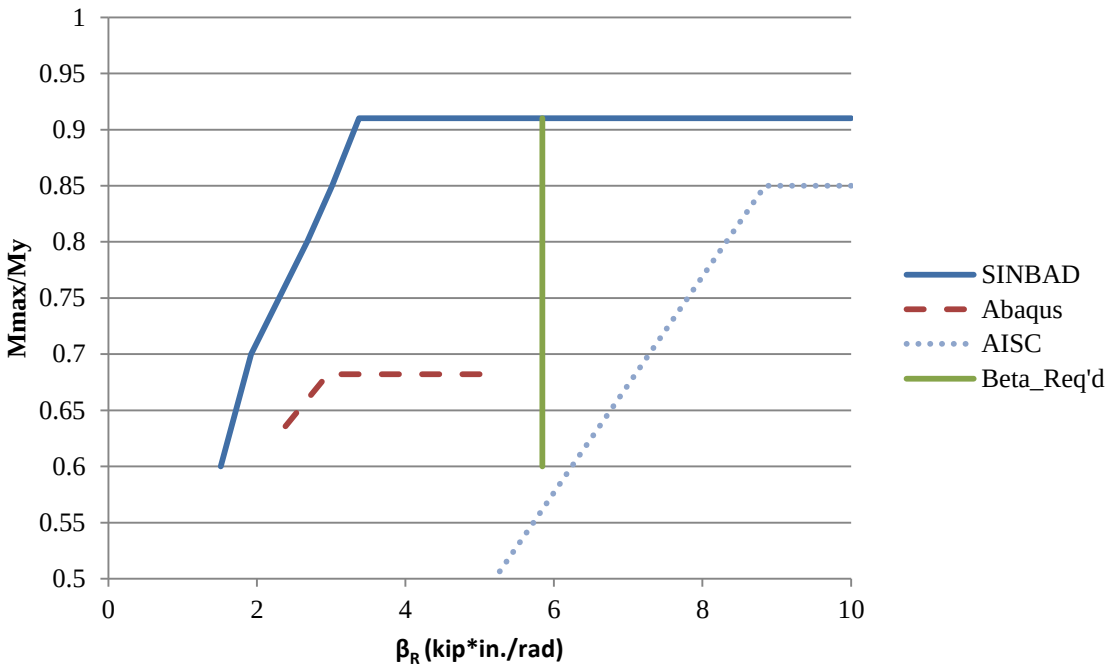

Figure 4.68: Case 4b; slender web section, uniform moment, 4 relative braces

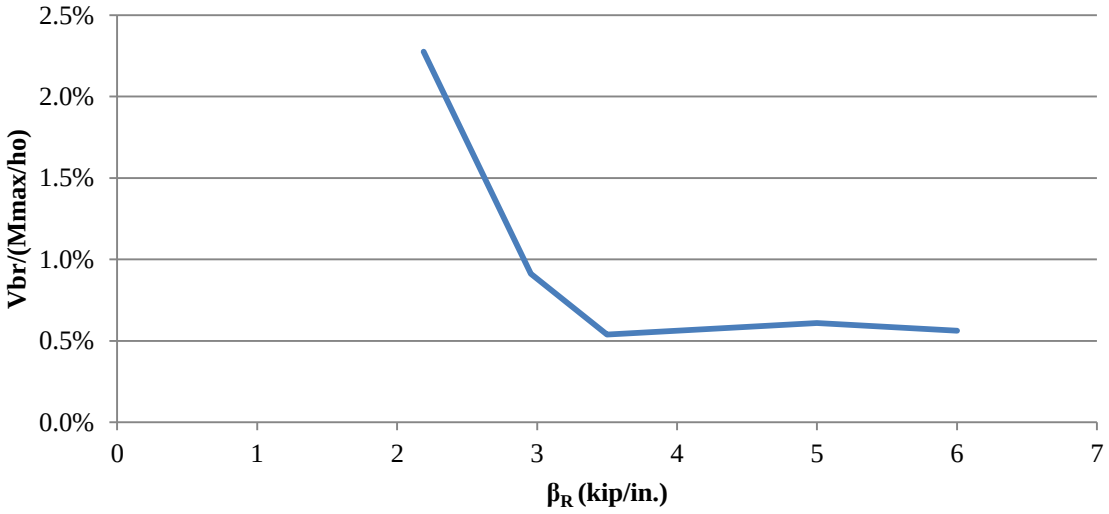

Figure 4.69: Case 4b; brace forces

4.6.4.3 Plastic Buckling Region

Case 3e:

Case 3e is the one example in this research that looks at the bracing requirements for developing full bracing for a member with an unbraced length in the plastic buckling region (with L_b less than L_p). Figure 4.70 shows the capacity of the section versus the applied bracing stiffness. Here, SINBAD over-predicts the solution from Abaqus, yet still suggests a $\beta_{Req'd}$ that reaches full bracing considering the simulation. The marked increase in capacity seen below from Abaqus to SINBAD can be attributed to the same reasoning given in Case 3a.

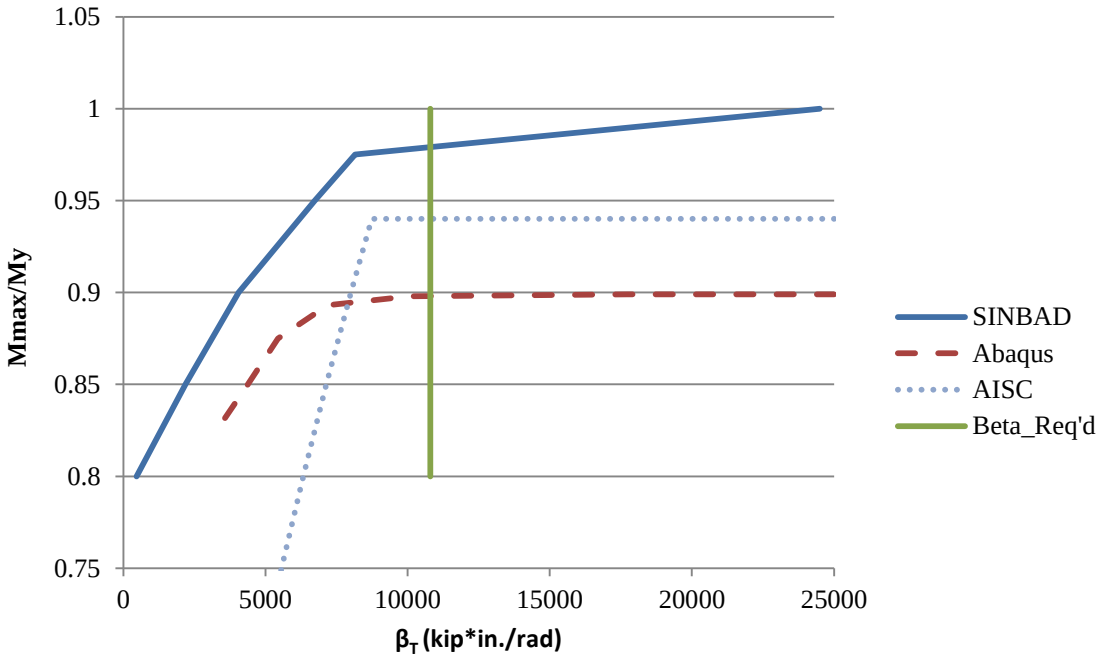

Figure 4.70: Case 3e; slender web section, uniform moment, 3 relative braces, plastic buckling

The brace force as a percentage of the applied moment is shown in Figure 4.71. For a given $\beta_{Req'd}$ of around 11000 kip*in./rad, the brace strength demand would be a normalized 1%.

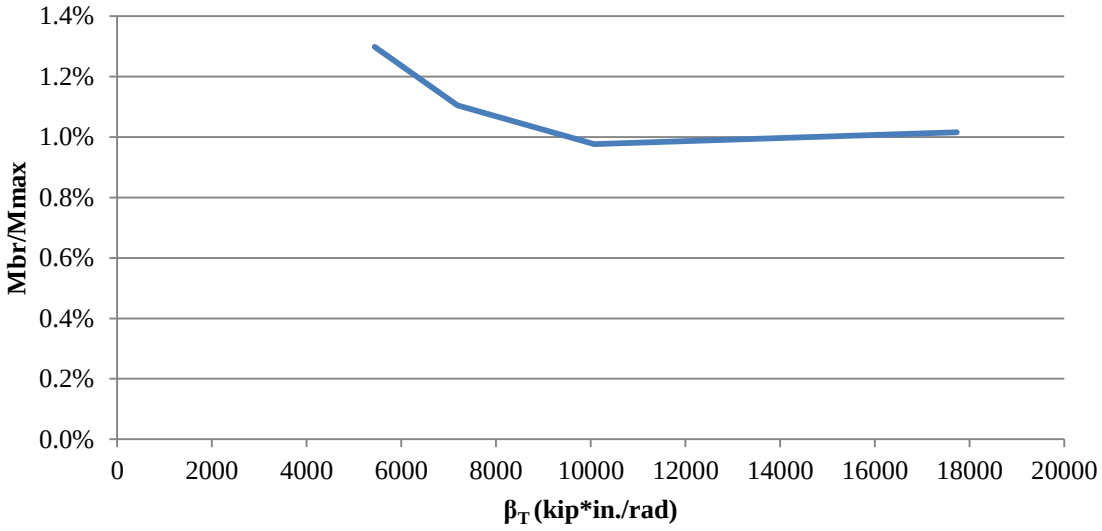

Figure 4.71: Case 3e; brace forces

4.6.5 Members Subjected to a Moment Gradient

Three examples are shown in this section for the bracing requirements required for inelastic eigenvalue buckling of members with non-uniform moment applied. Each of these cases has a maximum moment applied at one end and zero moment at the other end. With an interior brace at mid-span, M1/M2 for either section will be 0.5 and C_b is equal to 1.3 using the Commentary equation C-F1-1 (AISC 2010b).

Cases 1d and 1e:

Cases 1d and 1e are for a compact web section with either applied torsional or relative bracing along the member's length, respectively. The plots of capacity versus stiffness are shown for Case 1d in Figure 4.72 and for Case 1e in Figure 4.73.

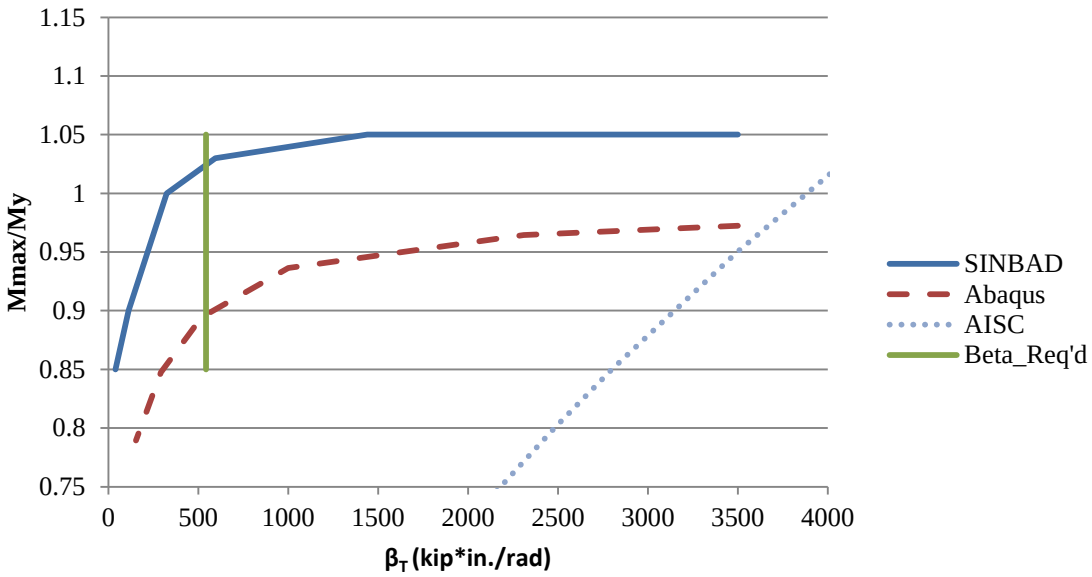

Figure 4.72: Case 1d; compact web section, M1/M2 = 0.5, 1 torsional brace

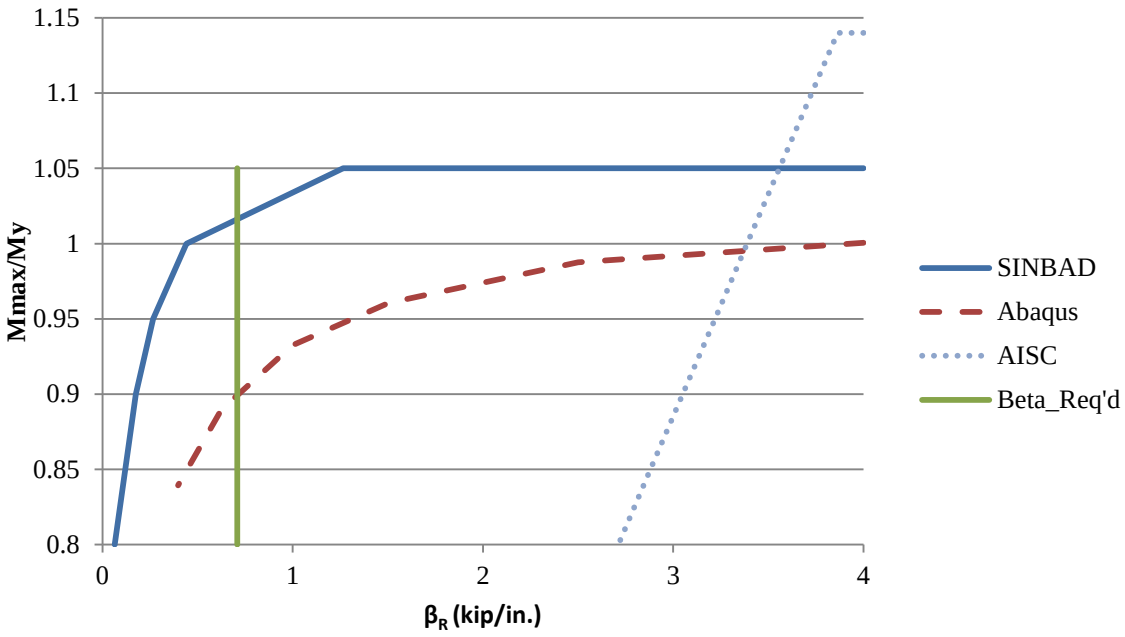

Figure 4.73: Case 1e; compact web section, M1/M2 = 0.5, 2 relative braces

Both Figures 4.72 and 4.73 show that SINBAD over-predicts the capacity results from Abaqus and suggest that slightly less bracing would be required to reach a full bracing condition. $\beta_{Req'd}$ from either plot is not quite enough to reach the plateau of the knuckle curve for the Abaqus solution but provides enough stiffness to reach approximately 90-95% of the rigidly-braced capacity. It is important to note that AISC's Appendix 6 equations for either torsional or relative bracing seem to do a better job at predicting the amount of bracing required for these two cases.

In reality for metal building systems, the typical design moment envelope will usually not have such a steep moment gradient over any one unbraced length. Yet, these plots are shown in an effort to validate how SINBAD works for many bracing configurations and applied loading conditions.

The brace force (or brace shear force) as a percentage of the maximum moment at mid-span (for Case 1d) and as a percentage of the maximum equivalent flange force at mid-span (for Case 1e) are shown in Figures 4.74 and 4.75, respectively. In both cases, the normalized brace forces are both under 1%.

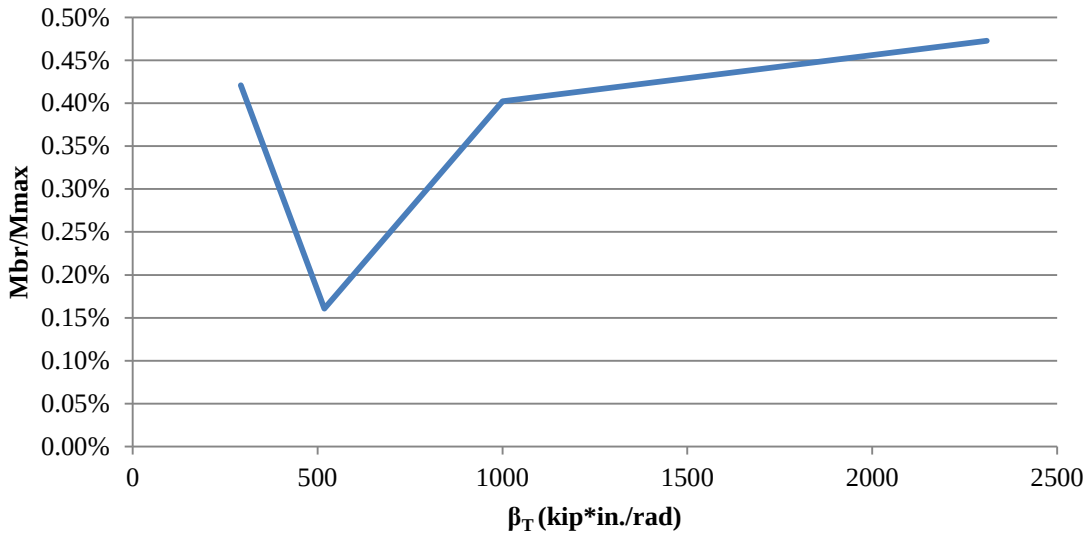

Figure 4.74: Case 1d; brace forces

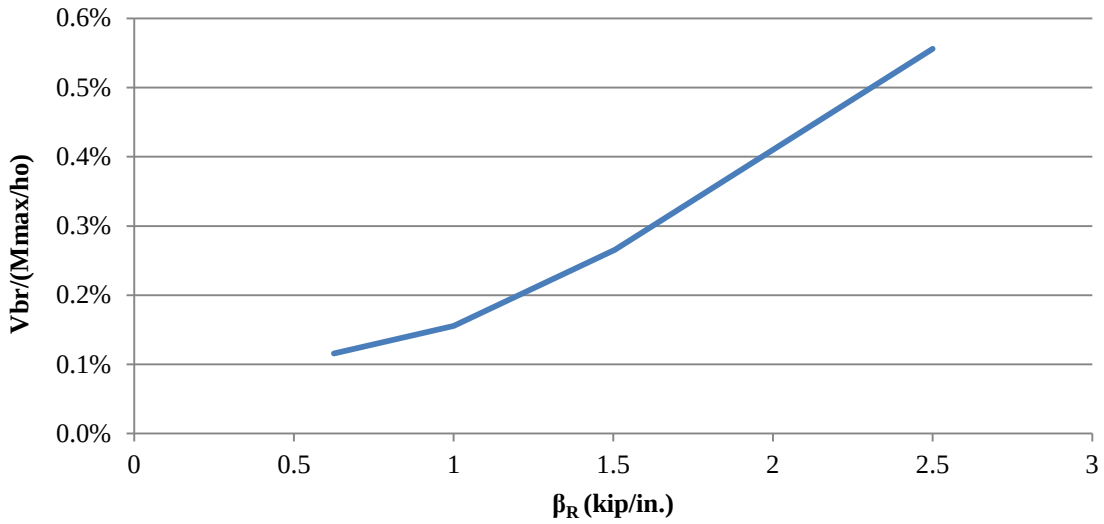

Figure 4.75: Case 1e; brace forces

Case 3f:

This example is similar to Case 1d, yet looks at the stiffness demands for an applied moment gradient for a slender web section. The plot of capacity versus bracing stiffness is shown in Figure 4.76. It should be noted that now, the difference in capacity between SINBAD and Abaqus is becoming quite large. However, $\beta_{Req'd}$ determined from the SINBAD results still provides the stiffness needed for Abaqus to reach approximately 95% of its fully-braced capacity. The requirement from AISC's Appendix 6 equations tends to be conservative in this example.

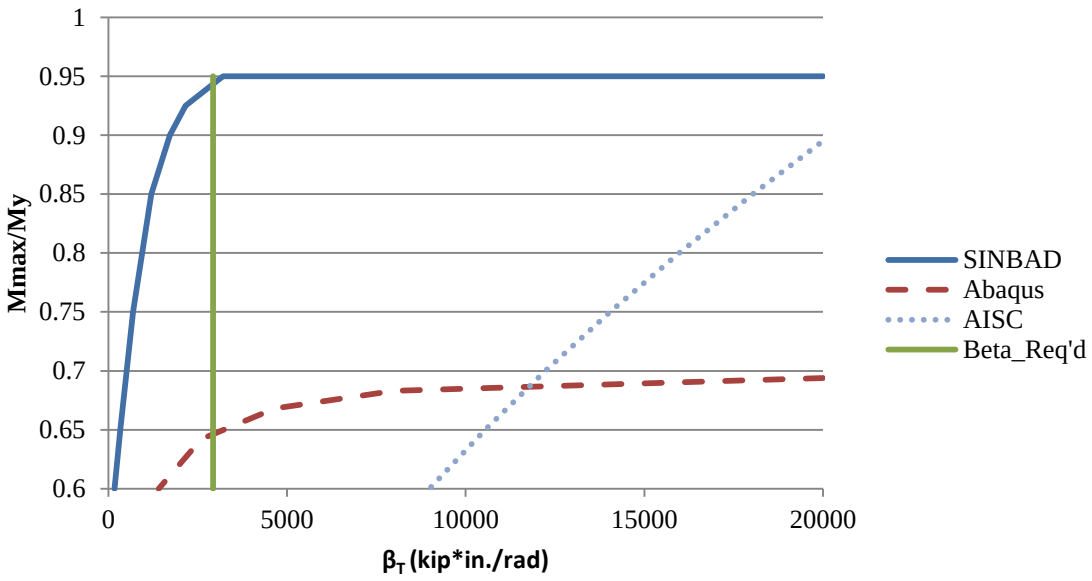

Figure 4.76: Case 3f; slender web section, M1/M2 = 0.5, 1 torsional brace

A plot of the brace force as a percentage of the maximum moment at mid-span is shown in Figure 4.77. In this example, given a wide range of applied stiffness, the normalized brace force varies only slightly between 1.1-1.5%.

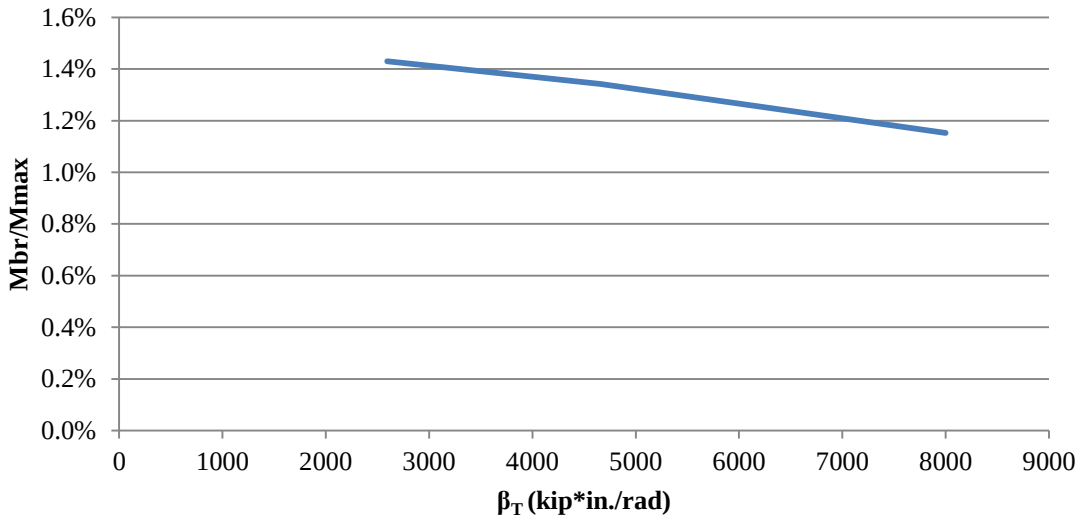

Figure 4.77: Case 3f; brace forces

4.6.6 Members with Unequal Brace Spacing

Two examples are presented where the brace layout along the member creates unequal unbraced lengths and the members are subjected to uniform bending. In these cases (Case 3b and 3c), the torsional braces are applied such that L_b = 48 in. for each end segment and L_b = 96 in. for the middle unbraced length. Both of these lengths are in the inelastic buckling region given the cross-section dimensions, yet at opposite ends (48" is closer to the plastic buckling region and 96" is closer to the elastic buckling region). These examples are outside the scope of AISC's Appendix 6 since they have unequal brace spacing.

Case 3b:

The plot of capacity versus bracing stiffness for Case 3b is shown in Figure 4.78. Again, the capacity reached by SINBAD over-predicts Abaqus for this slender web case for reasons discussed previously. Additionally, $\beta_{Req'd}$ suggests a bracing stiffness that is

close to the plateau level for the Abaqus simulation (around 15000 kip*in./rad). Lastly, it is important to note that AISC's Appendix 6 equations for torsional bracing are not derived for this case of unequal spaced braces. In Chapter 2, it was discussed that the fundamental equations rely on the assumption that the brace stiffness and spacing is uniform over the length of the member. Therefore, as shown in Figure 4.78, the stiffness values shown from AISC are the required stiffness based on the maximum required from either the 48 in. or 96 in. unbraced length, which is an ad hoc adaptation of the requirements selected by the author.

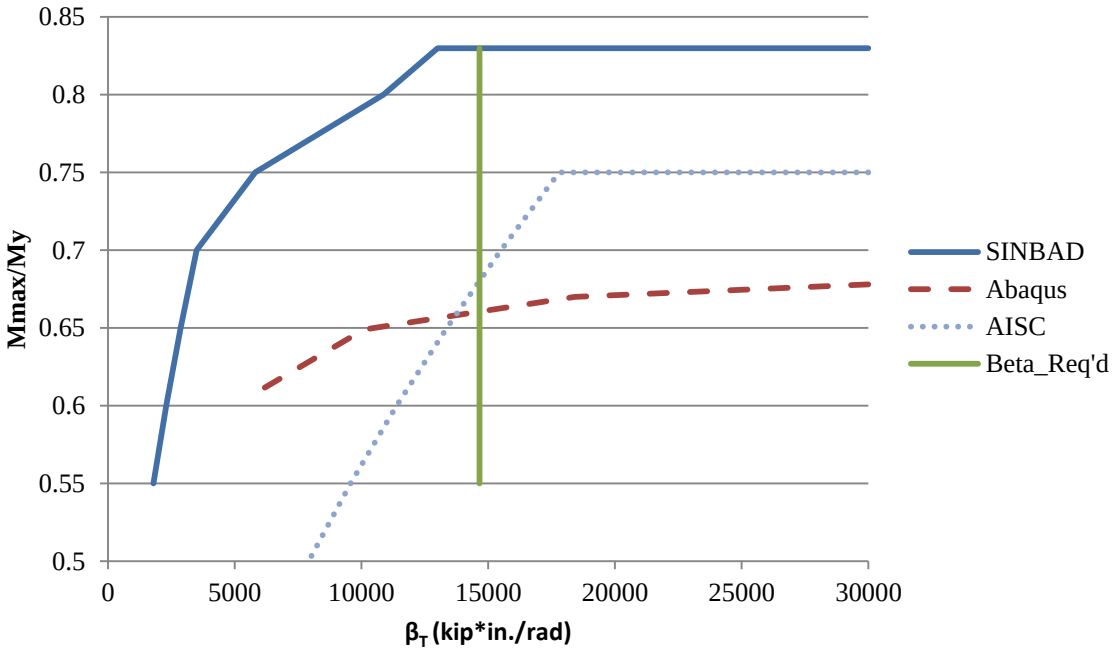

Figure 4.78: Case 3b; slender web section, uniform moment, 2 torsional braces unequally spaced

A contoured plot of the equivalent plastic strain for rigid bracing is shown in Figure 4.79. Any parts of the member that are not dark blue have yielded. This figure suggests that

the member is starting to develop significant yielding on the compression side of the compression flange as the bracing stiffness approaches full bracing.

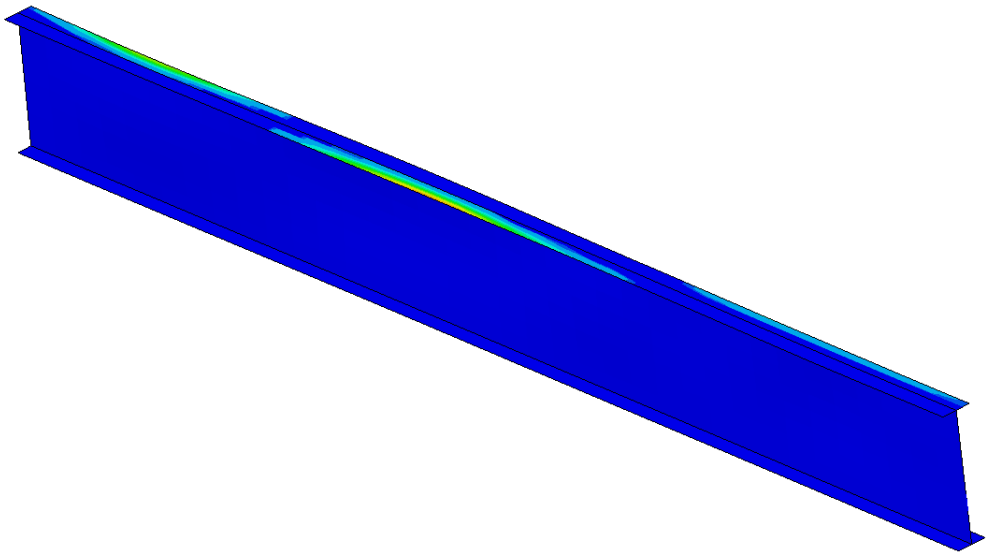

Figure 4.79: Contoured equivalent plastic strain, slender web section, uniform moment, rigid bracing (from Abaqus)

The results for the brace strength demands are shown in Figure 4.80 with a normalized brace force of less than 1.2% for the suggested bracing requirement of 15000 kip*in./rad.

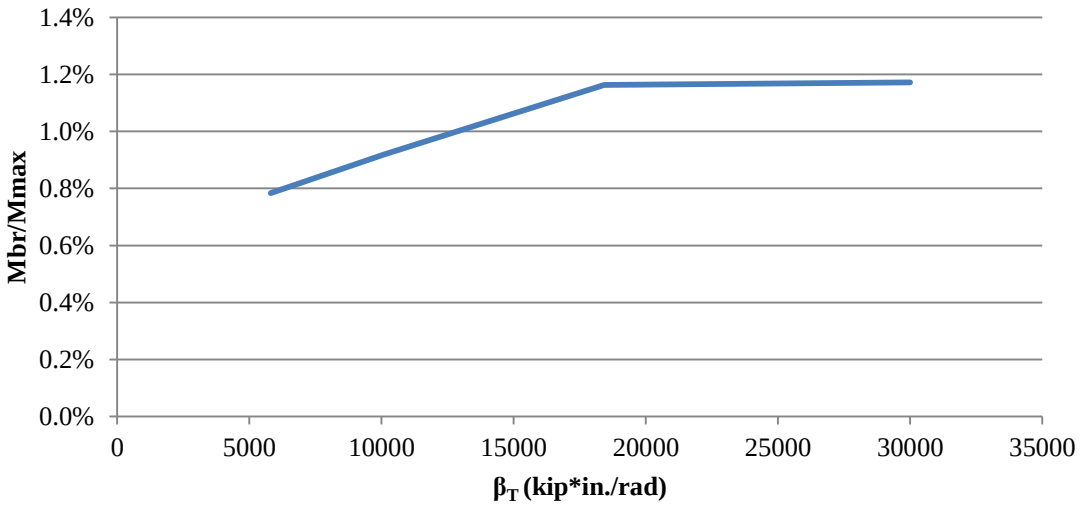

Figure 4.80: Case 3b; brace forces

Case 3c:

Case 3c presents a variation of Case 3b where the flange dimensions are different than typical for these member studies. For this case, the width of the flange was increased to 6.6 in. and the thickness was reduced to 0.2919 in. These new dimensions place the flange in the non-compact classification for F_y = 50 ksi. This case was chosen due to observations from numerous prior simulation studies by Sharma (2010) that showed that non-compact flanges can potentially reduce the bracing stiffness demands. However, if local buckling occurs in the flange, than brace point forces start to increase drastically. Figure 4.81 shows the capacity versus stiffness results for Case 3c and Figure 4.82 presents the normalized brace forces.

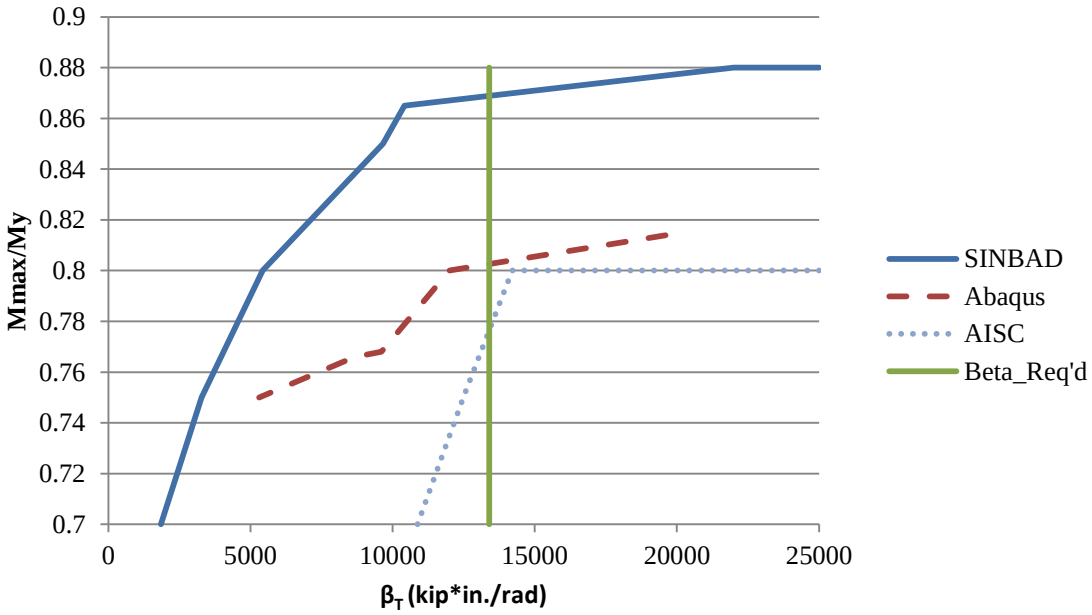

Figure 4.81: Case 3c; slender web section with 6.6" wide flanges, uniform moment, 2 torsional braces unequally spaced

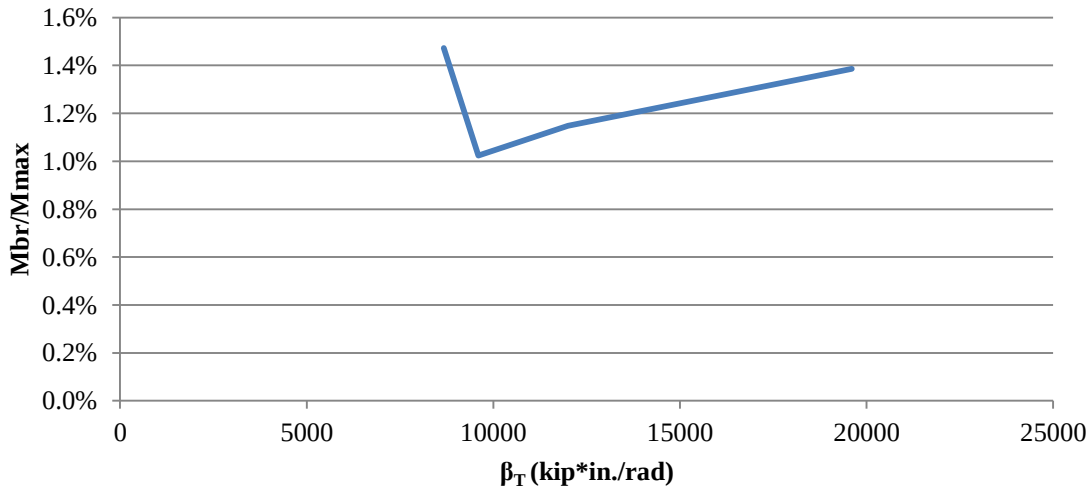

Figure 4.82: Case 3c; brace forces

In this case, where the flanges are deemed non-compact per the AISC Specification's Chapter B, the capacity of the section from AISC is controlled by flange local buckling. Due to the modeling of the flanges using cubic Hermitian beam element, the SINBAD solution does not capture the effect of flange local buckling. However, the Abaqus model employs shell elements for the flanges, which are able to capture the effects of flange local buckling and thus, provide the reduced capacity as compared to SINBAD (shown in Figure 4.81). The suggested required bracing stiffness is enough for the capacity of the section to reach 95% of its rigidly-braced strength.

The normalized brace forces associated with this stiffness requirement are on the order of 1.2%, as shown in Figure 4.82. This brace force is not significantly different from the brace forces depicted in Figure 4.80 suggesting that the observation made by Sharma (2010) of decreased brace forces for wider flanges is difficult to substantiate in this example. In Chapter 5, the concept of wider flanges potentially reducing the brace strength demands will be revisited for a 90 foot clear-span frame example.

4.6.7 Members with Combined Bracing Types

Cases 3h and 3j are examples where the torsional bracing is used in tandem with relative bracing under applied uniform bending. Both examples have a set relative stiffness of 1 kip/in., where Case 3h has the relative bracing applied to the *compression flange* and Case 3j has the relative bracing applied to the *tension flange*. For these two cases, the relative stiffness remains set at its provided value and only the torsional bracing stiffness will be varied in the tests. Figures 4.83 and 4.84 show the capacity versus bracing stiffness for Case 3h and Case 3j, respectively.

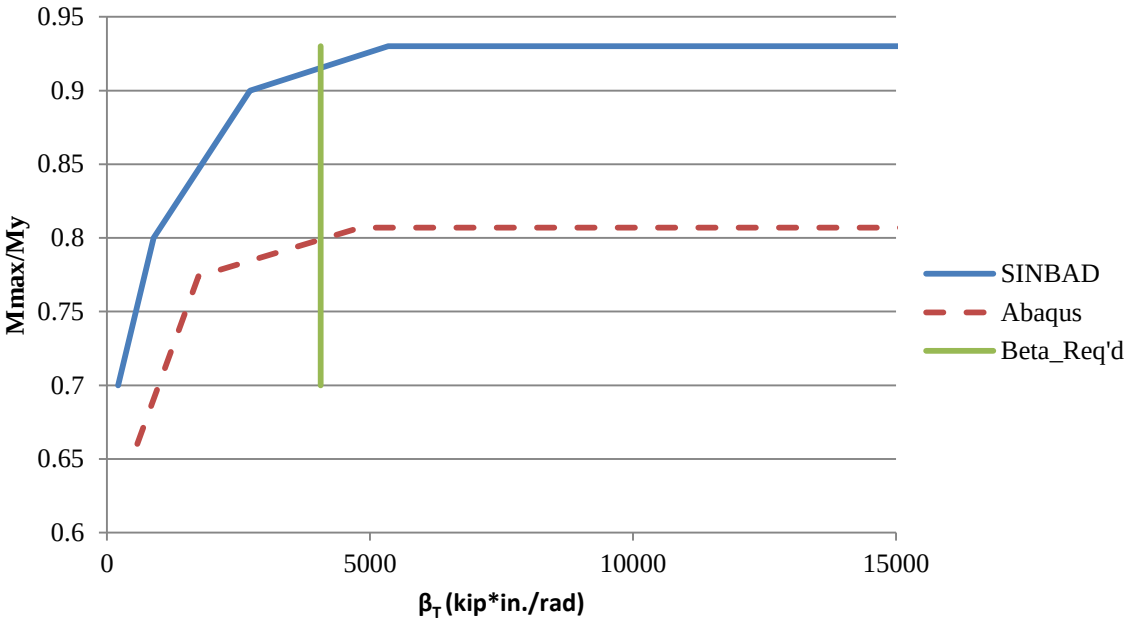

Figure 4.83: Case 3h; slender web section, uniform moment, 3 torsional braces & 4 relative braces applied to the *compression* flange

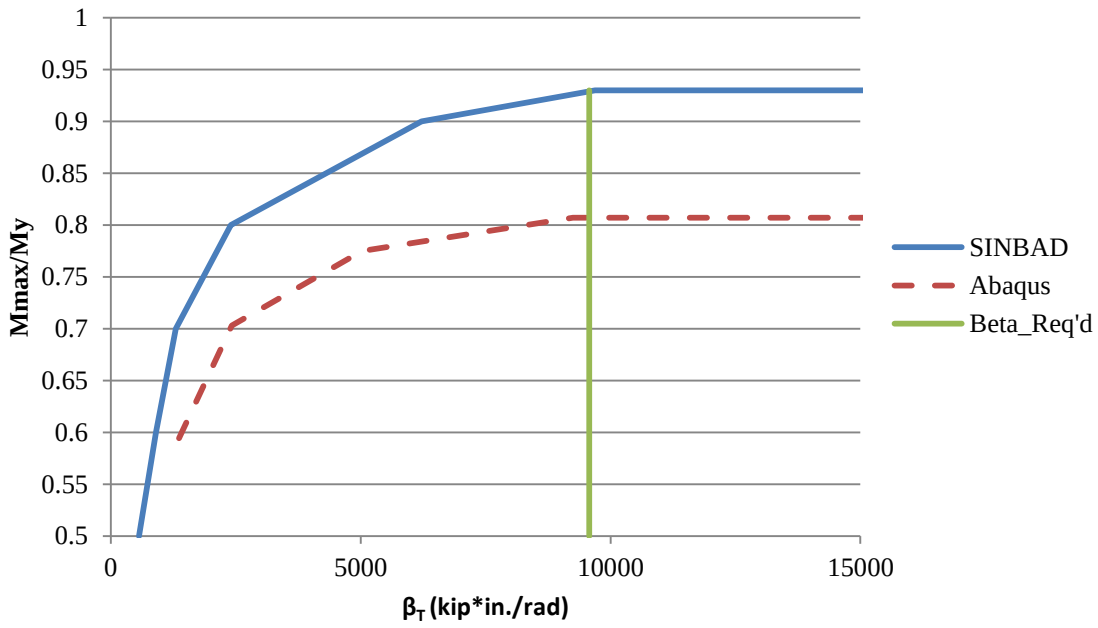

Figure 4.84: Case 3j; slender web section, uniform moment, 3 torsional braces & 4 relative braces applied to the *tension* flange

First, comparing Figures 4.83 and 4.84, one notices a general shift in the bracing requirements; leading to an increased stiffness requirement as the relative bracing system is moved from the compression flange to the tension flange. Since the tension flange is not buckling, it is able to provide some restraint to twist of the section. If a relative bracing system is attached to the tension flange and assumed to act in series with that flange, then the tension flange has an added stiffness that prevents it from displacing laterally. Conversely, if the relative bracing system is applied to the compression flange, it is working in parallel with the tension flange to prevent relative twist between the two flanges. Since preventing twist of the cross-section is paramount to bracing of beams, it makes sense that a compression flange relative bracing system would be more efficient than a system connected to the tension flange.

Next, if one compares Figures 4.83 or 4.84 back to the similar case without the addition of relative bracing (Case 3a, Figure 4.64), the application of relative bracing on the compression flange cuts the torsional stiffness requirements in half. Conversely, if relative bracing is applied to the tension flange, the torsional bracing requirement remains relatively unchanged. This emphasizes two key points:

1. The most efficient location to apply relative (lateral) bracing is on the compression flange, and
2. Adding relatively minimal relative bracing (taken as 1 kip/in. in these examples) to the compression flange can significantly reduce the torsional bracing requirements.

It is also important to note that AISC's Appendix 6 does not address the combination of bracing types. Therefore, the AISC stiffness requirements are not shown in the last two figures.

As has been shown here, significant economy may be achieved by using an inelastic eigenvalue buckling analysis to capture all the sources of bracing stiffness simultaneously. The suggested stiffness requirement for either Case 3h or 3j generally provides enough stiffness to reach close to the rigidly-braced capacity of the member.

Furthermore, if one selects a load level M/M_y = 0.77 to compare the stiffness requirements from the simulations, one would see that without relative bracing (Case 3a, Figure 4.64), the Abaqus simulation requires a stiffness of 5200 kip*in./rad, but if a small amount of relative bracing is included on the compression flange (1 kip/in. for Case 3h), the torsional bracing stiffness requirement drops to 1740 kip*in./rad. That's over a 60% reduction in the bracing stiffness requirement with just a slight addition in relative bracing stiffness on the compression flange. The reason for this steep drop can be explained by looking at the failure mode for Cases 3a and 3h at roughly the same load. Figure 4.85 shows the buckled shape with equivalent plastic strain contours (anything in dark blue is not yielded) and without relative bracing at M/M_y = 0.77. Figure 4.86 shows the buckled shape at a similar load level with equivalent plastic strain contours (anything in dark blue has not yielded) except with the addition of relative bracing on the compression flange.

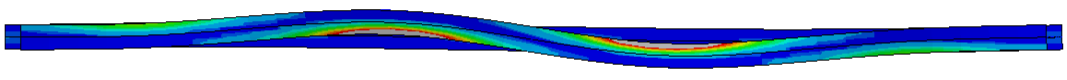

Figure 4.85: Equivalent plastic strain contours, slender web section, 3 torsional braces, plan view (from Abaqus, displacements scaled 10x)

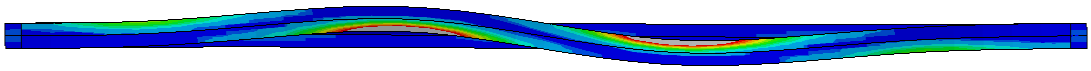

Figure 4.86: Equivalent plastic strain contours, slender web section, 3 torsional & 4 relative braces, plan view (from Abaqus, displacements scaled 10x)

Comparing Figures 4.85 and 4.86, one notices that the deflected shape at the limit load given the current bracing schemes are quite similar. Essentially the same level of yielding and stresses in the member are resisted by both relative and torsional bracing in Figure 4.86, yet by only torsional bracing in Figure 4.85. Therefore, it is to be expected that the requirements for torsional brace stiffness will decrease with the addition of relative bracing, since the similar displaced shape is ultimately resisted by both torsional and relative bracing. Similar results for a decrease in the torsional bracing stiffness requirements with the addition of compression flange relative bracing were noted by Sharma (2010) for bracing of complete frame systems. Therefore, it can be concluded and recommended that if possible, designers should provide relative bracing in tandem with torsional bracing to be able to more efficiently develop the required loads.

The mid-span torsional brace force as a percentage of the moment at the brace location remains relatively tame for these two examples. The normalized brace force is around 1% for the cases with relative bracing applied to the compression flange or the tension flange at the suggested bracing stiffness requirement, $\beta_{Req'd}$. Plots of the normalized torsional brace force versus stiffness are shown in Figures 4.87 and 4.88 for Case 3h and Case 3j, respectively.

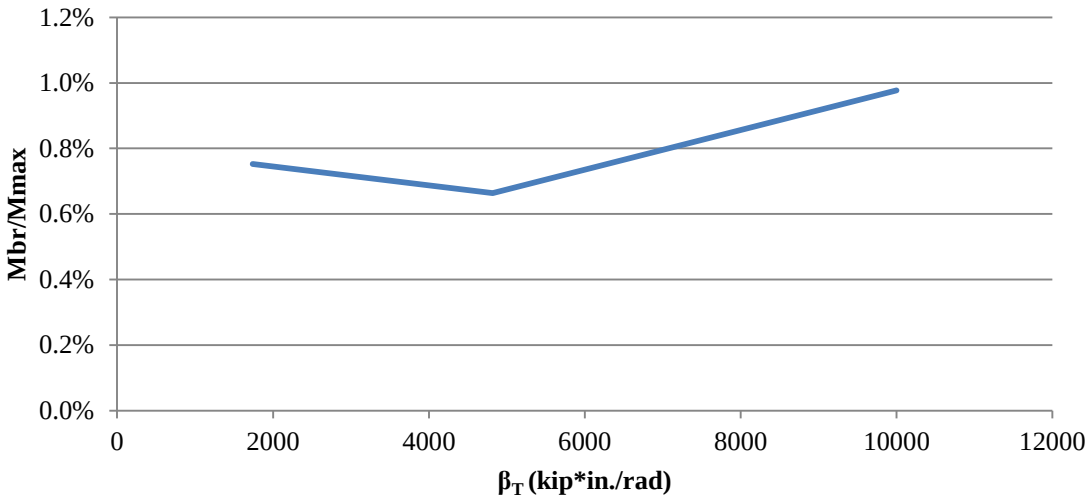

Figure 4.87: Case 3h; brace forces

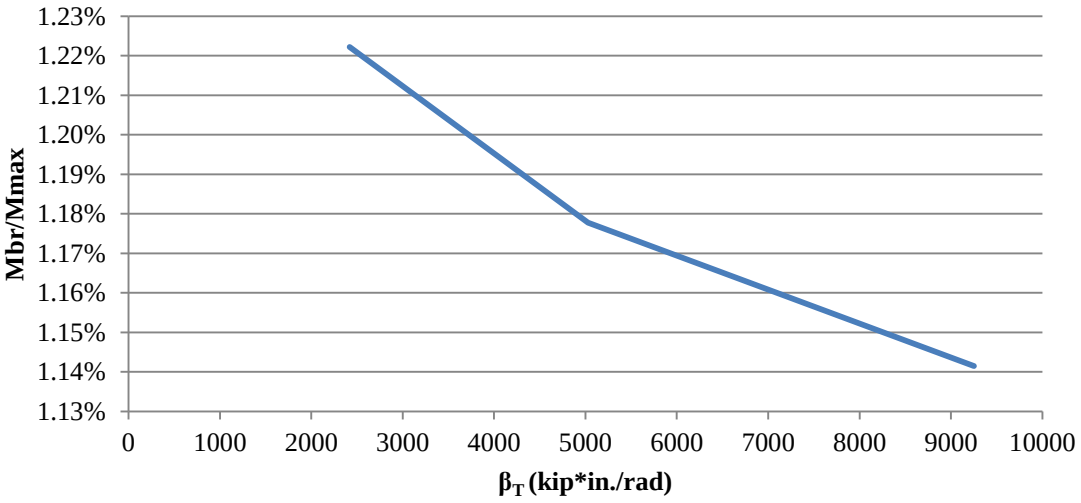

Figure 4.88: Case 3j; brace forces

The last item of note is that despite having combined bracing types for this example, no recommendation has been made on how to appropriately scale, in this case, the relative bracing stiffness requirement. As mentioned before, SINBAD provides the ideal bracing

stiffness given a member geometry, loading distribution, and bracing scheme. Yet, to limit brace point movement and effectively control brace forces, one needs some multiple of the ideal bracing stiffness. By varying the amount of torsional bracing in the present model while maintaining constant relative bracing, one does not have an idea of how the relative bracing may be affecting the stiffness of the system for any given loading condition. Therefore, and since the requirements for relative bracing requirements from AISC are derived from models that are much simpler to understand, the author recommends the use of the same AISC bracing stiffness factor equal to $2/\phi$ for the appropriate scaling of the relative bracing when SINBAD has been used to assess the sensitivity to the torsional bracing stiffness.

4.6.8 Beam-columns

Case 3g:

Case 3g combines both bending and axial loads onto the member in order to see if any increased stiffness demands for torsional bracing are required for beam-columns. The member has three interior torsional braces with four equal-length unbraced lengths. The axial load applied is $0.1*P_y$ when a load of M_y is applied to the section. This ratio of applied axial load to bending moment is held constant with different levels of applied moment for both the SINBAD and Abaqus models. The results for bracing moment capacity versus bracing stiffness are shown in Figure 4.89. Equivalent plastic strain contours (where the dark blue regions are not yielded) for a bracing stiffness from Abaqus equal to 25000 kip*in./rad are shown in Figure 4.90.

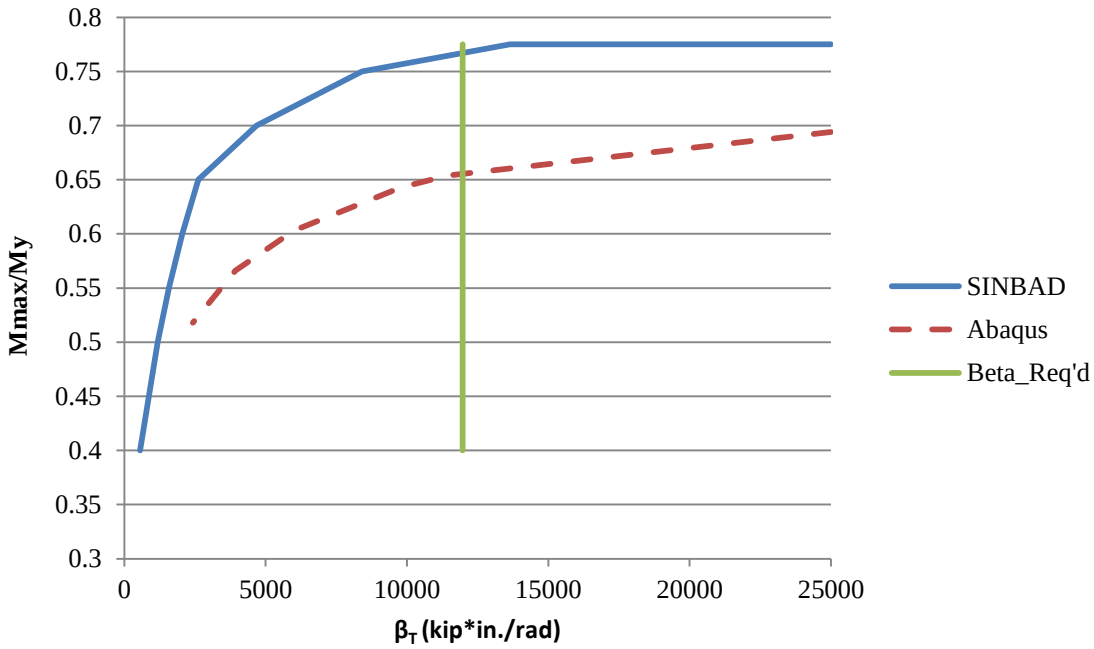

Figure 4.89: Case 3g; slender web section, uniform moment with axial load, 3 torsional braces

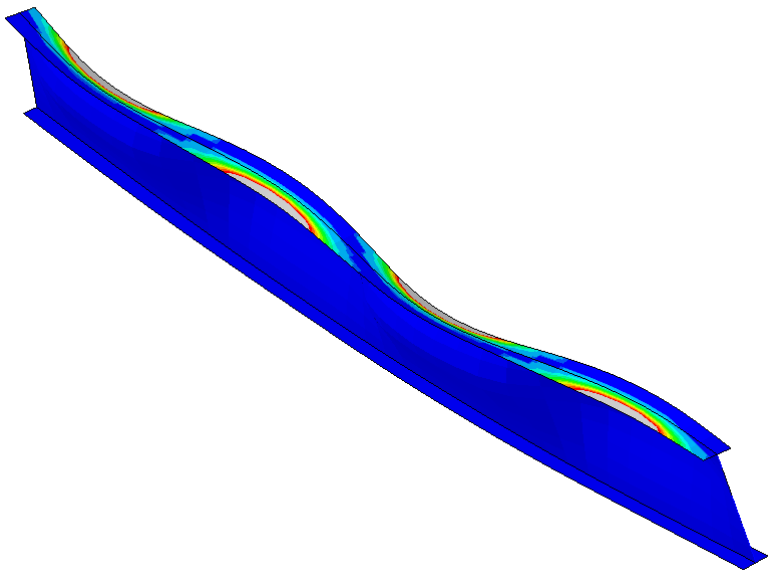

Figure 4.90: Contoured equivalent plastic strain, slender web section, uniform moment with axial load, rigid bracing (from Abaqus, displacements scaled 10x)

From Figure 4.89, one notices the gradual increase in capacity versus bracing stiffness exhibited by the Abaqus simulation, where the solution from SINBAD reaches its capacity with a relatively low stiffness requirement. The suggested stiffness requirement still provides roughly 90-95% of the capacity reached when full bracing is provided. Also, if Figure 4.89 is compared back to the similar example without the addition of axial load (Case 3a, Figure 4.64), it can be observed that the stiffness requirement increases from around 10000 kip*in./rad for the case without axial loading to 12000 kip*in./rad for the case with axial loading. This should come as no surprise, since the additional axial load on the compression flange will cause the flange plate to want to buckle at a lower applied moment. Therefore, one would expect the stiffness demands to generally increase to support the fully-braced capacity

Figure 4.90 shows that despite the addition of axial load (albeit a small force in comparison to the applied bending moment), the member still exhibits a failure mode where buckling between the brace on the compression flange is prevalent with no yielding on the tension flange. What may be happening here is that although there is additional compressive load on the compression flange, there is an equivalent reduction in tensile load on the tension flange. Therefore, for the case of rigid torsional bracing, the tension flange may be able to "assist" the member more by preventing out-of-plane movement of the tension flange at the brace location.

A plot showing the bracing force as a percentage of the maximum bending moment on the section is shown in Figure 4.91. Again, comparing back to Figure 4.65 from Case 3b, the brace forces increase for the suggested required bracing stiffness for beam-columns from roughly 1.5% to 2.8%. Given the discussion above, an increase in the bracing force requirements is to be expected when a beam is subjected to bending and axial loads.

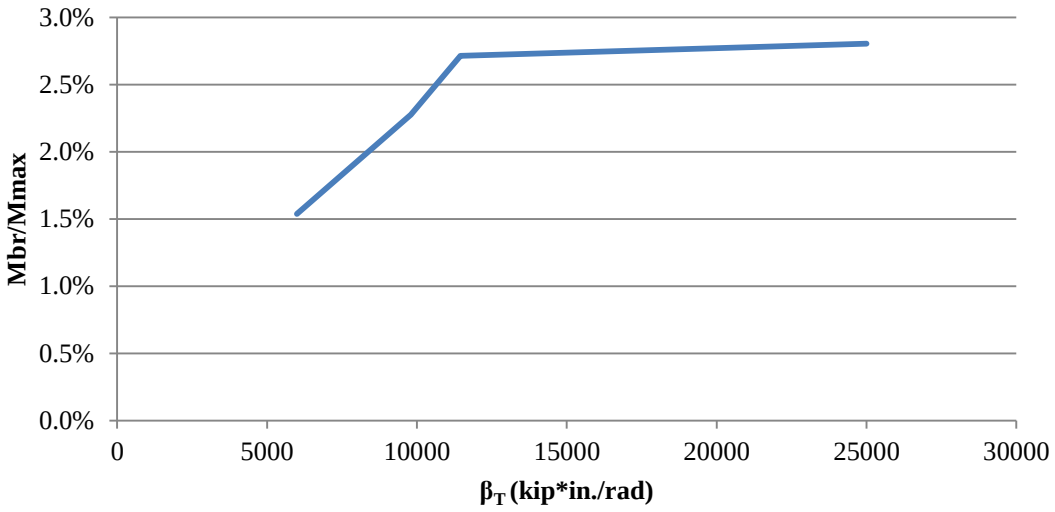

Figure 4.91: Case 3g, brace forces

4.7 Web-Tapered Rafter Example

A 45 ft web-tapered member is selected to assess how SINBAD handles members that are similar to sections typically used in the metal building industry. The flanges are selected first as 0.375 in. x 6 in. sections (compact flange elements for F_y = 50 ksi). Next, h/b_f = 6 is used at the deep end of the member. h/t_w = 180 is set as the web slenderness at the deep end of the rafter leading to a 0.2 in. x 36 in. web plate (slender element for F_y = 50 ksi). Finally, the member was tapered down to h/b_f = 2.5 at the shallow end (a little less than the h/b_f ratio of a W16x26 rolled wide-flange member). At the shallow end, the web depth was equal to 15 in. and the web is classified as compact. In summary, the member is selected that has compact flanges and tapers from a slender web at the deep end to a compact web at the shallow end.

The rafter has only torsional bracing and is spaced at 5 foot on-center. The boundary conditions are assumed to be pinned (although in a real rafter, there may be some

restraint provided by the connection to adjacent parts of the structure). The rafter is subjected to an arbitrary, uniformly distributed load that is applied as a series of point loads based on tributary area to the brace points (assumed to be purlin locations) at the top flange . An elevation view of the rafter model is shown below in Figure 4.92.

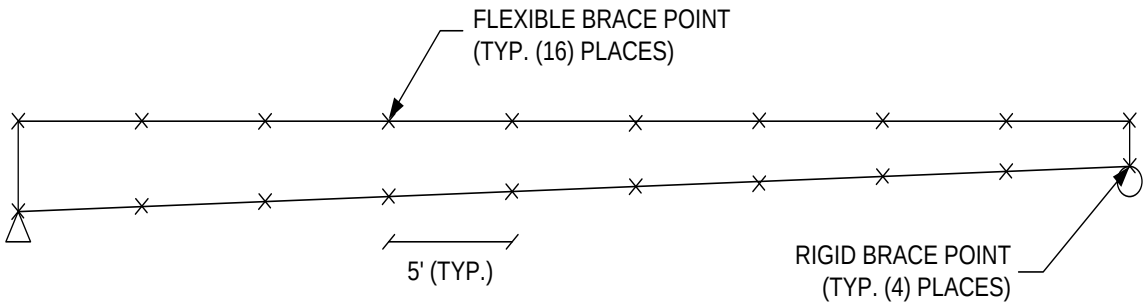

Figure 4.92: 45 ft web-tapered rafter, elevation view

Residual stresses are imposed in both the simulation and the eigenvalue buckling model pursuant to the patterns discussed in Chapter 3. Also, an initial imperfection based on the tolerances from the Code of Standard Practice (AISC 2010a) is seeded into the simulation. Two separate cases are considered: one that includes a sweep of the compression flange between brace points (selected to minimize the section capacity) and one that includes three separate analyses where the compression flange is “kinked” at the location of braces 4, then 5, and then 6 as counted from the deep end of the rafter. These three specific brace points were chosen to study the brace forces since they lie at locations of maximum flange stress. Plan views of the imperfection patterns are shown in Figure 4.93.

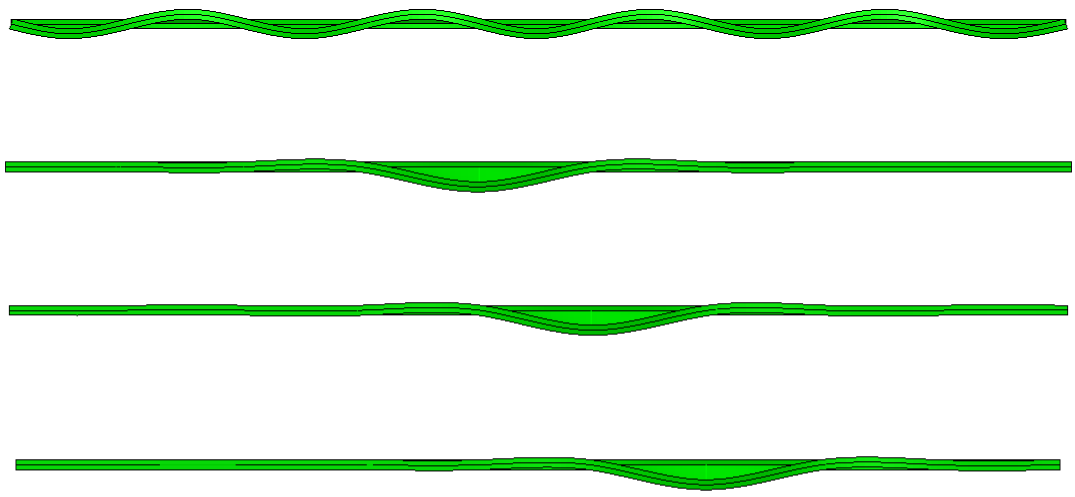

Figure 4.93: Initial imperfection patterns used in Abaqus, plan view (top flange is displacing laterally compared to the bottom flange, displacements scaled 100x)

Figure 4.94 shows the capacity versus torsional bracing stiffness demands for this example. For this case, Abaqus shows that the member continues to resist increases in loading with very large increases in the bracing stiffness requirements. Therefore, $\beta_{Req'd}$ suggests a bracing stiffness that would only permit the simulation model to reach roughly 90% of its rigidly-braced capacity. Again, with consideration of the fact that the initial imperfections and residual stresses are combined in a worst-case scenario for the simulations, this slight under-prediction of the bracing stiffness required for torsional bracing should not be cause for alarm.

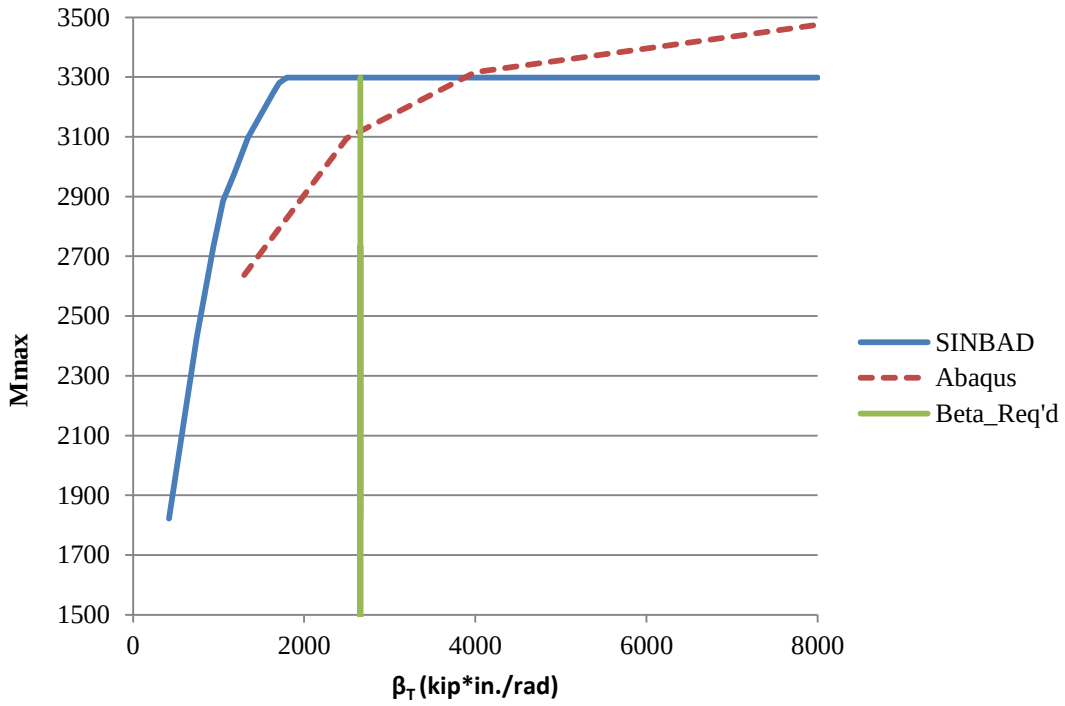

Figure 4.94: 45 ft web-tapered rafter knuckle curves

Figures 4.95 and 4.96 show the equivalent plastic strain contours at the limit load reached under rigid bracing, where Figure 4.96 is an enlargement of the critical section (the fourth span from the shallow end). In this case, significant yielding is occurring on the compression flange whereas the tension flange and bottom of the web are just beginning to yield within the critical segment.

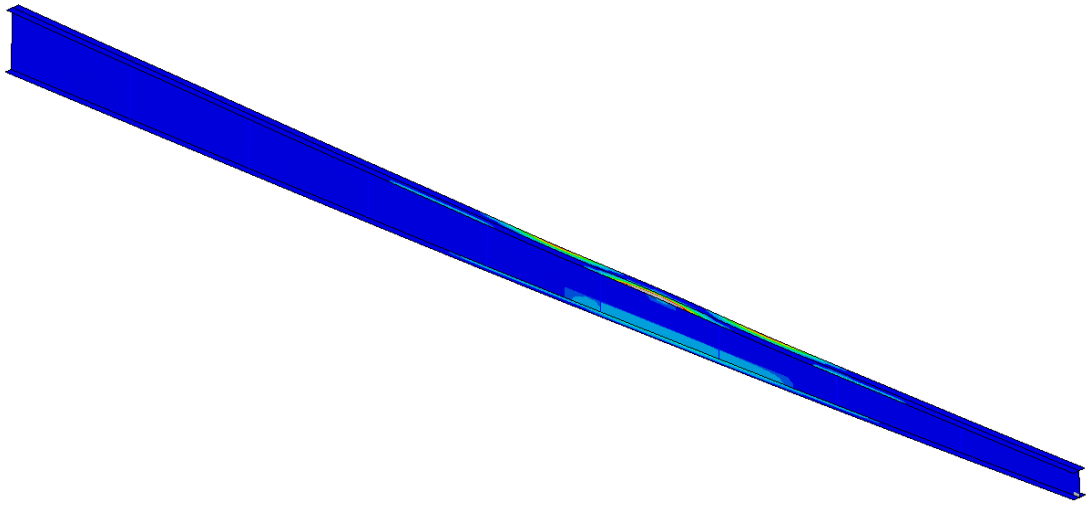

Figure 4.95: Equivalent plastic strain contours, 45 ft rafter (from Abaqus)

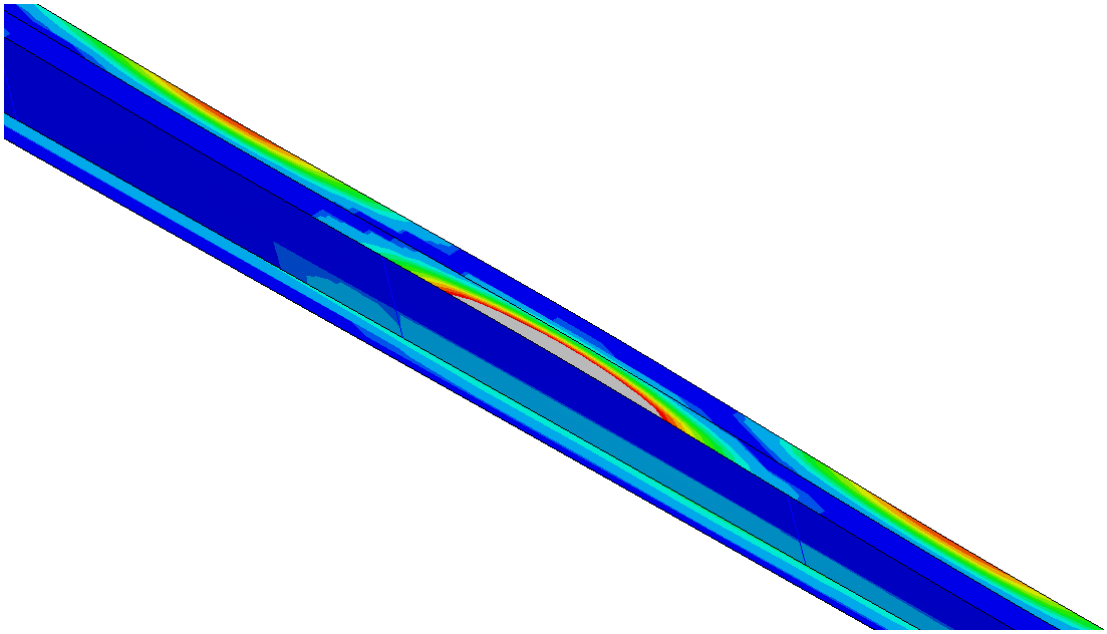

Figure 4.96: Equivalent plastic strain contours, 45 ft rafter's critical section (from Abaqus)

Figure 4.97 shows the brace forces as a percentage of the moment in the section at the location of the torsional brace. If the suggested required stiffness of 2700 kip*in./rad is

applied to all the torsional braces along the rafter, then the brace forces for the critical brace locations would range from 1-2%.

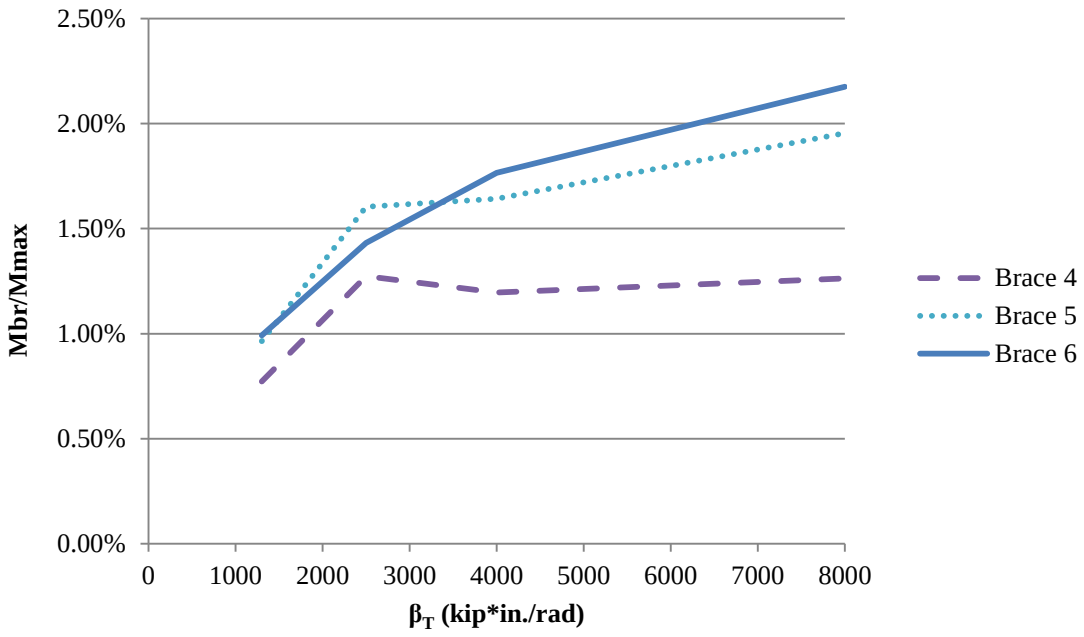

Figure 4.97: 45 ft rafter; brace forces

5. APPLICATION OF SINBAD TO FRAMES

This chapter details how the concepts presented in the previous chapter for members can be combined and extrapolated to predict the bracing stiffness requirements for more complicated framing systems. This chapter is organized around three examples: a 90 ft clear-span frame, a variation on the 90 ft clear-span frame with increased flange widths, and a 300 ft modular frame.

As was mentioned at the end of Chapter 3 and the start of Chapter 4, due to the nature of the solution algorithms, it is anticipated that the ideal stiffness based on an inelastic eigenvalue buckling analysis from SINBAD requires some scaling in order to approximate the stiffness required from the true, load-deflection solution. The same procedure used to determine $\beta_{Req'd}$ that was presented in Chapter 4 is implemented herein to provide this necessary scaling

5.1 Clear-span Frame

5.1.1 Frame Geometry and Loading

The 90' clear-span frame studied in this first example was introduced previously in Section 2.4 as a motivation for this research. Kim (2010) and Sharma (2010) studied this frame in-depth and the reader is referred to their individual theses for more detailed information, especially concerning the original design of the frame. Figure 2.5 is repeated here as Figure 5.1 for ease of reference and Table 5.1 lists the section properties at different locations along the frame.

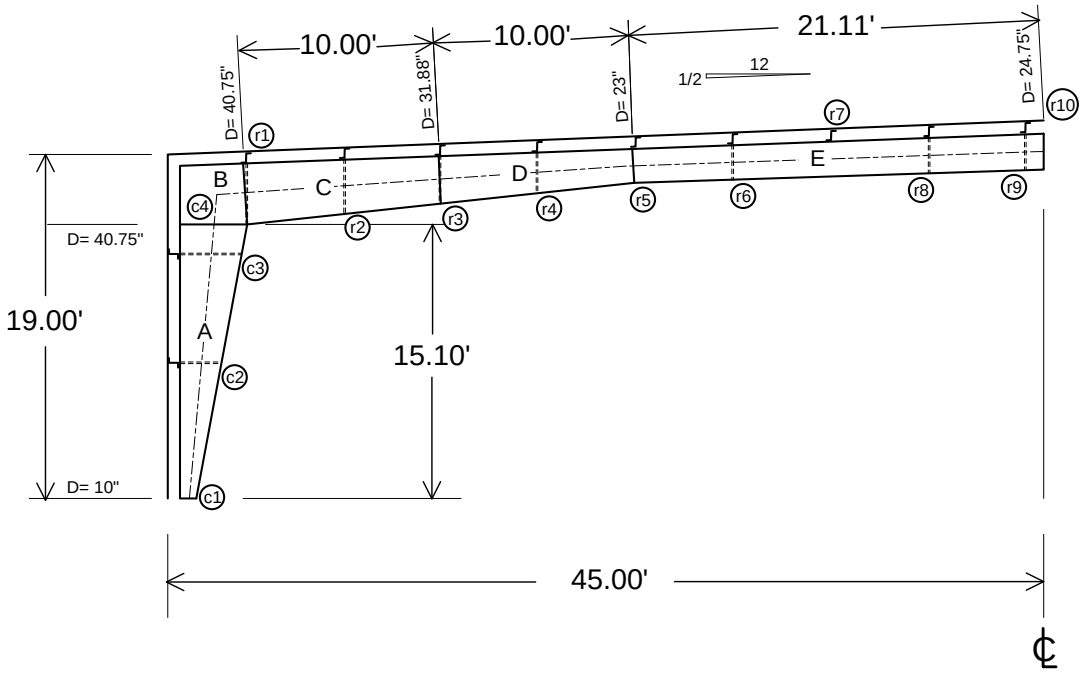

Figure 5.1: Elevation view of ninety foot clear-span frame (from Kim 2010)

Table 5.1: 90’ Clear-span frame geometry (from Sharma 2010)

Length	Location	Web				Inside Flange			Outside Flange		
		d (in)	t_w (in)	h/t_w*	h_c/t_w	b_f (in)	t_f (in)	$b_f/2t_f$	b_f (in)	t_f (in)	$b_f/2t_f$
A	c1	10.00	7/32	42	36	6.0	1/2	6.0	6.0	3/8	8.0
	c2	25.27		112	103						
	c3	37.49		167	157						
	c4	40.75		182	172						
B			7/32								
C	r1	40.75	1/4	160		6.0	3/8	8.0	6.0	3/8	8.0
	r2	36.31		142							
	r3	31.88		125							
D	r3	31.88	3/16	166		6.0	3/8	8.0	6.0	3/8	8.0
	r4	27.44		142							
	r5	23.00		119							
E	r5	23.00	5/32	142		6.0	3/8	8.0	6.0	3/8	8.0
	r6	23.42		145							
	r7	23.80		148							
	r8	24.25		150							
	r9	24.67		153							
	r10	24.75		154							

*For F_y = 55 ksi, the webs are compact for $h/t_w \leq 86$ and slender for $h/t_w \geq 130$.

In the original design of the frame, the ASD loading combination involving uniform roof snow load was deemed the critical load combination. Sharma (2010) and Kim (2010) studied this frame with an ASD load factor of 1.6, corresponding to the ultimate design load level. For the results presented in this research, it is simpler to work with a uniformly distributed factored load. That is, since no member design checks are performed, the origin of the loads applied in these examples is irrelevant.

5.1.2 Bracing Configuration

For the 90 ft clear-span frame, the wall panels and x-bracing are applied as relative braces in both the SINBAD and Abaqus models. No roof panels are used in the analysis of this frame, since typically for metal building systems, the roof panels are attached together using standing seams, which by design, are intended to allow movement associated with thermal expansion and contraction of the roofing system. It should be noted that some designers count on the friction between these panels and the rigid insulation inside the building to provide some restraint to movement and thus, consider some small addition to the bracing by the application of these types of roof panels in the design of the bracing systems. Figure 1.1 is repeated as Figure 5.2 below for reference during the discussion of the applied bracing in this example.

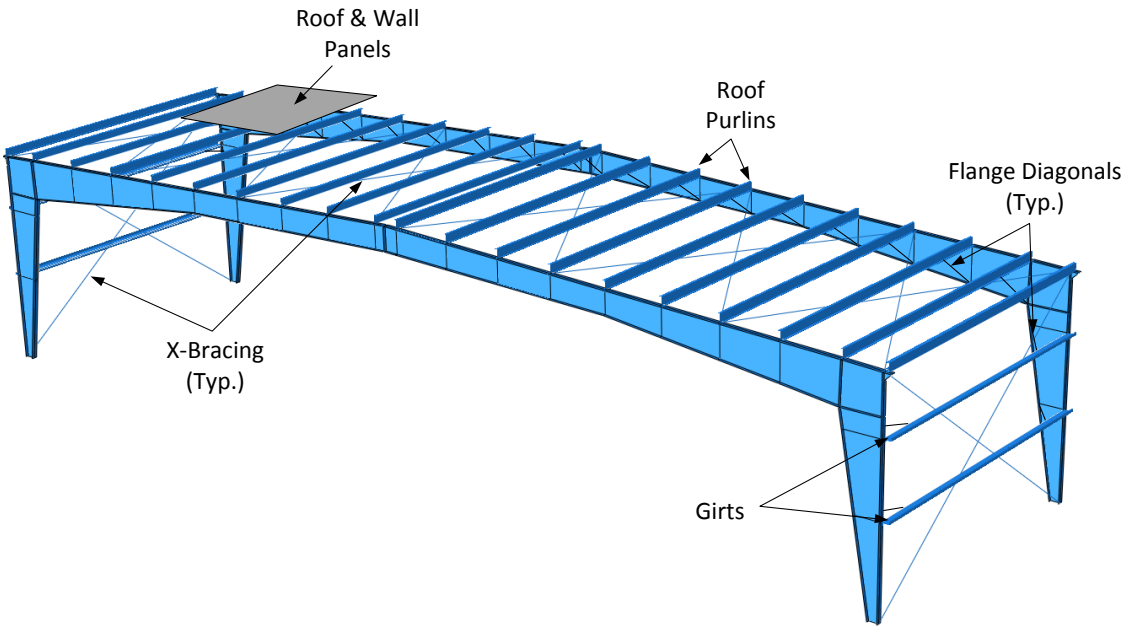

Figure 5.2: Two representative clear-span metal building frames (Sharma 2010)

The relative stiffness of the wall panels (shown as a roof panel in Figure 5.2) is taken as G' = 4.19 kip/in.; a value provided in the initial design of the frame (Sharma 2010). To determine the stiffness value applied in SINBAD and Abaqus, one calculates:

$$\beta_{diaphragm} = \frac{G' \sum s}{L_b} \tag{5.1}$$

where G' is the relative stiffness of the wall panels, Σs is generally the sum of the bay spacing along the entire length of the building, assumed to be the tributary spacing for one frame in this example, since the major interest lies in the analysis of one frame with a given wall panel and not the entire bracing system, and L_b is the length of the wall panel between girt locations (Sharma 2010). In the examples presented in this chapter, it is assumed that the stiffness provided by the wall bracing remains constant.

For the x-bracing in the plane of the wall and the roof (see Figure 5.2), rod bracing is employed and the methods detailed in Section 2.3.7 are used to determine the relative stiffness provided, assuming that for any given braced bay, only one rod acting in tension is providing the stiffness. That is, the rod in compression is considered to be ineffective when determining the stiffness provided in any given braced bay. In the examples presented in this chapter, it is assumed that the stiffness provided by the x-bracing remains constant.

The torsional bracing used in these models is the only bracing type that is varied to provide a measure of the capacity versus bracing stiffness and an assessment of the bracing strength requirements. Also for this analysis, it is assumed that all of the torsional bracing is at the same stiffness level. That is, while some economy may be gained by reducing the size and spacing of torsional bracing in regions of the frame that are less critical, that specific consideration is not introduced in this study.

5.1.3 Elastic Buckling Load Ratio

In some cases, it may be useful to calculate γ_e for a complete framing system. One would most likely not use such a value for design of the members, since sections of the frame with relatively low stress would be penalized by parts of the structure with higher stress. However, there may be some intrinsic value in determining γ_e as a measure of the reserve capacity in the frame, considering it remains elastic.

In this example, the 90’ clear-span frame is analyzed to determine the elastic buckling load ratio. That is, one is looking for what multiple of the applied frame loading will lead the frame to buckle elastically. The pertinent information needed for the determination of γ_e is:

- Applied, factored uniformly distributed load = 0.90825 klf on the horizontal project of the roof (corresponding to 1.4 x the controlling ASD combination from Sharma 2010 or Kim 2010)
- All bracing stiffness values are as provided in the design of the original frame (see Sharma 2010 or Kim 2010) and as described in the preceding section.

The elastic buckling load ratio determined from SINBAD is γ_e = 1.74. This means that if the applied uniform load were multiplied by this ratio, the frame would be at its elastic buckling capacity. Figure 5.3 shows an elevation of the frame from SINBAD. Figure 5.4 is a plan view (looking up from the ground toward the bottom flange of the rafter) of the buckled shape, which is a scaled eigenmode corresponding to the lowest eigenvalue = 1.74.

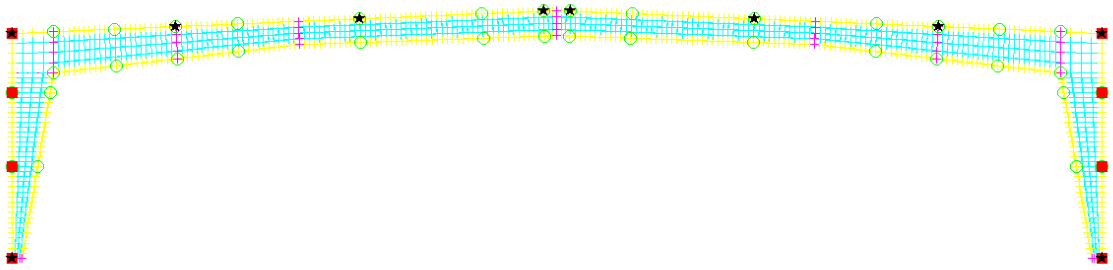

Figure 5.3: 90’ clear-span frame, elevation view from SINBAD

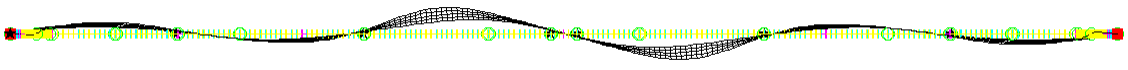

Figure 5.4: 90’ clear-span frame, buckled shape, plan view looking up toward bottom of rafter

In both Figures 5.3 and 5.4, the small green circles represent locations of torsional bracing, the black stars are locations of rod bracing, and the red squares in the plane of the wall represent the wall panels spanning between girt locations. The buckled shape depicted in Figure 5.4 shows that the rafter buckles between the cable-braced points at the elastic buckling load and that the torsional braces appear to “go along for the ride”. This observation is not unique to this frame. Whenever there is a member with a relatively long total length (or long length between fairly rigid bracing points, as is the case here where the lateral bracing is provided by rods at specific purlin locations along the outside flange of the rafter) and braced intermittently by closely spaced torsional bracing, the torsional bracing may effectively prevent twist of the cross-section, but cannot prevent the entire section from elastically buckling out-of-plane. This observation parallels the recommendation in Chapter 4 that more efficient bracing systems will include at least some relative bracing applied to the compression flange. Despite the fact that rod bracing is provided in the plane of the wall and roof in this example, the brace points are far enough apart that elastic buckling between the rod brace points controls the design of the elastic system over buckling between torsional bracing points.

5.1.4 Bracing for Inelasticity

5.1.4.1 Residual Stresses and Initial Imperfections

Residual stresses are applied to the frame in accordance with the patterns discusses in Chapter 3. The initial stress values are selected by using the section properties at the mid-depth of the column and the girder separately to calculate any reductions necessary due to web plate buckling.

Three main types of geometric imperfections are seeded in the model in keeping with the tolerances set forth in the Code of Standard Practice (AISC 2010a) and the Metal Building Systems Manual (MBMA 2006):

1. Canting of the frame in its plane by (eave height)/500 (Figure 5.5),
2. Out-of-plane flange sweeps in the vicinity of the knee (Figures 5.6 and 5.7), and
3. Out-of-plane web buckling modes (Figure 5.8).

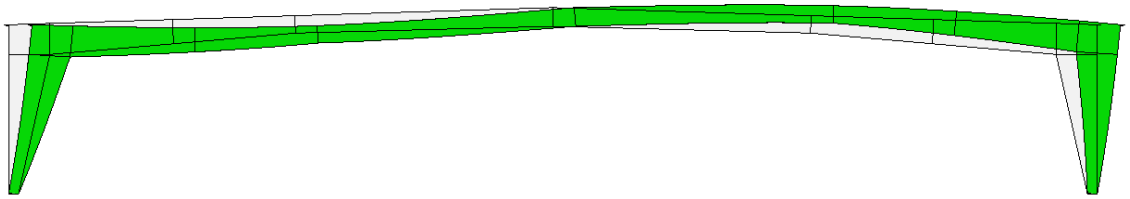

Figure 5.5: Imperfection 1: Canting of the frame by (eave height)/500 (scaled 50x, from Abaqus)

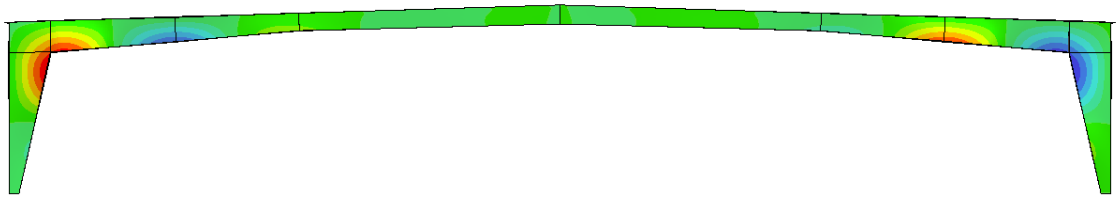

Figure 5.6: Imperfection 2: Contoured out-of-plane flange sweep (from Abaqus)

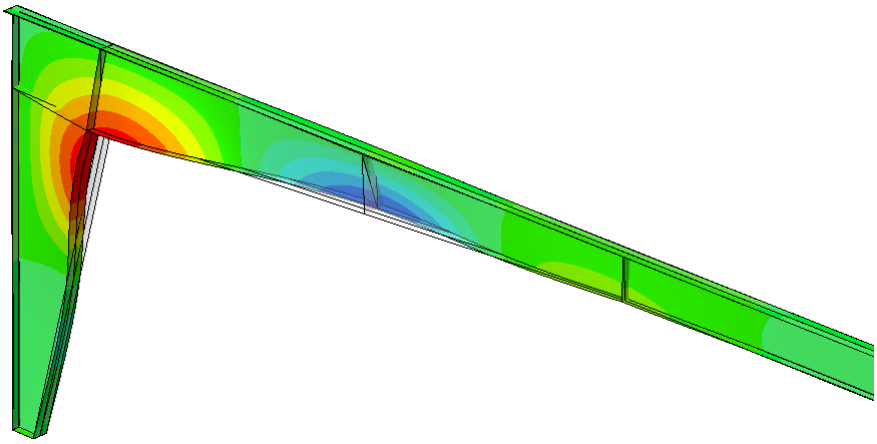

Figure 5.7: Imperfection 2: Contoured out-of-plane flange sweep, close-up at knee (scaled 50x, from Abaqus)

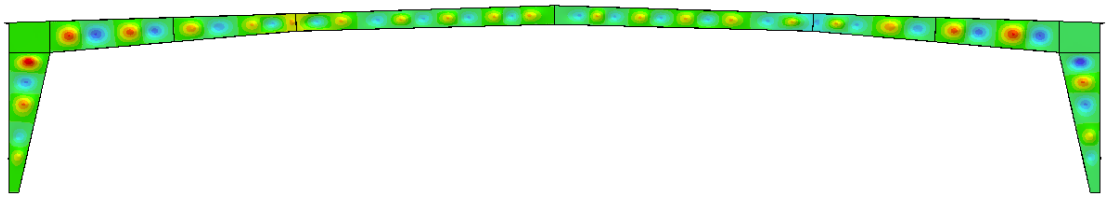

Figure 5.8: Imperfection 3: Contoured out-of-plane web local buckling modes (scaled 5x, from Abaqus)

The out-of-plane flange sweep is applied in the vicinity of the knee region due to the bending moment being the greatest in this region. With the application of gravity loading, the moment at the knee is such that the inside of the knee region is in compression. As presented previously in Chapter 4 during the discussion of critical imperfections for members, a kinking of the brace point out-of-plane by 1/500 generally leads to the highest brace forces (Wang and Helwig 2005). Therefore, in this example, the top torsional brace point in the column and the first torsional bracing point in the rafter are forced out-of-plane by 1/500 and in the same direction. Additionally, the third torsional

brace point in the rafter is also forced out-of-plane but in the opposite direction, in an effort to cause the largest change in curvature at the first rafter brace point and thus, maximize the brace forces in the knee region.

5.1.4.2 Brace Stiffness and Strength

The results for brace stiffness versus applied uniformly distributed load are presented in Figure 5.9. SINBAD predicts slightly more capacity than Abaqus, but more importantly, suggests an ideal bracing stiffness that is significantly lower than the full bracing requirement predicted by Abaqus. While the proposed bracing stiffness, $\beta_{Req'd}$, would still allow the frame to reach roughly 90% of the fully-braced capacity, one may be curious as to why the inelastic eigenvalue buckling solution from SINBAD reaches the fully-braced capacity of the frame at such a reduced bracing stiffness than indicated by Abaqus. One might also remember from Chapter 4 that the 45' web-tapered rafter example experienced a similar reduction in the prediction of bracing stiffness when comparing Abaqus to SINBAD.

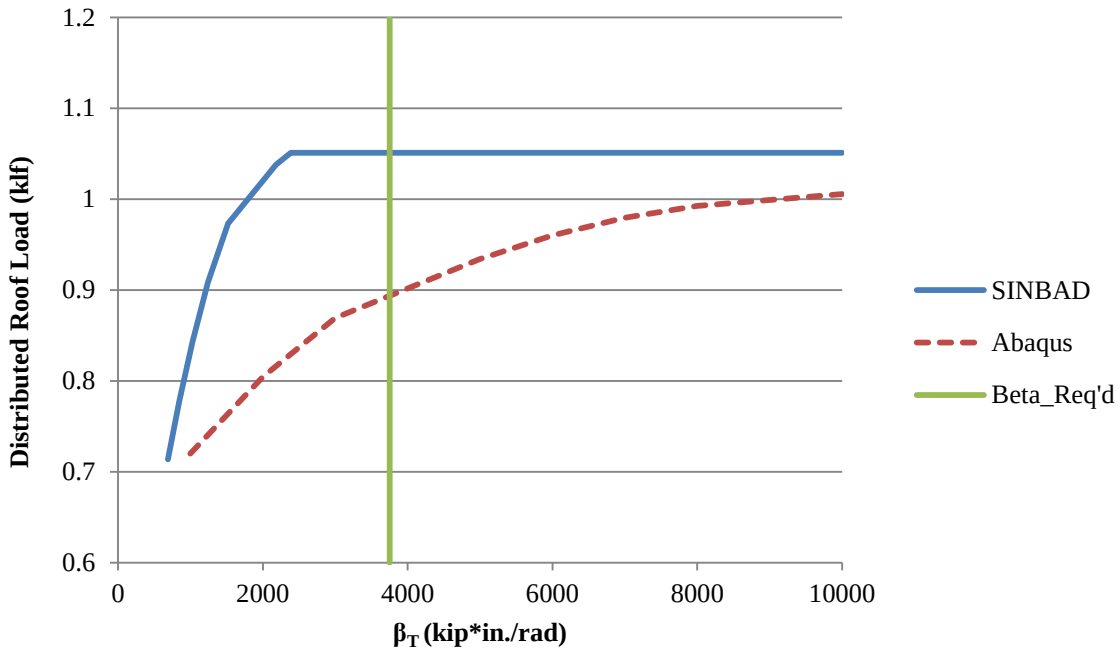

Figure 5.9: 90 ft clear-span frame; knuckle curves

The best explanation of this phenomenon is centered around Figures 5.10 and 5.11. The two figures show the contoured equivalent plastic strain at the capacity of the framing system for a case where the stiffness provided is very weak and a case where the stiffness provided is approaching full bracing, respectively. In these contour plots, anything that is not dark blue has yielded. When scrutinizing these figures, one notices that the yielding associated with Figure 5.11 (the full bracing case) is much more localized in the flange at the rafter as compared to Figure 5.10. Therefore, what may be happening is that the continued localization of yielding in the flanges as one moves from relatively weak to relatively stiff bracing leads to limit states where the individual cross-section dimensions of the member dictate that local buckling may control over a more global buckling mode. That is, with weaker bracing (as in Figure 5.10), the inside rafter flange and inside column flange move out-of-plane together, where stiffer torsional

bracing (as in Figure 5.11) forces local buckling in only the rafter flange, which, as mentioned in the development of the program, cannot be captured by SINBAD.

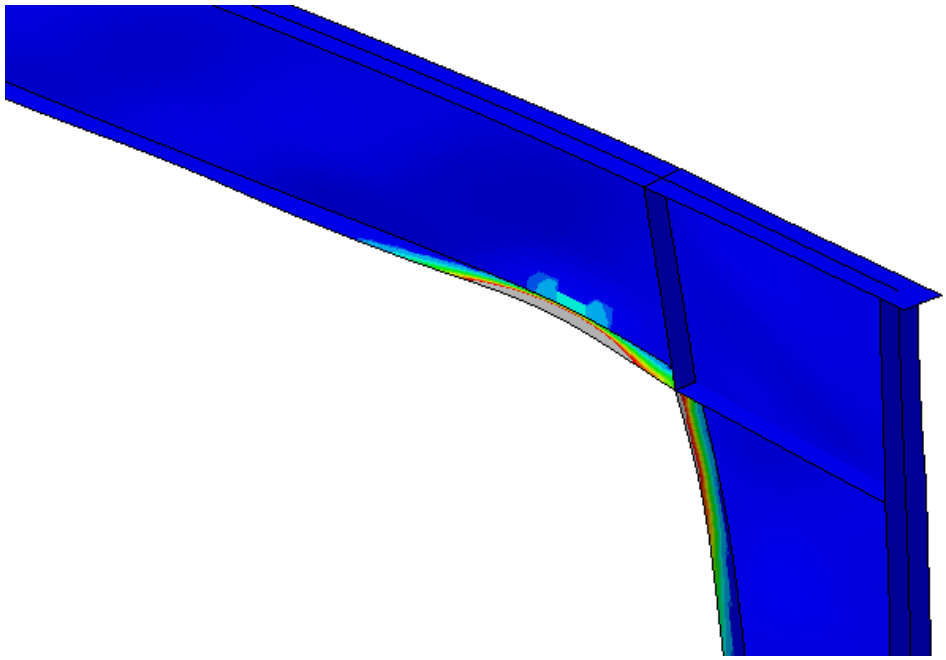

Figure 5.10: Contoured equivalent plastic strain for weak partial bracing, at the knee (from Abaqus)

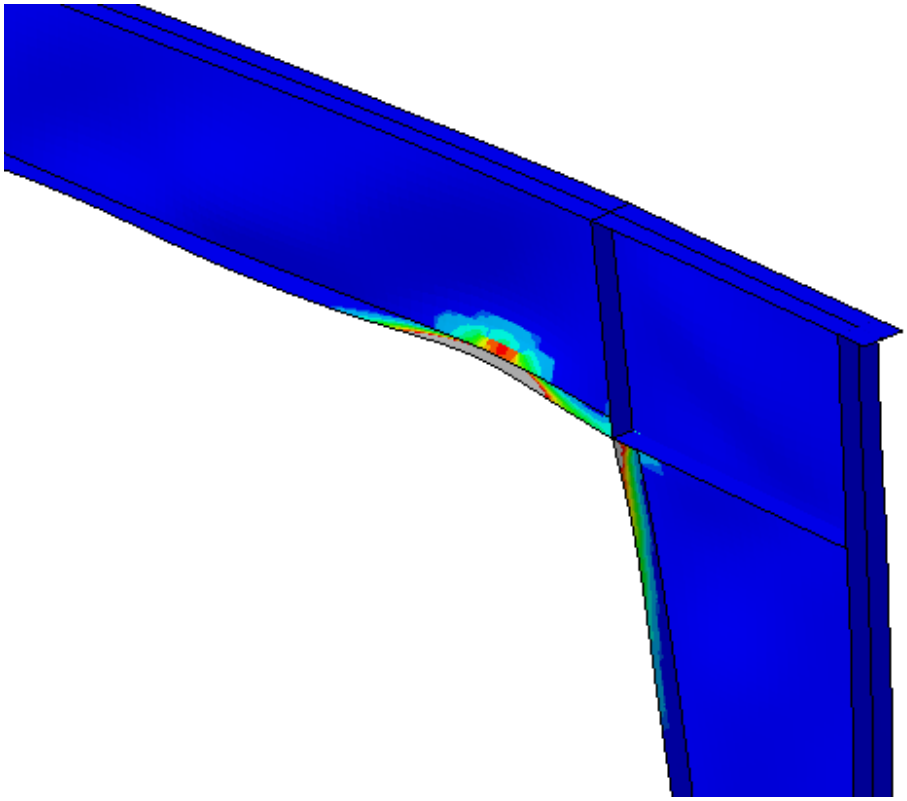

Figure 5.11: Contoured equivalent plastic strain for full bracing, at the knee (from Abaqus)

Figure 5.12 shows the brace force as a percentage of the moment in the frame for the last torsional brace on the column and the first torsional brace on the rafter (in the vicinity of the knee). The normalized flange force remains less than 3% for all results near the suggested stiffness, $\beta_{Req'd}$ = 3900 kip*in./rad.

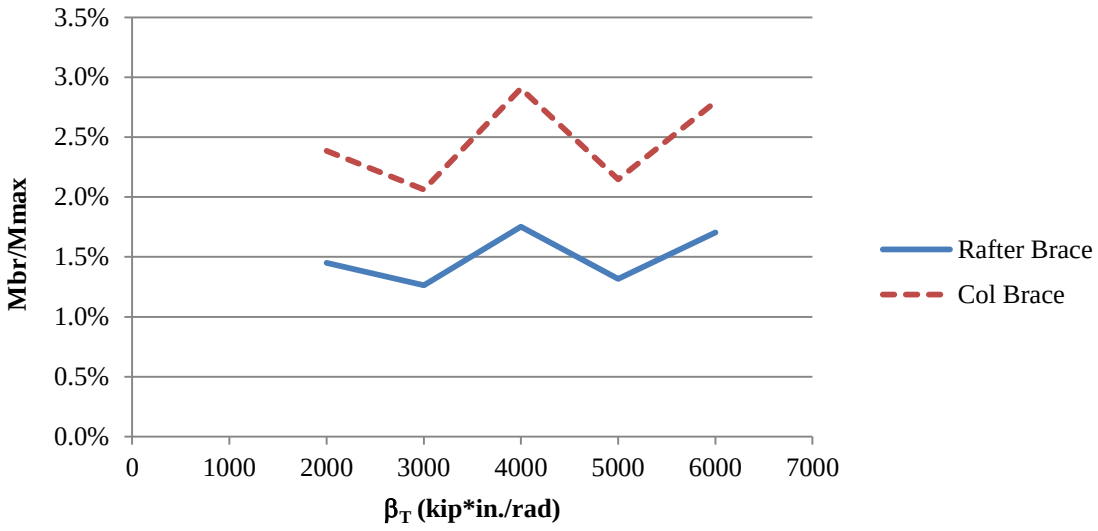

Figure 5.12: 90 ft clear-span frame; brace forces

5.2 Variation on the 90 ft Clear-span Frame

5.2.1 Introduction

This example explores how the use of flanges with increased widths affects the torsional stiffness and strength requirements. The frame, geometry, loading, residual stresses, and initial imperfections all remain exactly the same as in the previous example, with the only change coming from increasing the flange width from 6 inches to 8 inches. From the Specification, Chapter B (AISC 2010b), the limiting width-to-thickness ratio for a compact flange element is $0.38*\sqrt{(E/F_y)} = 8.7$ (with F_y = 55 ksi). Therefore, with λ = 8”/(2*0.5”) = 8 for the inside column flange and λ = 8”/(2*0.375”) = 10.67 for all other flanges, all flanges other than the inside column flange would be classified as non-compact. With this change to the flange compactness, the Specification now dictates that local limit states, such as flange local buckling or tension flange yielding, for a given member and loading must also be verified.

As has been discussed extensively, due to the use of beam elements for modeling of the flanges, SINBAD is unable to predict capacity limitations associated with local buckling limit states for the flanges (or technically, for the webs as well, since a new method was introduced in order to remove local buckling effects in the web). Therefore, one might expect the capacity determined using rigid bracing in SINBAD to over-predict the capacity reached in a simulation if flange local buckling or tension flange yielding controls for the critical segment.

Also, as a note when comparing the results for this example and the previous example with the original width flanges: the capacity reached by SINBAD or Abaqus will be different due to the effect that increased flange widths have on the cross-section moment of inertia and ultimately, the moment capacity. However, as was mentioned in the previous example, the overall magnitude of the load to reach the capacity of the frame is of little importance in this research where the major consideration lies in the bracing stiffness and strength requirements where the strength of the member or frame has essentially been normalized to rigorous, finite element simulations from Abaqus.

5.2.2 Brace Stiffness and Strength

The results for brace stiffness versus applied uniformly distributed load for the 90 ft frame with 8 inch flanges are presented in Figure 5.13.

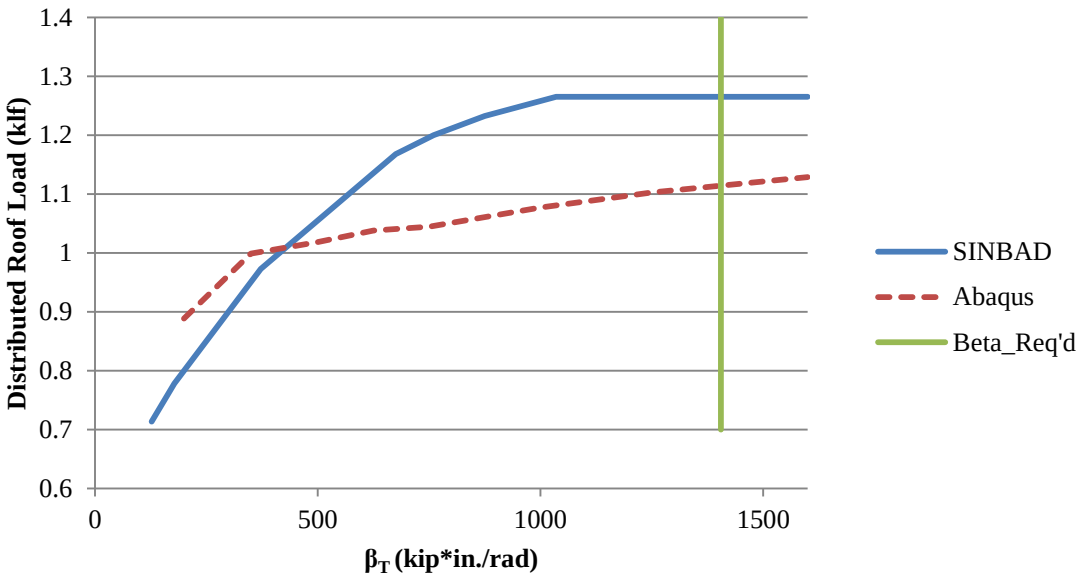

Figure 5.13: 90 ft clear-span frame with 8 in. flanges; knuckle curves

Similar to the previous example, SINBAD tends to over-predict the capacity from Abaqus and thus, slightly under-predicts the torsional stiffness requirements. However, again $\beta_{Req'd}$ suggests a bracing stiffness that approaches 90% of the fully-braced capacity of the frame, as determined from Abaqus.

Given the prior discussion about local buckling effects on the member, one may wonder why there is not an even larger variability in the capacities reached in this example, where the flanges are classified as non-compact versus the results from the previous example with compact flanges. The best explanation is that the increased out-of-plane moment of inertia has a larger effect on the capacity and bracing demands than the propensity for local buckling of the flange plates. This is evidenced by the fact that the bracing stiffness to reach the fully-braced condition (from either SINBAD or Abaqus) is significantly decreased by widening of the flanges.

Figure 5.14 shows the brace force as a percentage of the moment in the frame at that particular brace for the last torsional brace on the column and the first torsional brace on the rafter (in the vicinity of the knee). For a required bracing stiffness of 1400 kip*in./rad, the normalized force demands are less than 1% for either the column or rafter brace in question. Again, this is a large (almost three-fold) reduction in the bracing strength requirement as compared to the original frame design.

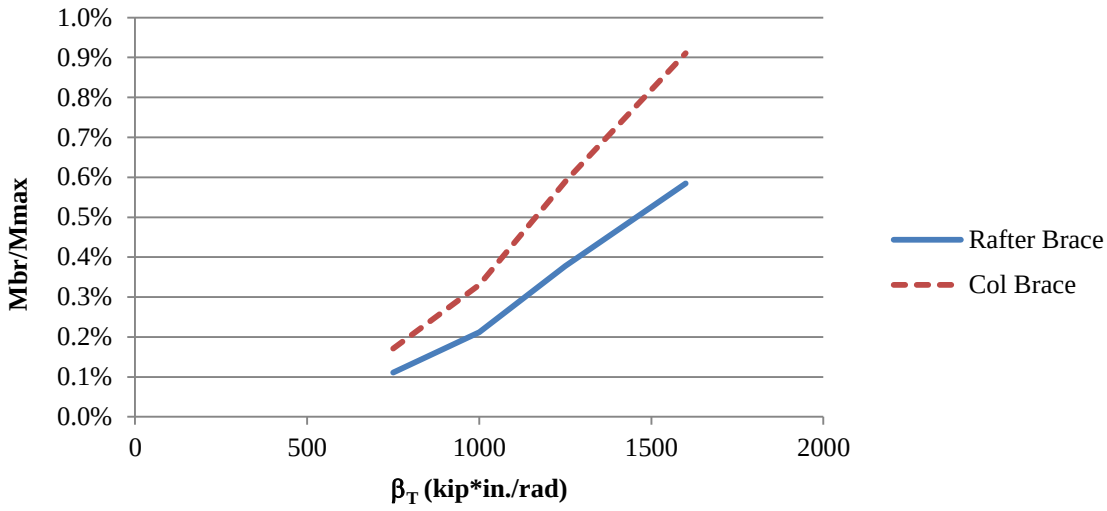

Figure 5.14: 90 ft clear-span frame with 8 in. flanges; brace forces

5.3 Modular Frame

5.2.1 Frame Geometry and Loading

The last frame example is a 300 ft modular frame. This frame was selected for study due to the complications arising with trying to determine the design bracing stiffness and strength requirements at an interior support. These locations in modular frames can experience tipping of the rafter with out-of-plane movement of the column, leading to

further destabilization of the rafter. This study shows that SINBAD can provide a reasonable estimate of the stiffness required to reach a full bracing condition.

An elevation view of this frame is presented in Figure 5.15 and a table of the pertinent geometry is provided in Table 5.2. This specific frame was originally designed by Mr. Duane Becker of Chief Industries. This modular frame has been extensively investigated by Sharma (2010), Kim (2010), and White and Kim (2006) and thus, the reader is referred to those publications for additional commentary.

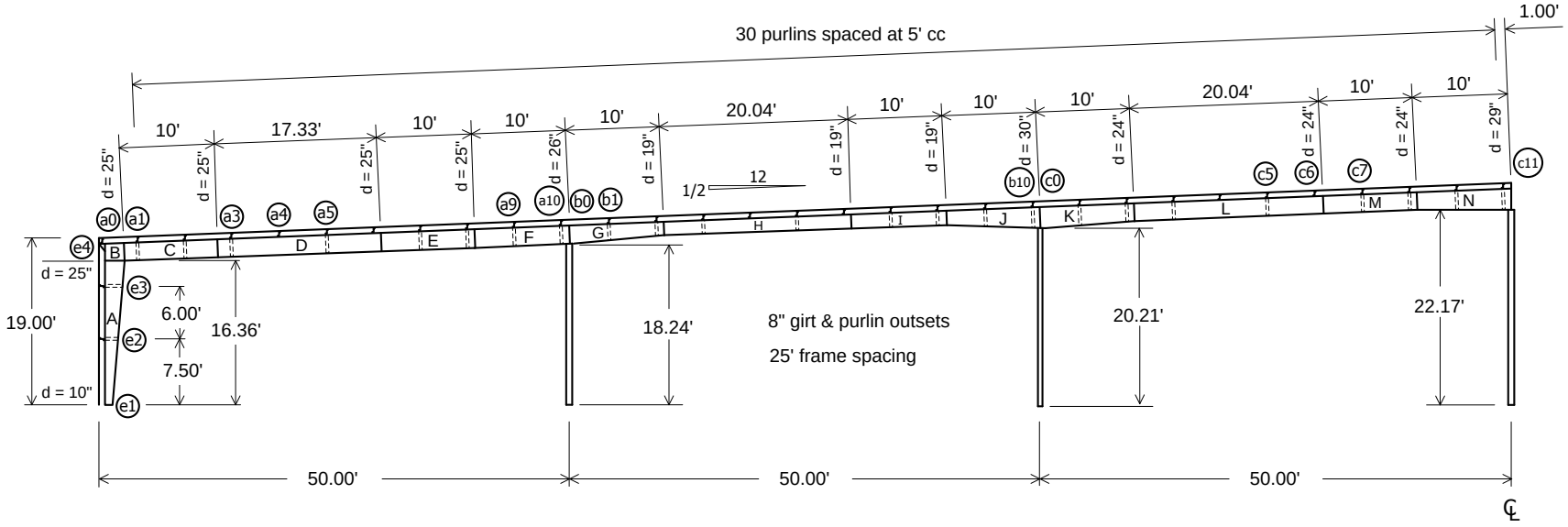

Figure 5.15: Elevation view of a 300 ft modular frame (only half of the frame is shown) (from Kim 2010)

Table 5.2: Summary of web and flange geometry, 300 ft modular frame[1] (from Sharma 2010)

Length	Location	Web				Inside Flange			Outside Flange		
		d (in)	t_w (in)	h/t_w*	h_c/t_w	b_f (in)	t_f (in)	$b_f/2t_f$	b_f (in)	t_f (in)	$b_f/2t_f$
A	e1	10	1/8	76		6.0	1/4	12.0	6.0	1/4	12.0
	e2	16.88		131							
	e3	22.38		175							
	e4	25		196							
B			5/32								
C	a0-a2'	25	5/32	157		6.0	1/4	12.0	6.0	1/4	12.0
D	a2'-a6'	25	1/8	196		6.0	1/4	12.0	6.0	1/4	12.0
E	a6'-a8'	25	5/32	157		6.0	1/4	12.0	6.0	1/4	12.0
F	a8'	25	3/16	130	124	6.0	3/8	8.0	6.0	5/16	9.6
	a9	25.41		132	126						
	a10	25.91		135	129						
	b0	26		135	129						
G	b0	26	3/16	135	129	6.0	3/8	8.0	6.0	5/16	9.6
	b1	23.13		120	114						
	b2	19.64		101	96						
	b2'	19		98	92						
H	b2'-b6'	19	5/32	118		6.0	1/4	12.0	6.0	1/4	12.0
I	b6'-b8'	19	1/8	148		6.0	1/4	12.0	6.0	1/4	12.0
J	b8'	19	3/16	98		6.0	5/16	9.6	6.0	5/16	9.6
	b9	23.46		122							
	b10	28.96		151							
	c0	30		157							
K	c0	30	3/16	157		6.0	5/16	9.6	6.0	5/16	9.6
	c1	27.57		144							
	c2	24.57		128							
	c2'	24		125							
L	c2'-c6'	24	3/16	123	133	6.0	1/2	6.0	6.0	3/8	8.0
M	c6'-c8'	24	3/16	123	133	6.0	1/2	6.0	6.0	3/8	8.0
N	c8'	24	7/32	107		6.0	1/4	12.0	6.0	1/4	12.0
	c9	26		117							
	c10	28.5		128							
	c11	29		130							

(1) The prime marks on the location symbols indicate positions corresponding to a cross-section transition. The symbols without prime marks represent purlin locations as shown in Fig. 8.1.*For F_y = 55 ksi, the web is compact for $h/t_w \leq 86$ and it is slender for $h/t_w \geq 130$.

Again, in the original design of the modular frame, the ASD loading combination involving uniform roof snow load was deemed the critical load combination. For the results presented in this thesis, the same scaling of a uniformly distributed factored load that was implemented in the two prior examples will be used herein.

5.3.2 Bracing Configuration

Similar to the analyses performed by Sharma (2010), it is assumed that all wall panels, roof panels, and x-bracing provided are infinitely stiff. That is, the outside flange of the rafter is considered rigidly braced at all purlin and girt locations. This assumption concerning the relative bracing allows one to directly assess how the torsional bracing stiffness affects the capacity of the frame.

5.3.3 Residual Stresses and Initial Imperfections

Residual stresses are applied to the frame in accordance with the discussed patterns in Chapter 3 by using the section properties at the mid-depth of the column and the girder separately to calculate any reductions necessary due to web plate buckling.

The same three classes of geometric imperfections presented in Section 5.1 are seeded in the model in keeping with the tolerances set forth in the Code of Standard Practice (AISC 2010a) and the Metal Building Systems Manual (MBMA 2006):

1. Canting of the frame in its plane by (eave height)/500 (Figure 5.16),
2. Out-of-plane flange sweeps in the vicinity of the knee and the first interior column (Figures 5.17 and 5.18), and
3. Out-of-plane web buckling modes (Figure 5.19).

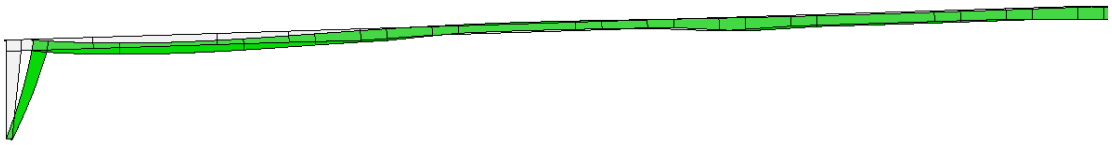

Figure 5.16: Imperfection 1: Canting of the frame by (eave height)/500, left-half of the frame shown (scaled 100x, from Abaqus)

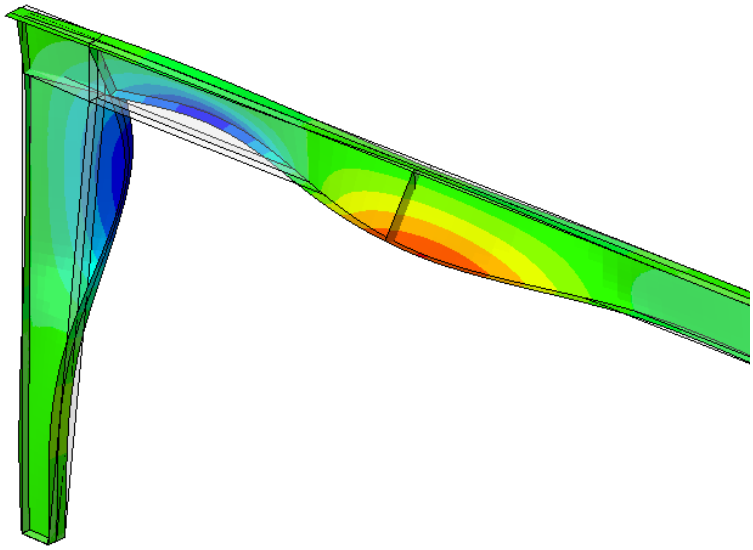

Figure 5.17: Imperfection 2: Contoured out-of-plane flange sweep at the knee (scaled 100x, from Abaqus)

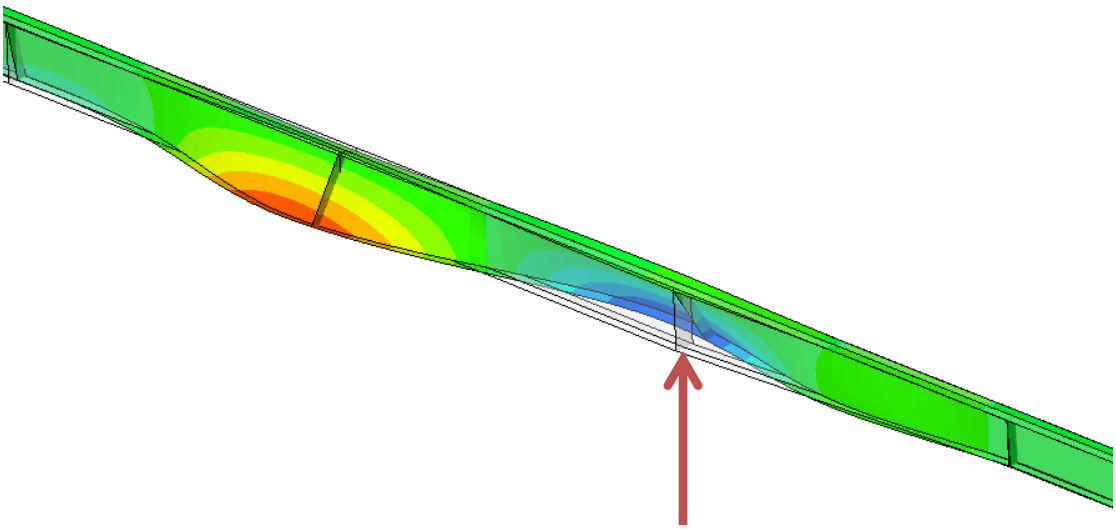

Figure 5.18: Imperfection 2: Contoured out-of-plane flange sweep at the first interior column (column location indicated by the red arrow, scaled 100x, from Abaqus)

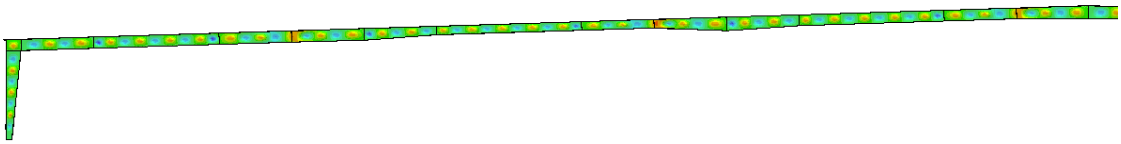

Figure 5.19: Imperfection 3: Contoured out-of-plane web local buckling modes, left-half of the frame shown (scaled 5x, from Abaqus)

The out-of-plane flange sweep is applied in the vicinity of the knee region and at the location of the first interior column due to the negative bending moments in these region (negative in the sense that the inside flange is in compression). The imperfections are applied in the same manner and with the same relative magnitudes as presented in the discussion of the 90 ft clear-span frame's imperfections.

5.3.4 Brace Stiffness and Strength

The results for brace stiffness versus applied uniformly distributed load for the 300 ft modular frame are presented in Figure 5.20.

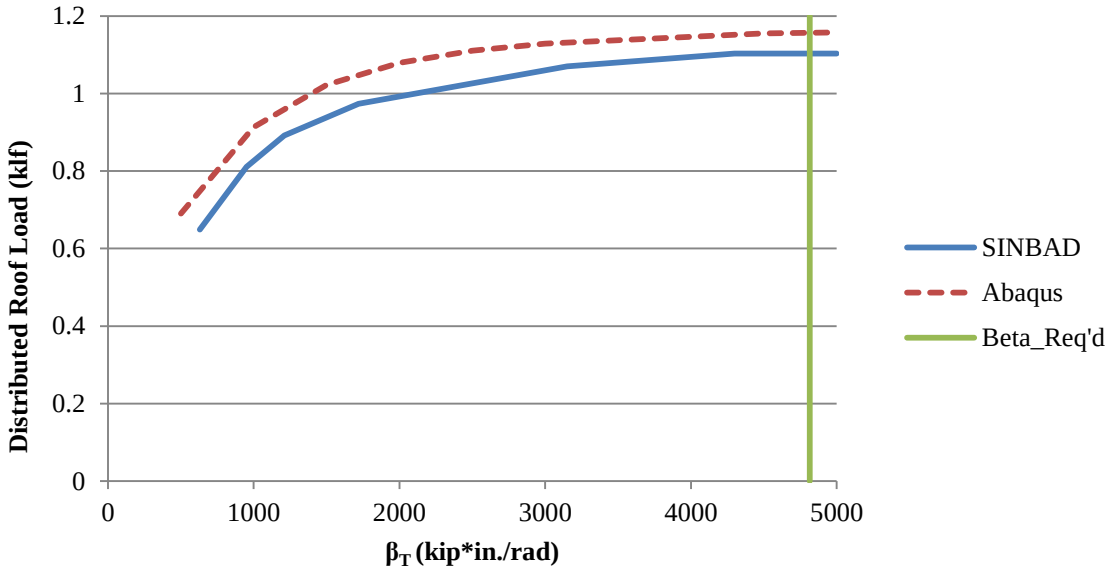

Figure 5.20: 300 ft modular frame; knuckle curves

As shown in Figure 5.20, this is a case where Abaqus slightly over-predicts the strength reached by the inelastic eigenvalue buckling solution from SINBAD. One possible reason for this discrepancy may be that while the imperfection patterns chosen and implemented in Abaqus may target the largest brace forces for bracing in the vicinity of the knee or the first interior column, they may not necessarily correlate with imperfections that are most deleterious to the capacity of the framing members. As was discussed and shown in Chapter 4 for the member cases, one generally targets one set

of imperfections that drive member capacity demands and another set of imperfections that target the largest brace force demands at a particular brace.

Another (albeit related) explanation for the difference in strengths may be due to the fact that the initial imperfections may be driving earlier yielding and local buckling of the webs that could potentially lead to redistribution of the loads away from the critical section. That is, with the application of loading, the initial web buckles and subsequent web yielding could potentially allow a pathway for stresses to be redirected to more lightly-loaded areas of the structure.

Despite the variance in capacity between Abaqus and SINBAD, $\beta_{Req'd}$ based on the inelastic eigenvalue-based knuckle curve from SINBAD is still able to almost develop fully-braced capacity that can be achieved in Abaqus.

Figures 5.21 and 5.22 are contour plots of the out-of-plane displacements near the first interior support and at the limit load on the structure for relatively weak torsional bracing and for torsional bracing that is approaching full bracing, respectively. The main difference between Figures 5.21 for weak, partial bracing and Figure 5.22 for full bracing lies in the localization of out-of-plane displacements. That is, for weaker torsional bracing, the failure mode is one where a larger portion of the rafter near the first interior column moves out-of-plane. Conversely, when torsional stiffness approaching the full bracing limit is used, the framing segment initially tries to move out-of-plane (similar to the case for weaker bracing), yet is arrested by the stiff torsional bracing, culminating in a failure mode incorporating buckling between brace points and as shown in Figure 5.22, local buckling of the compact flange plate.

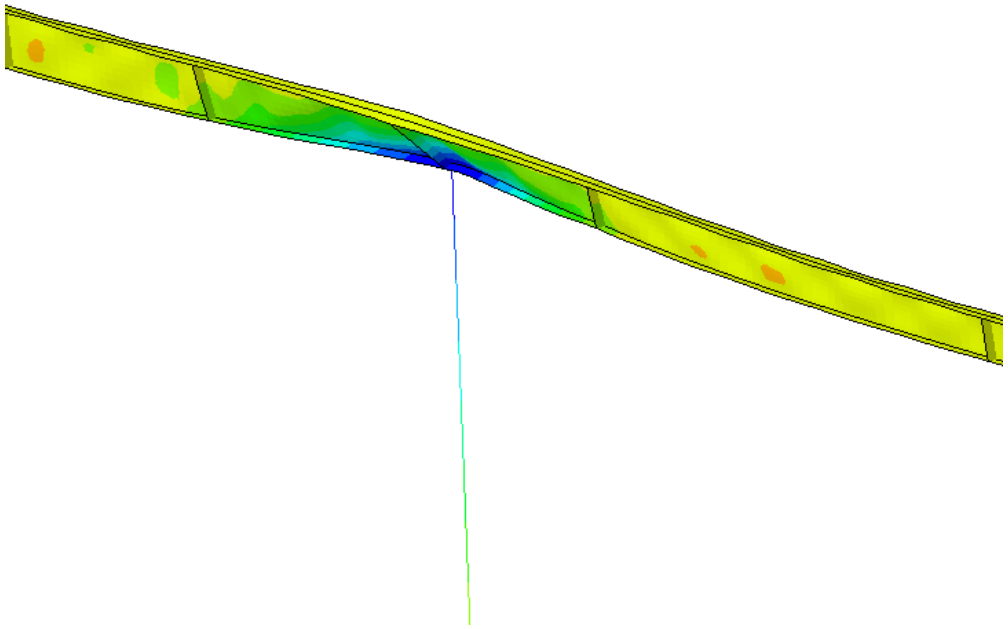

Figure 5.21: Contoured out-of-plane displacements at the first interior support with weak torsional bracing

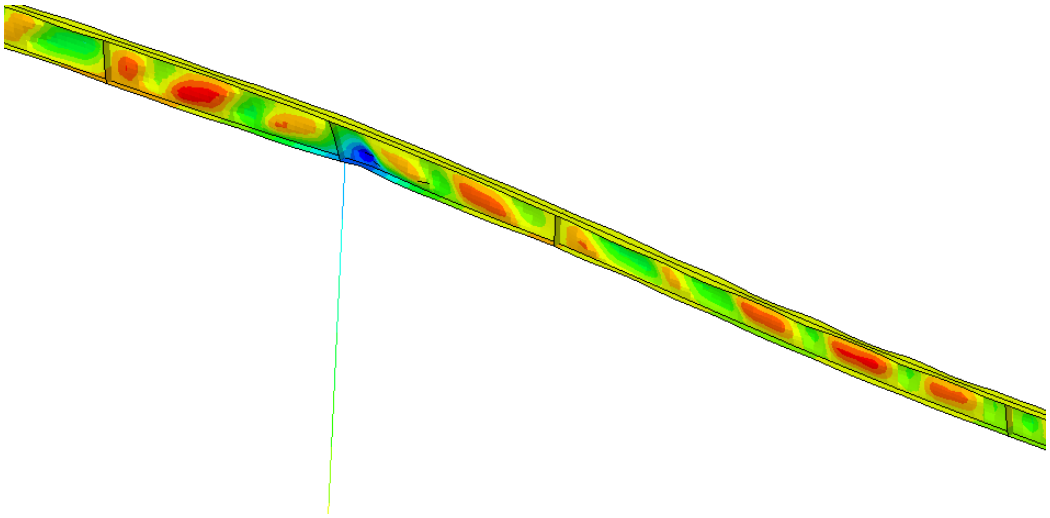

Figure 5.22: Contoured out-of-plane displacements at the first interior support with full torsional bracing

Lastly, Figure 5.23 shows the brace force as a percentage of the moment in the frame at the brace closest to the first interior support. For a required bracing stiffness of 4800 kip*in./rad, the normalized force demands are under 2%.

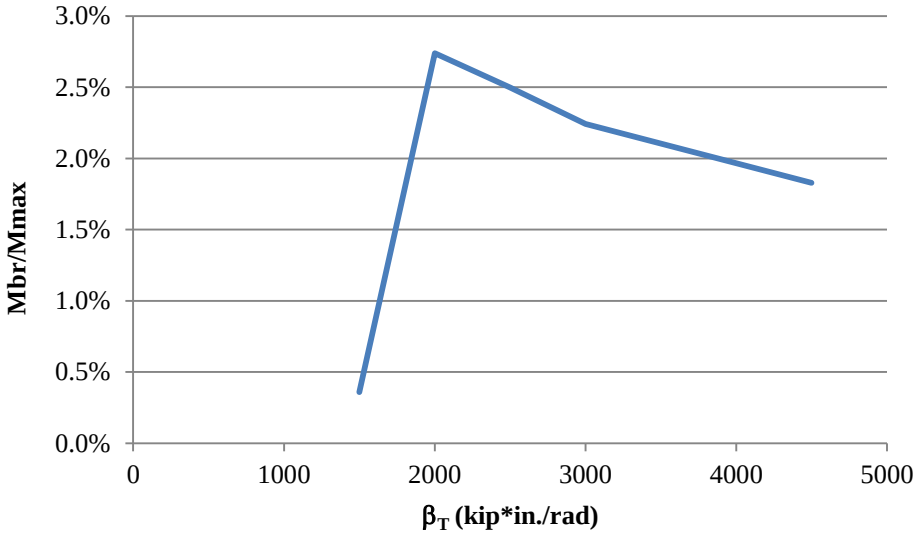

Figure 5.23: 300 ft modular frame; brace forces

6. SELECTION OF BRACING STRENGTH AND STIFFNESS FOR DESIGN

6.1 Design by Inelastic Analysis

Appendix 1 of AISC allows an engineer the freedom to perform any method of analysis that adheres to the rules stipulated therein. One benefit of pursuing such a complex analysis is that any limit states detected and accounted for within the analysis are not required to be checked via the main body of the Specification. The basic requirements of any inelastic analysis are that it must account for (AISC 2010b):

1. Flexural, shear, and axial deformations as well as any connection deformations,

   SINBAD considers flexural, shear, and axial deformations as well as any connection deformations that affect the deflections of the structure inherently through its analysis based on nonlinear finite elements. Any change in stiffness associated with yielding of the flange beam elements or of the web shell elements is tracked and recorded and the corresponding increased deflections are realized as part of the analysis.

2. Second-order effects (both of the P-Δ and P-δ variety),

   Second order effects are considered in SINBAD through the application of geometrically nonlinear beam and shell elements. That is, the equilibrium equations are formulated based on the element's deformed geometry, in

essence, capturing additional load effects as the internal forces act through the displaced geometry.

3. Geometric imperfections,

   SINBAD does NOT account for geometric imperfections, either explicitly or through the application of notional loads. This is due to the fact that SINBAD performs an eigenvalue buckling analysis procedure and not a load-deflection solution and thus, does not require initial out-of-plane movement to determine a measure of the out-of-plane response. Strictly speaking, any out-of-plane response produced in a buckling analysis is purely a scaling of the respective eigenmode and does not provide any physically measurable magnitude of the resulting out-of-plane deflections.

4. Any reductions of stiffness due to e.g., residual stresses or partial yielding, and

   It has been shown in Chapter 3 that SINBAD accounts for initial stress conditions through the application of residual stresses along the flange width and through the web depth. These residual stresses arise from the non-uniform cooling associated with the welding process. A single residual stress pattern has been proposed, justified, and utilized throughout this research.

5. Any uncertainty in member strength and stiffness.

   Uncertainty in stiffness and strength must be accounted for in order to use SINBAD for design. Therefore, a reduction factor must be placed on the yield

stress and stiffness prior to the analysis. Design by Inelastic Analysis as described in Appendix 1 requires that the material properties be factored by 0.9 to account for this uncertainty.

Another caveat for the use of Appendix 1 requires any analysis to be performed with the loads at their ultimate level. That is, load and resistance factor design (LRFD) pursuant to Section B3 of the Specification must be used in the analysis (AISC 2010b). It is NOT sufficient to perform an analysis under service level loads and then attempt to factor the results to reach an ultimate state, since generally, different levels of load will lead to a different distribution of stress and yielding and ultimately, a different in-plane solution and buckling capacity. More succinctly, the application of loads and the resulting stresses and deformations from an inelastic analysis are not related linearly.

SINBAD lacks the capacity to predict limit states associated with local buckling; namely, flange local buckling and web local buckling. Since the flanges and stiffeners are modeled using cubic Hermitian beam elements instead of shells, it is not possible for the beam elements to detect local buckling. For the shell elements used in the modeling of the web plates, a procedure was introduced in Chapter 3 to prevent inconsequential web local buckling from dominating the eigenvalue buckling modes. This procedure effectively condenses the internal stresses associated with the Gauss points and internal nodes to only allow out-of-plane movement at the web-flange juncture. This modification, while sufficient to produce accurate buckling results, effectively violates one of the major stipulations for the use of Appendix 1. However, all is not lost. The Specification does permit the use of inelastic analyses even if that analysis does not detect all limit states

provided that the engineer verifies with the general requirements laid out in the main body of the Specification that those limit states do not control the design of the section.

One last stipulation in AISC's Appendix 1 disallows its use for seismic design. The reader is referred to the Commentary to Appendix 1 (AISC 2010b) for a further discussion of the topic. The limitation is simply mentioned here for completeness and will be discussed in moderate detail in the discussion of the bracing strength requirements in Section 6.3.

Given the above requirements that are unmet by SINBAD, it is not permissible to use SINBAD to design or verify the specific *member capacities*. For example, if one created a knuckle curve for the capacity of a member versus applied bracing stiffness and noticed that the capacity predicted by SINBAD was higher than the intended design load, the engineer would not be able to necessarily conclude that a higher design load could be placed on the structure. Any change in the member design would require that all the limit states including local buckling effects not specifically addressed by SINBAD are re-verified by the designer.

Pursuant to the discussion above and in accordance with the limitations stipulated in Appendix 1, it is permissible to design the bracing system using SINBAD since all the ingredients required for such an analysis are included in the analysis package. Despite not having initial geometric imperfections applied in the model, the design of the bracing system, which acts as a secondary load-carrying system (secondary in the sense that the only loads applied to the bracing come from out-of-plane movements associated with the deflections of the primary load-carrying system, e.g., beams or frames) is permitted

using this computational tool, since the proclivity for members to buckle out-of-plane is captured accurately by an inelastic eigenvalue buckling analysis.

6.2 Bracing Stiffness Requirements for Design

As was introduced in Section 4.6.3, the recommendation from this research is that the bracing stiffness required to reach full bracing of the member should be provided. This recommendation is founded on the following two observations which will be discussed in the following two sections:

1. At the knuckle of the capacity versus stiffness plots shown throughout this thesis, any further reduction in the stiffness could result in a precipitous drop in the capacity of the member being braced, and
2. A reasonable level of bracing stiffness should be provided to minimize out-of-plane displacements and effectively keep the bracing strength requirements manageable.

6.2.1 Providing for the Plateau

The first observation can be substantiated through the many knuckle curve plots presented in this thesis. For these generalized plots of member (or frame) capacity versus bracing stiffness, it is wise to aim for levels of bracing stiffness on the plateau of the curve, such that any variation in the stiffness does not cause an unfortunate drop in the member strength.

Also shown in the knuckle curve plots was the AISC Appendix 6 requirement. This requirement is based on solutions from an *elastic* eigenvalue buckling analysis where

the ideal stiffness is subsequently scaled to ensure that an adequate level of stiffness was provided to reach the intended capacity of the section and to maintain manageable brace forces. While the requirements shown in the figures were generally conservative, a major problem is that there are a number of attributes of real structures that do not fit into the narrow scope required for the use of Appendix 6. In defense of the equations, it is practically impossible to provide codified equations that are able to accurately capture the many inherent complexities in determining the bracing requirements for complicated structures.

The use of an inelastic eigenvalue buckling analysis and then an appropriate scaling to ensure that an adequate level of bracing stiffness is provided directly parallels the procedure outlined in Appendix 6. The main difference is that instead of basing the requirements on the elastic state of the structure, SINBAD aims to assess the more realistic bracing requirements by accurately capturing the current state of stress and yielding.

Additionally, a specific procedure was proposed in Section 4.6.3 whereby an appropriate scaling was performed to ensure that any stiffness requirements from SINBAD were able to match the physical demands observed from simulation studies. The following is a concise step-by-step procedure for determining the required bracing stiffness from SINBAD:

1. Determine the load level corresponding to an eigenvalue equal to 1.0 when the braces are modeled as rigid constraints.

2. Apply a load value equal to 95% of the load reached in Step 1 and iterate the stiffness until an eigenvalue equal to 1 is obtained.
3. Apply a load value equal to 90% of the load reached in Step 1 and iterate the stiffness until and eigenvalue equal to 1 is reached.
4. The required bracing stiffness, $\beta_{Req'd}$, is then taken as the summation of stiffness determined in Step 3 and Step 4.

The reasoning behind the selection of stiffness values as 95% and 90% of the rigidly-braced capacity was discussed in Section 4.6.3. In essence, the main idea is to assess where one lies on the knuckle curve without having to create the entire curve. If the stiffness requirements from 95% and 90% of the rigidly-braced capacity are fairly close together, then that indicates that one is generally at or near the knuckle and the summation of the two requirements will provide up to two times the requirement to reach 95% of the strength (in the limit that one is on the vertical portion of the knuckle curve, the scaling would be exactly two times the 95% stiffness requirement). Conversely, if the difference in stiffness associated with 95% or 90% of the capacity is relatively far apart, this generally indicates that one is at or near the plateau and the addition of the 90% capacity to the 95% will not result in a large increase in the required stiffness. It should be noted that some results showed that this summation of bracing stiffness measures does not quite allow the member to reach the fully-braced capacity as indicated by Abaqus. However, generally the requirement was still able to reach 90 to 95% of the rigidly-braced capacity. While not specifically reaching the condition of full bracing may make some engineers uneasy, there is some consolation in the knowledge that it is highly unlikely that the worst case loading, imperfection pattern, and residual stress will

all occur at a location where the member is at its capacity limit simultaneously. Therefore, it is suggested that any bracing stiffness that provides on the order of 90 to 95% of the capacity of the system is “good enough”.

It should be noted that for cases involving unequal brace spacing and/or stiffness, the structural resistance is generally asymptotic to the rigid bracing strength with increase in brace stiffness. There is no specific bracing stiffness value where the rigid bracing capacity is reached. There is precedent for using the 95 % and 90 % of the rigid bracing strength as a design target in prior research such as Stanway et al. (1992a and b).

6.2.2 Managing Bracing Strength Requirements

Chapters 4 and 5 also showed how different selections for the applied bracing stiffness can affect the bracing strength demands. Relatively lower stiffness values generally drive brace point movement which in turn, leads to higher forces in the brace. However, this is not always so. Depending on the level of stiffness provided, in some cases it may not take much movement to force larger brace strength demands.

As mentioned previously, one of the main points to scaling the ideal bracing stiffness from SINBAD is to make sure that the brace force demands do not become “too large”. Obviously, there is some optimal combination of brace stiffness and brace strength demands that would lead to the most economical bracing scheme. However, to have an idea of the brace force demands, one must perform a load-deflection solution, since an eigenvalue buckling solution does not provide any information about the true magnitude of the out-of-plane displacements. Therefore, SINBAD must be corroborated with load-deflection solutions to ensure that any suggested stiffness recommendation comes with

a force (or strength) recommendation that can generally be achieved in practice. The specifics of the strength requirements will be deferred to the next section, but it has been shown (see Yura 2001, for example) that to maintain moderate brace forces, one generally needs to scale the ideal bracing stiffness by some amount (generally, $2/\phi$ in the Specification). Effectively, a scaling of the brace stiffness requirements is achieved by summing the brace stiffness requirements at 95% and 90% of the full-bracing capacity. It will be shown in Section 6.3 that this generally leads to reasonable brace forces.

6.2.3 Combined Bracing Types

The final item for discussion concerning the bracing stiffness requirements is how one should address multiple bracing types. Both Cases 3h and 3j presented in Chapter 4 were cases where relative bracing was used in tandem with torsional bracing. In the analysis for these two cases, only the torsional bracing was varied; i.e., it was assumed that the relative bracing remained constant. From these examples, the reader may be left thinking, how should the relative bracing stiffness be scaled to ensure that the relative bracing stiffness requirements approach full bracing in a manner similar to what is shown for the torsional bracing?

The answer to this question lies in the simple scaling of the "unadjusted" brace by the AISC factor of $2/\phi$. That is, when one holds the relative bracing constant and varies the torsional bracing, the torsional bracing will be scaled according to the procedure detailed in Section 6.2.1 and the relative bracing will simply be scaled by $2/\phi$. In contrast, if the torsional bracing is held constant while the relative bracing is varied to determine the

knuckle curve, than the relative bracing will implement Section 6.2.1 while the torsional bracing is scaled by $2/\phi$. The use of a “static” scaling of the brace that is not changed is purely to ensure that the bracing strength requirements are within reason. In essence, this procedure ensures that the stiffness required for the unadjusted bracing type is still some multiple of its ideal bracing stiffness. In general, it is not necessary to create two separate knuckle curves, one based on varying each bracing type while holding the other constant, since the generation of one curve provides a representative capacity of the system that can be reached given the entire bracing system.

6.3 Bracing Strength Requirements for Design

Sharma (2010) looked extensively into the bracing strength and stiffness requirements using full nonlinear finite element simulations of complete metal building frames. He determined that the strength requirements were rarely over 4% of the corresponding member internal moment for torsional bracing. In fact, Sharma found that usually around 2% of the internal moment was enough to allow the member to reach within 95% of its capacity. Lastly, he noted that the comparable relative bracing limit was around 1%.

In this research, the key concept is to determine the ideal stiffness directly and use some multiple of that stiffness as the torsional or relative stiffness requirement. However, if the bracing stiffness becomes too low, than substantial brace point movement can occur. And since brace point movement is directly proportional to the brace force (and strength requirement), it is very important to manage the out-of-plane movement of the brace. Currently, the AISC Specification Appendix 6 addresses this by embedding a factor of

two in the bracing stiffness requirement equation (see, e.g., Yura 2001 for a more complete discussion).

Table 6.1 is an amalgamation of the brace force plots shown in Chapter 4 for the member studies and lists the maximum and minimum normalized brace force as well as the normalized brace force when $\beta_{Req'd}$ is used. In this case, the term "normalized" is used to suggest that the bracing forces have been divided by the maximum moment or the equivalent flange force at the location of the brace. One should note that any subsequent references to "brace forces" or "brace force demands" (or similar) will mean the normalized values and not the actual brace force.

Table 6.1: Normalized brace forces from the member studies

Case	L	L_b	No. of Seg.	Brace Type	n_T or n_R	C_b	Notes:	Max. Brace Force	Min. Brace Force	Brace Force at $\beta_{Req'd}$
1a	192	48	4	T	3	1		4.0%	1.2%	1.8%
1b	192	48	4	R	4	1		1.3%	2.3%	1.4%
1c	432	144	3	T	2	1		2.6%	1.6%	1.8%
1d	192	96	2	T	1	1.3		0.47%	0.16%	0.20%
1e	192	96	2	R	2	1.3		0.56%	0.11%	0.13%
2a	192	48	4	T	3	1		2.6%	1.4%	2.3%
2b	192	48	4	R	4	1		2.4%	0.8%	0.9%
3a	192	48	4	T	3	1		1.9%	1.5%	1.6%
3b	192	48/96/48	3	T	2	1		1.2%	0.8%	1.1%
3c	192	48/96/48	3	T	3	1	Wide Flanges	1.5%	1.0%	1.2%
3d	432	144	3	T	2	1		3.4%	2.2%	2.4%
3e	90	30	3	T	2	1		1.3%	0.9%	1.0%
3f	192	96	2	T	1	1.3		1.5%	1.1%	1.4%
3g	192	48	4	T	3	1	Includes Axial Load	2.8%	1.6%	2.7%
3h	192	48	4	T & R	3/4	1	R = 1 kip/in. Comp. FL	1.0%	0.7%	0.7%
3j	192	48	4	T & R	3/4	1	R = 1 kip/in. Ten. FL	1.3%	1.2%	1.2%
4a	192	48	4	T	3	1		2.5%	1.6%	1.8%
4b	192	48	4	R	4	1		2.3%	0.5%	0.6%

A number of observations can be gleaned from Table 6.1 when looking at the brace force demands for an applied stiffness equal to $\beta_{Req'd}$:

1. The torsional bracing forces are never greater than 3% and often hover at or under 2%. The major exception to this statement is shown for Case 3g, where the brace force is around 2.7%. However, this example is subjected to bending and axial loads (beam-column) and thus, it is reasonable to expect that the brace stiffness and force demands will increase with the application of axial loads.
2. The relative bracing shear force is generally less than 1% except for the Case 1b, where the brace force is on the order of 1.4%.
3. The addition of relative bracing in tandem with torsional bracing reduces the brace force demands on the torsional bracing (comparing Cases 3h or 3j to Case 3a). This occurs since the relative bracing reduces brace point displacement, which in turn, limits rotation of the flanges relative to one another, ultimately reducing the brace force demands on the torsional bracing.

The results from the frame studies (see Chapter 5 for the brace force plots) show bracing forces at an applied $\beta_{Req'd}$ of:

- 2.8% in the column brace and 1.7% in the rafter brace for the 90 ft clear-span frame
- 0.75% in the column brace and 0.45% in the rafter brace for the variation on the 90 ft clear-span frame with 8 in. wide flanges
- 2% near the first interior column in the 300 ft modular frame

From the results from the member studies and the frame studies shown above, a reasonable recommendation for the bracing force requirement should be on the order of 2.5-3% for the case of torsional bracing and 1-1.5% for the case of relative bracing. These recommendations are on the same order of magnitude as those observed by Sharma (2010).

One specific caveat for the brace forcing requirements shown above is that these strength requirements are generally insufficient to support large cycles of loads, as may be experienced during a seismic event. In fact, the brace forces presented herein are determined based on the maximum force when the limit load of the structure is reached assuming static loading. That is, the members and frames have not been taken past their limit loads to assess bracing force demands for a post-peak response. Ongoing research in the field of seismic design for bracing systems is aiming to assess the true stiffness and strength requirements when metal building structures are subjected to seismic loads with large cycles in the loading magnitude and direction.

7. CONCLUDING REMARKS

7.1 Summary

This research incorporates a number of attributes of metal building frames that lie outside the scope of AISC's Appendix 6, namely:

- Consideration of web-tapered members,
- Unequal brace stiffness,
- Unequal brace spacing,
- Warping and lateral bending restraint from joints and continuity across brace points,
- Combination of bracing types, and
- Reduced demands in non-critical regions.

This research builds on prior work by Yura (1993, 1995, 1996, 2001), Yura and Helwig (2009), Tran (2009), Kim (2010), and Sharma (2010) and seeks to develop a method that is based on sound theory yet practical for use in design. By developing an inelastic eigenvalue buckling tool (SINBAD) and correlating it to extensive simulation studies, the engineer has a more accurate means with which to incorporate the above attributes into a safe structural design for bracing systems.

Differences in brace stiffness requirements between eigenvalue buckling analysis results from SINBAD and load-deflection simulations in Abaqus were addressed by scaling of the ideal bracing stiffnesses obtained by SINBAD in order to predict physical bracing stiffness demands and ensure that sufficient brace stiffness is provided in order to force

buckling between brace points. The necessary scale factors are determined such that the physical structure is effectively fully braced and such that the magnitudes of the brace forces are manageable.

7.2 Key Research Findings

The key findings from this research project are the following:

- An inelastic eigenvalue buckling solution can be used to predict bracing stiffness demands for a member or for a complex frame system. Through the inclusion of all bracing types, inherent consideration of warping and other continuities across brace points, coupled with the ability to specify any brace stiffness at any location, an inelastic eigenvalue buckling solution provides a more economical and less time-consuming method with which to design bracing.
- Efficient procedures are devised for determining the bracing stiffness requirements from an inelastic eigenvalue buckling solution. These procedures are benchmarked to rigorous, nonlinear finite element analysis simulations from Abaqus.
- Providing relatively stiff torsional bracing does not preclude a member from buckling in a global mode. Even under uniform bending of a compact section, the tension flange may not be sufficient to prevent global lateral movement of the entire system. This effect is more pronounced in longer spans that lack adequate lateral bracing. However, torsional bracing is effective at allowing the member to develop the load capacity associated with the assumption that the torsionally-braced locations are brace points.

- A new method is introduced to remove the web local buckling modes from an eigenvalue buckling solution. By removing local modes that correspond to stable post-buckled conditions, one can focus on the flange buckling modes that generally have the largest influence on brace strength and stiffness demands.
- Residual stresses and initial geometric imperfections often drive simulations to fail at loads smaller than an eigenvalue buckling analysis prediction. For slender-web sections this becomes even more true as the web buckles under the residual stress or small application of load and begins to shed load to the flanges. At the same time, the flanges are deflecting out-of-plane under in-plane loads due to these imperfections, further exacerbating yielding on one side of the flange.
- The application of geometric imperfection patterns to determine the most deleterious effects on any one brace can be a daunting endeavor. The imperfections need to be applied in an approach akin to the application of different load combinations to determine which imperfection patterns give the largest demands on the strength and stiffness of the different braces in the structure. Also, if one had many load combinations to perform, the number of possibilities of selecting the worst load case with the worst imperfection for each brace becomes endless. It is precisely for this reason that load-deflection solutions are so laborious and thus, not practical for a typical designer to use for assessment of stability bracing requirements.
- If possible, relative bracing should always be provided in tandem with torsional bracing, where the relative bracing is applied on the compression flange. This is

due to the fact that torsional bracing is excellent at preventing twist of the section, yet global lateral displacement can still occur. The most effective and efficient way to provide stability to a member or frame is through a combination of relative and torsional bracing.

- Lateral-torsional buckling of the member always leads to local buckling in the flange. As the member deflects laterally, one side of the compression flange continues compressing while the other side starts to relieve its compression. The amplification of the initial imperfection as the member displaces laterally causes one side of the flange to yield earlier and then ultimately, form a local buckle. This local buckling of the flange can lead to a sharp rise in the brace force demands, which could cause the brace components or connections to rupture.
- When the ideal bracing stiffness from SINBAD is appropriately scaled to the suggested bracing requirement (effectively providing full bracing), the torsional bracing force requirements are on the order of 2.5 to 3% of the moment at the brace location. Similarly, for full bracing as determined by SINBAD, the relative bracing shear force requirements are on the order of 1 to 1.5% of the equivalent flange lateral force at the location of the brace. These bracing forces are based on a static application of the load and are not sufficient for cyclic loading commonly experienced during a seismic event.

7.3 Recommendations for Future Work

The following are some recommendations for future work in assessing stability bracing requirements:

- Explore how cyclic loading drives brace strength and stiffness demands. The current research has focused on the static application of loads and the strength and stiffness required to stabilize the structure under those loads. More research needs to be performed in order to assess how the cyclic application of loads, potentially with the failure of individual components of the bracing system, affects the strength and stiffness that would be required for ductile seismic design.
- All the studies presented herein have assumed that the required stiffness and strength could be provided by typical stability bracing components and details. However, if for instance, a roof purlin is designed to brace the rafter and is also counted on as a component in the gravity framing system, how does the interaction between the secondary forces due to bracing and the primary forces due to gravity loading affect the ability of the bracing component to provide sufficient stiffness and strength to the member requiring bracing?
- As was mentioned briefly in the discussion of the LTB curves, what is driving the difference between simulation results and the AISC predictions for LTB? How do simulation results compare to other standards such as the European codes? Further investigations are needed to determine how the selection of different standards with varying predictions for the member's LTB strength affects bracing requirements for that member.
- There appears to be some sensitivity of the torsional bracing stiffness requirements to the compactness of the web for the member studies. Further cases should be analyzed and potentially tested experimentally to determine if

any generalizable conclusions can be drawn about the effects that the web compactness has on the torsional bracing stiffness requirements.

APPENDIX A

A. EXCEL WORKSHEET INTERFACE

The two options for importing data into SINBAD are the Excel worksheet interface and the application program interface. This appendix provides detailed information and screen shots of the information required for SINBAD from the Excel input only. For all the following figures, yellow (shaded) cells signify information that is editable by the user.

A.1 Beam Module

The beam module is broken into three separate input tabs:

1. General – Figure A.1 – A basic information tab that allows the user to specify the material properties, boundary conditions, and parameters for the solution algorithm.
2. Geometry – Figures A.2, A.3, and A.4 – The specific section properties tab where all of the section dimensions are included, the purlin/girt locations and bracing information is stipulated, and the stiffener geometry is specified. SINBAD has the capability to accept up to 30 section transitions, 30 purlin or girt bracing locations, and 30 stiffener locations.
3. Loading – Figure A.5 – The loading tab is where the user can specify the location, magnitude, and direction of loading. SINBAD is able to accept up to 30 different load locations for the given member.

E =	29000	ksi	v =	0.3					
Fy =	50	ksi	Et =	290					
Fu =	70	ksi	Est =	900					
# of Load Increments :			5		Initial Increment:	0.2	<===	It is highly recommend to leave	
Max. # of Equil. Iterations:			30				<===	these values unchanged.	
Boundary Condition:	pin-pin				☐	Torsionally Fixed - START			
					☐	Torsionally Fixed - END			

Figure A.1: Member “General” tab (from Excel input)

SECTION PROPETIES

Section	Length (ft)	tw (in.)	bfi (in.)	tfi (in.)	bfo (in.)	tfo (in.)	CumSum	ho start (in.)	ho end (in.)
1	5	0.25	5.5	0.345	5.5	0.345	5	15.355	15.355
2									
3									
4									
5									
6									
7									
8									
9									
10									
11									
12									
13									
14									
15									
16									
17									
18									
19									
20									
21									
22									
23									
24									
25									
26									
27									
28									
29									
30									
								Web Elem. =	4
								Fl. Elem. =	2

*Note: A new section must be defined every time either of the flanges or the web changes thicknesses.

Figure A.2: Member “Geometry” tab, section properties (from Excel input)

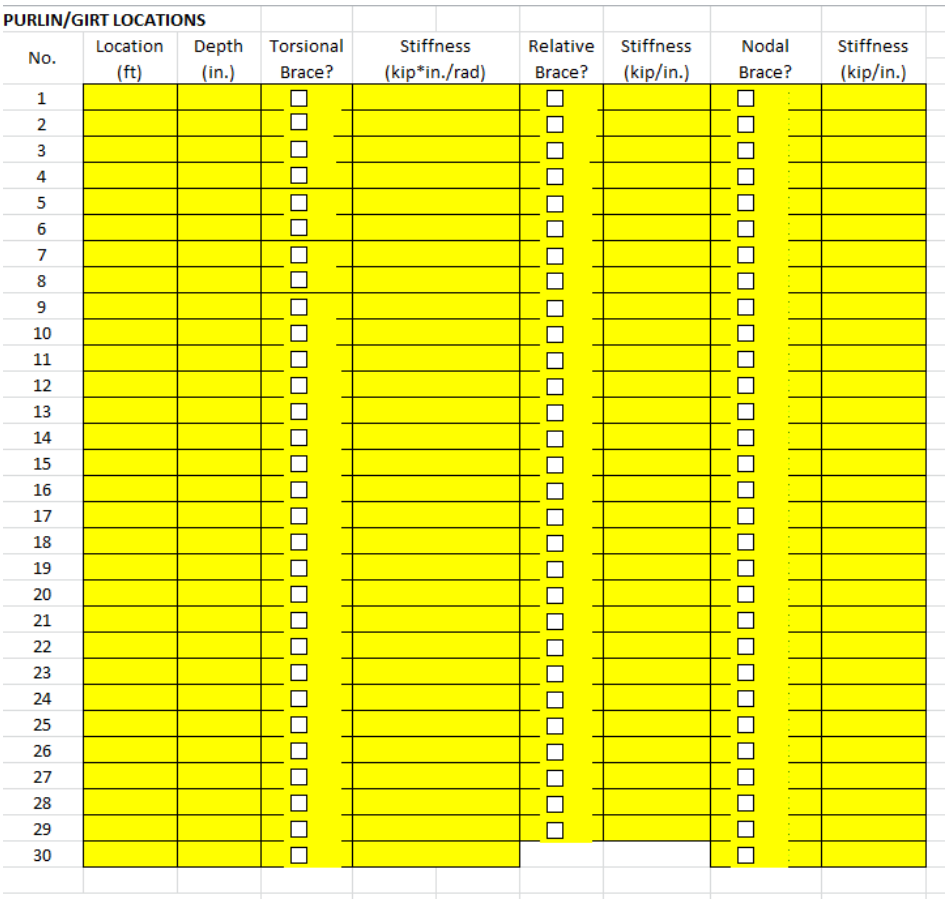

PURLIN/GIRT LOCATIONS

No.	Location (ft)	Depth (in.)	Torsional Brace?	Stiffness (kip*in./rad)	Relative Brace?	Stiffness (kip/in.)	Nodal Brace?	Stiffness (kip/in.)
1			☐		☐		☐	
2			☐		☐		☐	
3			☐		☐		☐	
4			☐		☐		☐	
5			☐		☐		☐	
6			☐		☐		☐	
7			☐		☐		☐	
8			☐		☐		☐	
9			☐		☐		☐	
10			☐		☐		☐	
11			☐		☐		☐	
12			☐		☐		☐	
13			☐		☐		☐	
14			☐		☐		☐	
15			☐		☐		☐	
16			☐		☐		☐	
17			☐		☐		☐	
18			☐		☐		☐	
19			☐		☐		☐	
20			☐		☐		☐	
21			☐		☐		☐	
22			☐		☐		☐	
23			☐		☐		☐	
24			☐		☐		☐	
25			☐		☐		☐	
26			☐		☐		☐	
27			☐		☐		☐	
28			☐		☐		☐	
29			☐		☐		☐	
30			☐				☐	

Figure A.3: Member “Geometry” tab, purlin/girt locations (from Excel input)

STIFFENER LOCATIONS

Stiffener	Location (ft)	Side	Thickness (in.)	Width (in.)
1	0	Both	10	5.5
2	5	Both	10	5.5
3		Both		
4		Both		
5		Both		
6		Both		
7		Both		
8		Both		
9		Both		
10		Both		
11		Both		
12		Both		
13		Both		
14		Both		
15		Both		
16		Both		
17		Both		
18		Both		
19		Both		
20		Both		
21		Both		
22		Both		
23		Both		
24		Both		
25		Both		
26		Both		
27		Both		
28		Both		
29		Both		
30		Both		

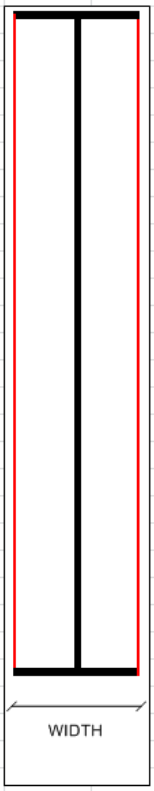

*NOTE: Inside is toward viewer when looking at the frame elevation.

Figure A.4: Member “Geometry” tab, stiffener locations (from Excel input)

Loading

Location (x) (ft)	Value (kip or kip*in.)	Type
0	1754	2
5	1754	2
1	1	1

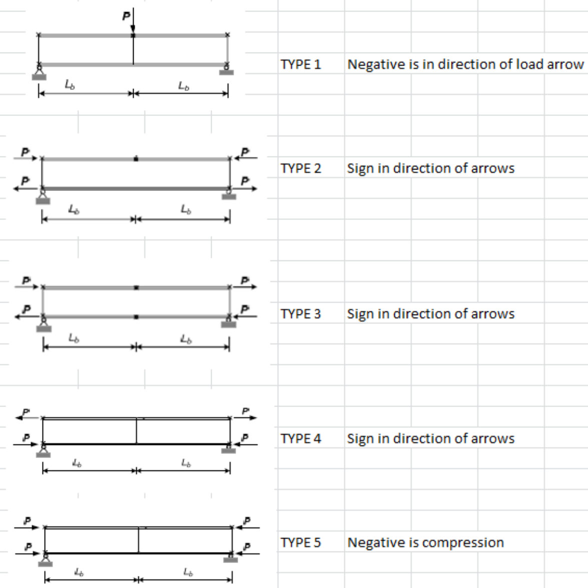

Figure A.5: Member “Loading” tab (from Excel input)

A.2 Frame Module

The frame module is broken into nine separate input tabs:

1. General – Figure A.6 – A basic information tab that allows the user to specify the material properties, boundary conditions, and parameters for the solution algorithm. Also, the user can specify whether or not the frame is symmetric. If so, the input from the tabs that include the right half of the frame is ignored.
2. L-Column – Figure A.7 – The specific section properties tab for the left column where all of the section dimensions are included, the purlin/girt locations and bracing information is stipulated, and the stiffener geometry is specified. SINBAD

has the capability to accept up to 10 section transitions, 10 purlin or girt bracing locations, and 10 stiffener locations for this member.

3. L-Knee – Figure A.8 – The specific section properties tab for the left knee region where all of the section dimensions are included, the purlin/girt locations and bracing information is stipulated, and the stiffener geometry is specified. SINBAD has the capability to accept up to 5 purlin or girt bracing locations within the knee. There is also the option to specify an eave strut and any associated bracing.
4. L-Rafter – Figures A.9, A.10, and A.11 – The specific section properties tab for the left rafter where all of the section dimensions are included, the purlin/girt locations and bracing information is stipulated, and the stiffener geometry is specified. SINBAD has the capability to accept up to 30 section transitions, 30 purlin or girt bracing locations, and 30 stiffener locations for this member. The user must also specify the slope of the rafter relative to the horizontal axis characterized by rise over run.
5. Rod-Cable Bracing – Figure A.12 – The locations and stiffness of any rod or cable bracing provided out-of-plane in the wall or roof. The locations are specified by bracing stiffness between specific purlins. For example, an engineer may specify that he has a rod brace between the base of the frame (purlin 1) and the eave strut at the top of the column/knee region (purlin 4).
6. Loading – Figure A.13 – The loading tab is where the user can specify the location, magnitude, and direction of loading. SINBAD is able to accept loading only at purlin locations. The user may also specify whether member self-weight should be included in the analysis.

7. R-Column – No figure provided – The exact same layout at L-Column, except that this tab pertains to the right column. This tab is only imported if the symmetry flag in the General tab is turned off.
8. R-Knee – No figure provided – The exact same layout at L-Knee, except that this tab pertains to the right knee region. This tab is only imported if the symmetry flag in the General tab is turned off.
9. R-Rafter – No figure provided – The exact same layout at L-Rafter, except that this tab pertains to the right rafter. This tab is only imported if the symmetry flag in the General tab is turned off.

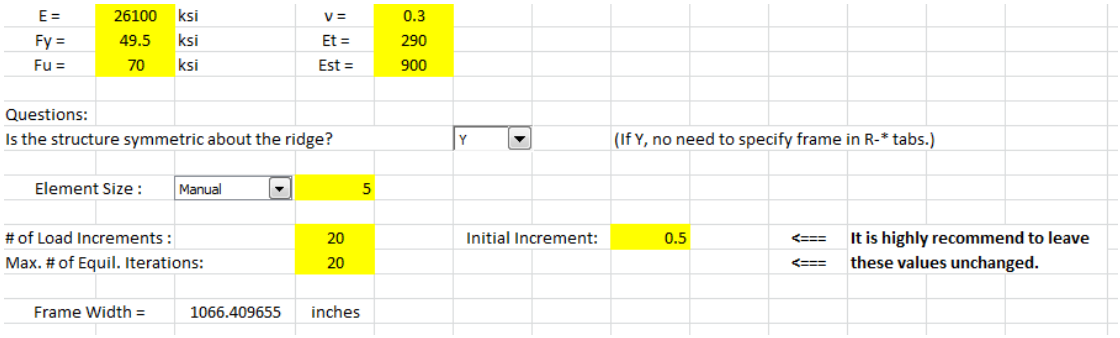

Figure A.6: Frame “General” tab (from Excel input)

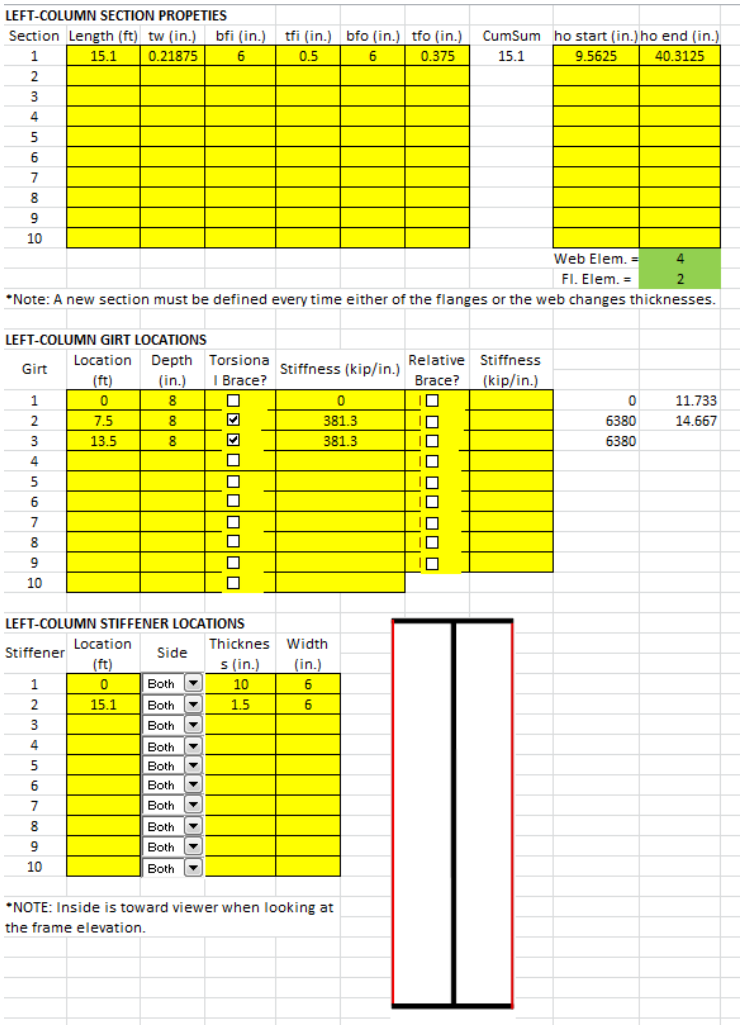

LEFT-COLUMN SECTION PROPETIES

Section	Length (ft)	tw (in.)	bfi (in.)	tfi (in.)	bfo (in.)	tfo (in.)	CumSum	ho start (in.)	ho end (in.)
1	15.1	0.21875	6	0.5	6	0.375	15.1	9.5625	40.3125
2									
3									
4									
5									
6									
7									
8									
9									
10									

Web Elem. = 4
Fl. Elem. = 2

*Note: A new section must be defined every time either of the flanges or the web changes thicknesses.

LEFT-COLUMN GIRT LOCATIONS

Girt	Location (ft)	Depth (in.)	Torsional Brace?	Stiffness (kip/in.)	Relative Brace?	Stiffness (kip/in.)		
1	0	8	☐	0	☐		0	11.733
2	7.5	8	☑	381.3	☐		6380	14.667
3	13.5	8	☑	381.3	☐		6380	
4			☐		☐			
5			☐		☐			
6			☐		☐			
7			☐		☐			
8			☐		☐			
9			☐		☐			
10			☐					

LEFT-COLUMN STIFFENER LOCATIONS

Stiffener	Location (ft)	Side	Thickness (in.)	Width (in.)
1	0	Both	10	6
2	15.1	Both	1.5	6
3		Both		
4		Both		
5		Both		
6		Both		
7		Both		
8		Both		
9		Both		
10		Both		

*NOTE: Inside is toward viewer when looking at the frame elevation.

Figure A.7: Frame “L-Column” tab (from Excel input)

LEFT-KNEE SECTION PROPETIES

ho lt. (in.)	ho rt. (in.)	tw (in.)	bf1 (in.)	tf1 (in.)	bf2 (in.)	tf2 (in.)	ho (in.)	Lo (in.)	
38.6125	40.375	0.21875	6	0.375	6	0.375	40.3125	4.25	0
Slope =	0.043721								

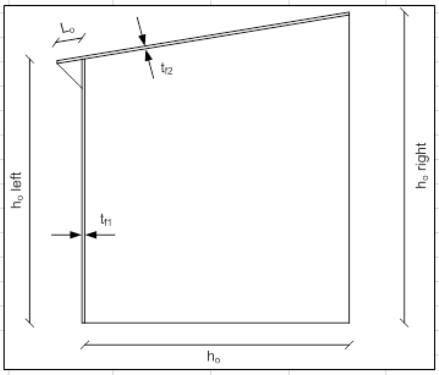

0

LEFT-KNEE VERTICAL GIRT LOCATIONS

Girt	Location (ft)	Depth (in.)	Torsional Brace?	Stiffness (kip*in./rad)	Relative Brace?	Stiffness (kip/in.)	
Previous	-	-	-	-	☐		15.087
1			☐		☐		
2			☐		☐		
3			☐		☐		
4			☐		☐		
5			☐		☐		

LEFT-KNEE HORIZONTAL PURLIN LOCATIONS

Purlin	Location (ft)	Depth (in.)	Torsional Brace?	Stiffness (kip*in./rad)	Relative Brace?	Stiffness (kip/in.)	
Previous	-	-	-	-			
1			☐		☐		
2			☐		☐		
3			☐		☐		
4			☐		☐		
5			☐				
Eave Strut?	☑	8			☐		28.089

Figure A.8: Frame “L-Knee” tab (from Excel input)

LEFT-RAFTER SECTION PROPETIES

Section	Length (ft)	tw (in.)	bfi (in.)	tfi (in.)	bfo (in.)	tfo (in.)	CumSum	ho start (in.)	ho end (in.)	Slope
1	10	0.25	6	0.375	6	0.375	10	40.375	31.505	-0.07392
2	10	0.1875	6	0.375	6	0.375	20	31.505	22.625	-0.074
3	21.11	0.15625	6	0.375	6	0.375	41.11	22.625	24.375	0.006908
4										#DIV/0!
5										#DIV/0!
6										#DIV/0!
7										#DIV/0!
8										#DIV/0!
9										#DIV/0!
10										#DIV/0!
11										#DIV/0!
12										#DIV/0!
13										#DIV/0!
14										#DIV/0!
15										#DIV/0!
16										#DIV/0!
17										#DIV/0!
18										#DIV/0!
19										#DIV/0!
20										#DIV/0!
21										#DIV/0!
22										#DIV/0!
23										#DIV/0!
24										#DIV/0!
25										#DIV/0!
26										#DIV/0!
27										#DIV/0!
28										#DIV/0!
29										#DIV/0!
30										#DIV/0!
										Min =
										Max =

Figure A.9: Frame “L-Rafter” tab, section properties (from Excel input)

							SLOPE:	
LEFT-RAFTER PURLIN LOCATIONS								12
Purlin	Location (ft)	Depth (in.)	Torsional Brace?	Stiffness (kip*in./rad)	Relative Brace?	Stiffness (kip/in.)	0.5	
1	0	8	☑	6380	☐		6380	20.95
2	5	8	☑	6380	☐		6380	
3	10	8	☑	6380	☐		6380	
4	15	8	☑	6380	☐		6380	
5	20	8	☐	0	☐		0	
6	25	8	☑	6380	☐		6380	
7	30	8	☐	0	☐		0	
8	35	8	☑	6380	☐		6380	
9	40	8	☑	6380	☐		6380	
10			☐		☐			
11			☐		☐			
12			☐		☐			
13			☐		☐			
14			☐		☐			
15			☐		☐			
16			☐		☐			
17			☐		☐			
18			☐		☐			
19			☐		☐			
20			☐		☐			
21			☐		☐			
22			☐		☐			
23			☐		☐			
24			☐		☐			
25			☐		☐			
26			☐		☐			
27			☐		☐			
28			☐		☐			
29			☐		☐			
30			☐					

Figure A.10: Frame “L-Rafter” tab, purlin locations (from Excel input)

LEFT-RAFTER STIFFENER LOCATIONS

Stiffener	Location (ft)	Side	Thickness (in.)	Width (in.)
1	0	Both	1.5	6
2	10	Both	1.5	6
3	20	Both	1.5	6
4	41.11	Both	1.5	6
5		Both		
6		Both		
7		Both		
8		Outside		
9		Both		
10		Both		
11		Both		
12		Both		
13		Both		
14		Both		
15		Both		
16		Both		
17		Both		
18		Both		
19		Both		
20		Both		
21		Inside		
22		Both		
23		Both		
24		Both		
25		Both		
26		Both		
27		Both		
28		Both		
29		Both		
30		Both		

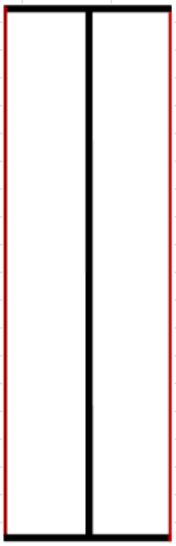

*NOTE: Inside is toward viewer when looking at the frame elevation.

Figure A.11: Frame “L-Rafter” tab, stiffener locations (from Excel input)

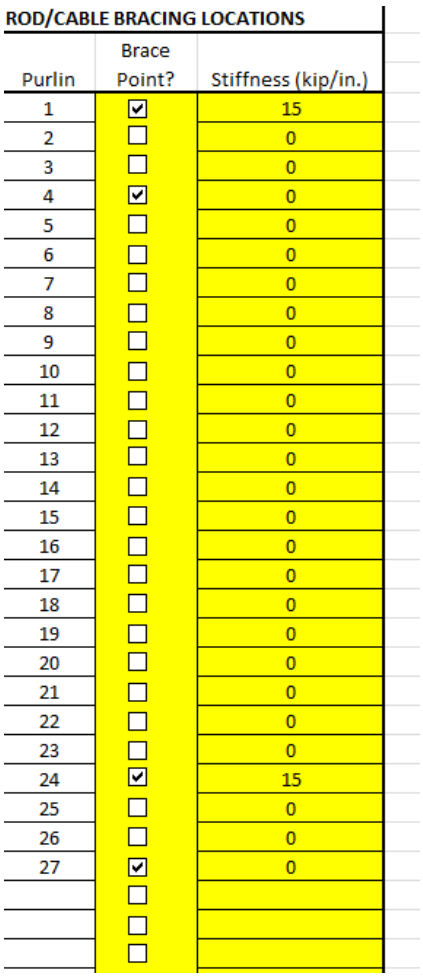

ROD/CABLE BRACING LOCATIONS

Purlin	Brace Point?	Stiffness (kip/in.)
1	☑	15
2	☐	0
3	☐	0
4	☑	0
5	☐	0
6	☐	0
7	☐	0
8	☐	0
9	☐	0
10	☐	0
11	☐	0
12	☐	0
13	☐	0
14	☐	0
15	☐	0
16	☐	0
17	☐	0
18	☐	0
19	☐	0
20	☐	0
21	☐	0
22	☐	0
23	☐	0
24	☑	15
25	☐	0
26	☐	0
27	☑	0
	☐	
	☐	
	☐	

Figure A.12: Frame “Rod-Cable Bracing” tab (from Excel input)

Analysis Type:	BUCKLE	2	Load No.	Descr.	Value (klf)	Factor	Status				
		0	1	DL	-0.039	0.8	ON				
Include Self-Weight?	NO	2	2	Coll DL	-0.06	0.8	ON		TOTAL LOAD:	-0.4152	klf
			3	Snow	-0.42	0.8	ON				
			4				OFF				
			5				OFF				

Purlin	Location	Trib Width	Load			Node #					
	0.3541667										
Eave	0	20.51041667	-0.70966			104500042					
1	40.3125	50.15625	-1.73541			204500038					
2	100.3125	60	-2.076			204500050					
3	160.3125	60	-2.076			204500062					
4	220.3125	60	-2.076			204500074					
5	280.3125	60	-2.076			204500086					
6	340.3125	60	-2.076			204500098					
7	400.3125	60	-2.076			204500110					
8	460.3125	60	-2.076			204500122					
9	520.3125	43.32	-1.49887			204500134					
10	533.6325										

Figure A.13: Frame “Loading” tab (from Excel input)

APPENDIX B

B. GRAPHICAL USER INTERFACE

The graphical user interface (GUI) implemented in SINBAD is based on the GUI creation wizard known as GUIDE from Matlab (2011). This appendix provides screen shots of the results that can be viewed using SINBAD. It should be noted that the colors representing the GUI have been inverted in the figures below in order to facilitate printing of this appendix.

The startup screen is shown below in Figure B.1. This is the screen that the user will see on execution of the program. Before an analysis is started, the user must specify whether or not to include residual stresses in the analysis and whether the user is interested in analyzing a beam or a frame.

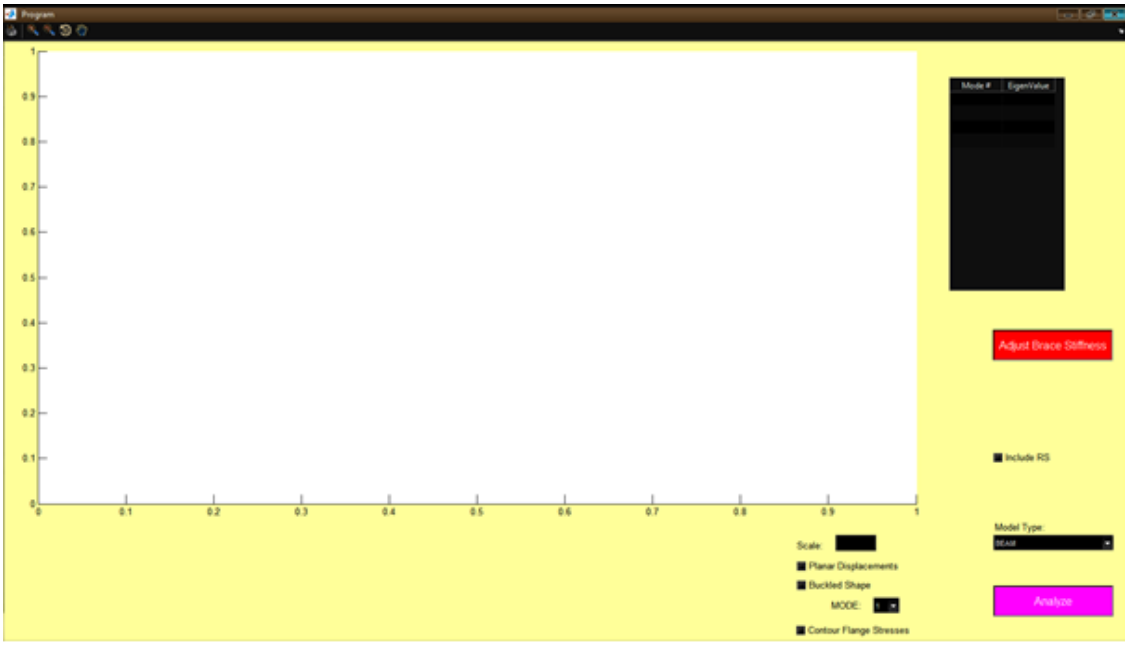

Figure B.1: Startup screen (from SINBAD)

After the analysis is complete, the GUI will display the initial, undeflected geometry for the member or frame in the main display window. Figures B.2 and B.3 show the results from a member and frame analysis, respectively.

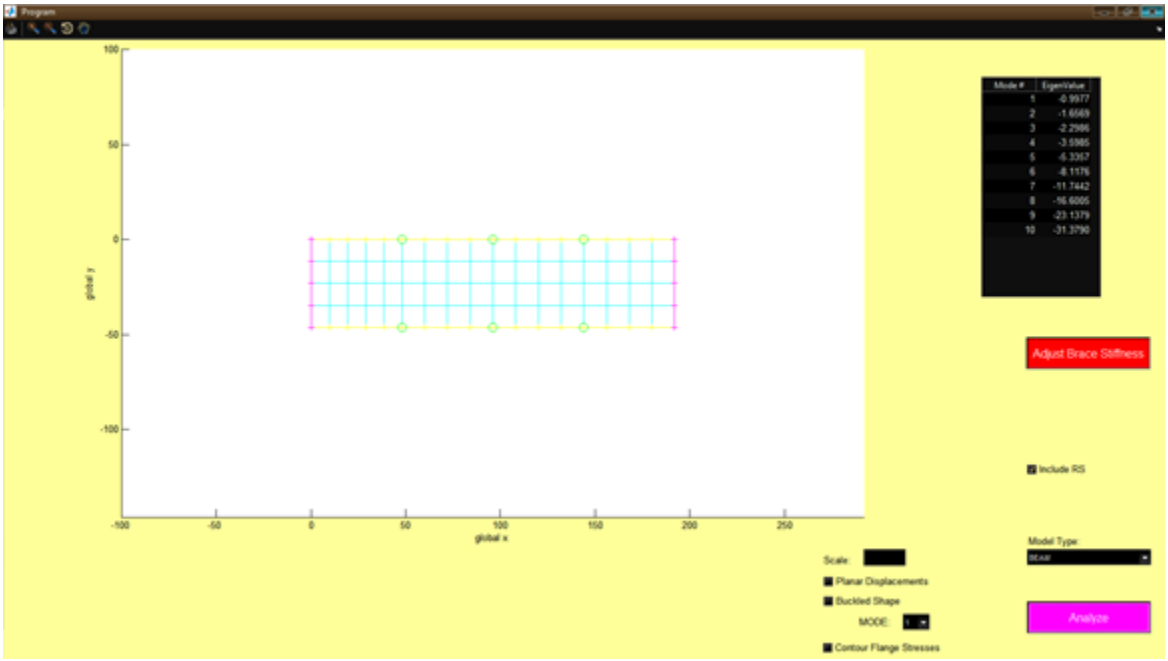

Figure B.2: Undeflected geometry after the member analysis (from SINBAD)

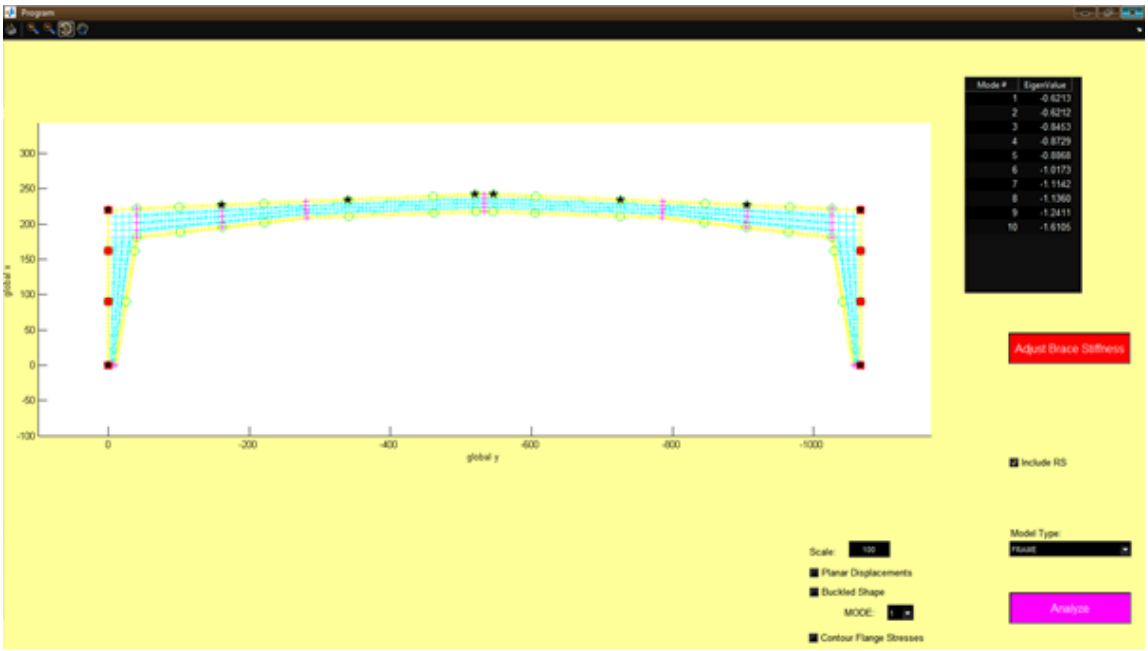

Figure B.3: Undeflected geometry after the frame analysis (from SINBAD)

SINBAD can display the in-plane displacements as shown in Figure B.4 for a member case subjected to loading such that the top flange is in compression and the beam is bending concave upwards.

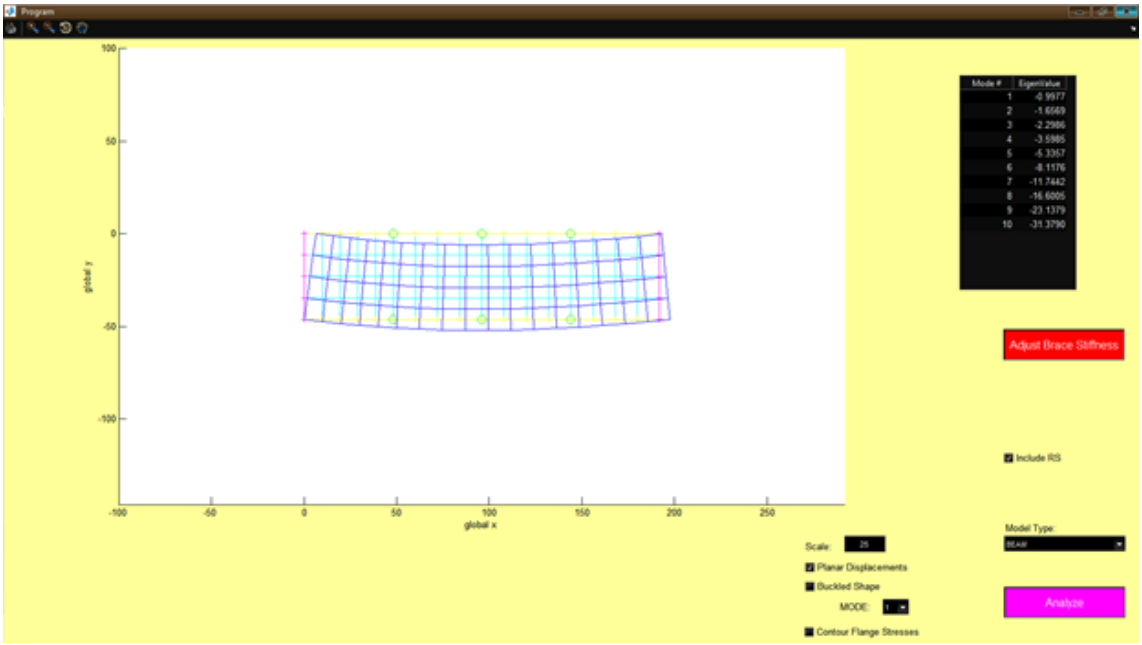

Figure B.4: In-plane deflected geometry after the member analysis (from SINBAD)

The mode shape corresponding to the lowest eigenvalue is shown in Figures B.5 and B.6 for an example member and in Figures B.7, B.8, and B.9 for an example frame.

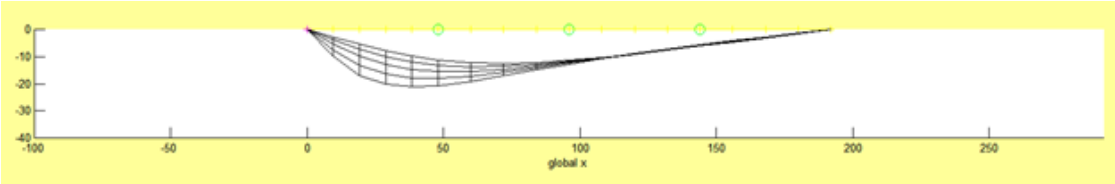

Figure B.5: Buckled mode shape after the member analysis, view 1 (from SINBAD)

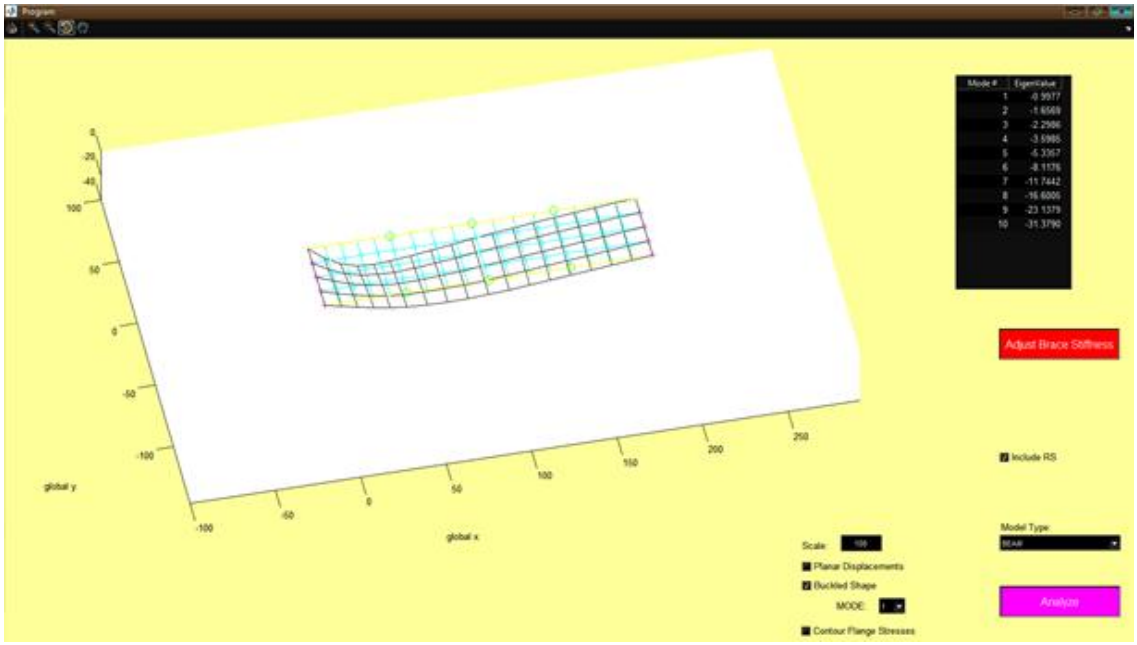

Figure B.6: Buckled mode shape after the member analysis, view 2 (from SINBAD)

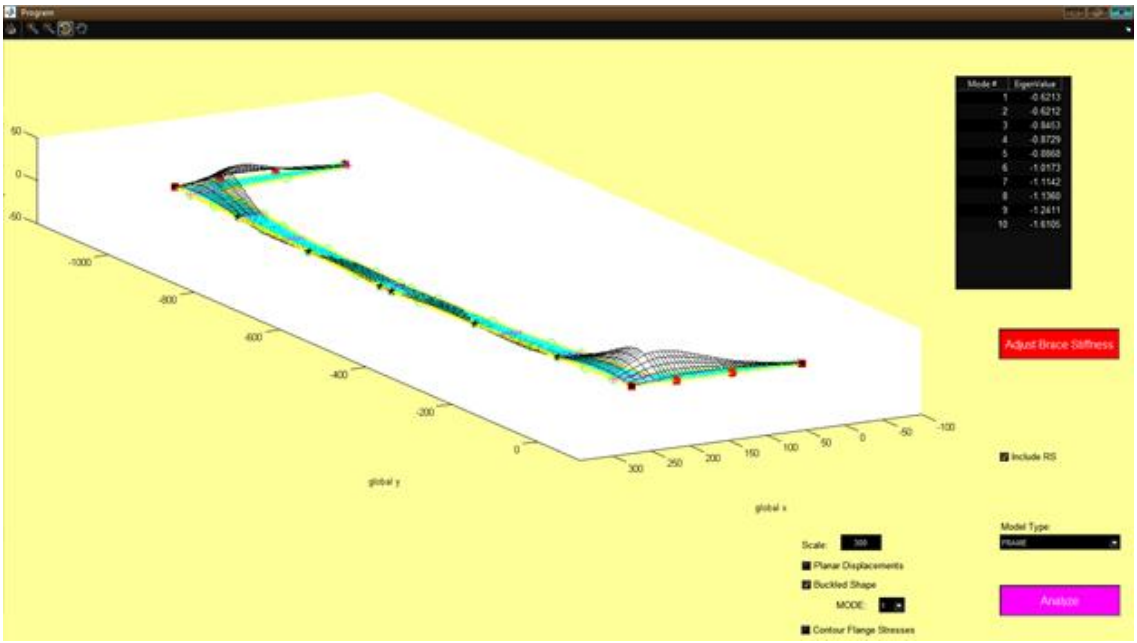

Figure B.7: Buckled mode shape after the frame analysis, view 1 (from SINBAD)

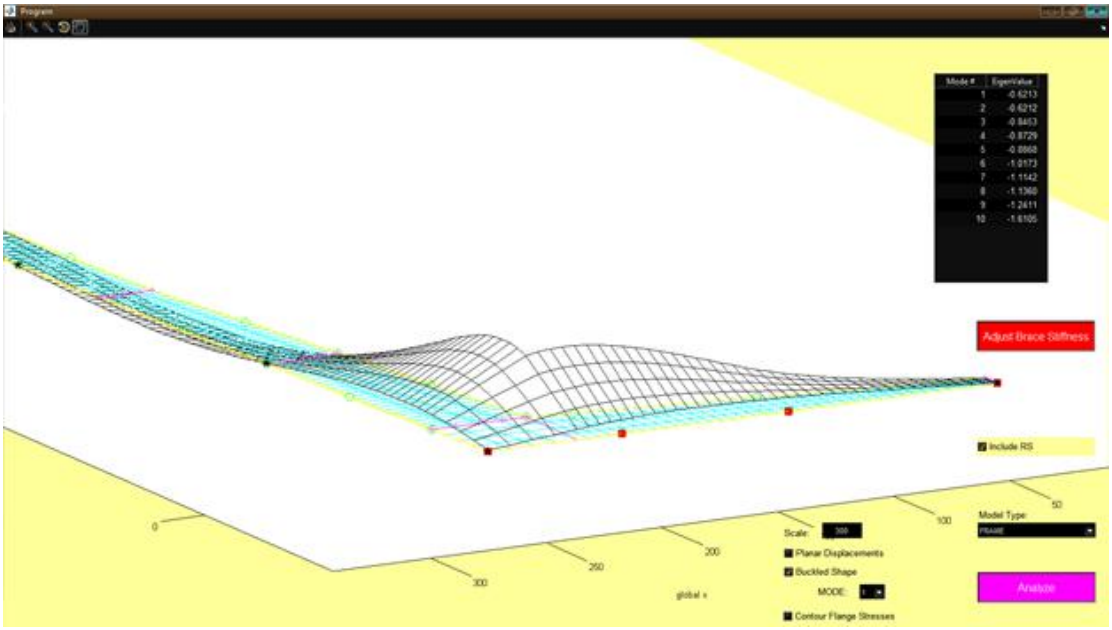

Figure B.8: Buckled mode shape after the frame analysis, view 2 (from SINBAD)

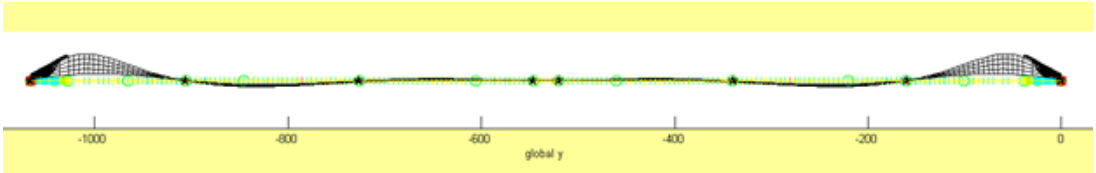

Figure B.9: Buckled mode shape after the frame analysis, view 3 (from SINBAD)

APPENDIX C

C. EXTERNAL GEOMETRIC STIFFNESS MATRIX FOR THE BEAM ELEMENT

As introduced in Chapter 3, the complete cubic Hermitian beam element external geometric stiffness matrix is shown in Table C.1, where *N* is the averaged element axial force at end 2, M_{z1} is the out-of-plane moment at end 1 and M_{z2} is the out-of-plane moment at end 2..

Table C.1: Beam element geometric stiffness matrix

$\mathbf{u_{x1}}$	$\mathbf{u_{y1}}$	$\mathbf{u_{z1}}$	$\boldsymbol{\theta}_{\mathbf{x1}}$	$\boldsymbol{\theta}_{\mathbf{y1}}$	$\boldsymbol{\theta}_{\mathbf{z1}}$	$\mathbf{u_{x2}}$	$\mathbf{u_{y2}}$	$\mathbf{u_{z2}}$	$\boldsymbol{\theta}_{\mathbf{x2}}$	$\boldsymbol{\theta}_{\mathbf{y2}}$	$\boldsymbol{\theta}_{\mathbf{z2}}$	
0	0	0	0	0	0	0	0	0	0	0	0	$\mathbf{u_{x1}}$
0	N/L	0	0	0	0	0	-N/L	0	0	0	0	$\mathbf{u_{y1}}$
0	0	N/L	M_{z1}/L	0	0	0	0	-N/L	M_{z2}/L	0	0	$\mathbf{u_{z1}}$
0	0	M_{z1}/L	0	0	0	0	0	$-M_{z1}/L$	0	0	0	$\boldsymbol{\theta}_{\mathbf{x1}}$
0	0	0	0	0	0	0	0	0	0	0	0	$\boldsymbol{\theta}_{\mathbf{y1}}$
0	0	0	0	0	0	0	0	0	0	0	0	$\boldsymbol{\theta}_{\mathbf{z1}}$
0	0	0	0	0	0	0	0	0	0	0	0	$\mathbf{u_{x2}}$
0	-N/L	0	0	0	0	0	N/L	0	0	0	0	$\mathbf{u_{y2}}$
0	0	-N/L	$-M_{z1}/L$	0	0	0	0	N/L	$-M_{z2}/L$	0	0	$\mathbf{u_{z2}}$
0	0	M_{z2}/L	0	0	0	0	0	$-M_{z2}/L$	0	$M_{z1}/6$ $-M_{z2}/3$	0	$\boldsymbol{\theta}_{\mathbf{x2}}$
0	0	0	0	0	0	0	0	0	$M_{z1}/6$ $-M_{z2}/3$	0	0	$\boldsymbol{\theta}_{\mathbf{y2}}$
0	0	0	0	0	0	0	0	0	0	0	0	$\boldsymbol{\theta}_{\mathbf{z2}}$

REFERENCES

AISC (2010a). “Code of Standard Practice for Steel Buildings and Bridges”, American Institute of Steel Construction, Inc. Chicago, IL. AISC 303-10.

AISC (2010b). “Specification for Structural Steel Buildings”, American Institute of Steel Construction, Inc. Chicago, IL. ANSI/AISC 360-10.

AISC (2002). “Example Problems Illustrating the Use of the New Bracing Provisions – Section C3, Spec and Commentary”, Ad hoc Committee on Stability Bracing, November (revised from original version of August 1998).

ASCE (1971). Plastic Design in Steel: A Guide and Commentary, Second Edition, A Joint Committee of the Welding Research Council and the American Society of Civil Engineers, ASCE, New York.

Ales, J.M. and Yura, J.A. (1993), “Bracing Design for Inelastic Steel Structures”, Is Your Structure Suitably Braced?, 1993 Conference, Structural Stability Research Council.

Avent, R.R. and Wells, S. (1979), “Factors Affecting the Strength of Thin-wall Welded Columns”, Report Submitted to Metal Building Manufacturers Association, Cleveland, OH, December.

Bathe, K. and Dvorkin, E. (1985), “A Four-node Plate Bending Element Based on Mindlin/Reissner Plate Theory and a Mixed Interpolation,” International Journal for Numerical Methods in Engineering, 21, Pp. 367-383.

Beedle, L. (1958). Plastic Design of Steel Frames, John Wiley and Sons, New York.

Clarke, M.J. and Hancock, G.J. (1990), “A study of incremental-iterative strategies for non-linear analyses”, International Journal for Numerical Methods in Engineering, 29(7), Pp. 1365-1391, May.

Cook, R., Malkus, D., Plesha, M., and Witt, R. (2002), Concepts and Applications of Finite Element Analysis, John Wiley and Sons, New York.

Crisfield, M.A. (1991). Non-linear Finite Element Analysis of Solids and Structures, Volume 1: Essentials, John Wiley and Sons, New York.

ECCS (1983). “Ultimate Limit State Calculations of Sway Frames with Rigid Joints,” Technical Working Group 8.2, Systems, Publication No. 33, European Commission for Constructional Steelwork, November, P. 20.

Galambos, T.V. and Surovek, A. E. (2008). Structural Stability of Steel: Concepts and Applications for Structural Engineers, John Wiley and Sons, New York.

Gil, H. (1996). “Bracing Requirements for Inelastic Steel Members”, Doctoral Dissertation, The University of Texas at Austin, Austin, TX, May.

Gil, H. and Yura, J.A. (1999). “Bracing Requirements for Inelastic Columns”, Journal of Constructional Steel Research, Vol. 51, Pp. 1-19, January.

Helwig, T.A. and Yura, J.A. (2008a). “Shear Diaphragm Bracing of Beams. I: Stiffness and Strength Behavior”, Journal of Structural Engineering, ASCE, Pp. 348-356, March.

Helwig, T.A. and Yura, J.A. (2008b). “Shear Diaphragm Bracing of Beams. II: Design Requirements”, Journal of Structural Engineering, ASCE, Pp. 357-363, March.

Kaehler, R.C., White, D.W., and Kim, Y.D. (2011). “Frame Design Using Web-Tapered Members”, AISC Steel Design Guide 25, American Institute of Steel Construction, Chicago, IL.

Kim, Y.D. (2010). “Behavior and Design of Metal Building Frames Using General Prismatic and Web-Tapered Steel I-Section Members”, Doctoral Dissertation, Georgia Institute of Technology, Atlanta, GA.

Li, G. and Yura, J.A. (2002). “Bracing Requirements for Inelastic Beams”, 2002 Conference, Structural Stability Research Council.

Lutz, A.L. and Fisher, J. (1985). “A Unified Approach for Stability Bracing Requirements”, AISC Engineering Journal, Vol. 22(4), Pp. 163-167.

MBMA (2006). Metal Building Systems Manual, Metal Building Manufacturers Association, Cleveland, OH.

MathWorks (2011). MATLAB, Software and Help Documentation, Version R2011b(7.13.0.564).

McGuire, W. (1968), Steel Structures, Englewood Cliffs, NJ: Prentice-Hall, Inc.

McGuire, W., Gallagher, R., and Ziemian, R. (2000), Matrix Structural Analysis, Second Edition, New York: John Wiley & Sons, Inc.

Nethercot, D.A. (1974), “Buckling of Welded Beams and Girders”, Proc. International Association for Bridge and Structural Engineering, Vol. 57, Pp. 291-306.

Prawel, S.P., Morrell, M.L. and Lee, G.C. (1974). “Bending and Buckling Strength of Tapered Structural Members,” Welding Research Supplement, Vol. 53, Pp. 75-84, February.

Seelye, Elwyn E. (1945), Data Book for Civil Engineers: Design, Vol. 1, John Wiley and Sons, New York.

Sharma, A. (2010). “Flange Stability Bracing Behavior in Metal Building Frame Systems”, In Partial Fulfillment of the Requirements for the Degree, Master of Science in the School of Civil and Environmental Engineering, Georgia Institute of Technology, Atlanta, GA.

Simo, J.C. and Taylor, R.L. (1986). “A Return Mapping Algorithm for Plane Stress Elastoplasticity,” International Journal for Numerical Methods in Engineering, 22, Pp. 649-670.

Simulia (2012). Abaqus, Software and Users’ Manuals, Version 6.12.

Simulia (2011). Abaqus Software, Version 6.10.

Smith, Matthew D. (2012a). “Cyclic Testing of Web-Tapered Rafters in Support of P695 Study, All Specimens Progress Report”. A presentation, July.

Smith, Matthew D. (2012b). “Cyclic Testing of Web-Tapered Rafters in Support of P695 Study, Progress Report: Specimen 4”. A presentation, May.

Stanway, G.S., Chapman J.C., and Dowling, P.J. (1992a). “A Simply Supported Imperfect Column with a Transverse Elastic Restraint at any Position. Part 1: Behaviour”. Proc. Instn. Civ. Engrs Structs & Bldgs, 94, Pp. 205-216, May.

Stanway, G.S., Chapman J.C., and Dowling, P.J. (1992b). “A Simply Supported Imperfect Column with a Transverse Elastic Restraint at any Position. Part 2: Design Models”. Proc. Instn. Civ. Engrs Structs & Bldgs, 94, Pp. 217-228, May.

Taylor, R., Beresford, P., and Wilson, E. (1976). “A Non-Conforming Element for Stress Analysis.” International Journal for Numerical Methods in Engineering, 10, Pp. 1211-1219.

Throop, C. Mortimer (1947), “Suggestions for Safe Lateral Bracing Design,” Engineering News-Record, McGraw Hill, 138, Pp. 218-219.

Timoshenko, S. and Gere, J. (1961), Theory of Elastic Stability, New York: McGraw-Hill.

Tran, D. Q. (2009). “Towards Improved Flange Bracing Requirements for Metal Building Frame Systems”, In Partial Fulfillment of the Requirements for the Degree, Master of Science in the School of Civil and Environmental Engineering, Georgia Institute of Technology, Atlanta, GA.

Wang, L. and Helwig, T. A. (2005). “Critical Imperfections for Beam Bracing Systems”, Journal of Structural Engineering, ASCE, Pp. 933-940, June.

White, D.W. (1985). “Material and Geometric Nonlinear Analysis of Local Planar Behavior in Steel Frames Using Interactive Computer Graphics”, In Partial Fulfillment of the Requirements for the Degree, Master of Science, Cornell University, Ithaca, NY, August.

White, D.W. (1988). “Analysis of Monotonic and Cyclic Stability of Steel Frame Subassemblages,” In Partial Fulfillment of the Requirements for the Degree, Doctor of Philosophy, Cornell University, Ithaca, NY, January.

White, D.W., and Kim, Y.D. (2006). “A Prototype Application of the AISC (2005) Stability Analysis and Design Provisions to Metal Building Structural Systems”, Report Prepared for Metal Building Manufacturers Association, January.

Will, K. and Zarco, B. (2011). “New Plane Stress, Plate Bending, and Plate Elements,” Presentation for GT STRUDL, June.

Winter, G. (1958), “Lateral Bracing of Columns and Beams,” Trans. ASCE, Part 1, 125, Pp. 809-925.

Yura, J.A. (2001), “Fundamentals of Beam Bracing,” Engineering Journal, AISC, 38(1), Pp. 11-26.

Yura, J.A. (1996), ‘‘Winter’s bracing approach revisited,’’ Engineering Structures 8(10), Pp. 821-825.

Yura, J.A. (1995), “Bracing for Stability – State-of-the-Art,” Is Your Structure Suitably Braced?, 1995 Conference, Structural Stability Research Council.

Yura, J.A. (1993), “Fundamentals of Beam Bracing,” Is Your Structure Suitably Braced?, 1993 Conference, Milwaukee, Wisconsin, Structural Stability Research Council, Bethlehem, PA, Pp. 1-40.

Yura, J.A. and Helwig, T.A. (2009). “Bracing for Stability,” Short course sponsored by the Structural Stability Research Council, North American Steel Construction Conference, Phoenix, AZ, April.

Yura, J.A., and Phillips, B. (1992). “Bracing Requirements for Elastic Steel Beams”, Report No. 1239-1, Center for Transportation Research, University of Texas at Austin. May, 88.

Yura, J.A., Phillips, B., Raju, S., and Webb, S. (1992). “Bracing of Steel Beams in Bridges”, Report No. 1239-4F, Center for Transportation Research, University of Texas at Austin. October, 80.

Ziemian, Ronald D. (2010), Guide to Stability Design Criteria for Metal Structures, 6th Edition, John Wiley & Sons, Inc., Hoboken, NJ.

Zuk, W. (1956), "Lateral Bracing Forces on Beams and Columns", Journal of the Engineering Mechanics Division, ASCE, 82 (EM3), 1032-1-1032-16.